

Designing a Scaffold-Free Bio-orthogonal Click Chemistry Method of Cell Assembly for Application in Tissue Engineering

Dmitry Rogozhnikov

A Thesis Submitted to the Faculty of Graduate Studies
In Partial Fulfillment of the Requirements
For the Degree of

Doctor of Philosophy

Graduate Program in Chemistry
York University
Toronto, Ontario

October 2017

©Dmitry Rogozhnikov, 2017

Abstract

Tissue engineering is a growing field of science that relies on the use of material chemistry, engineering, genetics, and cell biology to produce functional tissues for use in transplantation, drug testing and disease modelling. Presently, there is an urgent need for a technology which would enable assembly of cells into 3-dimensional multilayered tissues. Current cell-assembly technologies rely on biodegradable polymer scaffolds to assemble cells into 3D structures and to support the cell mass of the growing tissue. The presence of these materials in tissues, however, lowers the cell density and the process of scaffold biodegradation results in accumulation of monomer byproducts within the tissue. To overcome these issues we developed a scaffold free method of cell-assembly based on bio-orthogonal ligation reactions between oxyamine and ketone groups to form a stable oxime bond. The reaction is quick, specific and occurs under physiological conditions without a catalyst. To deliver the bio-orthogonal functionalities onto cell surfaces, ketone- and oxyamine- functionalized lipids were incorporated into liposomes which were subsequently fused with cell membranes. The surface engineered cells were assembled into three-dimensional tissues. Using this approach, we were able to produce functional cardiac and liver tissues with variable thicknesses and cell orientations for drug testing as well as the complex 3D co-cultures of stem cells to study stem cell differentiation. The rapid bio-orthogonal cell ligation process also enables assembly of cells into co-culture spheroids in flow, inside a microchannel. The introduction of a bi-functional oxyamine crosslinker molecule allowed for the rapid crosslinking of ketone-functionalized cells into 3D tissues. This bio-orthogonal click chemistry technology can be used with different cell types to produce customized tissues for applications in drug development and regenerative medicine.

Acknowledgements

I would like to thank my supervisor, Professor Muhammad. N. Yousaf for providing his guidance and support during my graduate training. He was the one who ignited my interest for the field of bio-orthogonal chemistry and opened my mind towards the infinite possibilities of interdisciplinary science. Professor Yousaf has been an amazing teacher and a patient mentor throughout the years of my studies in graduate school.

I am also grateful to my peers: Paul O'Brian and Sina Elahipanah, with whom I shared all happy and difficult moments and who have become my best friends. I would also like to thank Melanie Williams for proofreading this work.

Finally, I would like to express my sincere and heart-full gratitude to my mother, Liubov Rogozhnikova for her love, support, encouragement and sympathetic ear.

Table of Contents

	Page
Abstract.....	ii
Acknowledgements	iii
Table of Contents.....	iv
List of Tables	xi
List of Figures.....	xii
List of Acronyms.....	xvi
List of Journal Articles.....	xviii

Chapter 1: Introduction: Application of Bio-orthogonal Chemistry in Tissue Engineering

		Page
1	Introduction: Application of Bio-orthogonal Chemistry in Tissue Engineering	1
1.0	The three-dimensional architecture of organs and tissues.....	2
1.1	Areas of application for three-dimensional tissues.....	4
1.1.1	Transplantation.....	4
1.1.2	Drug Testing.....	5
1.1.3	A 3D Model for Intercellular Interactions.....	6
1.2	Scaffolds, Biomaterials and 3D printing.....	8
1.2.1	ECM-based scaffolds and hydrogels.....	8
1.2.2	Alginate.....	10
1.2.3	Polymer Scaffolds.....	11
1.3	Scaffold Fabrication Methods.....	15
1.3.1	Electrospinning.....	15
1.3.2	3D Printing.....	17
1.3.4	Decellularized Scaffolds.....	18

1.3.5	Organoids.....	20
1.4	Extracellular Matrix.....	22
1.4.1	Durotaxis.....	23
1.4.2	ECM composition.....	23
1.4.2.1	Collagen.....	24
1.4.2.2	Elastin.....	25
1.4.2.3	Fibronectin.....	25
1.4.2.4	Integrins.....	26
1.4.2.5	Glycosaminoglycans.....	26
1.5	Plasma Membrane.....	27
1.6	Cell Surface Engineering.....	30
1.6.1	Genetic Engineering.....	31
1.6.2	Metabolic Engineering.....	34
1.6.3	Layer by Layer Self-assembly Technique.....	36
1.7	Liposome Fusion.....	38
1.8	Bio-orthogonal Chemistry.....	45
1.8.1	Oxime chemistry.....	49
1.9	Bio-orthogonal Cell-Assembly Strategy.....	51
1.10	References.....	59

Chapter 2: Scaffold- Free Bio-orthogonal Assembly of 3-Dimensional Cardiac Tissue via Cell Surface Engineering

		Page
2	The Copyright Statement.....	73
2.1	Summary.....	74
2.2	Introduction.....	75
2.3	Experimental.....	77

2.3.1	Ethical Statement.....	77
2.3.2	Cardiomyocytes Isolation.....	77
2.3.3	Tissue culture.....	78
2.3.4	Preparation of Liposomes.....	78
2.3.5	Tissue Assembly.....	79
2.3.6	Immunohistochemistry and Confocal Microscopy.....	80
2.3.7	Immunostaining.....	80
2.3.8	Fluorescent Staining for Collagen and Elastin.....	81
2.3.9	Fluorescent Calcium Imaging.....	81
2.3.10	Cardiotoxicity Testing.....	82
2.3.11	Real Time Image Processing.....	82
2.4	Results and Discussion.....	83
2.5	Conclusion.....	96
2.6	References.....	98

Chapter 3: Generation of a Scaffold-Free Three-Dimensional Liver Tissue via a Rapid Cell-to-Cell Click Assembly Process

		Page
3	The Copyright Statement.....	101
3.1	Summary.....	102
3.2	Introduction.....	103
3.3	Experimental.....	105
3.3.1	Tissue Culture.....	105
3.3.2	Preparation of Liposomes.....	106
3.3.3	Liver Tissue Assembly.....	107
3.3.4	Fluorescent Staining for Collagen and Elastin in 2D and 3D Assemblies	107
3.3.5	Immunohistochemistry and Confocal Microscopy.....	108

3.3.6	Activation of Cytochrome P450 3A4.....	108
3.3.7	Albumin Analysis.....	109
3.3.8	Toxicity Assays.....	109
3.4	Results and Discussion.....	109
3.5	Conclusion.....	117
3.6	References.....	118

Chapter 4: Cell Polymerization via a Biocompatible Crosslinker

		Page
4.1	Summary.....	123
4.2	Introduction.....	124
4.3	Experimental.....	126
4.3.1	List of Materials.....	126
4.3.2	Synthesis of Dioxyamine Crosslinker.....	127
4.3.3	Preparation of Functionalized Liposomes.....	128
4.3.4	Cell Surface Engineering via Bio-orthogonal liposome fusion.....	128
4.3.5	Cell – Cell Crosslinking.....	129
4.3.6	Confocal Microscopy.....	130
4.3.7	Liver Tissue Assembly.....	130
4.3.8	Immunohistochemistry and Confocal Microscopy.....	131
4.3.9	Activation of Cytochrome P450 3A4.....	131
4.3.10	Liver Toxicity Assays.....	132
4.4	Results and Discussion.....	133
4.5	Conclusion.....	140
4.6	References.....	141

Chapter 5: Assembly of Cells into 3D Tissues via Bio-orthogonal Chemistry and Preferential Differentiation of Stem Cells in Co-cultures with Controlled Cell Orientations

	Page
5.1	Summary..... 145
5.2	Introduction..... 146
5.3	Experimental..... 148
5.3.1	Tissue Culture..... 148
5.3.2	Formation of Liposomes..... 148
5.3.3	Formation of Cell Multi-layers..... 149
5.3.4	Adipogenic Differentiation..... 149
5.3.5	Preferential Differentiation..... 150
5.3.6	Immunohistochemistry..... 150
5.3.7	Cell Viability Assay..... 151
5.3.8	Statistical Analysis..... 151
5.3.9	Confocal Microscopy..... 151
5.3.10	RT-PCR..... 152
5.4	Results and Discussion..... 153
5.5	Conclusion..... 162
5.6	References..... 163

Chapter 6: Spheroid and Tissue Assembly via Click Chemistry in Microfluidic Flow

	Page
6	The Copyright Statement..... 166

6.1	Summary.....	167
6.2	Introduction.....	168
6.3	Experimental.....	170
6.3.1	List of Materials.....	170
6.3.2	Cell Culture.....	170
6.3.3	Microfluidic Device Fabrication and Design.....	171
6.3.4	Liposome Formation and Formulation.....	171
6.3.5	Cell Surface Modification Using Liposome Fusion.....	172
6.3.6	General Method for Spheroid Generation in Microfluidic Device.....	172
6.3.7	Engineered Spheroid Growth Kinetics Using Microfluidics.....	173
6.3.8	Confocal Microscopy of RFP/GFP 3D Coculture Microtissues.....	174
6.3.9	Confocal Microscopy of Three-Cell Lines (Red/Green/Blue) Microtissues	174
6.3.10	3D Coculture Multilayers of HMSCs and 3T3 Fibroblasts.....	175
6.3.11	Collagen Based RFP and GFP Tissue Formation.....	176
6.3.12	3D Oriented Coculture Multilayers (RFP-GFP-RFP, thin).....	176
6.3.13	3D Oriented Coculture Multizones (RFP-GFP-RFP, thick).....	177
6.3.14	Oxime Bond Formation (Synthesis of 2-(Propan-2- ylideneaminoxy)acetic acid)	177
6.3.15	Oxime Hydrolysis Analysis.....	178
6.3.16	Oxime Formation Kinetics Conditions.....	178
6.3.17	Stem Cell Differentiation in Coculture. RT-PCR Analysis.....	179
6.3.18	Bubble Fusion via Oxime Chemistry.....	179
6.3.19	Spheroid Assembly.....	180
6.4	Results and Discussion.....	180
6.5	Conclusion.....	192
6.6	References.....	194

Chapter 7: Conclusions and Future Work

	Page
7	Conclusions and Future Work..... 197
7.1	References..... 201

Appendix

	Page
A1	Appendix A1..... 202

List of Tables

1.1	Advantages and disadvantages of applying scaffolds for tissue engineering.....	51
-----	--	----

List of Figures

Chapter 1: Application of Bio-orthogonal Chemistry in Tissue Engineering

	Page
1.1	Areas of application for three-dimensional tissues..... 3
1.2	The three-dimensional ECM scaffold..... 9
1.3	The alginate hydrogel..... 10
1.4	Two models of scaffold degradation..... 13
1.5	Generating scaffolds via electrospinning..... 16
1.6	Decellularized scaffolds..... 19
1.7	The formation of intestinal organoids..... 21
1.8	Detailed depiction of the extracellular matrix..... 24
1.9	The structure of the eukaryotic plasma membrane..... 27
1.10	Genetic transfection of cells via a liposomal transfection agent..... 30
1.11	Genetically engineered integrin receptors..... 33
1.12	Metabolic engineering..... 35
1.13	The layer by layer (LbL) self-assembly technique..... 37
1.14	Liposome delivery system..... 39
1.15	The mechanism of lipid membrane fusion depicting the key..... 41 intermediate structures
1.16	The membrane destabilization strategies..... 42
1.17	Bio-orthogonal chemistry as an effective molecular ligation strategy..... 46
1.18	The modified Staudinger ligation reaction..... 47
1.19	The copper-catalyzed azide–alkyne cycloaddition (CuAAC)..... 48
1.20	The strain-promoted alkyne-azide cycloaddition..... 49
1.21	The bio-orthogonal reaction between oxyamine and ketone..... 50
1.22	The synthesis of functionalized liposomes for cell surface engineering... 53

1.23	Cell surface engineering via liposome fusion.....	54
1.24	The bio-orthogonal cell ligation strategy.....	57

Chapter 2: Scaffold- Free Bio-orthogonal Assembly of 3-Dimensional Cardiac Tissue via Cell Surface Engineering

		Page
2.1	Schematic description for generating a scaffold free complex cardiac tissue by combining cell surface engineering and bio-orthogonal chemistry.....	84
2.2	The schematic diagram representing the process of generating scaffold free 3 dimensional cardiac tissue via cell surface engineering and bio-orthogonal chemistry.....	85
2.3	Confocal image representations of various 2D and 3D scaffold free cardiac tissue.....	86
2.4	Cell viability in 2D and 3D tissues measured using propidium iodide viability assay.....	87
2.5	Fluorescent antibody staining for expression of cardiac-specific markers 96h after tissue assembly.....	88
2.6	Fluorescent immunostaining for endothelial genetic marker CD31 expressed by HUVEC cells in 2D and 3D co-cultures 96h after tissue assembly.....	89
2.7	Fluorescent staining of collagen and elastin secreted over time by 2D monolayers and 3D tissues.....	90
2.8	Native propagation of calcium across cardiac tissues without external stimulation.....	92
2.9	Chronotropic effects of cardiac tissues under treatment with varying concentrations of isoprenaline and doxorubicin.....	95

Chapter 3: Generation of a Scaffold-Free Three-Dimensional Liver Tissue via a Rapid Cell-to-Cell Click Assembly Process

		Page
3.1	General schematic process of engineering cell surfaces with bio-orthogonal chemistry groups for the programmable assembly of multiple cell lines into complex coculture spheroids and tissues.....	110
3.2	Fluorescent images and digital photograph of single layer and three-dimensional liver tissue.....	111

3.3	Fluorescent image comparisons of extracellular matrix (ECM) production over time after two-dimensional co-culture monolayer and three-dimension multilayer tissue assembly.....	113
3.4	Fabrication and analysis of various types of liver chips generated via an intercell bio-orthogonal ligation strategy.....	114
3.5	Study of mitochondrial activity for evaluation of liver toxicity in different types of liver constructed chips.....	116

Chapter: 4 Cell Polymerization via a Biocompatible Crosslinker

		Page
4.1	Schematic of cell surface engineering and cross-linking surface-engineered cells.....	134
4.2	Schematic and fluorescent microscopy showing cross-linking and assembly of surface-engineered cells.....	136
4.3	Constructing model 3D liver tissue by the integrated surface engineering and cross-linking system.....	138
4.4	Constructed model 3D liver tissue for liver chip assay application.....	139

Chapter: 5 Assembly of Cells into 3D Tissues via Bio-orthogonal Chemistry and Preferential Differentiation of Stem Cells in Co-cultures with Controlled Cell Orientations

		Page
5.1	The schematic representation of cell surface engineering and the bio-orthogonal reaction between oxyamine and ketone functionalities.....	147
5.2	Schematic representation of 3D co-cultures of C3H 10T1/2 and hMSC generated via liposome fusion technology.....	153
5.3	Control of orientation and thickness of cell multilayers via bio-orthogonal chemistry.....	154
5.4	Multilayers of co-culture of human mesenchymal stem cells (hMSC) with murine (mouse) C3H10T1/2 fibroblasts and their adipogenic differentiation (visualized with Oil Red O staining).....	155
5.5	3D plot describing the rate of adipogenic differentiation based on stem cell orientation.....	157
5.6	Schematic representation of the experiment involving a choice of cell lineage.....	159

5.7	The orientation of stem cells in co-culture influences their lineage preference.....	159
5.8	Plot describing the differentiation of co-cultures with different cell orientations into adipocytes and osteoblasts after 18 days of incubation in media containing both adipogenic and osteogenic growth factors.....	161

Chapter 6: Spheroid and Tissue Assembly via Click Chemistry in Microfluidic Flow.

		Page
6.1	Schematic describing the cell surface tailoring strategy to generate complex coculture tissue assemblies.....	181
6.2	NMR study of the kinetics and stability of a bio-orthogonal oxime conjugation reaction under physiological conditions.....	183
6.3	Schematic describing the use of microfluidic technology and tailored cell lines to generate multilayer coculture tissues.....	184
6.4	Brightfield images of C3H10T1/2 cells at various stages of assembly in the microfluidic channel device.....	185
6.5	3D plot presenting the relationship between flow rate, channel distance, cell density, and resulting cell cluster size (spheroid) assembled within a microfluidic channel.....	186
6.6	Schematic cartoon and fluorescent images of resultant coculture spheroid assembly via click chemistry ligation.....	188
6.7	Range of confocal and bright-field images of various combinations of GFP NIH 3T3 fibroblasts, RFP neonatal fibroblasts, CMAC live stained C3H10T1/2 pluripotent embryonic fibroblast stem cells. HMSC cells and NIH Swiss 3T3 cells.....	190
6.8	Construction of a 3D tissue coculture system via intercell click ligation and application to stem cell differentiation.....	191

Appendix

		Page
A1	Control and stability studies for the formation of cell aggregates and Multilayers.....	202

List of Acronyms

3D	three-dimensional
2D	two-dimensional
ECM	extracellular matrix
iPSC	induced pluripotent stem cells
M	(1,4)-linked β -D-mannuronate
G	α -L-guluronate
FDA	American Food and Drug Administration
PGA	polyglycolide
PLA	polylactide
PCL	polycaprolactone
DNA	deoxyribonucleic acid
ES cells	embryonic stem cells
RGD	arginine, glycine, aspartic acid
GAG	glycosaminoglycans
IgE	immunoglobulin E
ManNAz	N-acetylmannosamine derivative containing an azidoacetyl group
LbL	layer by Layer Self-assembly Technique
FITC	Fluorescein isothiocyanate
SUV	small unilamellar vesicles
LUV	large unilamellar vesicles
GUV	giant unilamellar vesicles
POPC	phosphatidylcholine
SNARE	Soluble <u>NSF</u> Attachment Protein Receptor
DOTAP	1,2-dioleoyl-3 trimethylammonium-propane
CuAAC	copper-catalyzed azide-alkyne cycloaddition
hMSC	human mesenchymal stem cells

HUVEC human umbilical vein endothelial cells
ECGS endothelial cell growth supplement
FBS fetal bovine serum
DMEM Dulbecco's modified Eagle high glucose medium
PBS phosphate-buffered saline
CMAC 7-amino-4-chloromethylcoumarin
CMFDA 5-chloromethylfluorescein diacetate
TRITC tetramethylrhodamine
DMSO dimethyl sulfoxide
DAPI 4',6-diamidino-2-phenylindole
Cx 43 connexin 43
cTnT cardiac troponin T
RFP red fluorescent protein
GFP green fluorescent protein
STeC primary human hepatic stellate cells
EC primary human hepatic sinusoidal endothelial cells
TEG tetra ethylene glycol
THF tetrahydrofuran
DMAP 4-dimethylaminopyridine
DCM dichloromethane
EtOAc ethyl acetate
DMF dimethylformamide
MFE multifunction enhancing
SteCM stellate cell medium
SteCGS stellate cell growth supplements
EDTA ethylenediaminetetraacetic acid
MTT (3-(4,5-dimethylthiazol-2-yl)-2,5-diphenyl tetrazolium bromide

List of Journal Articles

Elahipanah, S., Paul J. O'Brien., **Rogozhnikov, D.**, & Yousaf, M.N. General Dialdehyde Click Chemistry for Amine Bioconjugation. **Bioconjugate Chem.** 28 (5), 422–1433 (2017)

O'Brien, P. J., Elahipanah, S., **Rogozhnikov, D.**, & Yousaf, M. N. Bio-Orthogonal Mediated Nucleic Acid Transfection of Cells via Cell Surface Engineering. **ACS Cent. Sci.** 3 (5), 489–500 (2017)

Rogozhnikov, D., Luo, W., Elahipanah, S., O'Brien, P,J & Yousaf, M.N. Scaffold- Free Bio-orthogonal Assembly of 3-Dimensional Cardiac Tissue via Cell Surface Engineering. **Nature Scientific Reports** 6:39806 (2016)

Rogozhnikov, D., Luo, W., Elahipanah, S., O'Brien, P,J & Yousaf, M.N. Generation of a Scaffold-Free Three-Dimensional Liver Tissue via a Rapid Cell-to-Cell Click Assembly Process. **ACS Bioconjug. Chem.** 27 (9), 1991–1998 (2016).

Elahipanah, S., Radmanesh, P., Luo, W., Paul J. O'Brien., **Rogozhnikov, D.**, & Yousaf, M.N. Rewiring Gram-Negative Bacteria Cell Surfaces with Bio-Orthogonal Chemistry via Liposome Fusion. **ACS Bioconjug Chem.** 27 (4), 1082–1089 (2016).

O'Brien, P. J., Luo, W., **Rogozhnikov, D.**, Chen, J. & Yousaf, M. N. Spheroid and Tissue Assembly via Click Chemistry in Microfluidic Flow. **ACS Bioconjug. Chem.** 26, 1939–1949 (2015).

Luo, W., Westcott, N., Dutta, D., Pulsipher, A., **Rogozhnikov, D.**, Chen, J., & Yousaf, M.N. A Dual Receptor and Reporter for Multi-Modal Cell Surface Engineering. **ACS Chem. Biol.** 10, 2219–2226 (2015).

Rogozhnikov, D., Luo, W., Elahipanah, S., O'Brien, P,J & Yousaf, M.N. Assembly of Cells into 3D Tissues via Bio-orthogonal Chemistry and Preferential Differentiation of Stem Cells in Co-cultures with Controlled Cell Orientations. (Submitted to **Nature Communications**).

Rogozhnikov, D., Luo, W., Elahipanah, S., O'Brien, P,J & Yousaf, M.N. Cell Polymerization via a Biocompatible Crosslinker. (Submitted to **Angewandte Chemie Int. Ed.**).

Chapter 1

Introduction: Application of Bio-orthogonal Chemistry in Tissue Engineering

1.0 The three-dimensional architecture of organs and tissues

In the body, cells exist in a complex environment and are an integral part of all vital processes. Every second, millions of cells undergo division, migration, differentiation and apoptosis. Each of these processes is regulated through a number of intricate molecular mechanisms, which facilitate intercellular communication as well as communication between cells and the environment.¹⁻³ Some cells, such as the red blood cells, are free-floating and circulate constantly inside the body, while others such as cardiomyocytes (the heart cells) and adipocytes (the fat cells) form tissues and organs. In a tissue, which in most cases is composed of different cells types, there exists a defined architecture, where cells are arranged in a specific structure serving to enhance functionality of the tissue. For example, the liver tissue is composed of multiple hexagonal units called lobules. This geometry allows for efficient exchange between the incoming materials and the secreted substances produced by the liver.⁴ Thus, the functionality of a specific organ depends entirely on the arrangement of cells in the tissue, their quantity, cell types and proportion. In order for organs to perform optimally, temporal coordination between the cells is required. For example, the heart's pumping action is achieved through the simultaneous contraction of all cardiomyocytes which is coordinated through pacemaker cells.⁵ Therefore, effective cell-cell communication is crucial for the tissue to perform its physiological function. Such communication is achieved through both physical contact and cytokine exchange, which are regulated with integrin proteins, tight junction proteins called connexins and various other membrane receptors.^{6,7}

For years, scientists worked to re-create functional tissues *in vitro*. In the emerging field of tissue engineering there have been multiple attempts to assemble single cells into a thick multicellular construct with defined architecture.⁸⁻¹³ The first tissue models were simple two-

dimensional (2D) monolayers of cells grown in Petrie dishes.^{14,15} Later, with development of polymer technologies and invention of scaffolds, the formation of the first thick three-dimensional tissues became possible.^{16,17} Areas of application for the engineered 3D tissues are numerous but this technology is especially important in transplantation medicine, drug testing and disease modeling (**Figure 1.0**). Below, I will describe how 3D tissue technology is used to solve problems specific to these fields.

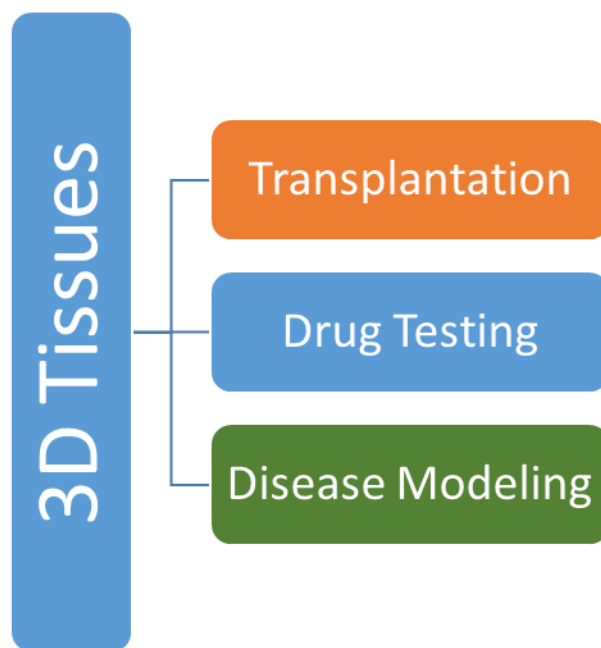


Figure 1.0: Areas of application for three-dimensional tissues. 3D tissues have become essential tools in biology and are currently used in the areas of transplantation, drug testing and disease modelling.

1.1 Areas of application for three-dimensional tissues.

1.1.1 Transplantation

A major problem encountered by medical professionals around the world today is a deficit of donor organs for transplantation. In 2006 alone, approximately 95,000 patients in North America were on the waiting list for organ transplants. Of those, only 28,140 patients received transplantations and 6120 died while waiting for an organ.¹⁸ The median waiting time for a kidney transplant in Ontario, Canada is 41 months.¹⁹ Such delays are caused by the lack of both living and deceased donors.

Few individuals agree to donate their organs, whether it is because of potential health complications or their ethical views. Organ donation for children is especially complicated due to both ethical and consent issues.²⁰

Finding an appropriate donor for organ transplant is challenging. The organ must be of the right size and have suitable cell surface receptors to prevent an autoimmune response. Even after successful transplantation there is a high risk of rejection.²¹ Successfully transplanted patients have to receive expensive immunosuppressive therapy over the duration of their life.²² The alternative supporting therapies such as dialysis used for kidney disorders are costly and significantly less effective than transplantation in terms of increasing the patient's life expectancy as well as improving the quality of their life.^{23,24}

Developing technologies that allow for the engineering of artificial organs and tissues will eliminate or reduce many problems associated with donor organ transplant. The custom-made tissues will solve these issues by utilizing the patient's own cells.^{25,26} This autologous

transplantation of artificial organs has potential to reduce the risk of autoimmunity and decrease the waiting time. Modern stem cell technologies are promising in terms of their ability to differentiate into a specific cell type. If assembled into 3D tissues with the right cell-assembly method, stem cells will become a powerful tool.²⁷ Therefore, developing the universal cell-assembly method is essential for the field of regenerative medicine.

1.1.2 Drug Testing:

Developing a new treatment for a specific condition is a long and expensive process. The average time for a drug to advance from bench to bedside is 17 years.²⁸ The process starts with *in vitro* screening of the selected molecule for its ability to inhibit the receptor target. Following that, the molecule is tested for safety, first in cell culture and then in animal studies. Finally, the new drug is administered to human subjects in the three stages of clinical trials. If the drug candidate demonstrates its efficiency in treating the condition as well as safety, it becomes approved for use as a treatment.²⁹ The average cost to develop a new therapy is estimated to be close to 2.6 billion dollars.³⁰

Since most of the potential drug candidates fail animal or human trials due to cytotoxicity, it is critical to develop a powerful *in vitro* system that would be capable to accurately demonstrate potentially toxic effects the molecule may induce if administered to a patient.³¹ The current *in vitro* test systems are based on monolayers of cells cultured on plastic substrates.³² The environment of this two-dimensional cell monoculture is drastically different from those of the three-dimensional multicellular tissue. Since in 2D cultures cells behave

differently than they do in *in vivo* conditions, the cell response to a specific drug concentration may also vary.³³ Therefore, it is important to create a functional three-dimensional tissue model containing the relevant cell types. The perfect model would recapitulate the 3D environment of tissue where cells would form functional intercellular connections while performing the same functions they perform in the body.

1.1.3 A 3D Model for Intercellular Interactions

Another important application of 3D co-cultures is to model cell-cell interactions in healthy and diseased tissues. Biological processes such as stem cell differentiation, organogenesis, cancer development, immune response and infections involve intercellular interactions between cells of different types.³⁴⁻³⁶ To study these processes biologists traditionally employed the standard animal models for *in vivo* and the 2D cell monoculture for *in vitro* experiments. Animals, such as transgenic mice with specific gene alterations have long been used to model disease manifestations and phenotypes similar to the conditions observed in humans.³⁷ Although used to replicate many diseases, animal models show limitations when applied to conditions like sepsis where mice and humans with the same disease phenotype demonstrate significant differences in the underlying molecular mechanisms.^{38,39} This inability to efficiently mimic human disease with a single animal model drives the need to employ multiple animal models such as *Drosophila* and *Caenorhabditis elegans* in the attempt to extrapolate the relevant data. The current 2D *in vitro* models, as mentioned above, are oversimplified and use a monoculture of cells which cannot recapitulate the organ-level structures including functions crucial for studying the intercellular interactions and their role in disease.⁴⁰

Recent efforts in the fields of chemistry, developmental biology and biological engineering have focused on creating complex functional multicellular 3D tissue models.^{41,42} The perfect model would be flexible and allow alteration of parameters such as the types of cells used, their proportion, tissue thickness as well as cell orientation and distribution in the co-culture. Such customized 3D tissue model will enable investigation of complex interactions between the cells in tissues and provide a universal platform to study pathologies.^{43,44}

Generating functional tissues for either transplantation, drug development or disease modeling is a challenging task which has attracted a lot of attention from specialists working in the fields of chemistry, bioengineering and developmental biology. To generate such tissues, one has to assemble single cells into a complex 3D structure. The challenge here is in the fact that healthy non-cancerous cells *in vitro* grow as a single layer. Thus, one has to create a robust method for the bottom to top cell assembly that would “glue” cells together without damaging their function. In functional tissue, cells must be connected with tight junctions for intercellular transport of proteins and ions.⁴⁵ In addition, the inner cell mass of thick tissues requires the supply of oxygen and nutrients, thus one has to induce the formation of blood vessels through the process of angiogenesis or by introducing pores or channels into the tissue architecture.^{46,47} Although this task is challenging, recent advances in tissue engineering have produced promising results.⁴⁸ The methods that will be reviewed in detail in this chapter are based on the use of natural, decellularized and polymer scaffolds, genetic engineering or employ our novel scaffold free bio-orthogonal tissue assembly technology which is the focus of this work.

1.2 Scaffolds and Biomaterials for Tissue Engineering.

Cells are normally grown as a monolayer in a 2D environment of plastic flasks *in vitro*.

However, *in vivo* the cells form complex multilayered 3D tissues. In order to obtain a complex 3 dimensional co-culture of cells, scientists have utilized different approaches varying from casting cells into polymer, ECM-based scaffolds via 3D printing or other means which can form simple organoids from induced pluripotent stem cells (iPSC).^{49,50} Each method has its advantages and disadvantages which are described below.

1.2.1 ECM-based scaffolds and hydrogels.

The extracellular matrix is a protein meshwork secreted by cells into intercellular space which plays an important role in the structural integrity of tissues (**Figure 1.2**). It regulates cell-cell adhesion and recognition, facilitates cell motility and performs many other biological tasks. The ECM is present in every tissue, but its content varies significantly depending on tissue type.⁵¹ Structural components of the ECM include collagen and fibronectin, proteins most extensively used for tissue engineering. The idea behind this method is to obtain a naturally-occurring biomaterial, which is native to tissues, and use it as scaffold to support cells. Since ECM proteins are naturally occurring, their application is supposed to lower the risk of cytotoxicity which is present in methods involving synthetic polymer scaffolds.⁵²

Collagen suspensions can be processed to have different physical properties for different applications by changing their formulations. One type of collagen suspension called hydrogel is a soft and elastic form which can absorb water and be molded into various shapes. The hard and dry form of collagen matrix called IntegraTM serves as a wound dressing.⁵³ The typical procedure of making collagen-based tissues involves mixing different types of cells with the liquid form of

collagen and then incubating the sample at 37°C for 30-60 min to induce crosslinking of collagen fibrils and harden the scaffold. The cells are trapped inside the scaffold where they easily adhere to collagen fibrils.⁵⁴ Alternatively, the cells can be seeded on top of a dry scaffold, where they penetrate through the pores and adhere to the inside. Collagen is a biodegradable material and can be degraded via enzymatic action of metalloproteases.⁵⁵ To obtain a wide range physical and biological properties collagen scaffolds often include different additives, such as growth factors, polymers, nanoparticles as well as other ECM components including glycosaminoglycans.⁵⁶ Wang and Stegemann (2010) constructed a collagen-chitosan scaffold to induce osteogenesis in 3D cultured bone marrow-derived human mesenchymal stem cells.⁵⁷ It was established that addition of chitosan (a polysaccharide material derived from crustacean exoskeletons) improved the formation of the bone tissue while collagen, due to presence of integrin-binding motifs, greatly enhanced the adhesive properties of cells.

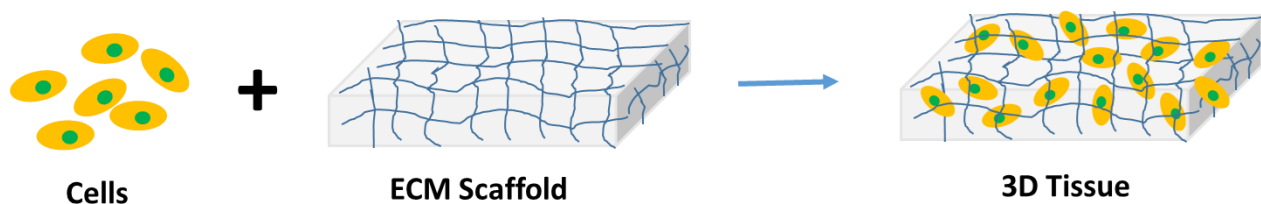


Figure 1.2: The three-dimensional ECM scaffold. Extracellular matrix proteins such as collagen and fibronectin are used for 3D tissue assembly. Cells are seeded on top of the ECM scaffold, where they adhere to ECM proteins to form a 3D tissue. Alternatively, cells can be mixed with liquid collagen or Matrigel, which solidifies trapping cells inside the gel.

1.2.2 Alginate

Another popular biomaterial used in tissue engineering is alginate. Alginate or alginic acid is an anionic polysaccharide found in the cell walls of brown algae. It consists of copolymers containing blocks of (1,4)-linked β -D-mannuronate (M) and α -L-guluronate (G) residues. The blocks can be composed of multiple consecutive or alternating M and G monomers arranged in linear geometry.⁵⁸ Alginate is a common food additive which recently found an application in drug encapsulation and wound dressing. The hydroscopic properties of alginate allow it to trap water during the process of gelation, thus providing cells that are enclosed inside the gel with the essential ions and nutrients contained in the medium. The process of alginate gelation is initiated with addition of calcium ions to the solution of sodium alginate. Ca^{+2} replaces sodium ions and crosslinks the polysaccharide chains (**Figure 1.3**). The sources of calcium ions are buffered solutions of simple inorganic salts such as CaCl_2 and CaSO_4 .⁵⁹ Just like collagen and fibronectin, alginate is biodegradable, non-immunogenic and is a very commonly used scaffold material in tissue-engineering experiments.

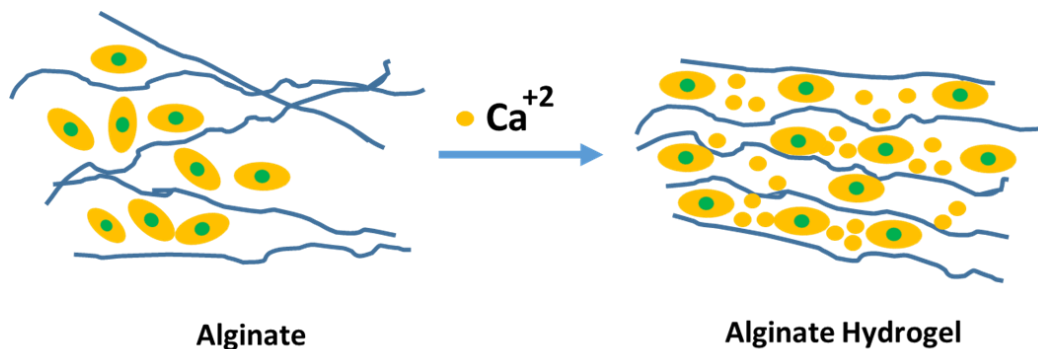


Figure 1.3: The alginate hydrogel. Alginate is an anionic polysaccharide derived from brown algae. To form an alginate scaffold, cells are mixed with a buffered solution of alginate; calcium ions are used to crosslink alginate strands to form a solid scaffold.

In addition, alginate is a moldable, elastic material which can sustain a significant stretch and is easy to handle. To construct harder structures such as bone tissue, hydroxyl apatite $\text{Ca}_5(\text{PO}_4)_3(\text{OH})$, is mixed with powder of sodium alginate and osteoblasts prior to gelation with a solution of calcium chloride.⁶⁰ The system however has several drawbacks. Unlike ECM-based scaffolds, alginate does not have integrin attachment sites such as RGD (Arginine-Glycine-Asparagine) motif which abolishes cell adhesion and spreading. Therefore, in alginate-based scaffolds, cells adopt a spherical shape, which is different from the star-like geometry of cells in a healthy tissue. In addition, high concentrations of calcium used in the gelation process are toxic to many types of cells.

1.2.3 Polymer scaffolds

Polymer-based scaffolds are another methodology for tissue engineering that has become popular in the last decade. Since different polymers have different physical and chemical properties, it is possible to build a scaffold with parameters that are suitable for a specific tissue. This high level of customization gives this system a significant advantage over other platforms where the properties of scaffolds cannot be easily changed.⁶¹ When constructing a polymer-based scaffold for optimal tissue growth, it is important to consider the following parameters:

- 1) **Stiffness:** It is known that some cell types such as osteoblasts and osteoclasts (bone cells) grow better on stiff surfaces while others such as neurons perform a lot better on softer materials. The stem cells, which are used extensively in tissue engineering, differentiate into different lineages depending on stiffness of the material.⁶²

- 2) Elasticity: In the body, tissues such as muscles and blood vessels undergo constant cycles of stretch and relaxation; therefore, it is important for the scaffold material to have proper elasticity to sustain the function of these tissues.⁶³
- 3) Porosity: While the scaffold is in place, cells must have an access to oxygen and nutrients. Since in some cases tissue thickness can reach 5 mm or more, it is important for cells that are found deep inside the scaffold to be exposed to the medium, which is achieved through use of porous scaffolds. The pores, however, must be of proper size: large enough to allow nutrient exchange, but small enough to keep the tissue intact, still allowing for cell-cell contact.⁶⁴
- 4) Biodegradability: The scaffold is designed to be a temporary structure, supporting the cell mass before the cells form intercellular junctions and, in the case of stem cells, differentiate into the right lineage. The scaffold, since it is an exogenous structure, must degrade away leaving the intact functional tissue. The process of degradation must proceed at the right pace allowing for gradual replacement of the polymer with growing cell mass.⁶⁵ There are two different mechanisms of scaffold degradation: via surface erosion or via bulk erosion (**Figure 1.4**). During surface erosion, the thin layers of polymers gradually degrade from the surface of the scaffold proportionally decreasing its overall size. In bulk erosion, the scaffold is degraded from within.⁶¹ The density of the material decreases while the overall shape of the scaffold is preserved. Each method is appropriate for a specific tissue type.
- 5) Non-cytotoxicity: During the process of scaffold biodegradation, by-products are produced; these by-products must be non-cytotoxic and non-immunogenic.⁶⁶ In addition,

they must not interfere with the process of tissue growth and diffuse from the scaffold shortly after being generated.

These are the essential parameters that need to be controlled for any scaffold system to be effective. These requirements significantly narrow the choice of polymers for tissue engineering.

There is a multitude of biodegradable polymers available for basic research which includes polyanhydrides, polyorthoesters, polyhydroxyalkanoates, and newly synthesized biomaterials, such as polypyrroles. Today, however, there are only three biodegradable polymers that have been approved by the American Food and Drug Administration (FDA): polyglycolide (PGA), polylactides (PLA) and polycaprolactone (PCL)^{67,68} These polymers belong to the polymer class of polyhydroxyalkanones and have long been used as sutures, grafts and prosthetic devices in medicine.

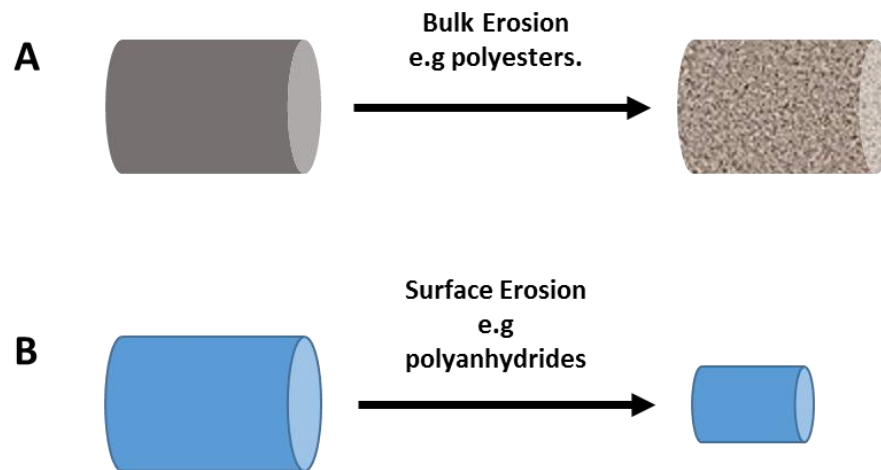


Figure 1.4: Two models of scaffold degradation. Scaffolds demonstrate different degradation patterns. **A)** Bulk erosion is common in materials made of polyesters while polyanhydrides **(B)** undergo surface erosion.

Recently, PGA, PLA, PCL and their co-polymers became essential for the tissue engineering field due to their biodegradability, biocompatibility and relatively low cytotoxicity.

Polyhydroxyalkanoates are degraded via hydrolysis and their by-products are non-cytotoxic in moderate amounts.^{69,70} For example, PLA is composed of lactic acid monomers – the natural components of glucose metabolism that accumulate in muscle tissue during exercise. During the hydrolysis of the PLA scaffold, lactic acid monomers are released into the body where they are metabolized through cellular metabolic pathways.^{71,72} The rate of degradation, however is strongly affected by the architecture of the scaffold and exposure of the polymer to water. Under certain conditions, a large portion of scaffold is exposed to water, which leads to quick polymer degradation and the release of a large amount of lactic acid molecules at once, causing a decrease in pH and thus cytotoxicity.^{69,73} PGA-based scaffolds are characterized by their high hydrophilicity and fast rate of degradation (4-8 weeks). Although suitable for fast growing tissues such as skin, quick degradation often limits the amount of time for tissue regeneration of other, more complex organs.⁷⁴

PCL-scaffolds contain multiples caprolactone monomers. The hydrolysis of PCL, however, is very slow and can last from 9 months to 3 years and is thus only suitable for slowly growing tissues such as bone and cartilage.⁷⁵ Since each given protein has its distinct properties and degradation rates, designing customized scaffolds often requires combining these materials in the form of co-polymers. Today PGA-PLA co-polymers are gaining popularity. The monomers are combined into different ratios providing properties such as tensile strength and changing the rate of degradation of the intermediate to the original PGA or PLA scaffolds.⁷⁶

Since, the growing tissue requires cytokine stimulation, specific growth factors are often embedded into polymer scaffolds. For example, VEGF is used to promote angiogenesis, while BMP4 is utilized to promote bone formation.^{77,78}

1.3 Scaffold Fabrication Methods

Both biodegradable polymers and naturally occurring biomaterials play an important role in building scaffolds for tissue engineering. Depending on the material in the manufacturing process, the properties of the resulting structure can differ substantially. The choice of material however is only one parameter that needs to be considered in tissue building process. The other one is the fabrication methodology. Building a scaffold is achieved through slow deposition of a polymer material which can be done via several methods.

1.3.1 Electrospinning.

Electrospinning is a unique method that utilizes electric force to draw charged threads of viscous polymer solution extending it to form thin fibers. The diameter of the fibers can range from 2-4 nm to several microns. The technique is applicable for a wide range of both natural and synthetic materials including chitosan, PLA, PGA, PLC, alginate and collagen.⁷⁹⁻⁸¹ The technique, developed in late 19th century, has been used ever since in various fields. The typical electrospinner setup looks the following way:^{79,82} A syringe containing polymer solution is inserted into an infusion pump - a device used to administer small amounts of liquid (**Figure 1.5**). A spinneret is a nozzle on a syringe which is made of conductive material and has an opening of small diameter. The spinneret is aimed towards the collector – a quickly rotating

drum. The voltage source is connected to the spinneret and is grounded onto the collector. The polymer solution is prepared in a volatile solvent and its concentration is carefully adjusted. The procedure starts when the syringe pump pushes the extruder and a small drop of polymer solution is formed on the tip of the spinneret. The drop is held on the tip with surface tension. When voltage is applied, the solution particles become charged, the electrostatic repulsion overtakes the surface tension and a jet of polymer solution is ejected towards the spinning collector.

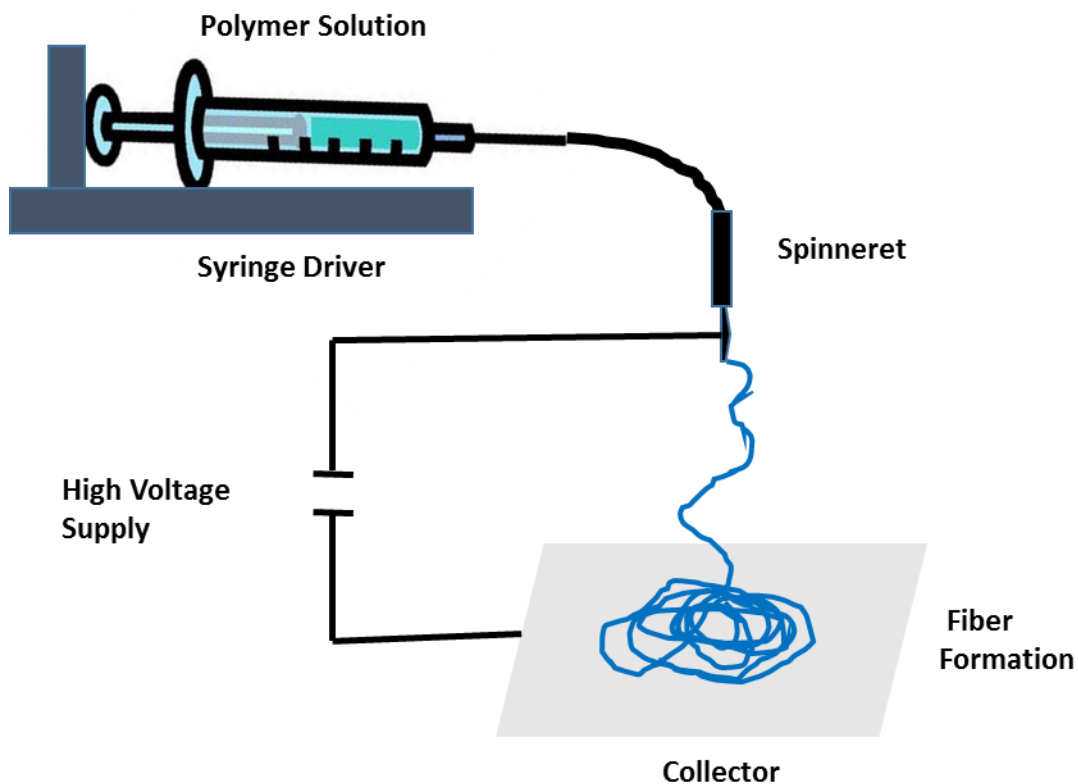


Figure 1.5: Generating scaffolds via electrospinning. In the process of electrospinning, a polymer solution is loaded into a syringe. The solution is ionized as it is extruded through the spinneret and thin threads of polymer fiber are formed on the collector screen.

The solvent evaporates quickly, leaving thin threads of polymer material. The method produces a patch made of a thick meshwork of polymer threads. The resulting material can be molded into a scaffold and seeded with cells. The cells can penetrate the scaffold through pores between the fibres, where they are trapped. The electrospinning technique has been used to produce tissues such as skin, bone and bladder.⁸³

1.3.2 3D Printing

The second method that has become popular in recent years is 3D printing. The technology is based on the successive addition of thin layers of material to produce a three-dimensional object. Just like in electrospinning, different types of polymers and biomaterials can be used in 3D printing.⁸⁴ The simplest design of a 3D printer involves a syringe, containing a viscous solution of collagen, alginate or synthetic polymer. The syringe is attached to a robotic arm that is capable of moving along the x, y and z axes.⁸⁵ The arm moves along the programmed path extruding layers of polymer, which are deposited on top of each other in layer-by-layer fashion allowing formation of a 3D object. More advanced versions of 3D printers can use solid materials such as PLA. The polymer is melted inside the machine and is then extruded through the printing head. This allows for high-resolution printing. If melting is not required, cells can be added directly into the solution of a biomaterial and thus be embedded into the structure of the resulting scaffold.⁸⁶⁻⁸⁸ 3D printing technology allows for the precise positioning of cells and the formation of complex structures. In 2015, Atala and colleagues utilized 3D printing to build an artificial tendon. They mixed C2C12 myoblasts and NIH/3T3 fibroblasts with a hydrogel containing hyaluronic acid, gelatin and fibrinogen in one syringe, while another syringe contained PCL.⁸⁹

The content of the syringes was simultaneously extracted producing a complex scaffold. This complex approach is called co-printing and is used to produce complex tissues. In this particular case, the scaffold contained cells embedded into a soft hydrogel covered with hard PCL polymer mimicking the tendon structure.

Similar to previous approaches used to create scaffolds with different properties, various proteins, growth factors or nanoparticles can be added into the biomaterial. In 2013, Mannoor et al, printed a bionic ear out of alginate containing chondrocytes and silver nanoparticles. Though the printed tissue morphology was different from the actual tissue, it demonstrated a step forwards method for creating a functional 3D organ.⁹⁰

1.3.3 Decellularized Scaffolds.

Engineering a functional 3D tissue on a scaffold is a complicated task which must take into account multiple parameters such as cell seeding density, degradation rate of a polymer material, porosity of scaffold, cell adhesion, migration and others. The level of complexity of natural tissues is hard to replicate in *in vitro* conditions.^{91,92} In 2010, Ott and colleagues developed a new method to build scaffolds using an extracellular matrix derived from the organs of a dead donor (**Figure 1.6**). The idea behind this method is to utilize the ECM from cadaveric organs or tissues to seed new cells and produce a living organ or tissue. The procedure includes the following steps.⁹⁴

- 1) An organ is removed from a dead body.

- 2) The organ is perfused with either trypsin or a chemical detergent to remove dead cells leaving a decellularized scaffold. The digestion must be very gentle so as not to damage ECM proteins.
- 3) Living cells are seeded onto the decellularized scaffold.
- 4) The cells attach to collagen or fibronectin fibers and migrate to the specific site guided by the physical cues received from the ECM. The future goal of this method is to re-create the cell niche, where cells can interact with each other and the extracellular matrix receiving all the necessary physical and chemical signals.
- 5) The resulting construct is then transplanted into the body of the recipient where it is supposed to perform all the functions of the replaced organ. In the case of paired organs such as the kidneys or lungs, the failed organ can be removed from the patient, decellularized and then seeded with cells from the second organ which is healthy. This procedure is supposed to reduce the immune response since both the cells and the ECM are obtained from the patient.

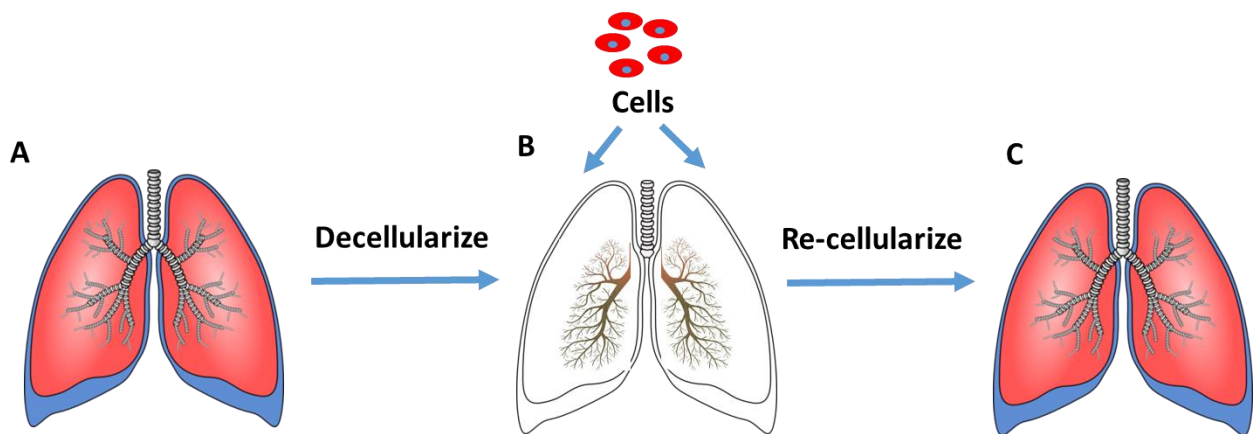


Figure 1.6: Decellularized scaffolds. **A)** Cadaverous organs or tissues are treated with a mild detergent or solution of protease to remove dead cells. **B)** The resulting carcass, which consists mainly of the components of the ECM, is seeded with patient or donor cells. **C)** The cells adhere to the matrix and restore some of the organ’s functions.

The decellularization technique has been used to build organs such as the heart, lung, liver and kidney.⁹⁵⁻⁹⁷ The constructs were transplanted into immunocompromised mice. Although, some of the tissue function was restored, there was still a very big difference in performance as well as structure between the healthy tissue and the re-seeded scaffold. The major limitation of this technique is that it does not control for the distribution of different cell types within the tissue.

1.3.4 Organoids

Significant steps towards creating artificial organs have been created by developmental biologists. The formation of any organ or tissue starts during the embryonic stage of human development. From the moment of fertilization and the formation of blastocyst, unspecialized totipotent stem cells undergo greater and greater degree of specialization leading to formation of organs and tissues.⁹⁸ In the early stages of embryogenesis, cells receive signals from other cells and the environment which, along with DNA markers, influence their choice of lineage. The resulting specialized cells of one cell type tend to self-aggregate excluding other cells. In this process, cells that belong to different cell types self-organize into complex tissues.

Using genetic engineering and co-culture techniques developmental biologists investigated the possibility of inducing the formation of a specific organ or tissue from pluripotent or totipotent stem cells (**Figure 1.7**). The stem cells commit to specific lineages, differentiate and then self-organize into miniature multicellular structures that resemble organs in their morphology and are called organoids.⁹⁹ A typical organoid contains two to three cell layers each containing a different cell type.

The first organoid developed from pluripotent stem cells was intestine. In the experiment by Spence et al (2011), human embryonic stem cells (ES cells) as well as induced pluripotent stem cells (iPSC) were treated with a combination of growth factors that play an important role in intestine development during embryogenesis.¹⁰⁰ Since the intestine is a part of endoderm (an inner germ layer inside an embryo), it was important to direct the stem cells towards endoderm development first.

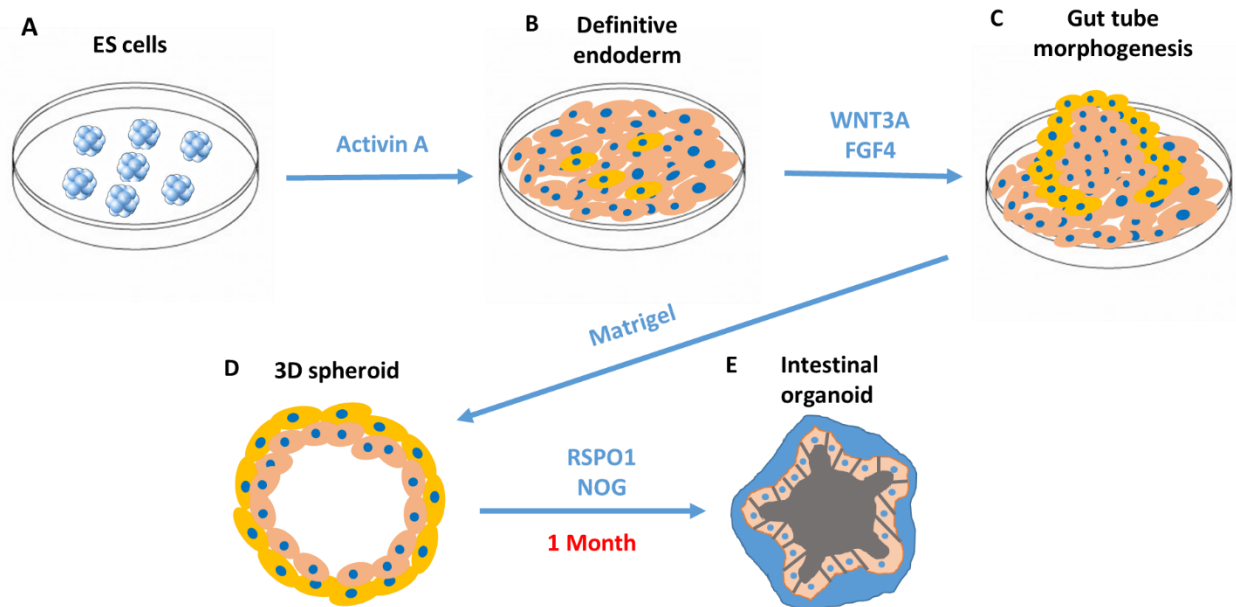


Figure 1.7: The formation of intestinal organoids. A) Embryonic stem cells are treated with activin A to induce formation of the definitive endoderm (B). Following that, the samples are treated with WNT3A and FGF4 to promote gut morphogenesis (C). Then, the tissues are transferred onto soft matrigel-coated plates to produce 3D spheroids (D), which are then treated with RSPO1 and NOG for the duration of 30 days to induce the formation of intestinal organoids.

Therefore, at day 1, the stem cells were treated with activin A – a nodal-related TGF- β molecule which induces endoderm formation. After 72h of activin A treatment the cells displayed endodermal markers and were subsequently treated with WNT3A and FGF4, the growth factors that directed further differentiation of stem cells into intestine-like organoids. At day 4, the dividing cells produced aggregate spheroids. Finally, at day 28, the spheroids transformed into organoids which contained morphological structures characterizing intestine (villus and crypts) and also expressed the intestine-specific markers: KLF5, CDX2, and SOX9.

As of today, several organoids have been generated including stomach, brain, heart, liver and kidney.¹⁰¹⁻¹⁰³ Organoids are capable of performing some functions of the corresponding organs and can be useful for studying cellular behavior in the process of organogenesis as well as for use as working models in the simulation of drug metabolism, infections and other processes. The disadvantage of this technique of cell assembly is that it is time-consuming and does not allow for flexibility in terms of the choice of cell types introduced into the organoid. Given that organoids are miniature structures and their generation is regulated indirectly (through the activation of genetic pathways), scaling this technology for commercial production may prove to be a challenge.

1.4 Extracellular Matrix

The extracellular matrix (ECM) is a meshwork of proteins and glycans secreted by cells into extracellular space. It provides a biochemical support to the surrounding cells and plays an important role in such processes as cell motility, stem cell differentiation, wound healing and angiogenesis.¹⁰⁴ To undergo these fundamental biological processes the cells must adhere to

different components of underlying the ECM. Upon adhesion, the cells receive molecular signals from ECM and respond to them in a specific manner. These physical and chemical interactions between the cell and ECM allow the cell to sense its position and orient itself correctly in space. The ECM also regulates intercellular communication and plays an integral role in supporting the tissue organization.¹⁰⁵

1.4.1 Durotaxis

The direction and rate of cell migration in the body are controlled through a process called durotaxis. This phenomenon is based on cells sensing the rigidity of ECM and migrating towards softer or harder regions.¹⁰⁶ ECM rigidity on the other hand is determined by the concentration of proteins such as collagen, elastin and fibronectin. Organs such as the brain have lower ECM rigidity, while in bone tissue the ECM rigidity is high.^{106,107} The content of ECM in tissues varies depending on their function. Typically, tissues that need to endure a lot of stress such as bone, skin and cartilage have higher ECM content (up to 72%) as compared to internal organs such as the heart, liver and brain.¹⁰⁸

The structure of ECM is dynamic and is being continuously modified. Specific protein complexes called metalloproteases are responsible for degradation of most ECM proteins, thus regulating the rigidity and composition of ECM and controlling such important processes as organogenesis and wound healing.¹⁰⁹

1.4.2 ECM composition

The ECM is a complex and dynamic structure composed of proteins such as collagen, elastin, fibronectin and laminin; glycosaminoglycans such as hyaluronan, heparin sulfate and chondroitin sulfate as well as proteoglycans such as perlecan and syndecan (**Figure 1.8**).¹¹⁰

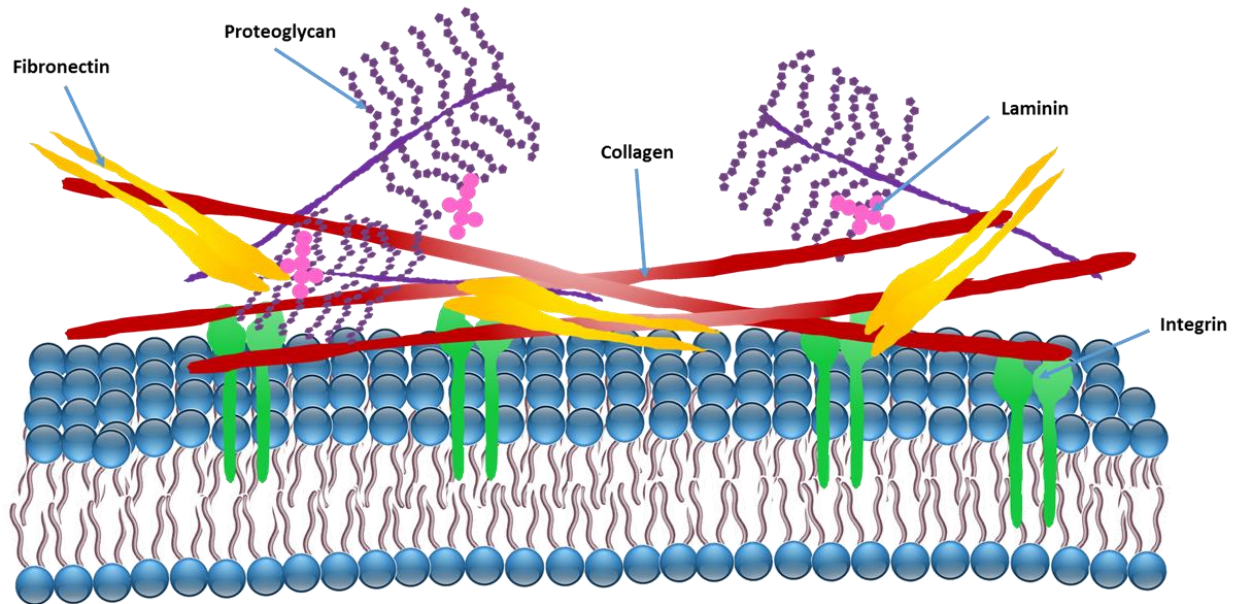


Figure 1.8: Detailed depiction of the extracellular matrix. The ECM is a complex dynamic structure which is composed of molecules secreted by cells. The ECM facilitates intercellular communication, cell-cell adhesion and provides structural and biochemical support for the surrounding cells.

1.4.2.1 Collagen:

Collagen is the most abundant protein in mammals and is a major component the ECM. In bone and skin collagen makes up 25% of the total protein mass. Collagen has a unique triple-stranded helical structure composed of three α chains. These α chains contain mainly glycine and proline, however, other amino acids such as alanine and glutamic acid are also abundant.¹¹¹ The α chains are made up of series of three amino acids such as Gly-Pro-X, where X can be any amino acid other than glycine or proline. Three α chains intertwine with each other to form triple

helices which are then assembled into a complex structure called collagen fibril. Oxidation of lysine residues initiates the assembly of multiple collagen fibrils into collagen fibre – a protein superstructure with high molecular weight. Collagen fibres provide tensile strength and physical support to tissues such as bones, skin, tendons and blood vessels.¹¹² In these tissues it is fibroblasts that are generally responsible for secretion of collagen. Depending on the content of amino acids, collagen can be classified into different types (collagen I–XII). Each collagen type has specific properties. For example collagens I, II, III, V and VI form fibrils, while collagen VII XI and XII anchor to the plasma membrane. Collagen IV fibres form durable β sheets.¹¹³

1.4.2.2 Elastin:

Elastin is hydrophobic protein that allows tissues to transiently stretch and is found in large quantities in tissues such as skin and blood vessels. Elastin is a complex protein which is produced via polymerization of 72 kD tropoelastin monomers.¹¹⁴ Tropoelastin is synthesized inside the cell and is then secreted into the ECM where it polymerizes to form elastin.

Tropoelastin has two alternating domains: hydrophilic and hydrophobic. The hydrophilic region contains lysine and alanine amino acids while the hydrophobic domain contains non-polar amino acids. It is the hydrophobic domain that is responsible for the stretching capabilities of elastin.

1.4.2.3 Fibronectin:

Fibronectin is a large (270kD) secreted glycoprotein composed of two dimers joined by a disulfide linkage.¹¹⁵ Fibronectin exists in multiple isoforms, one of which is soluble and participates such biological processes as blood clotting and wound healing. The other isoforms are insoluble; they are assembled on the cell surface and become the parts of ECM structure.

Fibronectin interacts with the cell through a protein called integrin. Integrin attaches to the

fibronectin through the focal adhesion points and links the actin filaments inside the cell with ECM. Fibronectin contains specific RGD (arginine, glycine, aspartic acid) amino acid repeats. Every motif containing RGD repeats is a binding site for integrin receptors. Although RGD is mainly present in fibronectin, it can be also found in laminin, fibrinogen vitronectin and some collagens.

1.4.2.4 Integrins

Integrins are transmembrane receptor proteins that link the ECM with the actin cytoskeleton inside the cell. Along with cadherins, selectins and syndecans, integrins can receive a mechanical signal from the ECM which can then be transferred to the nucleus through a specific signaling cascade, resulting in a biological response such as changing the cell shape, direction of movement or transferring to a different stage of the cell cycle.¹¹⁶ Integrins are structured as heterodimers and are composed of α and β transmembrane subunits. There are 18 α and 9 β subunits known which can combine to form 24 different integrin heterodimers. This immense complexity of integrin receptors is responsible for a great diversity of biological functions integrins can perform.¹¹⁷ These include cell-ECM and cell-cell adhesion, cell growth and differentiation, cell survival, organization of actin filaments and assembly of the cytoskeleton. Thus, integrins serve as a bridge between the cell's internal proteins and enzymes and the outside environment.

1.4.2.5 Glycosaminoglycans (GAGs)

In addition to protein components, the ECM contains carbohydrates. Glycosaminoglycans (GAGs) such as hyaluronic acid are important components of tissues such as skin and tendons. GAGs are hydrophilic and thus attract water molecules acting as a lubricant

or shock absorber which protects tissues from impact and shear stress. GAGs consist of repeating disaccharide units, typically amino sugar (*N*-acetylglucosamine or *N*-acetylgalactosamine) along with galactose or uronic sugar.¹¹⁸

1.5 Plasma Membrane

The cell membrane is a phospholipid bilayer that acts as semipermeable barrier between the cell cytoplasm and outside environment. The plasma membrane regulates the uptake and secretion of K^+ , Na^+ , Ca^{2+} , Cl^- ions, glucose, proteins, as well as water molecules.¹¹⁹

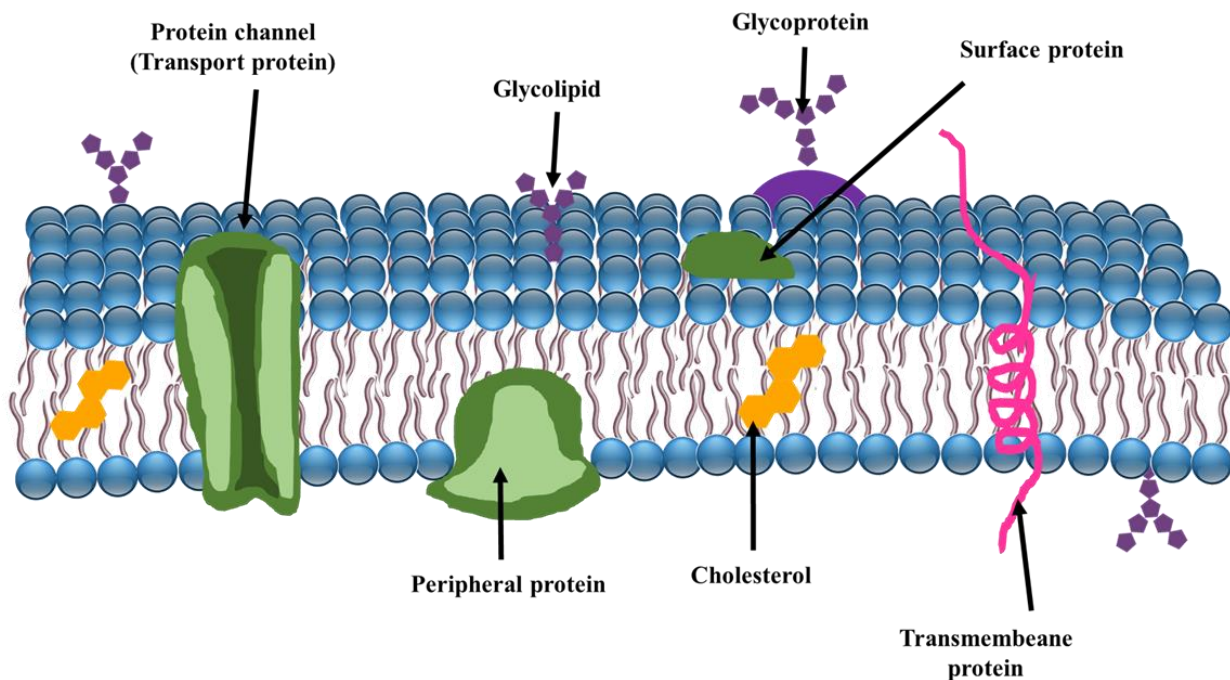


Figure 1.9: The structure of the eukaryotic plasma membrane. The plasma membrane is a phospholipid bilayer that separates the cellular interior from the external environment. It is semipermeable and regulates transport of molecules that enter and leave the cell. The plasma membrane contains various receptor and structural proteins which play an important role in maintaining membrane integrity, cell adhesion regulation, motility and intercellular communication facilitation.

Due to the amphiphilic structure of the plasma membrane, sporadic diffusion of substances across the lipid bilayer rarely happens, thus the transport is generally achieved through regulated protein channels or controlled endocytosis.¹²⁰

Communication between the cell and the surroundings as well as cell-cell communication takes place via both chemical and mechanical signaling, and in either case, it is the membrane-bound receptors that receive the signal and transmit them into the cell through signaling cascade **(Figure 1.9)**¹²¹.

Amphiphilic polar lipids make up the cellular membrane and are composed of hydrophobic tails and hydrophilic heads. Hydrophobic moieties have the propensity to self-associate which is driven entropically by water.¹²² Hydrophilic moieties, on the other hand, have a tendency to interact with the aqueous environment. These properties allow the cells to segregate the internal constituents from the external surroundings. Glycerophospholipids are the most abundant lipids in the plasma membrane. Phosphatidylcholine, phosphatidylethanolamine, phosphatidylserine, phosphatidylinositol and phosphatidic acid are the key structural components of the membrane. Each glycerophospholipid has a hydrophobic diacylglycerol portion which contains two saturated or *cis*-unsaturated acyl chains of different lengths.

The lipid membrane is a dynamic structure which contains both liquid and solid regions. Membrane fluidity is regulated by different proportions of saturated and unsaturated fats. Phosphatidylcholine is the most common glycerophospholipid and constitutes more than 50% of all plasma membrane lipids. It has one *cis*-unsaturated fatty acyl chain, one saturated fatty acid chain and a polar head group.¹²³ Remarkably, the molecules have nearly cylindrical shape and self-assemble into a lipid bilayer in the aqueous environment. The *cis*-unsaturated acyl chains in phosphatidylcholine molecules give the plasma membrane its fluidity.

The eukaryotic plasma membrane, although mostly fluid, contains solid patches called lipid rafts. Lipid rafts are composed of non-polar cholesterol molecules, sphingolipids and integral membrane proteins such as caveolin which are anchored inside the lipid raft. Sphingolipids such as sphingomyelin, ceramide and sphingosine contain a polar head group and a long saturated hydrocarbon tail.¹²⁴ Due to their saturated structure and streamline geometry, sphingolipids are able to tightly pack together, producing solid regions in plasma membrane. In addition to that, sphingolipids can form structurally stable complexes with cholesterol. Lipid rafts can incorporate various transmembrane proteins into their structure, which play an integral role in different biological process such as antigen detection in immunology (B and T antigen receptors as well as the anchored IgE protein) and cell-cell signaling.

Membrane charge is a very important physical property of the plasma membrane. Under typical physiological conditions, the mammalian plasma membrane has a negative charge provided by negatively charged lipid phosphatidylserine as well as by glycolipids and glycoproteins found in glycocalyx.^{125,126} This negative charge on the membrane prevents unspecific binding of proteins to the cell surface, thus promoting selective entry of exogenous proteins i.e cytokines through designated protein channels or endosome-facilitated endocytosis. In addition, it helps to protect the cell from the entry of pathogens such as viruses that have a lipid coating which would easily fuse with plasma membrane if it was neutral. Membrane distribution of negatively charged phosphatidylserine lipids is also an important factor for cell survival. The lipid belongs to the cytosolic leaflet in a healthy cell where sporadic migration into the outer leaflet is prevented by the flippase enzyme which “flips” phosphatidylserine lipids back to inside. In a damaged cell, on the other hand, this catalysis is abolished, thus leading to accumulation of the negatively charged lipids in the outer leaflet which triggers apoptosis.¹²⁷

Glycolipids and glycoproteins are essential components of plasma membrane. They contain long chains of carbohydrates which stick out towards the aqueous environment and form a thick polysaccharide matrix of glycocalyx. Glycocalyx can be as thick as 11 μm and plays an important role in cell adhesion, cell-cell signaling, modulation of red blood cell volume as well as immune recognition.¹²⁸ Each individual has a unique combination of sugar monomers in glycocalyx and which for instance can enable a transplant patient's immune system to differentiate between the host and the donor organ, thus triggering the immune response and organ rejection.¹²⁹

In addition to carbohydrates and lipids, the eukaryotic plasma membrane contains many complex proteins. Channel proteins such as aquaporins are responsible for regulated intake of water, ABC transporters pump out toxins; sodium and potassium channels regulate the ion balance. In addition, intercellular communication is accomplished through gap junction proteins called connexins that can span across the plasma membranes of two cells and allow for direct exchange of cytoplasmic content between the cells in the tissue which plays an important role in cardiac muscle depolarization and proper embryonic development.¹³⁰⁻¹³²

The immense complexity of both the ECM and the plasma membrane allows for intercellular communication and formation of complex tissues and organs.

1.6 Cell Surface Engineering

The cell membrane is a lipid bilayer containing proteins that span either side, and serves as barrier between the cytoplasm and the outside environment. It is responsible for many key

processes that are essential for cell survival. The membrane has a sensory function, mediates communication between the cell and its surroundings, promotes intercellular communication, aids in locomotion, and controls the inflow and secretion of substances.¹³³ Since the role of cellular membrane is important, its modification can be used to control the cellular behaviour. Cell surface engineering can be used to modify the cellular membrane for a variety of purposes. Such modifications include labeling with fluorescent probe for imaging, expressing a receptor protein on a lymphocyte surface to target a cancer cell, homing a stem cell towards the injured region of heart muscle, assembling cells into a functional tissue and many others.^{134,135} Cell surface engineering however is challenging due to the dynamic nature of plasma membrane. Lipids, glycoproteins and proteoglycans are being constantly modified, displaced, internalized and replaced with de novo synthesis.¹³⁶ Thus, functionalization of cellular membrane with target molecules, chemical tags, recombinant receptors and nanomaterials has become an important area of research in the fields of chemistry and molecular biology.^{137,138} Applying the right strategy to decorate the plasma membrane enables control over such important cellular processes as adhesion, migration, differentiation and apoptosis. There are several cell surface engineering strategies that are in use today.

1.6.1 Genetic Engineering

Genetic engineering is the most widespread technique used for modification of cell surface. It is based on genetic expression of surface proteins via the standard molecular biology techniques. Well known, widely used, genetic engineering allows for on demand expression of natural and unnatural proteins (**Figure 1.10**). The technique is based on host DNA modification which is performed in the following way:^{139,140}

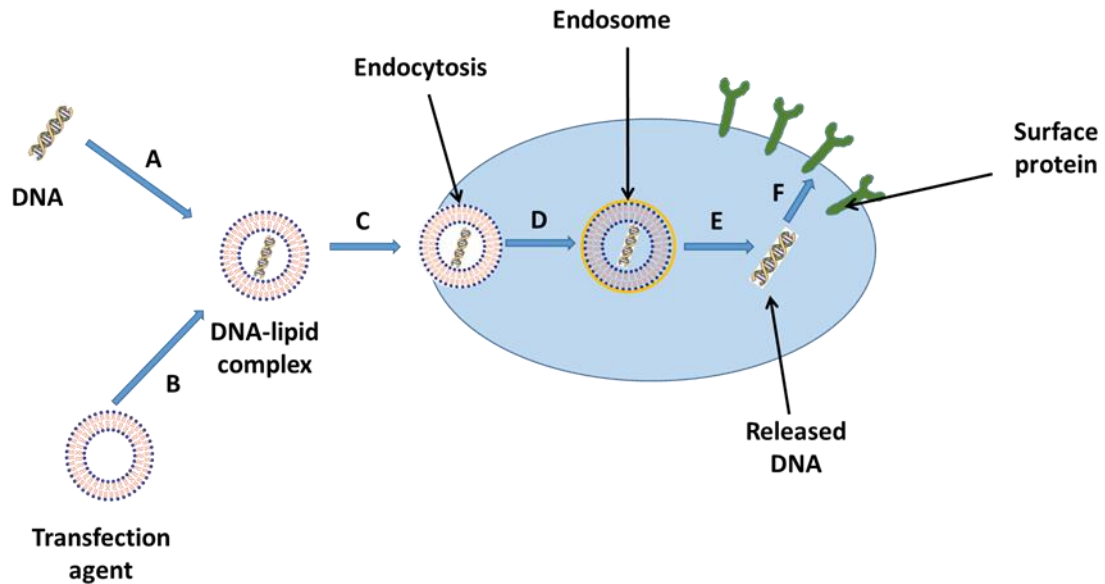


Figure 1.10: Genetic transfection of cells via a liposomal transfection agent. DNA plasmid containing the gene of interest (**A**) is encapsulated into the structure of the liposomal transfection agent (**B**) to form a DNA-lipid complex which is then endocytosed by the cell (**C,D**). The DNA is then released from the endosome and translated into the receptor protein (**E**) which is displayed on the cell surface (**F**).

The DNA sequence which codes for the gene of interest is delivered into the cell via a DNA plasmid. For this purpose, both the plasmid and the DNA fragment containing the gene of interest are digested with restriction enzymes producing the sticky ends. The DNA fragment is then ligated into the plasmid next to the promoter. The plasmid is delivered inside the cell, where the gene is then expressed producing the protein of interest. The modern methods of DNA transfection are based on liposome delivery strategy (**Figure 1.10**). DNA is incorporated into liposome and is delivered into the cell via endocytosis. Other methods of DNA modification are based on viral transduction and the novel CRISPR-cas9 system. The biggest advantage of genetic engineering is that one can produce a variety of recombinant proteins for specific purposes. In

one such experiment Kato and Mrksich produced a chimeric integrin protein to adhere specifically to a surface coated with benzenesulfonamide — a synthetic ligand (**Figure 1.11**).¹⁴² The chimeric receptor was constructed from $\alpha 5\beta 1$ integrin, a common transmembrane protein which binds to the components of extracellular matrix. The chimeric protein was constructed by fusing the intracellular and transmembrane domains of $\beta 1$ protein with an extracellular domain of carbonic IV anhydrase. Carbonic IV anhydrase binds specifically to benzenesulfonamide, therefore the chimeric integrin had affinity for the artificial surface. As the result, genetically modified cells were able to attach and migrate on the surface coated with artificial ligand which would not be possible for cells with natural form of integrin.

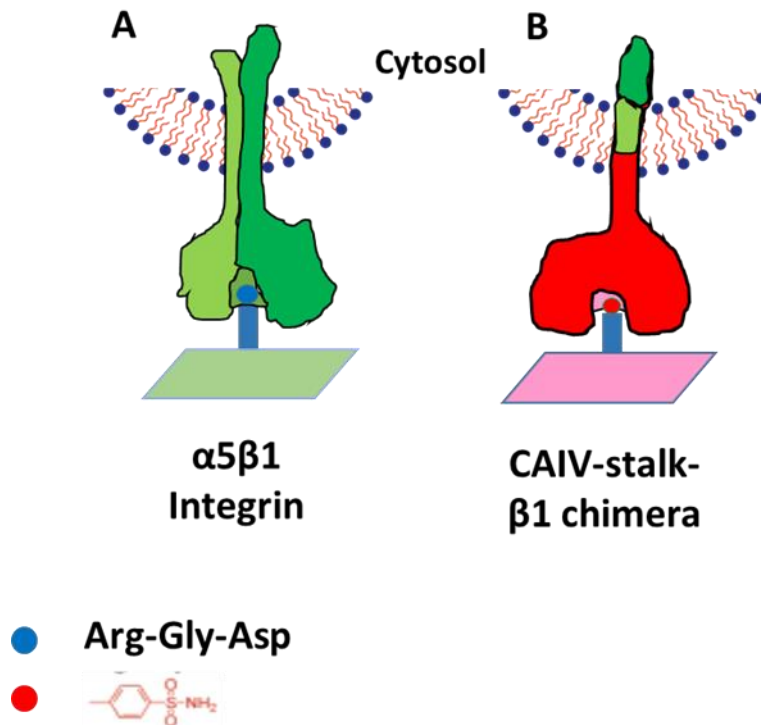


Figure 1.11: Genetically engineered integrin receptors. Surface receptors can be modified to bind a synthetic ligand. **A)** The $\alpha 5\beta 1$ integrin which normally binds Arg-Gly-Asp (RGD) peptide was modified into a chimeric receptor protein which binds an artificial benzenesulfonamide surface ligand **(B)**.

Molecular biology is a powerful tool for cell surface engineering, since it allows generating different surface proteins for different tasks. The method however has several intrinsic drawbacks. It is relatively complicated for commercial use. Prolonged expression and secretion of proteins does not allow for rapid cell surface engineering. The technique relies on DNA modifications, thus permanently alters the biological processes inside the cell. Finally, the application of this method is restricted by the use of proteins that span the plasma membrane, thus not every protein or ligand can be introduced to the cell surface.

1.6.2 Metabolic Engineering

The alternative technique to engineer cell surfaces is by metabolic engineering. As opposed to genetic engineering, this method does not require permanent genetic modifications, thus expression of surface ligands has temporal effect. Metabolic engineering utilizes the cell's metabolism machinery to deliver specific proteins or carbohydrates onto cell surface. The convenience of this technique comes from the fact that the precursors of the required ligands can be added directly to the cell medium, absorbed by the cell as the nutrient, metabolized inside the cell and then secreted onto the cell surface in the final form. Bertozzi and colleagues used this approach to tether cells with biomolecules and fluorescent markers.¹⁴³ They utilized a sugar biosynthetic pathway to incorporate the azide-functionalized sugar into the structure of a glycoprotein (**Figure 1.12**). N-acetylmannosamine derivative (ManNAz) containing an azidoacetyl group was introduced into cell culture medium.

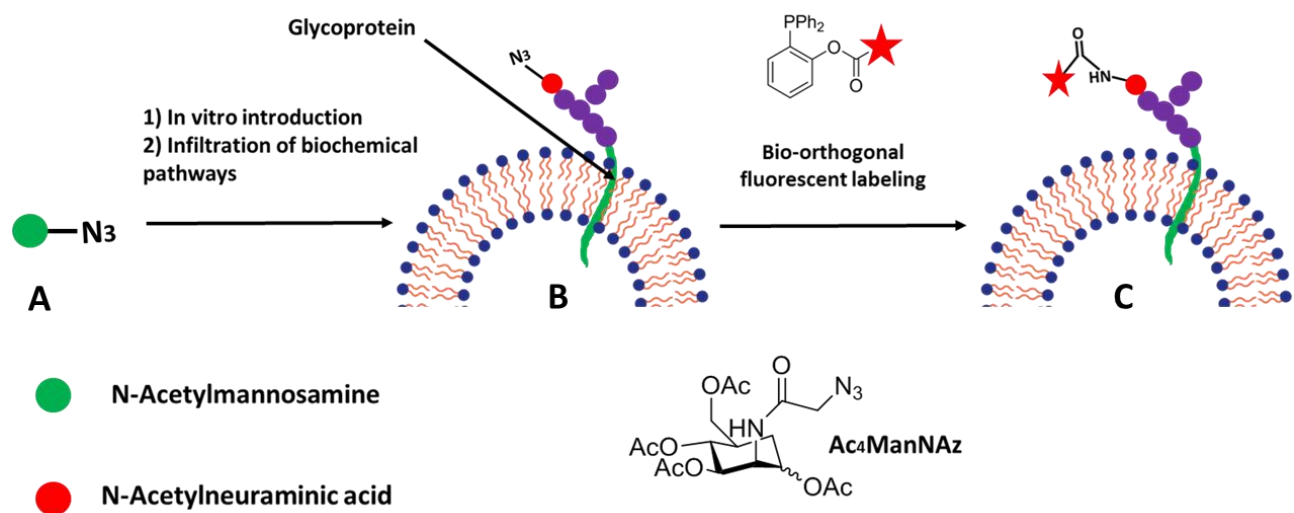


Figure 1.12: Metabolic engineering. **A)** An azide-functionalized N-Acetylmannosamine (Ac₄ManNAz) is introduced into the cell medium. **B)** The carbohydrate is introduced into the biochemical pathway, converted into N-Acetylneuraminic acid and incorporated into a glycoprotein, bringing the azide functionality onto the cell surface. **C)** Bio-orthogonal fluorescent labeling is achieved via the click-reaction between the surface-presented azide and the phosphine.

Given that azide group is relatively small, ManNAz was effectively incorporated into a biosynthetic pathway, brought to the cell surface and inserted into the glycoprotein in a form of sialic acid. The glycoprotein was then labeled with fluorescent probe via the bio-orthogonal click chemistry reaction of Staudinger ligation.

Although metabolic cell surface engineering opens new possibilities for chemical modification of cellular membranes and provides a non-genetic alternative of cell surface engineering, the method has several limitations. Since sialic acid's functions inside the cell are

diverse, the metabolic processes inside the cell can be affected which might cause unwanted biological changes. In addition to this, large quantities of functionalized sugars can be lost inside an organism if the azide-functionalized sugar is introduced systemically in *in vivo* studies, which can potentially be toxic.

1.6.3 Layer by Layer Self-assembly Technique

Another important self-surface engineering method is the layer by layer self-assembly technique (LbL). The technology is based on coating the cell surface with a very thin layer of polymer (6-300 nm thick) with given properties. The advantage of this technique is that it does not utilize the cellular metabolic processes and does not rely on genetic modifications, which means any change is transient and can be made and removed at any given time.¹⁴⁴ This technology allows for the deposit of different synthetic materials, such as polymers, small molecules and nanoparticles, thus providing cells with new (i.e magnetic) properties that would be impossible to introduce with the standard molecular biology tools. Swiston et. al utilized the layer by layer approach to introduce three different layers of polymers (**Figure 1.13**).¹⁴⁵ The first layer is the cell-adhesive region, the region containing a hydrogel that binds directly to the cell membrane. The second layer is the payload region, a part that contains the cargo nanoparticles and FITC stain for visualization. And finally, the release region containing a temperature-sensitive polymer due to which a cell can attach to and detach from any surface with a slight temperature change. Due to presence of Fe₂O₃ nanoparticles, the cell acquires magnetic properties and can be moved with magnetic field.

The Lbl methodology however has major drawback. The layers of polymer create a barrier between the cell surface and the environment which can detrimental to cell-cell interactions as well as to intake of water, ions and nutrients and excretion of the products of metabolism.

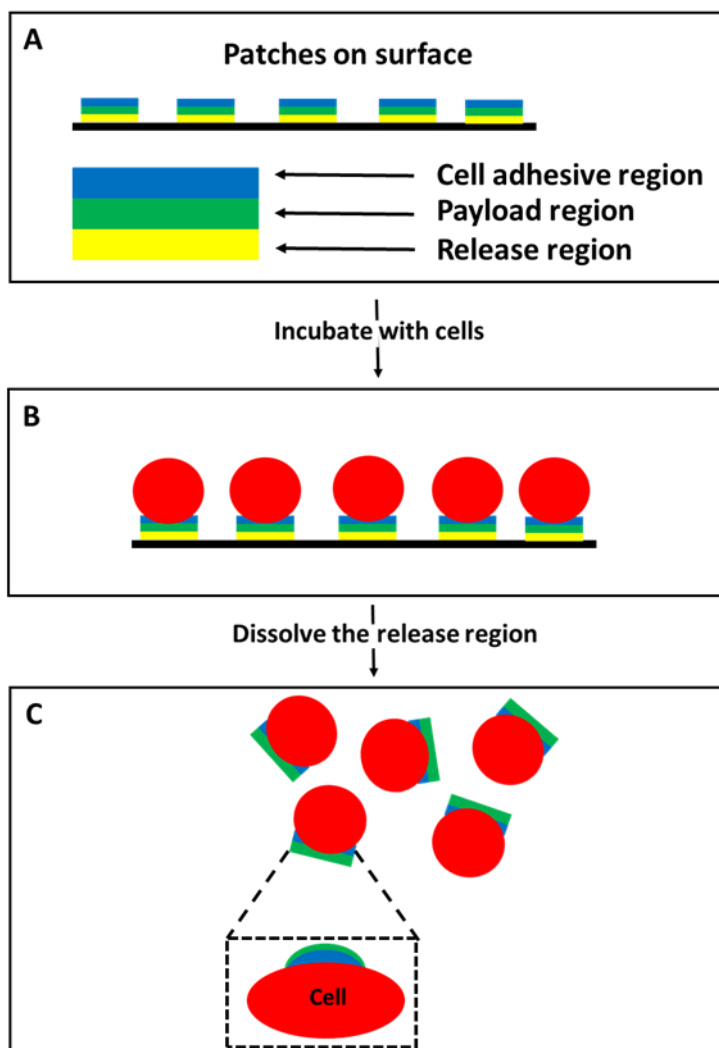


Figure 1.13: The layer by layer (LbL) self-assembly technique. The technique is used to deposit layers of material onto the plasma membrane to effectively modify the cell surface properties. **A)** The substrate surface is coated with patches of material and each patch has three layers. The cell adhesive layer is composed of hydrogel which binds the cell membrane. The payload region contains FITC stain and nanoparticles. The release region is attached to the substrate. **B)** The cells are deposited onto the coated surface and the material from the patches is transferred onto the cell membrane. **C)** The release region is dissolved promoting release of cells which are now functionalized with both: the fluorescent FITC stain and Fe_2O_3 nanoparticles.

1.7 Liposome Fusion

Another method used in engineering of the cell surface is liposome fusion. Liposomes are small artificial spherical vesicles composed mainly of amphiphilic phospholipids. Liposomal properties can vary considerably with size, surface charge and membrane composition.¹⁴⁶ Since the lipid composition of a typical liposome is very similar to the composition plasma membrane, liposome fusion can occur without damaging the membrane and is also considered to be non-cytotoxic. Liposome fusion is an established technology that has been around for several decades and is currently used for intercellular drug delivery, DNA transfection and vaccination.¹⁴⁷

Liposomes can have different architecture but the classical liposome is a spheroid phospholipid bilayer with an aqueous core. The lipid membrane of liposome is composed of polar phospholipids arranged in a form of a bilayer containing two leaflets. In aqueous solvents hydrophilic heads of the phospholipids lipids of the outer leaflet are facing the environment, and the ones belonging to inner leaflet face the aqueous core (**Figure 1.14**). The hydrophobic tails on both leaflets are stacked in the membrane creating the hydrophobic environment inside the bilayer.¹⁴⁸ This creates three different carrier slots that can be used for delivery of different types of molecules. Water soluble molecules (ie polysaccharides) can readily be transported into the aqueous core of the liposome.¹⁴⁹ Non- polar drugs (ie hormones) and amphiphilic lipids can be inserted inside the phospholipid bilayer. Finally, if a liposome contains positively charged lipids in its structure, negatively charged molecules such as DNA can find their place on the liposomal membrane surface.¹⁵⁰⁻¹⁵³

Lipid composition directly influences the properties of the liposome. A typical liposome contains lipids that are identical or similar in structure to those usually found in eukaryotic

plasma membrane. The presence of saturated or unsaturated hydrophobic tails impact the stability and thus degradation properties of a liposome. Unsaturated fats promote greater fluidity of the phospholipid bilayer while saturated fats make the structure more rigid.^{154,155}

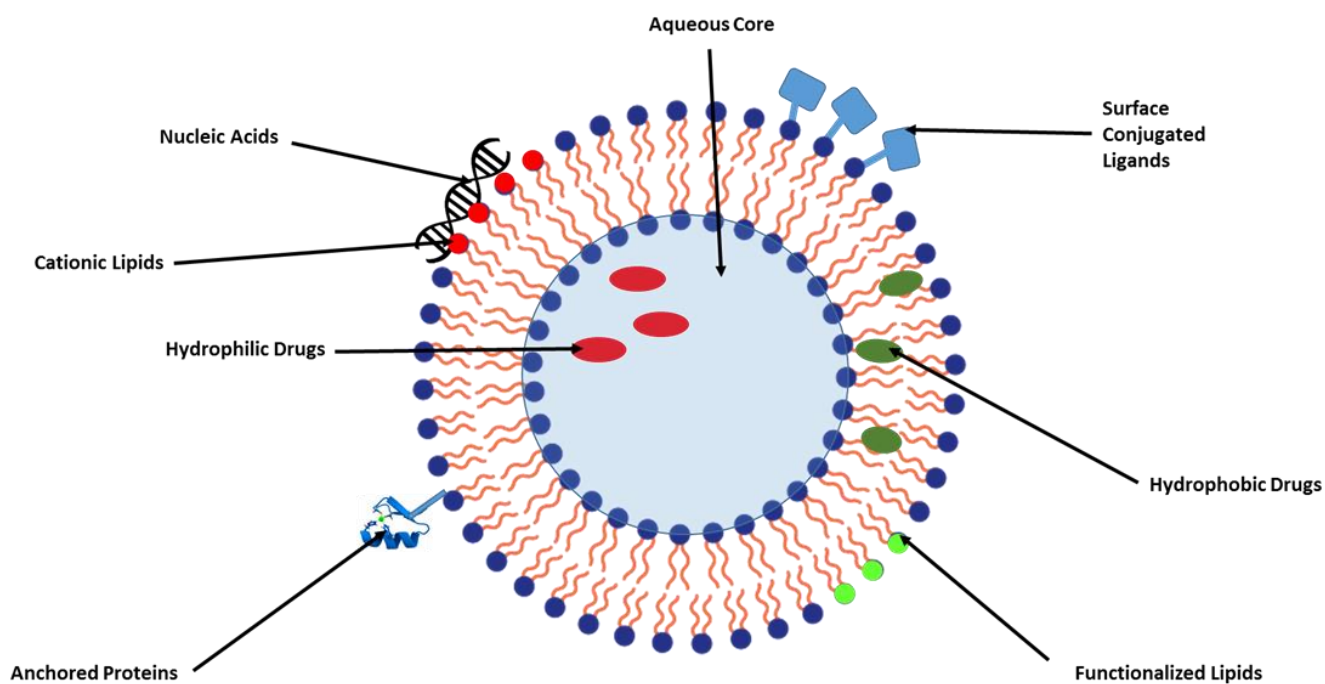


Figure 1.14: Liposome delivery system. Liposomes are versatile carriers capable of transporting a wide range of molecules into cells. Hydrophobic drugs are incorporated into the lipid bilayer, while water-soluble drugs are found in the aqueous core. In addition, liposomes are capable of carrying nucleic acids, anchored lipids as well as surface conjugated ligands. Synthetic lipids can be inserted into liposomes and delivered onto cell membrane.

Liposome size can vary considerably depending on the purpose of use. The typical size of a liposome varies from very small (30 nm) to large (25 μm). Small liposomes with sizes ranging from 20nm to 100nm are called small unilamellar vesicles (SUVs). Large unilamellar vesicles (LUVs) have sizes ranging from 100 nm to 400 nm. Finally, the giant unilamellar vesicles (GUVs) can often be larger than 1 μm . The vast majority are composed of only one lipid bilayer (unilamellar vesicles), however some of them can have an onion-like structure with two and more phospholipid bilayers (multilamellar vesicles).¹⁵⁶⁻¹⁵⁸

Liposome fusion involves the fusion of lipid membranes, a process where two initially distinct lipid bilayers with hydrophobic cores fuse to produce a single interconnected structure. Membrane fusion is involved in many cellular processes such as fertilization of an egg by sperm, exocytosis and formation of lysosome to excrete metabolic waste products. In addition, membrane fusion is a key step in lipid transport from the site of lipid synthesis to the plasma membrane. Even pathogenic processes such as viral infections utilize lipid membrane fusion to transport their genetic material into the host cell.¹⁵⁹

If the liposome contains only uncharged lipids, such as phosphatidylcholine (POPC), this process is thermodynamically unfavourable and involves four steps (**Figure 1.15**).¹⁵⁹ At first, the liposome must approach the plasma membrane closely (few nanometers) through aggregation. Second, the liposome must come very close to the plasma membrane so that the distance does not exceed a few angstroms. At this distance it is important that two surfaces remain at least partially dehydrated as the water molecules if they remain between the lipid membranes will at this distance cause strong repulsion between the bilayers. Third, a destabilization must occur between the lipid surfaces.¹⁶⁰ It is this important that it happens simultaneously between the two leaflets of lipid bilayers, which is very difficult in the aqueous

environment since the hydrophobic lipid tails strongly avoid any contact with water. If only one leaflet from each bilayer is destabilized, hemifusion occurs. In the event of hemifusion, lipid exchange between outer leaflets of the liposome and the plasma membrane can occur; the inner leaflets, however remain intact thus the mixing of the internal content is impossible.

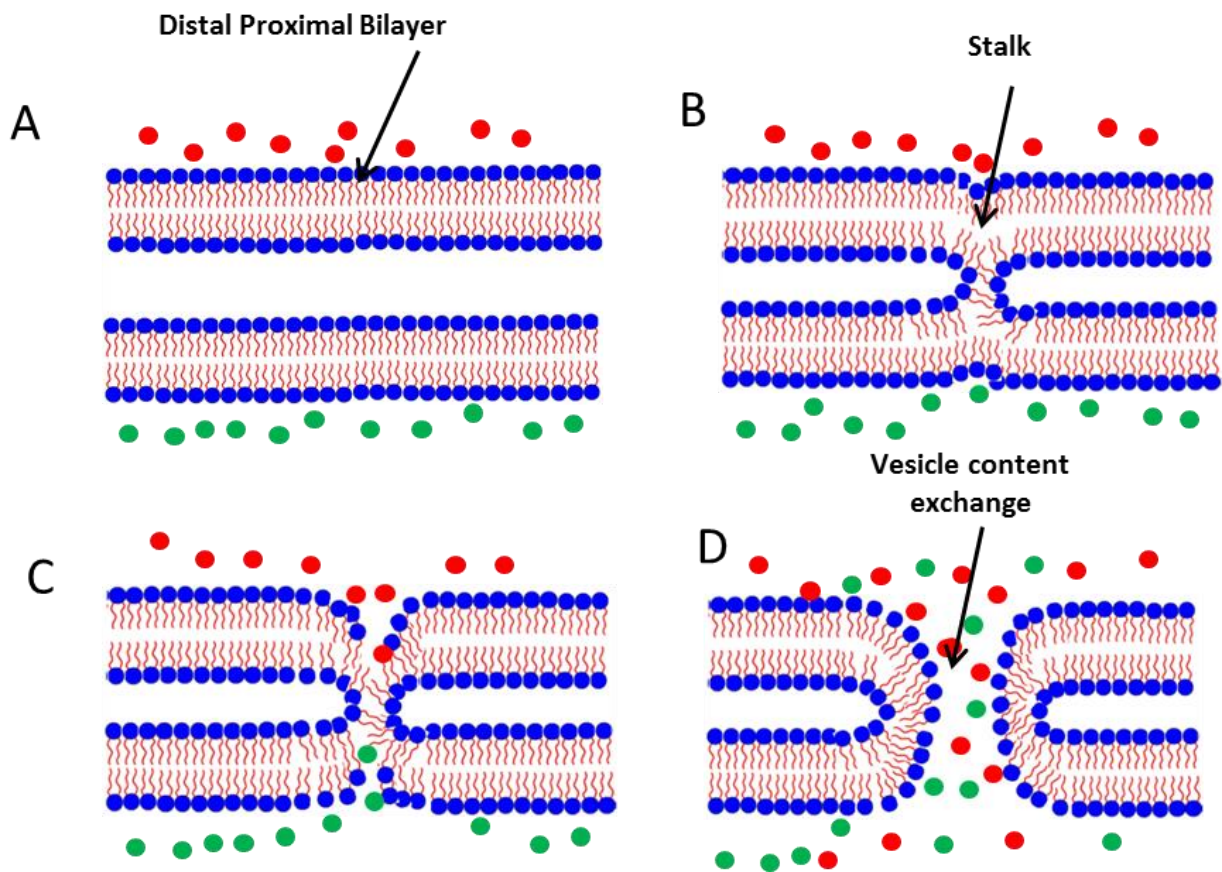


Figure 1.15: The mechanism of lipid membrane fusion depicting the key intermediate structures. A) Two lipid membranes approach each other until the distance between them does not exceed 10-15Å. **B)** Membrane destabilization occurs between the two inner leaflets leading to the formation of a stalk. Lipid exchange between the inner leaflets is initiated promoting membrane destabilization. **C)** Lipid exchange between the outer leaflets is initiated enlarging the stalk and resulting in pore formation. **D)** The pore grows and the content of fusing vesicles is exchanged.

Finally, in the event of complete fusion two leaflets of each bilayer come into contact. Destabilization produces a fusion pore which grows and causes the content of liposome to mix with the cytosol from the cell. This exchange enlarges the pore and leads to the complete fusion. Fusion between the uncharged liposome and the negatively charged membrane does not happen simultaneously. Therefore, liposomal structure must be modified to promote membrane destabilization and subsequently fusion (**Figure 1.16**).

One way is based on inserting specific proteins into the structure of a liposome. This method was adapted from the natural events which occur with lipid vesicles trafficking protein and lipid cargo between the endoplasmic reticulum and the Golgi apparatus. Specific proteins called SNAREs are found on lipid vesicles and on the target organelles.

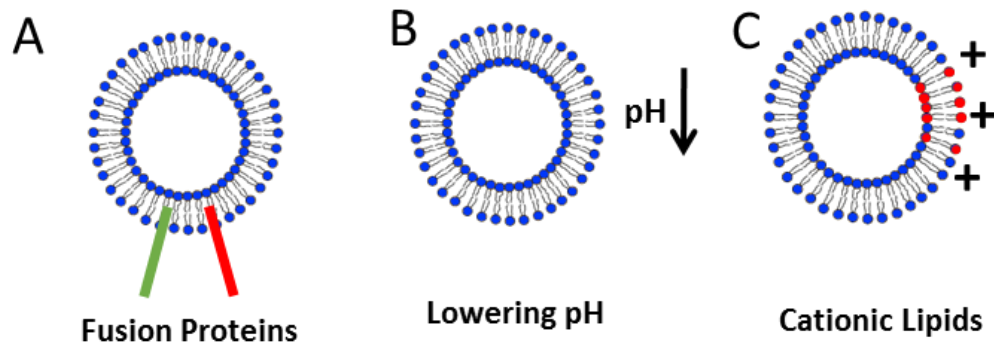


Figure 1.16: The membrane destabilization strategies: A) Fusion proteins destabilize lipid membranes and promote liposome fusion. B) Lowering pH causes protonation of negatively charged glycolyx and facilitates liposome fusion. C) Cationic lipids incorporated into the liposome structure will enhance fusion with the negatively charged eukaryotic plasma membrane.

SNAREs promote lipid membrane destabilization and subsequent fusion of the vesicle and the lipid membrane of the organelle. The ability of liposomes to fuse with the plasma membrane was greatly increased with the introduction of proteins. The liposome is decorated with short amphiphilic peptides which when inserted into the plasma membrane promote destabilization of the lipid bilayer with subsequent liposome fusion. Protein-functionalized liposomes can be used to target cells which express specific surface receptors and thus facilitate the delivery of substances such as drugs or other cargo to the place where it is needed.^{161,162} This approach however, has a major disadvantage. In *in vivo* applications the presence of exogenous proteins can trigger an immune response which is greatly undesirable.

Another important feature that was employed to promote membrane destabilization is alteration of the pH. Decreasing pH would cause protonation of negatively charged lipids thus reducing the electrostatic repulsion between the liposome and the plasma membrane and promoting liposome fusion.¹⁶³ A similar effect can be achieved with introduction of calcium and magnesium ions.¹⁶⁴ Since the environment around malignant tissues is mildly acidic (pH=6.5), the pH sensitive approach is very useful, because liposomes loaded with anticancer drugs can fuse to the area of malignancy, thus promoting targeted drug delivery.¹⁶⁵

The introduction of cationic lipids into the liposome structure was proven to be an effective method to promote liposome fusion. Positively charged lipids such as 1,2-dioleoyl-3-trimethylammonium-propane (DOTAP) can be incorporated into otherwise uncharged liposomes containing natural phospholipids such as palmitoyl-oleoyl phosphatidylcholine (POPC). The positively charged liposome can be electrostatically attracted to the negatively charged plasma

membrane and fuse with it under physiological conditions with pH 7.4.¹⁶⁶ The approach is simple, reliable and non-cytotoxic, thus is our method of choice for cell surface engineering.

There are multiple applications for liposome technology, the most popular being drug delivery. Liposomes provide an ideal environment for drug transport. Drugs with different properties can be carried inside the liposome within the aqueous layer inside the lipid bilayer if they are hydrophobic or outside on the membrane if they are charged. In 2012, there were 8 liposome based drugs on the market that are used to treat such conditions as influenza, hepatitis A, fungal infections and different types of cancer.¹⁶⁷

Liposomes are also used for immunization. Liposome-based adjuvants are gaining popularity and there are several liposome-based vaccines on the market. To induce an immune response, T cells and B cells are activated with proteins delivered via liposomes. The proteins are typically attached to a lipid linker which is inserted into the lipid bilayer, thus displaying the antigen on the outer layer.¹⁶⁸ The antigen stimulates the lymphocytes and induces the immune response.

Recent advances in chemistry have allowed for creation of liposome-based DNA/RNA transfection system such as LipofectamineTM. The cationic lipids in the liposome electrostatically attract the negatively charged nucleic acids promoting rapid delivery into the cell. Liposome technology is an outstanding tool for cell surface engineering. Liposome fusion allows for easy delivery of natural and synthetic lipid moieties onto the cell surface.¹⁶⁹ The engineered liposomes can fuse to the cell surface and transform the plasma membrane with different ligands for various purposes such as fluorescent labeling, DNA transfection and cell assembly. Since the technology

is simple, predictable and non-cytotoxic liposome fusion opens many possibilities for cell surface engineering.

1.8 Bio-orthogonal Chemistry

The term bio-orthogonal click chemistry was introduced in 2003 by an American scientist Carolyn Bertozzi.¹⁷⁰ Bio-orthogonal reactions are chemical reactions that do not interact or interfere with biological processes in a biological system or living organism, exhibiting no cellular toxicity and providing high specificity (**Figure 1.17**). These biologically inert click-chemistry reactions are of great importance for the coupling of cells and biological macromolecules (lipids, carbohydrates and proteins).¹⁷¹

For a chemical reaction to be applicable for biological purposes it has to satisfy the following criteria. 1) It has to proceed under physiological conditions: 37°C pH 7. 2) The reaction has to proceed in an aqueous environment. 3) Reactants and products of the reaction have to be non-cytotoxic. 4) Products of the reaction should not undergo hydrolysis and must be stable in an aqueous environment. 5) The reaction must be specific, thus the reactants must react exclusively with each other and be inert towards the cellular proteins, carbohydrates or lipids. Out of all the diversity of organic reactions which lead to formation of covalent bonds, only few can be classified as bio-orthogonal.^{171,172}

The first such reaction was introduced by Bertozzi and colleagues in the year of 2000.¹⁷³ It involved a modified version of the well-known Staudinger Ligation. This is a reaction between an azide, a soft nucleophile, and a phosphine, a soft electrophile. The original Staudinger ligation reaction was prone to hydrolysis. To avoid this Bertozzi and colleagues modified the classic

Staudinger ligation reaction mechanism by introducing an ester group ortho to the phosphorus atom on the aryl ring (**Figure 1.18**). This led to the formation of the aza-ylide intermediate. Addition of an ester group yielded the second intermediate which upon hydrolysis led to a stable amide-linked product. This was the first attempt to generate a quick bioorthogonal reaction. Although non-cytotoxic, the reaction however had very slow kinetics with a second-order constant of only $0.0020 \text{ M}^{-1}\text{s}^{-1}$.

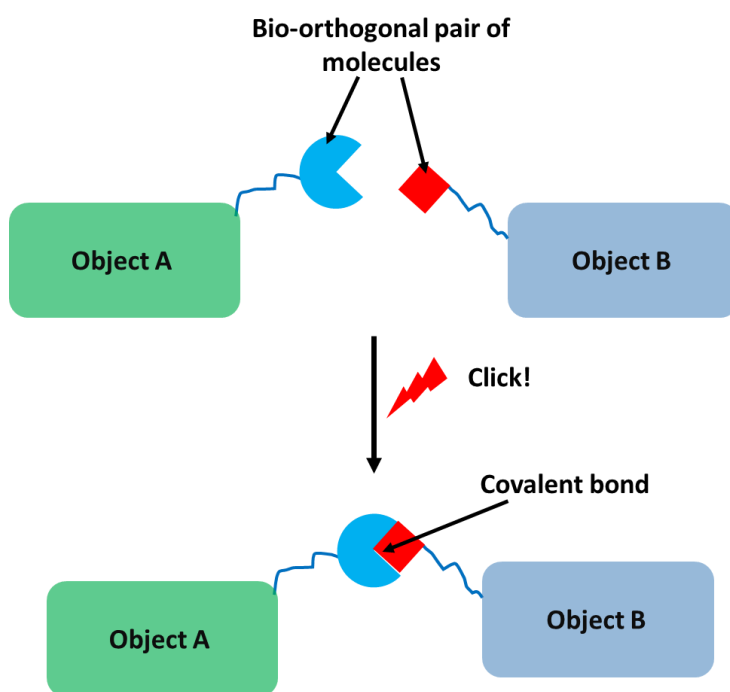


Figure 1.17: Bio-orthogonal chemistry as an effective molecular ligation strategy. Bio-orthogonal ligation is a robust and specific method that can be used to assemble small molecules, biological ligands, nanoparticles and cells into complex structures. These objects can be tethered with a bio-orthogonal pair of molecules which interact exclusively with each other and are completely inert towards reactions with other substances. The reaction between the moieties happens instantaneously resulting in the formation of a strong covalent bond. As the result, the two objects are assembled into a single structure.

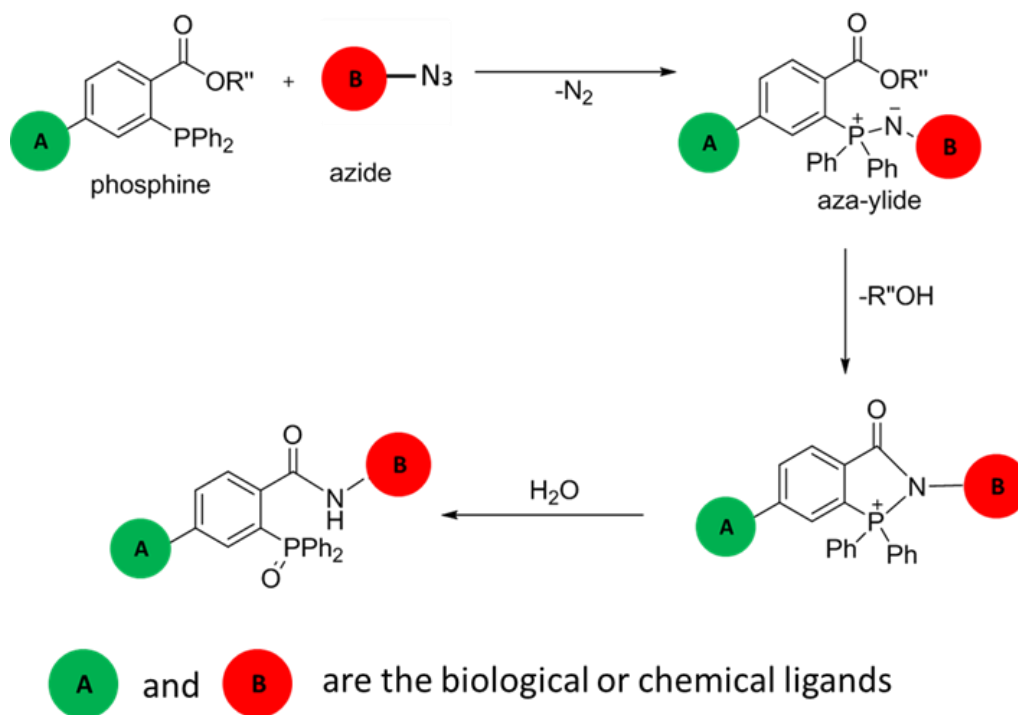


Figure 1.18: The modified Staudinger ligation reaction. The first bio-orthogonal reaction used for ligation of biomolecules. Phosphine, which is a soft electrophile, is attacked by an azide, a soft nucleophile, to form an aza-ylide intermediate. Due to the presence of an ester group, the final product is resistant to hydrolysis.

In the early 2000s, Sharpless and Meldal introduced a copper-catalyzed azide-alkyne cycloaddition (CuAAC) - a variation of Huisgen cycloaddition method in which the rate of reaction between an azide and alkyne is dramatically increased via Cu(I) catalysis (Figure 1.19).¹⁷⁴ Due to weak acidity and basicity of both alkyne and azide, their interaction with biological molecules is limited, making the reaction very specific. Today, it is the most widely used *in vitro* click-chemistry reaction. It can proceed in aqueous buffers under physiological conditions. CuAAC was demonstrated to work for labelling glycoproteins, nucleic acids and glycans with fluorescent tags and crosslinking them with each other.^{175,176} In 2003,

Finn and colleagues reported the use of CuACC for labeling Cowpea mosaic virus.¹⁷⁷ They coupled the azide-functionalized chemical linkers to the surface of viral protein and then coupled an alkyne-functionalized dye. This was the first example of the use of click chemistry within a biological system. The process of bio-orthogonal functionalization of bio-molecules however requires a complicated chemical synthesis which can be potentially damaging to the bio-molecule of interest. In addition, the use of copper in living cells and organisms is associated with increased cytotoxicity, which is strongly undesirable in biological experiments.

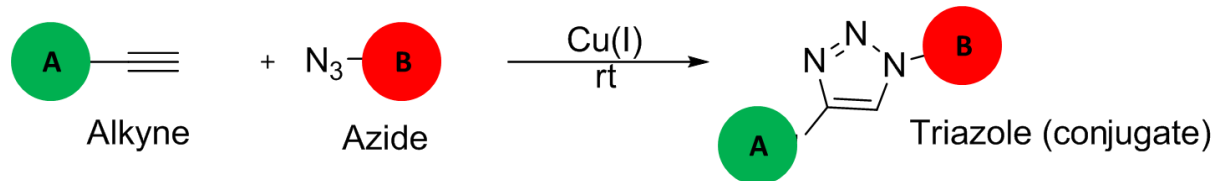


Figure 1.19: The copper-catalyzed azide–alkyne cycloaddition (CuAAC). Organic azides are capable of reacting with terminal alkynes to produce the stable triazole conjugate. The reaction requires copper for catalysis.

In order to eliminate the use of copper and still preserve the high rate of reaction, Bertozzi and colleagues came up with an idea to apply the steric strain onto alkyne group to activate the alkyne towards the reaction with the azide (**Figure 1.20**). The alkyne functionality in the form of cyclooctyne, due to the ring strain, reacts selectively with azides through strain-promoted cycloaddition.¹⁷⁸ The first copper-free click chemistry reactions with cyclooctyne had very slow kinetics with the second-order constant of only $0.0024 \text{ M}^{-1} \text{ s}^{-1}$. Later, the rate of reaction was significantly enhanced with addition of two electron-withdrawing fluorine atoms yielding difluorinated cyclooctyne with $k = 0.076 \text{ M}^{-1} \text{ s}^{-1}$.¹⁷⁹ Despite decreased cytotoxicity and increased reaction rates, this reaction still has significant limitations. One of which is low water solubility of alkyne-functionalized moieties due their hydrophobicity, which can ultimately

change the solubility and reactivity of alkyne-conjugated biological molecules. This increased hydrophobicity can also result in non-specific sticking to proteins and insertion into lipid membranes. The low stability of cyclooctynes also decreases the range of their application.

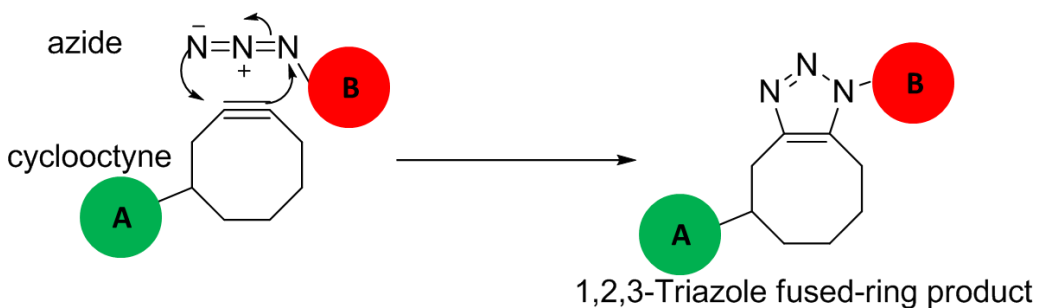


Figure 1.20: The strain-promoted alkyne-azide cycloaddition. To obviate the need to use cytotoxic copper, the activation energy for the reaction between alkyne and azide was effectively lowered by introducing the ring-strained cyclooctyne. The free energy from this bond deformation was sufficient enough to induce the reaction of the alkyne with the azide under mild conditions.

Finally, Fox and colleagues (2008) demonstrated the use of the inverse electron-demand Diels-Alders cycloaddition of strained cyclooctene with tetrazine. This is the fastest bioorthogonal reaction known today with rate constants ranging from 10^3 to $10^6 \text{ M}^{-1}\text{s}^{-1}$.¹⁸⁰ The technology was applied to label antibodies with radioactive probes and eradicating tumors in mouse models. The system however has the same limitations as the cyclooctyne-azide coupling reaction.

1.8.1 Oxime chemistry

In the present study we have demonstrated the use of covalent bioorthogonal reaction between an oxyamine and ketone to form a stable oxime (**Figure 1.21**). The reaction is quick, stable and

specific; it requires no catalysis and can proceed at low temperatures. These properties can be explained by the increased nucleophilicity of oxyamine. Unlike the regular amine, oxyamine is strongly nucleophilic due to alpha-effect created by the presence of an oxygen atom with two lone pairs of electrons adjacent to the nitrogen atom with one lone pair. Kinetics studies by O'Brian et al (2015) demonstrated that the reaction is fast ($k = 0.0098 \text{ M}^{-1}\text{s}^{-1}$) with $t_{1/2} = 9\text{s}$.¹⁸¹ The oxime is resistant to hydrolysis under physiological conditions in the aqueous environment of phosphate buffered saline (pH 7.4) and is known to be stable for at least three weeks. Oximes are non-existent in biological systems and do not interact with enzymes and other biomolecules. The only by-product of oxime formation is water, thus the reaction between oxyamine and ketone is non-cytotoxic.^{181,182}



Figure 1.21: The bio-orthogonal reaction between oxyamine and ketone. The reaction between oxyamine and ketone results in the formation of a stable covalent oxime bond. The reaction can occur under physiological conditions (37 C, pH 7.2), requires no catalyst and is resilient to hydrolysis. All reactants and products of this reaction are non-cytotoxic. The process provides significant atom economy and the only by-product produced in this reaction is water.

Another advantage of oxime chemistry is that both oxyamine and ketone are small and polar chemical groups. This makes it easy to create both ketone and oxyamine functionalized biomolecules, such as proteins, carbohydrates and lipids without significant alteration of their properties (i.e solubility). For example, ketone and oxyamine lipids just like the regular

phospholipids will contain polar heads and non-polar tails, which makes them suitable for incorporation into the cellular membrane via the process of liposome fusion.

Ketone-functionalized lipids such as dodecanone are commercially available and the oxyamine-functionalized lipids can be obtained via a simple two-step organic synthesis. These properties make bio-orthogonal oxime chemistry our system of choice.

1.9 Bio-orthogonal Cell-Assembly Strategy

Over the last decade, a number of new methods to build 3D tissues have appeared. These tissue assembly methods have been described above and most of them rely either on the use of exogenous scaffolds to support the cell mass or on genetic engineering to create organoids from stem cells.^{183,184} Scaffold technologies, although providing structural support for the cells, have some disadvantages. When using the scaffold system one has to account for many parameters such as the degradation rate of scaffold material, porosity of the scaffold and the ability of cells to adhere to the material among many others.¹⁸⁵

Advantages	Disadvantages
<ul style="list-style-type: none">• Provide support for cells• Easy to handle• Can be tuned for different applications• A large selection of polymer materials is available	<ul style="list-style-type: none">• Occupy volume in a tissue• Create a barrier between cells• Lower the cell density• Potential toxicity of products of scaffolds degradation

Table 1.1: Advantages and disadvantages of applying scaffolds for tissue engineering.

Scaffolds are made of biodegradable materials which leach degradation byproducts in tissue and can potentially be toxic for the cells or trigger an immune response.^{186,187} In addition, in scaffold-based tissues a large portion of tissue volume is occupied by polymer material; this material may create a barrier between the cells, lowering the cell density and preventing formation of cell-cell junctions thus disrupting extracellular communication.¹⁸⁸

Approaches based on developmental biology and use of stem cells result in organoids — structures reminiscent of organs. These constructs capture some of the 3D structure of the real organ and do not require a scaffold to be built. The system however is not flexible and does not allow for formation of tissues with variable dimensions and architecture. It is impossible to control what cell types are used to build the tissue and the ratios in which they can be combined.¹⁸³ In addition, stem cell differentiation is a time consuming process and the methods that involve use of human embryonic stem cells are controversial.¹⁸⁹ Therefore, the most optimal method to construct a functional 3D tissue for either transplantation, drug testing or disease modeling would be the one that requires no scaffold, is robust and easily customizable for a variety of applications.

The method of cell assembly presented in this work is scaffold-free and does not utilize any polymer materials. The technology is based on a bio-orthogonal click chemistry reaction between an oxyamine and ketone functionalities to form a stable covalent oxime bond. This ligation reaction is quick, specific and requires no catalyst. The reaction occurs under physiological conditions, is stable, and produces no toxic byproducts. The only byproduct of this reaction is water.

For delivery onto the cell membrane, oxyamine and ketone lipids are incorporated into liposomes (**Figure 1.22**). The liposome composition includes a neutral POPC lipid, DOTAP – a positively charged lipid which enables destabilization of the negatively charged lipid membrane initiating the membrane fusion.¹⁹⁰ Ketone and oxyamine functionalities are incorporated into the liposome in the form of dodecanone and *O*-dodecyloxyamine lipids. Liposome technology is a well-established and safe method of drug delivery. There are currently 8 drugs that utilize liposome fusion to deliver the therapeutic molecules into cells.¹⁶⁷ Our group was the first to use liposome fusion for cell surface engineering.¹⁹¹

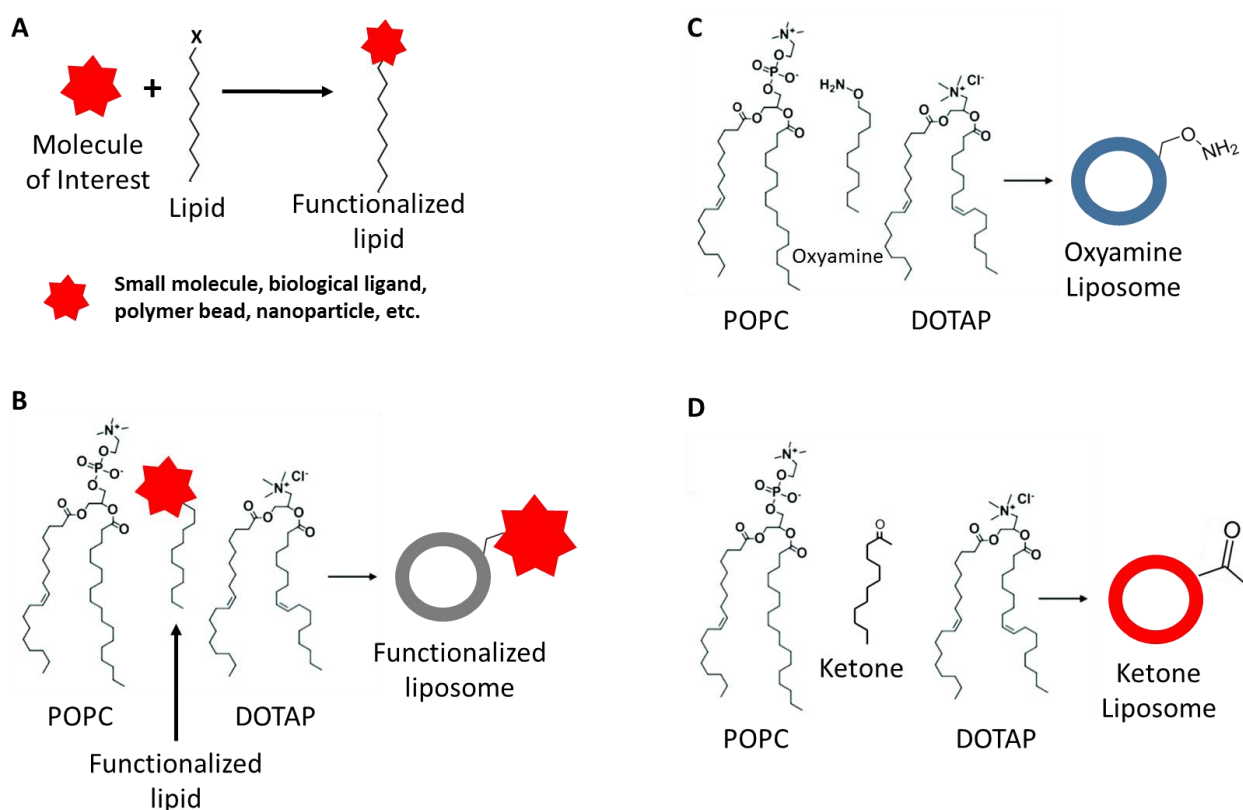


Figure 1.22: The synthesis of functionalized liposomes for cell surface engineering. **A)** A ligand of choice which can be either a biological molecule, a chemical moiety, a polymer bead or a nanoparticle is functionalized with hydrophobic lipid tail for incorporation into a liposome with subsequent delivery onto the cell membrane. **B)** The functionalized lipid is mixed with the background lipids (POPC and DOTAP) and sonicated to produce a liposome tethered with the molecule of interest. Oxyamine **(C)** and ketone **(D)** liposomes are used for the shuttling of bio-orthogonal moieties onto cell surfaces for the purpose of tissue assembly.

Through liposome fusion, cell membranes can be tethered with ketone or oxyamine moieties (**Figure 1.23**). The process quick, simple and requires less than 5 minutes. After that, the cells with engineered membranes can be assembled into spheroid cell aggregates within seconds. These spheroids then adhere to the substrate, the cells secrete an extracellular matrix and spread forming tissues.¹⁹² Only ~10,000 oxyamine or ketone molecules per cell are required to effectively assemble cells, and this chemistry is gradually diluted out as the cells divide renewing the membrane.¹⁹¹

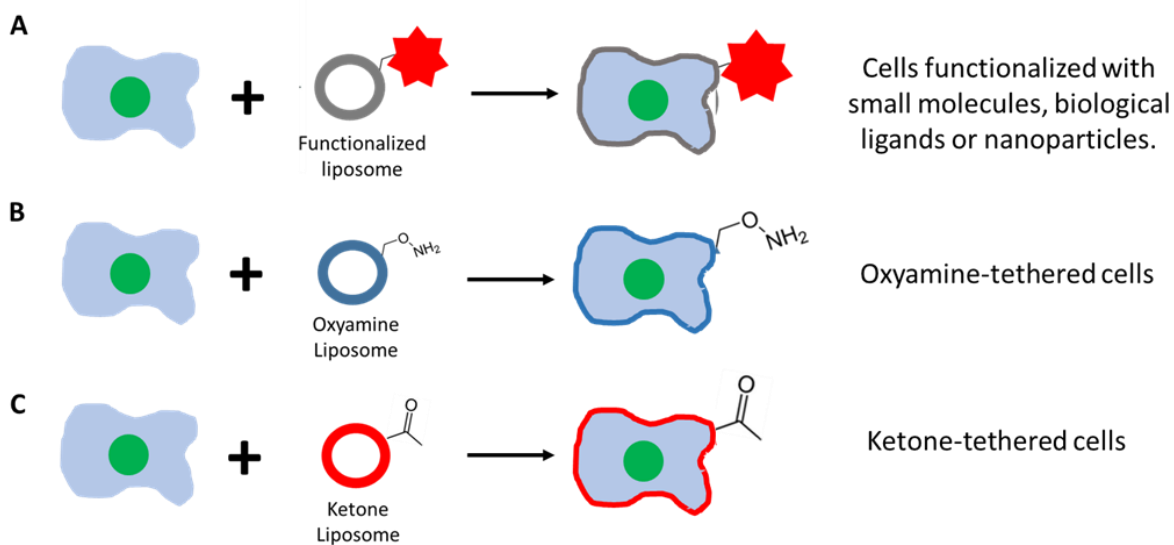


Figure 1.23: Cell surface engineering via liposome fusion. Liposomes rapidly fuse with the cell membrane delivering the ligands onto cell surfaces. **A)** Cell surfaces can be functionalized with biological ligands, nanoparticles or small molecules for different purposes such as fluorescent labeling, cell sorting and immunological studies. Using this approach, cells can be labeled with bio-orthogonal oxyamine and ketone groups (**B,C**).

The ketone and oxyamine-functionalized lipids are incorporated into liposomes and delivered onto the cell membrane via liposome fusion. This cell surface engineering method is robust, simple and applicable to all cell-types. The ketone and oxyamine-tethered cells clicked together resulting in cell assembly.¹⁹³

Although in this work cell surface engineering was applied for tissue assembly, other applications of this technology are possible. Surface engineering enables binding of practically any ligand to the cell surface. The ligand must contain an oxyamine or ketone functionality and can be tethered to a membrane-engineered cell.¹⁹⁴ The ligand can be a fluorescent molecule for microscopic visualization, a cytokine to induce a specific cellular response, a drug molecule, or a physical object, such as nanoparticle or a polymer bead for cell-sorting and purification. In the case of protein ligands, this approach is especially useful because it eliminates the need to use genetic engineering. Since genetically expressed proteins need to utilize biochemical pathways to be delivered to the cell surface, the only the proteins inserted into plasma membrane are the ones that have the right amino acid sequence, size and conformation. Since oxime chemistry works from the outside of the cell, a wide range of proteins with different characteristics can be installed onto cell surface.

Liposome fusion has long been used for targeted drug delivery and DNA transfection. Although a lot of progress has been made in these areas of research, the bottleneck of the current technologies is the low efficiency of the fusion process which happens as result of lipid vesicles being too stable. In other words, a large percentage of vesicles come in contact with the cell membrane and bounce off without fusion. Adding oxime chemistry to the cell surface and the liposome will fix the liposome in proximity to the cell membrane, induce membrane

destabilization and promote fusion. Cell surface engineering is a promising method in the creation of technologies that can be used for efficient DNA transfection and drug delivery.¹⁹⁵

The liposome cell surface engineering method is used not only for eukaryotic, but also for prokaryotic organisms. The ketone and oxyamine-functionalized lipids were incorporated into liposomes and delivered onto the cell membrane via liposome fusion. This cell surface engineering method is robust, simple and applicable to all cell-types. The ketone and oxyamine-tethered cells clicked together resulting in cell assembly.

Bio-orthogonal liposome fusion technology can be used not only with eukaryotic, but also with prokaryotic organisms. Using bio-orthogonal chemistry our team engineered the cellular surfaces of *E.coli* bacteria with oxyamine and ketone moieties via liposome fusion.¹⁹⁶ This chemistry enabled functionalization of ketone tethered bacterial cells with fluorescent oxyamine- FITC dye. Likewise, an oxyamine biotin molecule was introduced to the cell surface and subsequently tagged with fluorescent streptavidin protein. Thus, aside from tissue engineering, oxime chemistry is also a powerful tool for functionalization of eukaryotic and prokaryotic cell surfaces with a wide variety of ligands.

Bio-orthogonal oxime chemistry is a powerful tool that can be used to assemble cells into multicellular 3D tissues. It enables tissue assembly without the use of exogenous polymers or scaffolds. The system is versatile and can be used with different cell types. The chemistry can be used to assemble multiple cell types into a functional tissue with varied thickness and geometry (**Figure 1.24**). In my research work, I have conducted five different projects.

In the first two projects, I demonstrated how the click-assembled 3D tissues can be used to assess the test cardiac and liver drug toxicity *in vitro*. Using this scaffold- free technology, I

was able to construct functional 3D cardiac and liver tissues, which contained cells from different cell types. The tissue performance was characterized with the standard function assays. The samples were subsequently treated with variable concentrations of drugs for different time periods to assess drug toxicity.

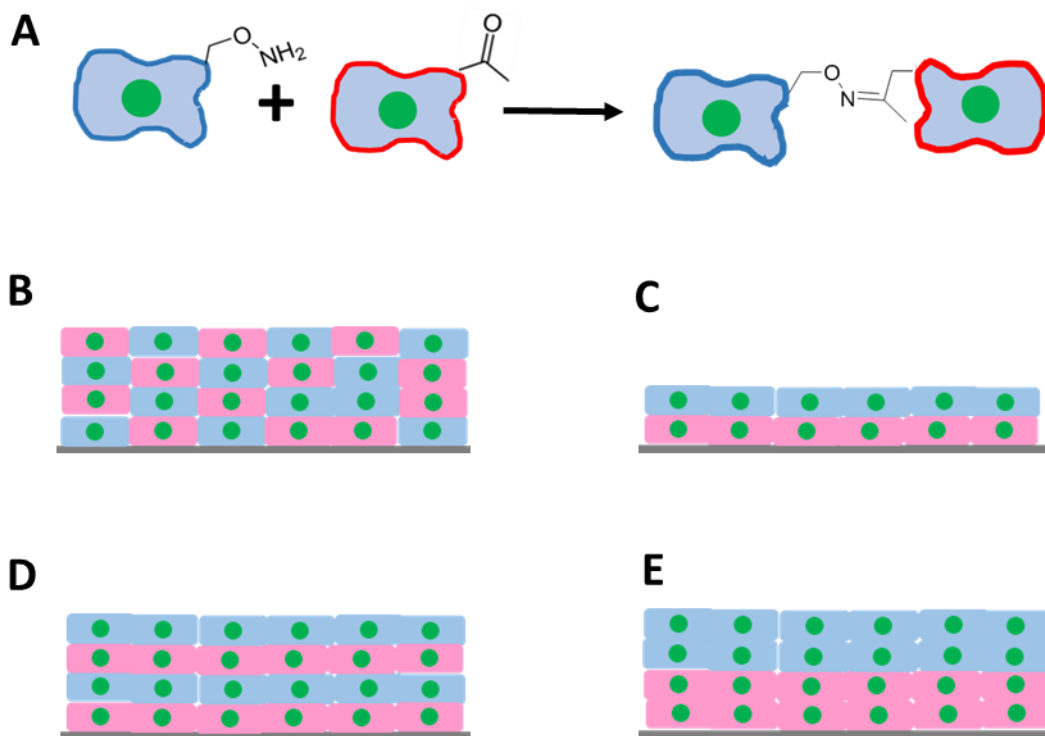


Figure 1.24: The bio-orthogonal cell ligation strategy. A) When oxime-labeled and ketone-labeled cells are brought into contact, the bio-orthogonal chemical groups displayed on the cell surface react with each other producing a stable oxime bond linking the cells together. Using this approach, a variety of functional tissues can be assembled. These tissues may contain various cell types and have different configurations. The cells can be mixed (B) or deposited layer by layer to yield thin (C) or thick (D,E) three-dimensional co-cultures with the defined cell-layer orientation.

In the body, cells form distinct patterns which are determined by the function of the specific tissue they belong to. Tissues such as skin are composed of multiple cell layers where each cell layer contains specific cell types. Our methodology allows the formation of such stratified tissues. One of the possible applications for such tissues is in the modelling of cell behavior in a complex 3D environment. In my third project, I created a multilayered 3D co-culture of human mesenchymal stem cells (hMSC) and C3H10T1/2 cells. The position of cells in the co-culture (at the top, at the bottom or mixed) determined the rate of stem cell differentiation as well as the choice of lineage.

The reaction between oxyamine and ketone is rapid, specific and can proceed in the aqueous environment which allows the assembly of cells into tissues via microfluidics. Oxyamine and ketone-tethered cells can click together as they flow inside a microfluidic channel. The four's introduces microfluidics system as a powerful tool for rapid cell assembly.

In my last project, I created a di-oxyamine crosslinker, a molecule which crosslinks ketone-functionalized cells into tissues. The resulting 3D construct is a polymer composed of multiple monomers which are cells. The technology allows to create a hybrid polymer that can potentially include several components at once: cells, cytokines, nanoparticles, polymer beads, etc. The construct can be used for transplantation, drug testing and disease modeling.

1.10 References

1. Gregory, C. D. & Pound, J. D. Cell death in the neighbourhood: direct microenvironmental effects of apoptosis in normal and neoplastic tissues. *J. Pathol.* **223**, 178–195 (2011).
2. Trepap, X., Chen, Z. & Jacobson, K. in *Comprehensive Physiology* (John Wiley & Sons, Inc., 2012). doi:10.1002/cphy.c110012
3. Doyle, A. D., Petrie, R. J., Kutys, M. L. & Yamada, K. M. Dimensions in cell migration. *Curr. Opin. Cell Biol.* **25**, 642–649 (2013).
4. Ho, C.-T. *et al.* Liver-cell patterning Lab Chip: mimicking the morphology of liver lobule tissue. *Lab Chip* **13**, 3578 (2013).
5. Boyett, M. The sinoatrial node, a heterogeneous pacemaker structure. *Cardiovasc. Res.* **47**, 658–687 (2000).
6. Chiba, H., Osanai, M., Murata, M., Kojima, T. & Sawada, N. Transmembrane proteins of tight junctions. *Biochim. Biophys. Acta - Biomembr.* **1778**, 588–600 (2008).
7. Boengler, K., Schulz, R. & Heusch, G. Connexin 43 signalling and cardioprotection. *Heart* **92**, 1724–1727 (2006).
8. Murphy, S. V & Atala, A. 3D bioprinting of tissues and organs. *Nat. Biotechnol.* **32**, 773–785 (2014).
9. Domansky, K. *et al.* Perfused multiwell plate for 3D liver tissue engineering. *Lab Chip* **10**, 51–58 (2010).
10. Fennema, E., Rivron, N., Rouwkema, J., van Blitterswijk, C. & de Boer, J. Spheroid culture as a tool for creating 3D complex tissues. *Trends Biotechnol.* **31**, 108–115 (2013).
11. Gauvin, R. *et al.* Microfabrication of complex porous tissue engineering scaffolds using 3D projection stereolithography. *Biomaterials* **33**, 3824–3834 (2012).
12. Wagner, I. *et al.* A dynamic multi-organ-chip for long-term cultivation and substance testing proven by 3D human liver and skin tissue co-culture. *Lab Chip* **13**, 3538 (2013).
13. Bajaj, P., Schweller, R. M., Khademhosseini, A., West, J. L. & Bashir, R. 3D Biofabrication Strategies for Tissue Engineering and Regenerative Medicine. *Annu. Rev. Biomed. Eng.* **16**, 247–276 (2014).

14. Templeton, I. E., Houston, J. B. & Galetin, A. Predictive Utility of In Vitro Rifampin Induction Data Generated in Fresh and Cryopreserved Human Hepatocytes, Fa2N-4, and HepaRG Cells. *Drug Metab. Dispos.* **39**, 1921–1929 (2011).
15. Peters, M. F., Lamore, S. D., Guo, L., Scott, C. W. & Kolaja, K. L. Human Stem Cell-Derived Cardiomyocytes in Cellular Impedance Assays: Bringing Cardiotoxicity Screening to the Front Line. *Cardiovasc. Toxicol.* **15**, 127–139 (2015).
16. Liu, X., Holzwarth, J. M. & Ma, P. X. Functionalized Synthetic Biodegradable Polymer Scaffolds for Tissue Engineering. *Macromol. Biosci.* **12**, 911–919 (2012).
17. Liao, J., Guo, X., Grande-Allen, K. J., Kasper, F. K. & Mikos, A. G. Bioactive polymer/extracellular matrix scaffolds fabricated with a flow perfusion bioreactor for cartilage tissue engineering. *Biomaterials* **31**, 8911–8920 (2010).
18. Abouna, G. M. Organ Shortage Crisis: Problems and Possible Solutions. *Transplant. Proc.* **40**, 34–38 (2008).
19. The Canadian Council for Donation and Transplantation. at <https://professionaleducation.blood.ca/sites/msi/files/Kidney_Allocation_FINAL.pdf>
20. Pediatric Organ Donation and Transplantation. *Pediatrics* **125**, 822–828 (2010).
21. Sánchez-Fueyo, A. & Strom, T. B. Immunologic Basis of Graft Rejection and Tolerance Following Transplantation of Liver or Other Solid Organs. *Gastroenterology* **140**, 51–64.e2 (2011).
22. Dandel, M., Lehmkuhl, H. B., Knosalla, C. & Hetzer, R. Impact of different long-term maintenance immunosuppressive therapy strategies on patients' outcome after heart transplantation. *Transpl. Immunol.* **23**, 93–103 (2010).
23. Meier-Kriesche, H.-U. & Kaplan, B. Waiting time on dialysis as the strongest modifiable risk factor for renal transplant outcomes: a paired donor kidney analysis. *Transplantation* **74**, 1377–81 (2002).
24. Schold, J. D. Which Renal Transplant Candidates Should Accept Marginal Kidneys in Exchange for a Shorter Waiting Time on Dialysis? *Clin. J. Am. Soc. Nephrol.* **1**, 532–538 (2006).
25. Strauer, B. E. Repair of Infarcted Myocardium by Autologous Intracoronary Mononuclear Bone Marrow Cell Transplantation in Humans. *Circulation* **106**, 1913–1918 (2002).
26. Tsai, R. J.-F., Li, L.-M. & Chen, J.-K. Reconstruction of Damaged Corneas by Transplantation of Autologous Limbal Epithelial Cells. *N. Engl. J. Med.* **343**, 86–93 (2000).

27. Gu, X., Ding, F., Yang, Y. & Liu, J. Construction of tissue engineered nerve grafts and their application in peripheral nerve regeneration. *Prog. Neurobiol.* **93**, 204–230 (2011).
28. Morris, Z. S., Wooding, S. & Grant, J. The answer is 17 years, what is the question: understanding time lags in translational research. *J. R. Soc. Med.* **104**, 510–520 (2011).
29. Trounson, A., Thakar, R. G., Lomax, G. & Gibbons, D. Clinical trials for stem cell therapies. *BMC Med.* **9**, 52 (2011).
30. DiMasi, J. A., Grabowski, H. G. & Hansen, R. W. Innovation in the pharmaceutical industry: New estimates of R&D costs. *J. Health Econ.* **47**, 20–33 (2016).
31. Saha, S., New, L. S., Ho, H. K., Chui, W. K. & Chan, E. C. Y. Investigation of the role of the thiazolidinedione ring of troglitazone in inducing hepatotoxicity. *Toxicol. Lett.* **192**, 141–149 (2010).
32. Lübberstedt, M. *et al.* HepaRG human hepatic cell line utility as a surrogate for primary human hepatocytes in drug metabolism assessment in vitro. *J. Pharmacol. Toxicol. Methods* **63**, 59–68 (2011).
33. Fey, S. J. & Wrzesinski, K. Determination of Drug Toxicity Using 3D Spheroids Constructed From an Immortal Human Hepatocyte Cell Line. *Toxicol. Sci.* **127**, 403–411 (2012).
34. Grapin-Botton, A. Three-dimensional pancreas organogenesis models. *Diabetes, Obes. Metab.* **18**, 33–40 (2016).
35. Masamune, A. & Shimosegawa, T. Pancreatic stellate cells: A dynamic player of the intercellular communication in pancreatic cancer. *Clin. Res. Hepatol. Gastroenterol.* **39**, S98–S103 (2015).
36. Hinrichs, C. S. & Rosenberg, S. A. Exploiting the curative potential of adoptive T-cell therapy for cancer. *Immunol. Rev.* **257**, 56–71 (2014).
37. Müller, B. & Grossniklaus, U. Model organisms — A historical perspective. *J. Proteomics* **73**, 2054–2063 (2010).
38. Mestas, J. & Hughes, C. C. W. Of mice and not men: differences between mouse and human immunology. *J. Immunol.* **172**, 2731–8 (2004).
39. Lin, S. *et al.* Comparison of the transcriptional landscapes between human and mouse tissues. *Proc. Natl. Acad. Sci.* **111**, 17224–17229 (2014).
40. Edmondson, R., Broglie, J. J., Adcock, A. F. & Yang, L. Three-Dimensional Cell Culture Systems and Their Applications in Drug Discovery and Cell-Based Biosensors. *Assay Drug Dev. Technol.* **12**, 207–218 (2014).

41. Zhao, D. *et al.* Notch Signaling Pathway Regulates Angiogenesis via Endothelial Cell in 3D Co-Culture Model. *J. Cell. Physiol.* **232**, 1548–1558 (2017).
42. Hwa, A. J. *et al.* Rat liver sinusoidal endothelial cells survive without exogenous VEGF in 3D perfused co-cultures with hepatocytes. *FASEB J.* **21**, 2564–2579 (2007).
43. Dolznig, H. *et al.* Modeling Colon Adenocarcinomas in Vitro. *Am. J. Pathol.* **179**, 487–501 (2011).
44. Lang, M. *et al.* Thymoquinone attenuates tumor growth in ApcMin mice by interference with Wnt-signaling. *Mol. Cancer* **12**, 41 (2013).
45. Friend, D. S. & Gilula, N. B. Variations in tight and gap junctions in mammalian tissues. *J. Cell Biol.* **53**, 758–76 (1972).
46. Laschke, M. W. *et al.* Angiogenesis in Tissue Engineering: Breathing Life into Constructed Tissue Substitutes. *Tissue Eng.* **12**, 2093–2104 (2006).
47. Soker, S., Machado, M. & Atala, A. Systems for therapeutic angiogenesis in tissue engineering. *World J. Urol.* **18**, 10–18 (2000).
48. Zisch, A. H. Tissue engineering of angiogenesis with autologous endothelial progenitor cells. *Curr. Opin. Biotechnol.* **15**, 424–429 (2004).
49. Van Vlierberghe, S., Dubruel, P. & Schacht, E. Biopolymer-Based Hydrogels As Scaffolds for Tissue Engineering Applications: A Review. *Biomacromolecules* **12**, 1387–1408 (2011).
50. Yin, X. *et al.* Engineering Stem Cell Organoids. *Cell Stem Cell* **18**, 25–38 (2016).
51. Frantz, C., Stewart, K. M. & Weaver, V. M. The extracellular matrix at a glance. *J. Cell Sci.* **123**, 4195–4200 (2010).
52. Kim, B.-S. *et al.* Design of artificial extracellular matrices for tissue engineering. *Prog. Polym. Sci.* **36**, 238–268 (2011).
53. Parenteau-Bareil, R., Gauvin, R. & Berthod, F. Collagen-Based Biomaterials for Tissue Engineering Applications. *Materials (Basel)*. **3**, 1863–1887 (2010).
54. Zhu, J. & Kaufman, L. J. Collagen I Self-Assembly: Revealing the Developing Structures that Generate Turbidity. *Biophys. J.* **106**, 1822–1831 (2014).
55. Lauer-Fields, J. L., Juska, D. & Fields, G. B. Matrix metalloproteinases and collagen catabolism. *Biopolymers* **66**, 19–32 (2002).

56. Dong, C. & Lv, Y. Application of Collagen Scaffold in Tissue Engineering: Recent Advances and New Perspectives. *Polymers (Basel)*. **8**, 42 (2016).
57. Wang, L. & Stegemann, J. P. Thermogelling chitosan and collagen composite hydrogels initiated with β -glycerophosphate for bone tissue engineering. *Biomaterials* **31**, 3976–3985 (2010).
58. Lee, K. Y. & Mooney, D. J. Alginate: Properties and biomedical applications. *Prog. Polym. Sci.* **37**, 106–126 (2012).
59. Murakami, K. *et al.* Hydrogel blends of chitin/chitosan, fucoidan and alginate as healing-impaired wound dressings. *Biomaterials* **31**, 83–90 (2010).
60. Masoumeh Nazarpak & Farzaneh Pourasgari. Fabrication of Tissue Engineering Scaffold from Hydroxyapatite/Alginate Composite. *Int. J. Biosci. Biochem. Bioinforma.* **4**, 142–145 (2014).
61. Shoichet, M. S. Polymer Scaffolds for Biomaterials Applications. *Macromolecules* **43**, 581–591 (2010).
62. Lee, J., Abdeen, A. A. & Kilian, K. A. Rewiring mesenchymal stem cell lineage specification by switching the biophysical microenvironment. *Sci. Rep.* **4**, 5188 (2015).
63. Riboldi, S. A., Sampaolesi, M., Neuenschwander, P., Cossu, G. & Mantero, S. Electrospun degradable polyesterurethane membranes: potential scaffolds for skeletal muscle tissue engineering. *Biomaterials* **26**, 4606–4615 (2005).
64. Byrne, D. P., Lacroix, D., Planell, J. A., Kelly, D. J. & Prendergast, P. J. Simulation of tissue differentiation in a scaffold as a function of porosity, Young's modulus and dissolution rate: Application of mechanobiological models in tissue engineering. *Biomaterials* **28**, 5544–5554 (2007).
65. Shin, H. J. *et al.* Electrospun PLGA nanofiber scaffolds for articular cartilage reconstruction: mechanical stability, degradation and cellular responses under mechanical stimulation in vitro. *J. Biomater. Sci. Polym. Ed.* **17**, 103–119 (2006).
66. Reing, J. E. *et al.* Degradation Products of Extracellular Matrix Affect Cell Migration and Proliferation. *Tissue Eng. Part A* **15**, 605–614 (2009).
67. Okamoto, M. & John, B. Synthetic biopolymer nanocomposites for tissue engineering scaffolds. *Prog. Polym. Sci.* **38**, 1487–1503 (2013).
68. Tyler, B., Gullotti, D., Mangraviti, A., Utsuki, T. & Brem, H. Polylactic acid (PLA) controlled delivery carriers for biomedical applications. *Adv. Drug Deliv. Rev.* **107**, 163–175 (2016).

69. Sinha Ray, S. Polylactide-Based Bionanocomposites: A Promising Class of Hybrid Materials. *Acc. Chem. Res.* **45**, 1710–1720 (2012).
70. Armentano, I., Dottori, M., Fortunati, E., Mattioli, S. & Kenny, J. M. Biodegradable polymer matrix nanocomposites for tissue engineering: A review. *Polym. Degrad. Stab.* **95**, 2126–2146 (2010).
71. Shin, H., Jo, S. & Mikos, A. G. Biomimetic materials for tissue engineering. *Biomaterials* **24**, 4353–4364 (2003).
72. Bendix, D. Chemical synthesis of polylactide and its copolymers for medical applications. *Polym. Degrad. Stab.* **59**, 129–135 (1998).
73. Lopes, M. S., Jardini, A. L. & Filho, R. M. Poly (Lactic Acid) Production for Tissue Engineering Applications. *Procedia Eng.* **42**, 1402–1413 (2012).
74. Li, Y. *et al.* Polyglycolic Acid Fibrous Scaffold Improving Endothelial Cell Coating and Vascularization of Islet. *Chin. Med. J. (Engl.)* **130**, 832 (2017).
75. Suwantong, O. Biomedical applications of electrospun polycaprolactone fiber mats. *Polym. Adv. Technol.* **27**, 1264–1273 (2016).
76. You, Y., Min, B.-M., Lee, S. J., Lee, T. S. & Park, W. H. In vitro degradation behavior of electrospun polyglycolide, polylactide, and poly(lactide-co-glycolide). *J. Appl. Polym. Sci.* **95**, 193–200 (2005).
77. Kanczler, J. M. *et al.* The effect of mesenchymal populations and vascular endothelial growth factor delivered from biodegradable polymer scaffolds on bone formation. *Biomaterials* **29**, 1892–1900 (2008).
78. Lu, H. *et al.* Spatial immobilization of bone morphogenetic protein-4 in a collagen-PLGA hybrid scaffold for enhanced osteoinductivity. *Biomaterials* **33**, 6140–6146 (2012).
79. Bhardwaj, N. & Kundu, S. C. Electrospinning: A fascinating fiber fabrication technique. *Biotechnol. Adv.* **28**, 325–347 (2010).
80. Pham, Q. P., Sharma, U. & Mikos, A. G. Electrospun Poly(ϵ -caprolactone) Microfiber and Multilayer Nanofiber/Microfiber Scaffolds: Characterization of Scaffolds and Measurement of Cellular Infiltration. *Biomacromolecules* **7**, 2796–2805 (2006).
81. Mo, X. ., Xu, C. ., Kotaki, M. & Ramakrishna, S. Electrospun P(LLA-CL) nanofiber: a biomimetic extracellular matrix for smooth muscle cell and endothelial cell proliferation. *Biomaterials* **25**, 1883–1890 (2004).

82. Ekaputra, A. K., Prestwich, G. D., Cool, S. M. & Hutmacher, D. W. Combining Electrospun Scaffolds with Electrospayed Hydrogels Leads to Three-Dimensional Cellularization of Hybrid Constructs. *Biomacromolecules* **9**, 2097–2103 (2008).
83. Haidar, M. & Eroglu, H. Nanofibers: New Insights for Drug Delivery and Tissue Engineering. *Curr. Top. Med. Chem.* **17**, 1564–1579 (2017).
84. Murphy, S. V & Atala, A. 3D bioprinting of tissues and organs. *Nat. Biotechnol.* **32**, 773–785 (2014).
85. Malda, J. *et al.* 25th Anniversary Article: Engineering Hydrogels for Biofabrication. *Adv. Mater.* **25**, 5011–5028 (2013).
86. Peltola, S. M., Melchels, F. P. W., Grijpma, D. W. & Kellomäki, M. A review of rapid prototyping techniques for tissue engineering purposes. *Ann. Med.* **40**, 268–280 (2008).
87. Chia, H. N. & Wu, B. M. Recent advances in 3D printing of biomaterials. *J. Biol. Eng.* **9**, 4 (2015).
88. Fedorovich, N. E., Alblas, J., Hennink, W. E., Öner, F. C. & Dhert, W. J. A. Organ printing: the future of bone regeneration? *Trends Biotechnol.* **29**, 601–606 (2011).
89. Merceron, T. K. *et al.* A 3D bioprinted complex structure for engineering the muscle–tendon unit. *Biofabrication* **7**, 35003 (2015).
90. Mannoor, M. S. *et al.* 3D Printed Bionic Ears. *Nano Lett.* **13**, 2634–2639 (2013).
91. Song, J. J. & Ott, H. C. Organ engineering based on decellularized matrix scaffolds. *Trends Mol. Med.* **17**, 424–432 (2011).
92. GILBERT, T., SELLARO, T. & BADYLAK, S. Decellularization of tissues and organs. *Biomaterials* (2006). doi:10.1016/j.biomaterials.2006.02.014
93. Ott, H. C. *et al.* Regeneration and orthotopic transplantation of a bioartificial lung. *Nat. Med.* **16**, 927–933 (2010).
94. Crapo, P. M., Gilbert, T. W. & Badylak, S. F. An overview of tissue and whole organ decellularization processes. *Biomaterials* **32**, 3233–3243 (2011).
95. Ott, H. C. *et al.* Perfusion-decellularized matrix: using nature’s platform to engineer a bioartificial heart. *Nat. Med.* **14**, 213–221 (2008).
96. Song, J. J. *et al.* Regeneration and experimental orthotopic transplantation of a bioengineered kidney. *Nat. Med.* **19**, 646–651 (2013).

97. Uygun, B. E. *et al.* Organ reengineering through development of a transplantable recellularized liver graft using decellularized liver matrix. *Nat. Med.* **16**, 814–820 (2010).
98. Lancaster, M. A. & Knoblich, J. A. Organogenesis in a dish: Modeling development and disease using organoid technologies. *Science (80-.)*. **345**, 1247125–1247125 (2014).
99. Uygun, B. E. *et al.* Organ reengineering through development of a transplantable recellularized liver graft using decellularized liver matrix. *Nat. Med.* **16**, 814–820 (2010).
100. Spence, J. R. *et al.* Directed differentiation of human pluripotent stem cells into intestinal tissue in vitro. *Nature* **470**, 105–109 (2011).
101. Lancaster, M. A. *et al.* Cerebral organoids model human brain development and microcephaly. *Nature* **501**, 373–379 (2013).
102. Voges, H. K. *et al.* Development of a human cardiac organoid injury model reveals innate regenerative potential. *Development* **144**, 1118–1127 (2017).
103. Huch, M., Boj, S. F. & Clevers, H. Lgr5⁺ liver stem cells, hepatic organoids and regenerative medicine. *Regen. Med.* **8**, 385–387 (2013).
104. Kim, S.-H., Turnbull, J. & Guimond, S. Extracellular matrix and cell signalling: the dynamic cooperation of integrin, proteoglycan and growth factor receptor. *J. Endocrinol.* **209**, 139–151 (2011).
105. Rozario, T. & DeSimone, D. W. The extracellular matrix in development and morphogenesis: A dynamic view. *Dev. Biol.* **341**, 126–140 (2010).
106. Whang, M. & Kim, J. Synthetic hydrogels with stiffness gradients for durotaxis study and tissue engineering scaffolds. *Tissue Eng. Regen. Med.* **13**, 126–139 (2016).
107. Lazopoulos, K. A. & Stamenović, D. Durotaxis as an elastic stability phenomenon. *J. Biomech.* **41**, 1289–1294 (2008).
108. NEUMAN, R. E. & LOGAN, M. A. The determination of collagen and elastin in tissues. *J. Biol. Chem.* **186**, 549–56 (1950).
109. Mancini, A. Transcriptional regulation of matrix metalloprotease gene expression in health and disease. *Front. Biosci.* **11**, 423 (2006).
110. Hynes, R. O. The extracellular matrix: not just pretty fibrils. *Science* **326**, 1216–9 (2009).
111. Di Lullo, G. A., Sweeney, S. M., Korkko, J., Ala-Kokko, L. & San Antonio, J. D. Mapping the Ligand-binding Sites and Disease-associated Mutations on the Most Abundant Protein in the Human, Type I Collagen. *J. Biol. Chem.* **277**, 4223–4231 (2002).

112. Shoulders, M. D. & Raines, R. T. Collagen Structure and Stability. *Annu. Rev. Biochem.* **78**, 929–958 (2009).
113. Heino, J. The collagen family members as cell adhesion proteins. *BioEssays* **29**, 1001–1010 (2007).
114. Rodgers, U. R. & Weiss, A. S. Cellular interactions with elastin. *Pathol. Biol.* **53**, 390–398 (2005).
115. Mao, Y. & Schwarzbauer, J. E. Fibronectin fibrillogenesis, a cell-mediated matrix assembly process. *Matrix Biol.* **24**, 389–399 (2005).
116. Katsumi, A., Orr, A. W., Tzima, E. & Schwartz, M. A. Integrins in Mechanotransduction. *J. Biol. Chem.* **279**, 12001–12004 (2004).
117. Ruoslahti, E. Integrins. *J. Clin. Invest.* **87**, 1–5 (1991).
118. Imberty, A., Lortat-Jacob, H. & Pérez, S. Structural view of glycosaminoglycan–protein interactions. *Carbohydr. Res.* **342**, 430–439 (2007).
119. Tillman, T. S. & Cascio, M. Effects of Membrane Lipids on Ion Channel Structure and Function. *Cell Biochem. Biophys.* **38**, 161–190 (2003).
120. Doherty, G. J. & McMahon, H. T. Mechanisms of Endocytosis. *Annu. Rev. Biochem.* **78**, 857–902 (2009).
121. van Meer, G., Voelker, D. R. & Feigenson, G. W. Membrane lipids: where they are and how they behave. *Nat. Rev. Mol. Cell Biol.* **9**, 112–124 (2008).
122. Dowhan, W. MOLECULAR BASIS FOR MEMBRANE PHOSPHOLIPID DIVERSITY: Why Are There So Many Lipids? *Annu. Rev. Biochem.* **66**, 199–232 (1997).
123. Wirtz, K. Phospholipid Transfer Proteins. *Annu. Rev. Biochem.* **60**, 73–99 (1991).
124. Lingwood, D. & Simons, K. Lipid Rafts As a Membrane-Organizing Principle. *Science (80-)*. **327**, 46–50 (2010).
125. Tarbell, J. M. & Cancel, L. M. The glycocalyx and its significance in human medicine. *J. Intern. Med.* **280**, 97–113 (2016).
126. VANCE, J. & STEENBERGEN, R. Metabolism and functions of phosphatidylserine. *Prog. Lipid Res.* **44**, 207–234 (2005).
127. Daleke, D. L. Regulation of transbilayer plasma membrane phospholipid asymmetry. *J. Lipid Res.* **44**, 233–242 (2003).

128. Reitsma, S., Slaaf, D. W., Vink, H., van Zandvoort, M. A. M. J. & oude Egbrink, M. G. A. The endothelial glycocalyx: composition, functions, and visualization. *Pflügers Arch. - Eur. J. Physiol.* **454**, 345–359 (2007).
129. Parker, W. *et al.* Fate of antigen in xenotransplantation: implications for acute vascular rejection and accommodation. *Am. J. Pathol.* **152**, 829–39 (1998).
130. Vinken, M. *et al.* Connexins and their channels in cell growth and cell death. *Cell. Signal.* **18**, 592–600 (2006).
131. Verkman, A. S. Aquaporins in Clinical Medicine. *Annu. Rev. Med.* **63**, 303–316 (2012).
132. Borst, P. & Elferink, R. O. Mammalian ABC Transporters in Health and Disease. *Annu. Rev. Biochem.* **71**, 537–592 (2002).
133. Loose, M. & Schwille, P. Biomimetic membrane systems to study cellular organization. *J. Struct. Biol.* **168**, 143–151 (2009).
134. Rabuka, D., Forstner, M. B., Groves, J. T. & Bertozzi, C. R. Noncovalent Cell Surface Engineering: Incorporation of Bioactive Synthetic Glycopolymers into Cellular Membranes. *J. Am. Chem. Soc.* **130**, 5947–5953 (2008).
135. Wang, H. *et al.* Cellular Membrane Enrichment of Self-Assembling d -Peptides for Cell Surface Engineering. *ACS Appl. Mater. Interfaces* **6**, 9815–9821 (2014).
136. Cone, R. E., Marchalonis, J. J. & Rolley, R. T. Lymphocyte membrane dynamics. Metabolic release of cell surface proteins. *J. Exp. Med.* **134**, 1373–84 (1971).
137. Lee, J.-J., Son, J., Ha, H.-H. & Chang, Y.-T. Fluorescent labeling of membrane proteins on the surface of living cells by a self-catalytic glutathione S-transferase omega 1 tag. *Mol. Biosyst.* **7**, 1270 (2011).
138. Stephan, M. T. & Irvine, D. J. Enhancing cell therapies from the outside in: Cell surface engineering using synthetic nanomaterials. *Nano Today* **6**, 309–325 (2011).
139. Liao, K.-W. *et al.* Stable expression of chimeric anti-CD3 receptors on mammalian cells for stimulation of antitumor immunity. *Cancer Gene Ther.* **10**, 779–790 (2003).
140. Sadelain, M., Brentjens, R. & Rivière, I. The promise and potential pitfalls of chimeric antigen receptors. *Curr. Opin. Immunol.* **21**, 215–223 (2009).
141. Ran, F. A. *et al.* Genome engineering using the CRISPR-Cas9 system. *Nat. Protoc.* **8**, 2281–2308 (2013).
142. Kato, M. & Mrksich, M. Rewiring Cell Adhesion. *J. Am. Chem. Soc.* **126**, 6504–6505 (2004).

143. Hang, H. C., Yu, C., Kato, D. L. & Bertozzi, C. R. A metabolic labeling approach toward proteomic analysis of mucin-type O-linked glycosylation. *Proc. Natl. Acad. Sci.* **100**, 14846–14851 (2003).
144. Wilson, J. T. *et al.* Cell Surface Engineering with Polyelectrolyte Multilayer Thin Films. *J. Am. Chem. Soc.* **133**, 7054–7064 (2011).
145. Swiston, A. J. *et al.* Surface Functionalization of Living Cells with Multilayer Patches. *Nano Lett.* **8**, 4446–4453 (2008).
146. Felice, B., Prabhakaran, M. P., Rodríguez, A. P. & Ramakrishna, S. Drug delivery vehicles on a nano-engineering perspective. *Mater. Sci. Eng. C* **41**, 178–195 (2014).
147. Bozzuto, G. & Molinari, A. Liposomes as nanomedical devices. *Int. J. Nanomedicine* **975** (2015). doi:10.2147/IJN.S68861
148. Ulrich, A. S. Biophysical aspects of using liposomes as delivery vehicles. *Biosci. Rep.* **22**, 129–50 (2002).
149. Clerc, S. & Barenholz, Y. Loading of amphipathic weak acids into liposomes in response to transmembrane calcium acetate gradients. *Biochim. Biophys. Acta* **1240**, 257–65 (1995).
150. Saxon, D. N., Mayer, L. D. & Bally, M. B. Liposomal Anticancer Drugs as Agents to be used in Combination with other Anticancer Agents: Studies on a Liposomal Formulation with two Encapsulated Drugs. *J. Liposome Res.* **9**, 507–522 (1999).
151. Noble, G. T., Stefanick, J. F., Ashley, J. D., Kiziltepe, T. & Bilgicer, B. Ligand-targeted liposome design: challenges and fundamental considerations. *Trends Biotechnol.* **32**, 32–45 (2014).
152. Medina, O. P., Zhu, Y. & Kairemo, K. Targeted liposomal drug delivery in cancer. *Curr. Pharm. Des.* **10**, 2981–9 (2004).
153. Shim, G., Kim, M.-G., Park, J. Y. & Oh, Y.-K. Application of cationic liposomes for delivery of nucleic acids. *Asian J. Pharm. Sci.* **8**, 72–80 (2013).
154. Ikeda, A., Funada, R. & Sugikawa, K. Different stabilities of liposomes containing saturated and unsaturated lipids toward the addition of cyclodextrins. *Org. Biomol. Chem.* **14**, 5065–5072 (2016).
155. Gracià, R. S., Bezlyepkina, N., Knorr, R. L., Lipowsky, R. & Dimova, R. Effect of cholesterol on the rigidity of saturated and unsaturated membranes: fluctuation and electrodeformation analysis of giant vesicles. *Soft Matter* **6**, 1472 (2010).

156. Bhatia, T. *et al.* Preparing giant unilamellar vesicles (GUVs) of complex lipid mixtures on demand: Mixing small unilamellar vesicles of compositionally heterogeneous mixtures. *Biochim. Biophys. Acta - Biomembr.* **1848**, 3175–3180 (2015).
157. Lin, C.-M., Li, C.-S., Sheng, Y.-J., Wu, D. T. & Tsao, H.-K. Size-Dependent Properties of Small Unilamellar Vesicles Formed by Model Lipids. *Langmuir* **28**, 689–700 (2012).
158. Akbarzadeh, A., Rezaei-Sadabady, R., Davaran, S., Joo, S. W., Zarghami, N., Hanifehpour, Y., ... Nejati-Koshki, K. (2013). Liposome: classification, preparation, and applications. *Nanoscale Research Letters*, 8(1), 102. <http://doi.org/10.1186/1556-276X-8-102>
159. Chernomordik, L. V & Kozlov, M. M. Mechanics of membrane fusion. *Nat. Struct. Mol. Biol.* **15**, 675–683 (2008).
160. Jahn, R., Lang, T. & Südhof, T. C. Membrane Fusion. *Cell* **112**, 519–533 (2003).
161. Hernandez, J. M., Kreutzberger, A. J. B., Kiessling, V., Tamm, L. K. & Jahn, R. Variable cooperativity in SNARE-mediated membrane fusion. *Proc. Natl. Acad. Sci.* **111**, 12037–12042 (2014).
162. Hernandez, J. M., Kreutzberger, A. J. B., Kiessling, V., Tamm, L. K. & Jahn, R. Variable cooperativity in SNARE-mediated membrane fusion. *Proc. Natl. Acad. Sci.* **111**, 12037–12042 (2014).
163. Drummond, D. C., Zignani, M. & Leroux, J.-C. Current status of pH-sensitive liposomes in drug delivery. *Prog. Lipid Res.* **39**, 409–460 (2000).
164. Martín-Molina, A., Rodríguez-Beas, C. & Faraudo, J. Effect of Calcium and Magnesium on Phosphatidylserine Membranes: Experiments and All-Atomic Simulations. *Biophys. J.* **102**, 2095–2103 (2012).
165. Karanth, H. & Murthy, R. S. R. pH-Sensitive liposomes-principle and application in cancer therapy. *J. Pharm. Pharmacol.* **59**, 469–483 (2007).
166. Zuris, J. A. *et al.* Cationic lipid-mediated delivery of proteins enables efficient protein-based genome editing in vitro and in vivo. *Nat. Biotechnol.* **33**, 73–80 (2014).
167. Sercombe, L. *et al.* Advances and Challenges of Liposome Assisted Drug Delivery. *Front. Pharmacol.* **6**, (2015).
168. Schwendener, R. A. Liposomes as vaccine delivery systems: a review of the recent advances. *Ther. Adv. Vaccines* **2**, 159–182 (2014).
169. Dalby, B. Advanced transfection with Lipofectamine 2000 reagent: primary neurons, siRNA, and high-throughput applications. *Methods* **33**, 95–103 (2004).

170. Hang, H. C., Yu, C., Kato, D. L. & Bertozzi, C. R. A metabolic labeling approach toward proteomic analysis of mucin-type O-linked glycosylation. *Proc. Natl. Acad. Sci.* **100**, 14846–14851 (2003).
171. Sletten, E. M. & Bertozzi, C. R. From Mechanism to Mouse: A Tale of Two Bioorthogonal Reactions. *Acc. Chem. Res.* **44**, 666–676 (2011).
172. Sletten, E. M. & Bertozzi, C. R. Bioorthogonal Chemistry: Fishing for Selectivity in a Sea of Functionality. *Angew. Chemie Int. Ed.* **48**, 6974–6998 (2009).
173. Kiick, K. L., Saxon, E., Tirrell, D. A. & Bertozzi, C. R. Incorporation of azides into recombinant proteins for chemoselective modification by the Staudinger ligation. *Proc. Natl. Acad. Sci.* **99**, 19–24 (2002).
174. Rostovtsev, V. V., Green, L. G., Fokin, V. V. & Sharpless, K. B. A Stepwise Huisgen Cycloaddition Process: Copper(I)-Catalyzed Regioselective ‘Ligation’ of Azides and Terminal Alkynes. *Angew. Chemie Int. Ed.* **41**, 2596–2599 (2002).
175. Zhang, X. & Zhang, Y. Applications of Azide-Based Bioorthogonal Click Chemistry in Glycobiology. *Molecules* **18**, 7145–7159 (2013).
176. Gramlich, P. M. E., Wirges, C. T., Manetto, A. & Carell, T. Postsynthetic DNA Modification through the Copper-Catalyzed Azide-Alkyne Cycloaddition Reaction. *Angew. Chemie Int. Ed.* **47**, 8350–8358 (2008).
177. Wang, Q. *et al.* Bioconjugation by Copper(I)-Catalyzed Azide-Alkyne [3 + 2] Cycloaddition. *J. Am. Chem. Soc.* **125**, 3192–3193 (2003).
178. Agard, N. J., Prescher, J. A. & Bertozzi, C. R. A Strain-Promoted [3 + 2] Azide-Alkyne Cycloaddition for Covalent Modification of Biomolecules in Living Systems [*J. Am. Chem. Soc.* **2004**, *126*, 15046–15047]. *J. Am. Chem. Soc.* **127**, 11196–11196 (2005).
179. Agard, N. J., Baskin, J. M., Prescher, J. A., Lo, A. & Bertozzi, C. R. A Comparative Study of Bioorthogonal Reactions with Azides. *ACS Chem. Biol.* **1**, 644–648 (2006).
180. Blackman, M. L., Royzen, M. & Fox, J. M. Tetrazine Ligation: Fast Bioconjugation Based on Inverse-Electron-Demand Diels–Alder Reactivity. *J. Am. Chem. Soc.* **130**, 13518–13519 (2008).
181. O’Brien, P. J., Luo, W., Rogozhnikov, D., Chen, J. & Yousaf, M. N. Spheroid and Tissue Assembly via Click Chemistry in Microfluidic Flow. *Bioconjug. Chem.* **26**, 1939–1949 (2015).
182. Park, S. & Yousaf, M. N. An Interfacial Oxime Reaction To Immobilize Ligands and Cells in Patterns and Gradients to Photoactive Surfaces. *Langmuir* **24**, 6201–6207 (2008).

183. Kretzschmar, K. & Clevers, H. Organoids: Modeling Development and the Stem Cell Niche in a Dish. *Dev. Cell* **38**, 590–600 (2016).
184. Van Vlierberghe, S., Dubruel, P. & Schacht, E. Biopolymer-Based Hydrogels As Scaffolds for Tissue Engineering Applications: A Review. *Biomacromolecules* **12**, 1387–1408 (2011).
185. Tajbakhsh, S. & Hajiali, F. A comprehensive study on the fabrication and properties of biocomposites of poly(lactic acid)/ceramics for bone tissue engineering. *Mater. Sci. Eng. C* **70**, 897–912 (2017).
186. Williams, D. F. On the mechanisms of biocompatibility. *Biomaterials* **29**, 2941–2953 (2008).
187. Kean, T. & Thanou, M. Biodegradation, biodistribution and toxicity of chitosan. *Adv. Drug Deliv. Rev.* **62**, 3–11 (2010).
188. ZIMMERMANN, W. *et al.* Heart muscle engineering: An update on cardiac muscle replacement therapy. *Cardiovasc. Res.* **71**, 419–429 (2006).
189. Mintrom, M. Policy entrepreneurs and controversial science: governing human embryonic stem cell research. *J. Eur. Public Policy* **20**, 442–457 (2013).
190. Chen, H., Zhang, H., Thor, D., Rahimian, R. & Guo, X. Novel pH-sensitive cationic lipids with linear ortho ester linkers for gene delivery. *Eur. J. Med. Chem.* **52**, 159–172 (2012).
191. Dutta, D., Pulsipher, A., Luo, W., Mak, H. & Yousaf, M. N. Engineering Cell Surfaces via Liposome Fusion. *Bioconjug. Chem.* **22**, 2423–2433 (2011).
192. Rogozhnikov, D., O'Brien, P. J., Elahipanah, S. & Yousaf, M. N. Scaffold Free Bio-orthogonal Assembly of 3-Dimensional Cardiac Tissue via Cell Surface Engineering. *Sci. Rep.* **6**, 39806 (2016).
193. Dutta, D., Pulsipher, A., Luo, W., Mak, H. & Yousaf, M. N. Engineering Cell Surfaces via Liposome Fusion. *Bioconjug. Chem.* **22**, 2423–2433 (2011).
194. Pulsipher, A., Griffin, M. E., Stone, S. E., Brown, J. M. & Hsieh-Wilson, L. C. Directing Neuronal Signaling through Cell-Surface Glycan Engineering. *J. Am. Chem. Soc.* **136**, 6794–6797 (2014).
195. O'Brien, P. J., Elahipanah, S., Rogozhnikov, D. & Yousaf, M. N. Bio-Orthogonal Mediated Nucleic Acid Transfection of Cells via Cell Surface Engineering. *ACS Cent. Sci.* **3**, 489–500 (2017).
196. Elahipanah, S. *et al.* Rewiring Gram-Negative Bacteria Cell Surfaces with Bio-Orthogonal Chemistry via Liposome Fusion. *Bioconjug. Chem.* **27**, 1082–1089 (2016).

Chapter 2

Scaffold Free Bio-orthogonal Assembly of 3-Dimensional Cardiac Tissue via Cell Surface Engineering

This work has been published in Nature Scientific Reports, Volume 6, Article number 39806 in 2016 under the title " Scaffold Free Bio-orthogonal Assembly of 3-Dimensional Cardiac Tissue via Cell Surface Engineering" It is reprinted with permission (© Nature Publishing Group 2016). Rogozhnikov, D., O'Brien, P. J., Elahipanah, S. & Yousaf, M. N are co-authors of this work."

Contributions

M.N.Y. designed the study. D.R., P.J.O. and S.E. performed the experiments. M.N.Y., D.R., P.J.O., and S.E. analyzed the data. D.R., and M.N.Y. wrote the manuscript.

2.1 Summary

There has been tremendous interest in constructing *in vitro* cardiac tissue for a range of fundamental studies of cardiac development and disease and as a commercial system to evaluate therapeutic drug discovery prioritization and toxicity. Although there has been progress towards studying 2-dimensional cardiac function *in vitro*, there remain challenging obstacles to generate rapid and efficient scaffold-free 3-dimensional multiple cell type co-culture cardiac tissue models. Herein, we develop a programmed rapid self-assembly strategy to induce specific and stable cell-cell contacts among multiple cell types found in heart tissue to generate 3D tissues through cell-surface engineering based on liposome delivery and fusion to display bio-orthogonal functional groups from cell membranes. We generate, for the first time, a scaffold free and stable self-assembled 3 cell line co-culture 3D cardiac tissue model by assembling cardiomyocytes, endothelial cells and cardiac fibroblast cells via a rapid inter-cell click ligation process. We compare and analyze the function of the 3D cardiac tissue chips with 2D co-culture monolayers by assessing cardiac specific markers, electromechanical cell coupling, beating rates and evaluating drug toxicity.

2.2 Introduction

The generation of complex three-dimensional (3D) tissues with multiple cell types in vitro is the pinnacle of the lab on a chip, tissue engineering and artificial organ research fields.¹⁻³

Innovations in developing these types of tissues and assemblies are needed in order to revolutionize transplantation medicine, biomedical and drug discovery research.⁴⁻⁶

Multidisciplinary approaches combining cell biology, bioengineering, polymer chemistry and regenerative medicine have resulted in the first wave of artificial tissue prototypes spanning pancreas, liver, kidney, skin and lung.⁷⁻¹⁰ Although each organ has a specific architecture and comprise of multiple cell types, a special challenge in the artificial tissue field is the generation of cardiac tissue. The heart is a very cell dense muscular organ which pumps blood through arteries and veins of the circulatory system. Cardiovascular associated diseases are the leading cause of death globally and account for 40% of deaths in North America.¹¹ Furthermore, during the drug discovery process, cardiotoxicity is one of the major obstacles that result in the removal of drug candidates from clinical trials.¹² Therefore, production of 3-dimensional artificial cardiac tissues for fundamental studies of heart disease, transplantation and evaluation of drug toxicity is an important and intense area of research. A key design criteria to create a functional tissue in vitro is a method to assemble multiple cell types into a 3D structure.¹³ The assembly method has to be efficient, inexpensive, non-immunogenic and non-cytotoxic. Techniques currently used for making 3D tissues include trapping cells in synthetic and natural polymer scaffolds. Natural scaffolds include collagen, matrigel, alginate, gelatin, chitosan as well as silk fibers and synthetic scaffolds include polymers such as polylactic acid, polyglycolic acid and their composites.¹⁴⁻¹⁶ These materials have revolutionized tissue engineering research and allowed for 3D cell

encapsulation and provide tunable mechanical properties such as controlled stiffness and elasticity. However, there are many parameters that need to be considered to make a scaffold-based tissue. These include: scaffold stability, porosity for oxygen and nutrients exchange, the rate of scaffold degradation, cytotoxicity of degradation by-products and potential inflammatory responses.¹⁷ Furthermore, each scaffold type has a certain cross-linking density and therefore volume, and when mixed with cells, significantly reduces the cell density in the matrix/tissue hybrid material. This excluded volume from the scaffold creates a barrier for formation of high-density cell-cell junctions to establish intercellular communication. Such inter-connections are especially crucial for cardiac tissue, which requires a very high density of cells in order to enable long-range communication between cells via propagation of electrical signals to produce mechanical contractions that pump blood through long range synchronous beating. Cardiac tissue generation via polymer scaffolds in vitro is particularly challenging due to the much higher density of cells contained in the heart compared to any other organ (2–3% of heart tissue contains extracellular matrix while skin contains approximately 70%).¹⁸ In order to achieve synchronized long distance beating of tissue, the cells must have control of uninterrupted ion flow through their cytoplasm, which is only possible when they are physically interconnected through intercellular junction proteins called connexins.¹⁹

Herein, we present a scaffold-free method to generate high density 3- dimensional cardiac tissue consisting of multiple cardiac cell types. The self-assembly strategy combines for the first time, cell surface engineering and bio-orthogonal chemistry to rapidly click together 3 different cell types to generate a functional in vitro cardiac tissue. No external scaffold is used and the cells are the only building blocks of the generated cardiac tissue. We evaluate the self-assembled cardiac tissue with several assays including antibody markers, electromechanical

beating rates, extracellular matrix production and influence of drugs on 2D and 3D synthesized cardiac tissues. To our knowledge, this is the first example of a 3-dimensional cardiac tissue that initially only consists of cells and does not contain any external supporting structure or scaffold.

2.3 Experimental

2.3.1 Ethical Statement

Experimental animals were housed in a temperature controlled environment under 12 h light and 12 h dark conditions, and were fed ad-libitum. Animal facilities met Canadian Council on Animal Care guidelines and all protocols used were approved by the York University Animal Care Committee.

2.3.2 Cardiomyocytes isolation

Neonatal cardiomyocytes were isolated from newborn 1–2 day old Sprague Dawley rat pups. The pups were euthanized via spinal dislocation and their hearts were excised. The atrial parts of the hearts were removed and the hearts were cut in half to remove blood fluid. The procedure was performed in CBFHH buffer: 137 mM NaCl, 20 mM Hepes, 0.44 mM KH₂PO₄, 5.6 mM dextrose, 5.4 mM KCl, 0.8 mM MgSO₄, pH 7.4. The hearts were then trimmed with surgical scissors into small pieces (1–1.5 mm²). The cardiac tissue was digested via serial digestion in enzymatic buffer: CBFHH buffer + 1.5 mg/ml of trypsin. Digestion was performed in a series of steps, 5 min each at 37 °C. The digests were collected into a test tube containing 5 mL of concentrated FBS. The cells were centrifuged at 800 rpm for 5 min. The cells were placed in a

flask containing Ham's F-12 Medium (10% FBS, 1% penicillin/streptomycin) medium and incubated for 45 min, to allow cardiac fibroblasts present in the tissue to adhere to the bottom of the flask. The medium containing purified cardiomyocytes was then transferred to a separate flask.

2.3.3 Tissue culture

Human umbilical vein endothelial cells (HUVEC) were purchased from ATCC (Canada). The cells were cultured on round 10 cm plastic tissue culture plates. The medium used was F-12K Medium (Kaighn's Modification of Ham's F-12 Medium) with 10% fetal bovine serum (FBS), 0.1 mg/ml heparin (Sigma), 0.05 mg/ml endothelial cell growth supplement (ECGS) (Sigma) and 1% penicillin/streptomycin. The cells were incubated at 37 °C, 5% CO₂, the medium was replaced every 48 h and the cells were passaged upon reaching 90% confluence. Human neonatal dermal fibroblasts were purchased from ATCC (Canada). The fibroblasts were cultured in Dulbecco's modified Eagle high glucose medium (DMEM) with 10% FBS and 1% penicillin/streptomycin.

2.3.4 Preparation of liposomes

To prepare oxyamine and ketone-tethered liposomes, chloroform solutions of palmitoyl-oleoyl phosphatidylcholine (POPC), 1,2 dioleoyl-3-trimethylammonium-propane (DOTAP) were mixed with O-dodecylamine (for oxyamine-tethered liposomes) or dodecanone (for ketone-tethered liposomes) on the following ratios: POPC (430 µL, 10 mg/mL in CHCl₃ at 86 mol%); DOTAP

(10 μ L, 10 mg/mL in CHCl_3 at 2 mol%); and O-dodecyloxyamine or dodecanone (60 μ L, 10 mM in CHCl_3 at 12 mol%). The mixtures of lipids were thoroughly dried and then re-suspended in 3 ml of phosphate-buffered saline (PBS). The suspension was then sonicated with a tip sonicator at the power of 20 Watts for 20 min until it was clear.

2.3.5 Tissue assembly

Isolated cardiomyocytes were centrifuged at 600 rpm for 5 min and the medium was discarded. HUVECs and human neonatal fibroblasts were allowed to achieve 85–90% confluence prior to tissue assembly and were trypsinized and centrifuged at 800 rpm for 5 min. 500 μ l of oxyamine- or ketone-tethered liposomes were added to the cell pellet, the cells were re-suspended and incubated at 37 °C for 5 min. The cells were then washed with PBS and re-centrifuged. The PBS was discarded and the oxyamine- and ketone- labeled cardiomyocytes, HUVECs and fibroblasts were mixed in a small volume of combined (1:1) Ham's F12: F-12K Kaighn's medium with heparin and ECGF. The total cell concentration was 5×10^6 cells/ml. 50 μ L drops of the concentrated re-suspended cell solutions were then placed on 1 cm^2 nitrocellulose-coated glass slides and given a slight shake to induce cell assembly. Each mixed (co-culture) 2D or 3D sample contained 1×10^5 cardiomyocytes, 1×10^5 HUVECs and 5×10^4 fibroblasts. Each 2D and 3D cardiomyocyte-only culture (monoculture) contained 1×10^5 cells. The cells were then incubated at 37 °C and 5% CO_2 for 24 h to achieve full spreading into tissues. Upon spreading of cells, fresh medium was added to the plates. Cells in the control samples were treated with non-functionalized liposomes.

2.3.6 Immunohistochemistry and confocal microscopy

Prior to tissue assembly, cells were incubated in serum-free medium containing fluorescent live stain (Life Technologies) dyes. Neonatal rat cardiomyocytes, HUVECS, and human neonatal fibroblasts were treated with 25 μ M CellTracker™ Blue CMAC (7-amino-4-chloromethylcoumarin), 25 μ M CellTracker™ Green CMFDA (5-chloromethylfluorescein diacetate), and 25 μ M CellTracker™ Red CMTPX respectively. The cells were incubated at 37 °C for 45 min, and then washed thoroughly with PBS and incubated in serum-free medium for an additional 45 min. The cells were then assembled into 3D tissues and incubated for 24 h. Subsequently, the tissues were fixed with 4% formalin for 10 min and visualized with LSM-700 (Zeiss) confocal microscope.

2.3.7 Immunostaining

The cells were fixed with 4% formalin for 10 min at room temperature and washed 4 times with PBS. To permeabilize the cell membrane, the samples were incubated in cold (−20 °C) 90% methanol for 5 min at 4 °C. Methanol was decanted and the cells were rinsed 3 times with PBS. The samples were treated with a blocking solution of 5% FBS in PBS at 37 °C for 60 min. While blocking, the dilution of primary monoclonal antibodies were prepared in 5% FBS. The 500–600X dilutions of anti-connexin 43, anti-cardiac troponin T or anti-CD31 primary antibodies (Abcam) were used. The blocking solution was removed and the samples were incubated with the solution of primary antibodies at 4 °C for 12 h. The solution was aspirated and the samples were washed 3 times with PBS. Following that, the samples were incubated in solution 900X-diluted FITC- and TRITC-conjugated secondary antibodies in the dark for 2 h at room

temperature. The samples were washed 3 times with PBS and visualized under fluorescent microscope.

2.3.8 Fluorescent staining for Collagen and Elastin

To observe the secretion of ECM over time for the various assembled 2D and 3D tissues, the samples were treated with Col-F fluorescent probe (Immunochemistry Technologies, MN), which has an affinity for collagen and elastin. The stock solution of Col-F (20 mM) was prepared in DMSO. The medium was replaced with the medium containing 20 μ M Col-F. The cells were incubated at 37 °C for 60 min, after which they were washed thoroughly with PBS and fixed with 4% formalin for 10 min with subsequent staining with DAPI for visualization of cellular nuclei. The samples were visualized under fluorescent microscope with excitation wavelength of 488 nm and emission of 520 nm.

2.3.9 Fluorescent Calcium Imaging

The tissues were incubated with 5 μ M of the calcium-sensitive dye Fluo-4 AM (Life Technologies) for 20 min at 37 °C. The samples were washed with Tyrode salt solution for 20 min and calcium transients were recorded using fluorescent imaging with excitation wavelength of 488 nm. Recording was performed for the duration of 10 s with the frequency of 67 frames per second (fps).

2.3.10 Cardiotoxicity testing

72 h upon tissue assembly, the tissue response to cytotoxic effects of two drugs, isoprenaline and doxorubicin (Sigma) were evaluated. The stock solutions of the drugs were prepared in DMSO. Each drug was dissolved in the culture medium and added to the slide containing assembled tissue. The control samples were treated with DMSO containing medium. The samples were incubated for 25 min with the corresponding drug and the change in the beating rate relative to the control was measured. Twenty independent experiments were performed for each drug to obtain statistically reliable data.

2.3.11 Real time image processing

To measure the variances in cardiomyocyte beating in response to drug treatment, a movie of beating cardiomyocytes in 3D co-cultures was captured under a light microscope. The series of images that make up the movie were analyzed using ImageJ software plugin SSIM index. This program compares two images and assigns a similarity score (SSIM index). Identical images receive a SSIM index of 1, and completely different – a similarity index of 0. The image with the tissue being completely contracted was taken for reference and assigned a similarity index of 1 and all other images of tissue undergoing different stages of contraction was measured against the reference image. As a result, when the tissue fully contracted, its SSIM index approached a value of 1.0, and as it was relaxing, the SSIM index was decreasing. To eliminate the noise signal, the image series of non-moving fixed tissues were recorded. The average SSIM measurement of non-moving fixed tissues was taken as the control and was subtracted from each result. The resulting number was plotted and resulted in a cardiogram-like graph.

2.4 Results and Discussion

Cardiac tissue is one of the most cell dense organs due to the cardiomyocytes requirement to be physically connected in order to propagate electrical signals that result in large scale mechanical rhythmic beating with a synchronous pattern. Most of the heart organ is made up of cells with very little extracellular matrix proteins. For eg. other organs, such as aorta 25.7%, skin 64.5–72.1%, bone 15.1%, chordae (tendons) 77.1% contain much higher amounts of extracellular matrix and much less cell density than heart.^{18,19}

In order to generate scaffold free functional 3-dimensional cardiac tissue, we used the combination of liposome fusion, cell surface engineering and bio-orthogonal chemistry.²⁰⁻²³ We have previously shown the rapid installation of bio-orthogonal ketone and oxyamine groups to a range of cell types via liposome fusion (ViaGlue).²⁴⁻²⁶ As ketone and oxyamine presenting cells come into contact the cells rapidly click together via the stable oxime ligation and assemble into spheroids and then tissues (**Figure 2.1**). The interfacial oxime reaction is fast, chemoselective, occurs at physiological conditions (37 °C, pH 7) and requires no catalyst.²⁷⁻²⁹ Furthermore, the resulting oxime bond has no side reactions with biomacromolecules, is bio-orthogonal and therefore does not interfere with native biological processes.³⁰

The delivery of the bio-orthogonal groups to cells' is based on rewiring the cell membranes with oxyamine and ketone moieties under mild conditions through the rapid process of liposome fusion. Ketone and oxyamine-functionalized lipids (O-dodecyloxyamine and dodecanone) together with widely used phospholipid palmitoyl-oleoyl phosphatidylcholine (POPC) and a cationic lipid 1,2 dioleoyl-3-trimethylammonium-propane (DOTAP) are incorporated into a liposome. When the bio-orthogonal liposomes (ViaGlue) are added to cells in

cell culture, the liposomes rapidly fuse with the cellular membrane resulting in delivery of chemical functionality onto the cell surface. Membrane-engineered cardiac cells from different cell types are then clicked together to form a complex multicellular cardiac 3D tissue.

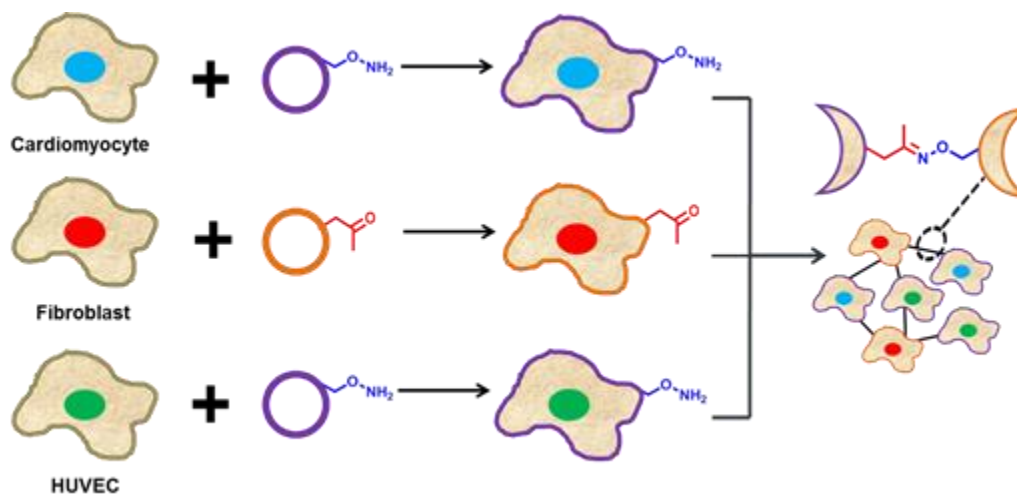


Figure 2.1: Schematic description for generating a scaffold free complex cardiac tissue by combining cell surface engineering and bio-orthogonal chemistry. The cells are initially treated with a rapid and mild liposome fusion method to install the bio-orthogonal groups onto the cell surface. Ketone and oxyamine groups on cell surface have been shown to rapidly click cells together via the oxime linkage and to form stable cell assemblies and tissues.

The delivery of the bio-orthogonal groups to cells' is based on rewiring the cell membranes with oxyamine and ketone moieties under mild conditions through the rapid process of liposome fusion. Ketone and oxyamine-functionalized lipids (O-dodecyloxyamine and dodecanone) together with widely used phospholipid palmitoyl-oleoyl phosphatidylcholine (POPC) and a cationic lipid 1,2 dioleoyl-3-trimethylammonium-propane (DOTAP) are incorporated into a liposome. When the bio-orthogonal liposomes (ViaGlue) are added to cells in cell culture, the liposomes rapidly fuse with the cellular membrane resulting in delivery of chemical functionality

onto the cell surface. Membrane-engineered cardiac cells from different cell types are then clicked together to form a complex multicellular cardiac 3D tissue.

In this work, primary cardiomyocytes were harvested from newborn Sprague Dawley rat pups (**Figure 2.2**). Harvested cardiomyocytes together with HUVEC's and fibroblasts were treated with ketone or oxyamine-containing liposomes.

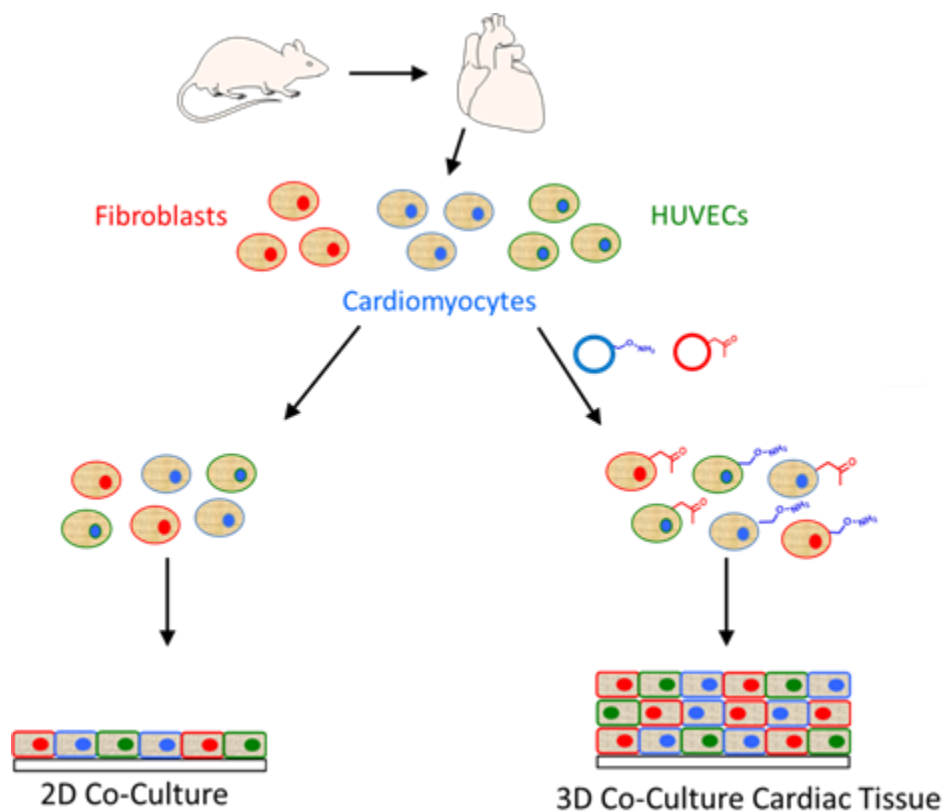


Figure 2.2. The schematic diagram representing the process of generating scaffold free 3 dimensional cardiac tissue via cell surface engineering and bio-orthogonal chemistry. The heart organ was first excised from new-born 24h rat pups. The neonatal cardiomyocytes were isolated from the hearts. The fresh cardiomyocytes were immediately decorated with bio-orthogonal groups via liposome fusion and mixed with similarly engineered neonatal fibroblasts and human vascular endothelial cells (HUVECS) to form 3-dimensional cardiac tissue. The cells that were not treated with liposomes do not form a 3D tissue but instead form a standard 2D monolayer.

The liposome fusion process occurs in seconds to minutes and installs the bio-orthogonal groups onto the cell surface. It should be noted that the liposome fusion/bio-orthogonal delivery technology works on many mammalian cell types and is fast, mild and works within seconds to tailor cell surfaces on freshly harvested cardiomyocytes from rat hearts. The 3 surface-engineered cell types were mixed and rapidly clicked together and assembled into 3D tissues. The non-treated control cells (empty liposomes, or with unpaired bio-orthogonal groups) when mixed did not assemble and as expected formed only a single monolayer of cells in culture.

Figure 2.3 shows confocal images of various 2 dimensional and 3 dimensional cardiac tissues.

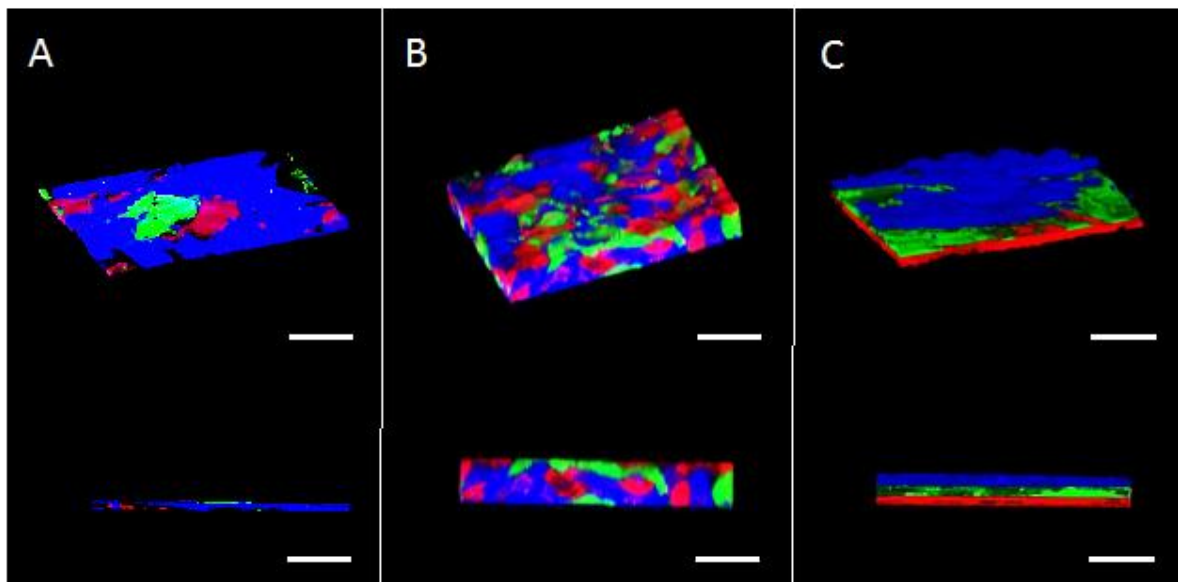


Figure 2.3: Confocal image representations of various 2D and 3D scaffold free cardiac tissue. Cardiomyocytes, HUVEC and fibroblast cells were live stained with fluorescent dyes (blue, green and red respectively). (A) The three cell types were mixed together and formed a single monolayer (10 μm thick). (B) The three cell types presented bio-orthogonal groups and when mixed clicked together and formed a random 3-dimensional multi-layer cardiac tissue (55 μm thick). (C) The three bio-orthogonal presenting cells were added sequentially to generate an oriented 3-dimensional cardiac tissue (20 μm thick). Scale bar = 60 μm .

The ability to generate scaffold free thick 3D tissues as well as 3D tissues with controlled orientation was demonstrated via liposome fusion, cell surface engineering and bio-orthogonal chemistry. Prior to assembly, the cardiomyocytes HUVEC's and fibroblasts were labeled with live-cell stain dyes, treated with liposomes and assembled into 3D tissues. Using oxime chemistry, it was possible to generate thick (55 μ M) complex 3D tissues. In addition, this technology allows for assembly of tissues with defined multi-layer orientation when the different cell types are added in sequential order. **Figure 2.3C** shows three cell types may be oriented in layers allowing for strict pattern control. In the control sample, the cells were not treated with liposomes or treated with non-functionalized liposomes and as a result only 2D monolayers were obtained with an average thickness of 10 μ M. The 3 dimensional tissues generated by the ViaGlue strategy were stable for several weeks (**Figure 4**).

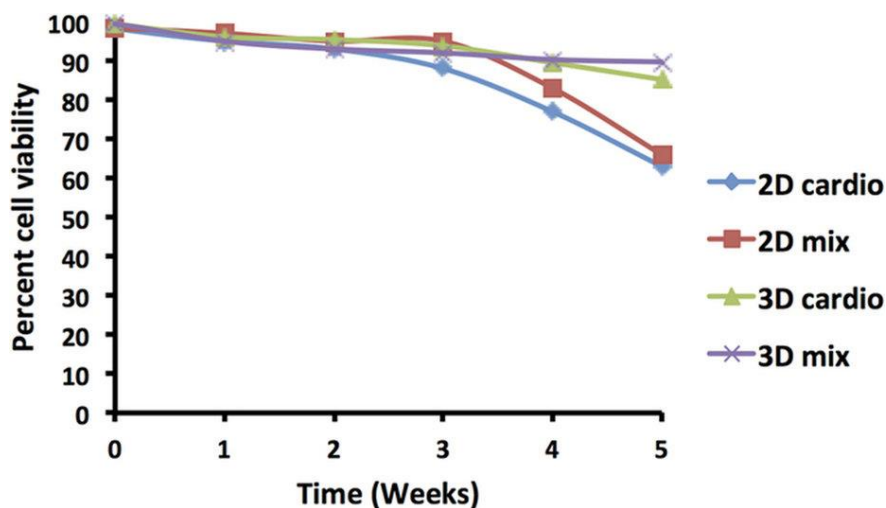


Figure 2.4: Cell viability in 2D and 3D tissues measured using propidium iodide viability assay. The various tissue constructs were stable and viable for several weeks. 2D Cardio = monolayer of cardiomyocytes. 2D mix = monolayer of mixed cardiomyocytes, fibroblasts and HUVEC cells. 3D cardio = 3 dimensional tissue comprising of only cardiomyocytes assembled via bio-orthogonal cell surface chemistry. 3D mix = 3 dimensional multilayer of mixed cardiomyocytes, fibroblasts and HUVEC cells assembled via bio-orthogonal cell surface chemistry.

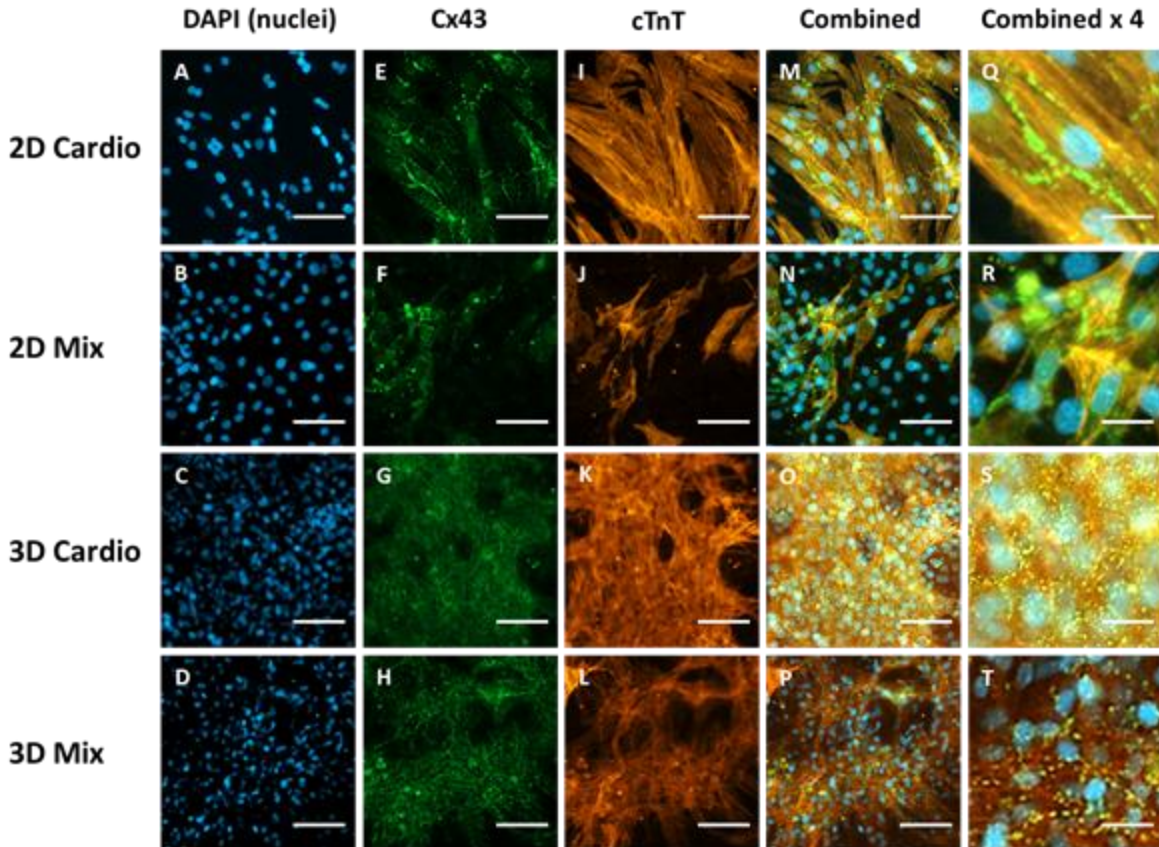


Figure 2.5: Fluorescent antibody staining for expression of cardiac-specific markers 96h after tissue assembly. 2D Cardio = monolayer of cardiomyocytes. 2D mix = monolayer of mixed cardiomyocytes, fibroblasts and HUVEC cells. 3D cardio = 3 dimensional tissue comprising of only cardiomyocytes assembled via bio-orthogonal cell surface chemistry. 3D mix = 3 dimensional multilayer of mixed cardiomyocytes, fibroblasts and HUVEC cells assembled via bio-orthogonal cell surface chemistry. (A-D) DAPI nuclear staining. (E-H) Expression of cardiac gap-junction protein Connexin 43 (Cx 43) in 3D tissues and 2D control monolayers. (I-L) Expression of myocardial regulatory protein cardiac troponin T (cTnT). (M-P). Merged fluorescent images. (Q-T) Merged fluorescent images magnified four times. (A-P) Scale bar = 80 μ M. (Q-T) Scale bar = 20 μ M.

To evaluate the function of the scaffold free 3-dimensional assembled cardiac tissues, the various tissues were immunostained for the expression of cardiac-specific genetic markers (**Figure 2.5**).

Cardiac troponin T (cTnT) is responsible for contraction of cardiac muscle and is present in

healthy tissue.³² Connexin 43 (Cx 43) is a gap junction transmembrane protein that is expressed in working myocardium and facilitates propagation of calcium ions.³³ Both proteins are expressed in both 2D monolayers and 3D tissues. However, the 3D mixed tissues showed higher levels of expression in both cTnT and Cx 43, compared to the 2D mix monolayer. Both proteins are expressed in 3D cardiac and 3D mixed tissues demonstrating that the cardiomyocytes are well connected and the tissues are functional.

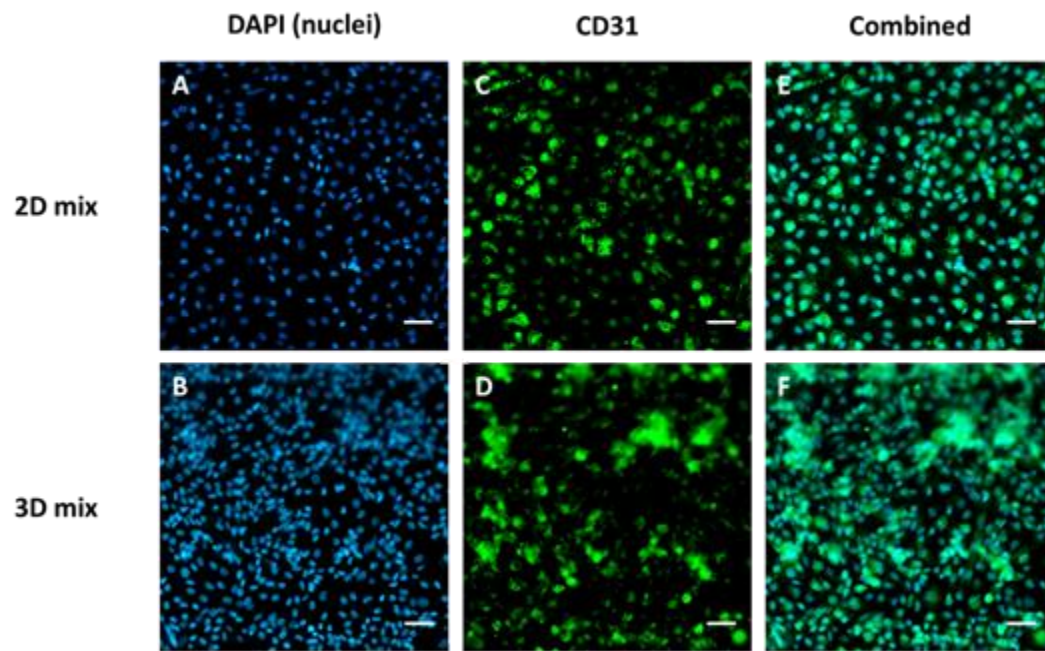


Figure 2.6: Fluorescent immunostaining for endothelial genetic marker CD31 expressed by HUVEC cells in 2D and 3D co-cultures 96h after tissue assembly. (A-B) DAPI staining of cell nuclei. (C-D) Expression of CD 31 marker by HUVEC cells. (E-F) The merged fluorescent image. Scale bar = 60 μ M.

To demonstrate the proper function of HUVEC cells in 3D tissue, the tissues were also stained for CD31, a genetic marker expressed on endothelial cells. CD31 is known to have various roles

in vascular biology including angiogenesis, platelet function, and thrombosis. It is a mechanosensor of endothelial cell response to fluid shear stress and it is involved in the regulation of leukocyte migration through venular walls.³⁴ **Figure 2.6B** shows high levels of expression for CD31 marker in 3D co-cultures compared to the 2D control. This demonstrates the proper functioning of HUVEC cells in 3D co-cultures.

Expression of extracellular matrix (ECM) by cells constituting myocardium is essential for proper functioning of cardiac tissue. The bio-orthogonal cell surface engineering strategy allows for the initial contact and assembly of the cells. However, over time, the cells in the assembly secrete their own extracellular matrix. The interfacial oxime bond click reaction initially nucleates the cell assembly process that does not naturally occur without scaffolds in vitro. To visualize production of ECM over time after the click cell assembly, the cells were stained with fluorescent probe markers specific for collagen and elastin (**Figure 2.7**).³⁵

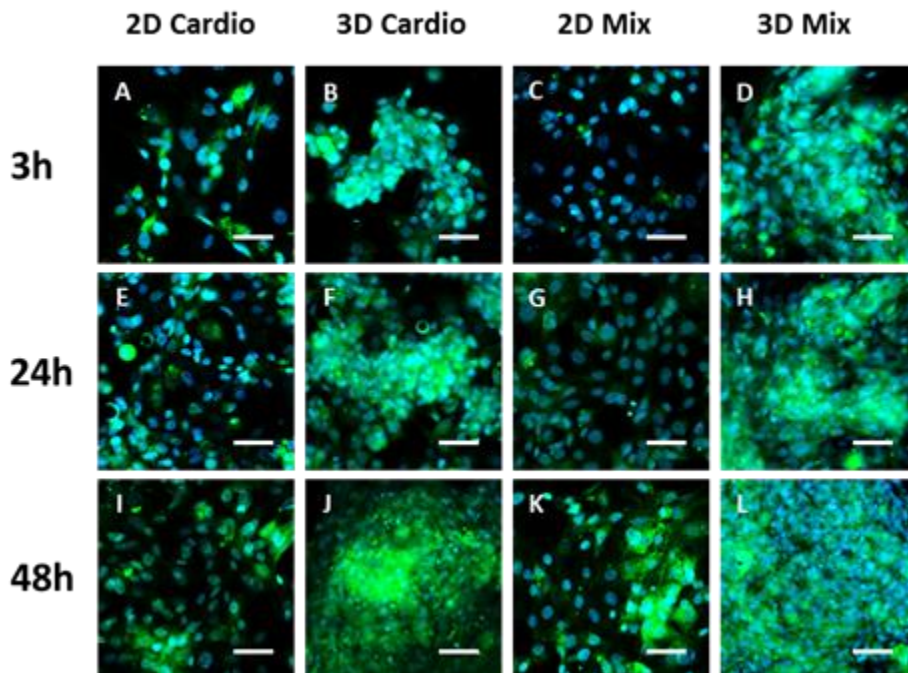


Figure 2.7: Fluorescent staining of collagen and elastin secreted over time by 2D monolayers and 3D tissues. The cells were assembled into tissues and stained for collagen and elastin with Col-F fluorescent dye at selected time points: 3h (**A-D**), 24h (**E-H**) and 48h (**I-L**). Green is the fluorescent dye Col-F, blue is the DAPI nuclear stain. Scale bar = 80 μ M

Upon tissue assembly, the cells were treated with the dye marker and fixed with 4% formalin for various durations. The images show gradual secretion of ECM. It is observed that 3D tissues secrete more extracellular matrix than 2D tissues, even 3h after cell assembly. After 48h, the amount of ECM expressed is the highest, which demonstrates that the stability of the cell associations in the tissue is primarily through secretion of extracellular matrix and that the bio-orthogonal cell surface click chemistry is used primarily to initiate the assembly process. Over time, the cells excrete their own extracellular matrix, which then becomes the main adhesive glue that holds the cells and tissues together. Taken together, the bio-orthogonal cell surface engineering method does not interfere with normal cell processes in tissue formation.

For cardiac tissue to function properly, the propagation of Ca^{+2} , Na^{+} and K^{+} ions is essential for contractile activity throughout the myocardium.³⁶ The propagation of signal is also necessary to synchronize the electromechanical beating between the cells in the myocardium. Calcium staining was performed to measure the rate of signal wave through the various assembled 2D and 3D tissue constructs (**Figure 2.8**). To demonstrate that there is an uninhibited calcium ion flow through the cell cytoplasm of interconnected cells via connexins, which are formed upon tissue assembly. After 48h assembly, the various tissues were treated with fluo-4 – a calcium-binding fluorescent dye and visualized with fluorescence microscopy.

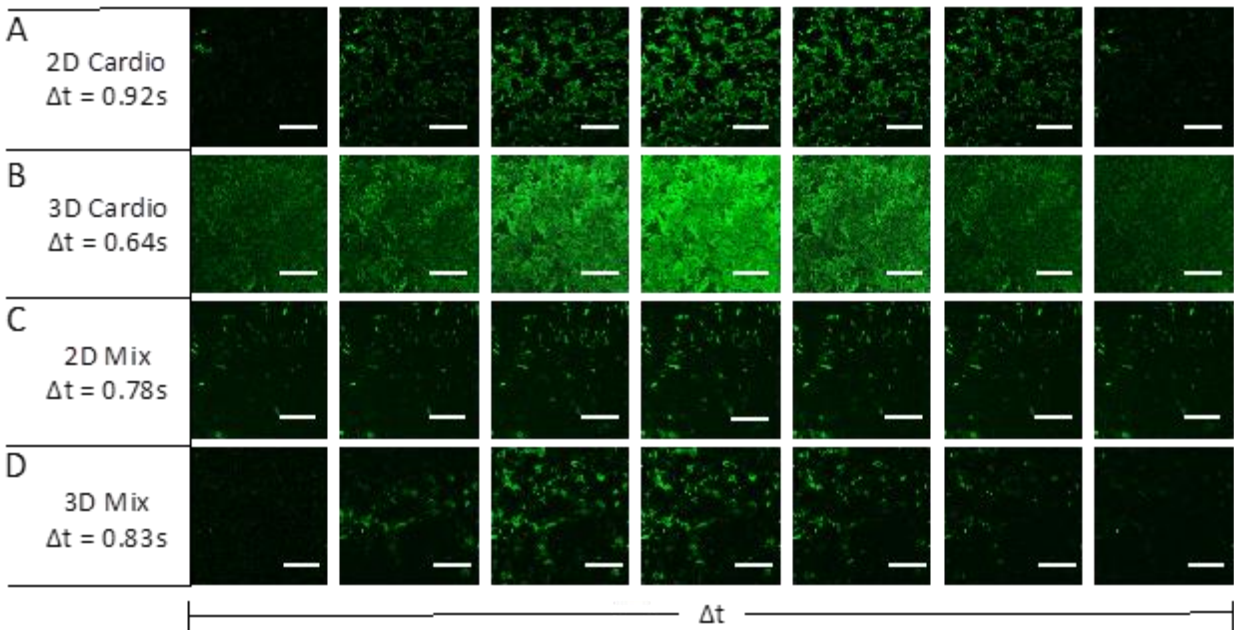


Figure 2.8: Native propagation of calcium across cardiac tissues without external stimulation. 48h after assembly, the tissues were life-stained with Fluo-4 calcium binding fluorescent probe. The propagation of calcium wave was recorded as the video time series. The fluorescent pulse rate differed depending on the type of cell assembly and was 0.92s for 2D cardiomyocytes (**row A**), 0.64s for 3D cardiomyocytes (**row B**), 0.78s for 2D mix. (**row C**) and 0.83s for 3D mix (**row D**). Scale bar = 80 μ M.

Snapshots were taken with frequency of 67 fps (frames per second) for 10s, and combined into a video. The frequency of calcium pulses varied across the different tissue types: in 3D cardiomyocytes, the frequency was the greatest: every 0.64s vs 0.83s for 3D mixed tissues. The normal heart rate is approximately 0.80s, which corresponds well with the mix 3D tissue generated. The intensity of fluorescence was the greatest in 3D cardiomyocytes monoculture and was due to the highest density of cardiomyocytes. In mixed 3D co-culture, the cardiomyocytes constitute only ~ 40% of all cells and the intensity of fluorescence is weaker. Overall, cardiac calcium signal propagation shows that there are proper cell-cell junctions between the cells in the tissue as well

as a coordinated, simultaneous contraction of all cells. These scaffold free 3 dimensional tissues show intrinsic long range beating throughout the tissue without the application of an external voltage. This result is significant to show that the cells are tightly packed through the tissue and can conduct ion flow over large areas in order to beat synchronously as an entire unit. In our laboratory, we have found polymer or scaffold containing 3 dimensional cardiomyocyte tissues require an external applied current in order for all the cells to beat synchronously. We observed, in a hydrogel or collagen scaffold that there are local high density regions of beating cardiomyocytes that are independent populations and not synchronized to other regions due to the polymer matrix inhibiting physical contact between various populations of cells throughout the tissue (data not shown). Our method is scaffold free where the cells are self-assembled via cell surface engineering and therefore there is no need for outside stimulation for a synchronous beating of tissue.

Cardiac toxicity is a major cause for drug candidates to fail clinical trials. Standard in vitro cytotoxicity studies, utilize 2D monocultures of cardiomyocytes. 2D monolayers, however cannot recapitulate the complex 3D environment of myocardium and therefore, new in vitro 3D models are needed for accurate assessment of cardiac cytotoxicity of drug candidates. A major criteria for testing drugs in 3D cell culture versus 2D cell culture is that cells in three dimensions form multi-layers of cells, whereas cells grown in two dimensions form a single monolayer. When testing a drug in two dimensions, it needs only to diffuse a short distance across the cell membrane in order to reach its intended target cell. However, in three dimensions, the situation is more realistic to an organ and a drug needs to diffuse across multi-layers of cells. The diffusion across multi-layers of cells more closely mimics the challenges found in the human body or in cancer tissues in which a drug needs to diffuse through multiple layers of cells before it reaches its intended target.

Furthermore, cells in three dimension tissues will form natural barriers to drugs, such as extracellular matrix and tight junctions that bind cells together and block or slow the diffusion of drugs, again making for a more realistic test model. For example, in a comparison of microarray data for gene expression of 3D cultured Hodgkin lymphoma line L1236 cells, of 2D cultured L1236 cells and of tumor samples from biopsy, gene expression patterns of the 3D cells were found to be more closely related to those of tumor samples than those cultured in two dimensions, with a marked difference for cell-substrate (2D) and cell-matrix (3D) adhesion molecules.³⁷

In this study, we evaluated the effect on beating rate of two chronotropic drugs, isoprenaline and doxorubicin on the various cardiac tissues (**Figure 2.9**).^{38,39} Both drugs are known to affect the beating rate of cardiomyocytes. Isoprenaline is a drug used for treatment of bradycardia (slow heart rate) and asthma (acts as a bronchiadilator). Doxorubicin is an anticancer drug commonly used to treat stomach cancer, leukemia, as well as soft tissue sarcomas. The most profound side effect of doxorubicin and isoprenaline is cardiomyopathy, which leads to congestive heart failure. The tissues were treated with different concentrations of isoprenaline (5nM and 10nM) or doxorubicin (100μM and 200μM) for the duration of 25 min, followed by light microscopy videos to record the alteration in tissue beating. **Figure 2.9A** shows percent increase (for isoprenaline) or decrease (for doxorubicin) in beating rate of cardiomyocytes in 2D or 3D tissues compared to the control samples (treated with DMSO only). All tissues had an increase in beating rate in response to an increase of concentration of isoprenaline. As expected, the 2D cardiomyocytes were the most sensitive due to the accessibility of the drug to the cells in a monolayer compared to a 3D tissue. This phenomena of 2D sensitivity over 3D is well known and indicative that 2D monolayers are not realistic model systems of organ function. Doxorubicin treatment decreased the beating rate of cardiomyocytes and had the greatest effect on 3D mixed tissues. Cardiogram-like graphs

were constructed to graphically represent the effect of isoprenaline and doxorubicin on cardiac beating rate (Figure 2.9B).

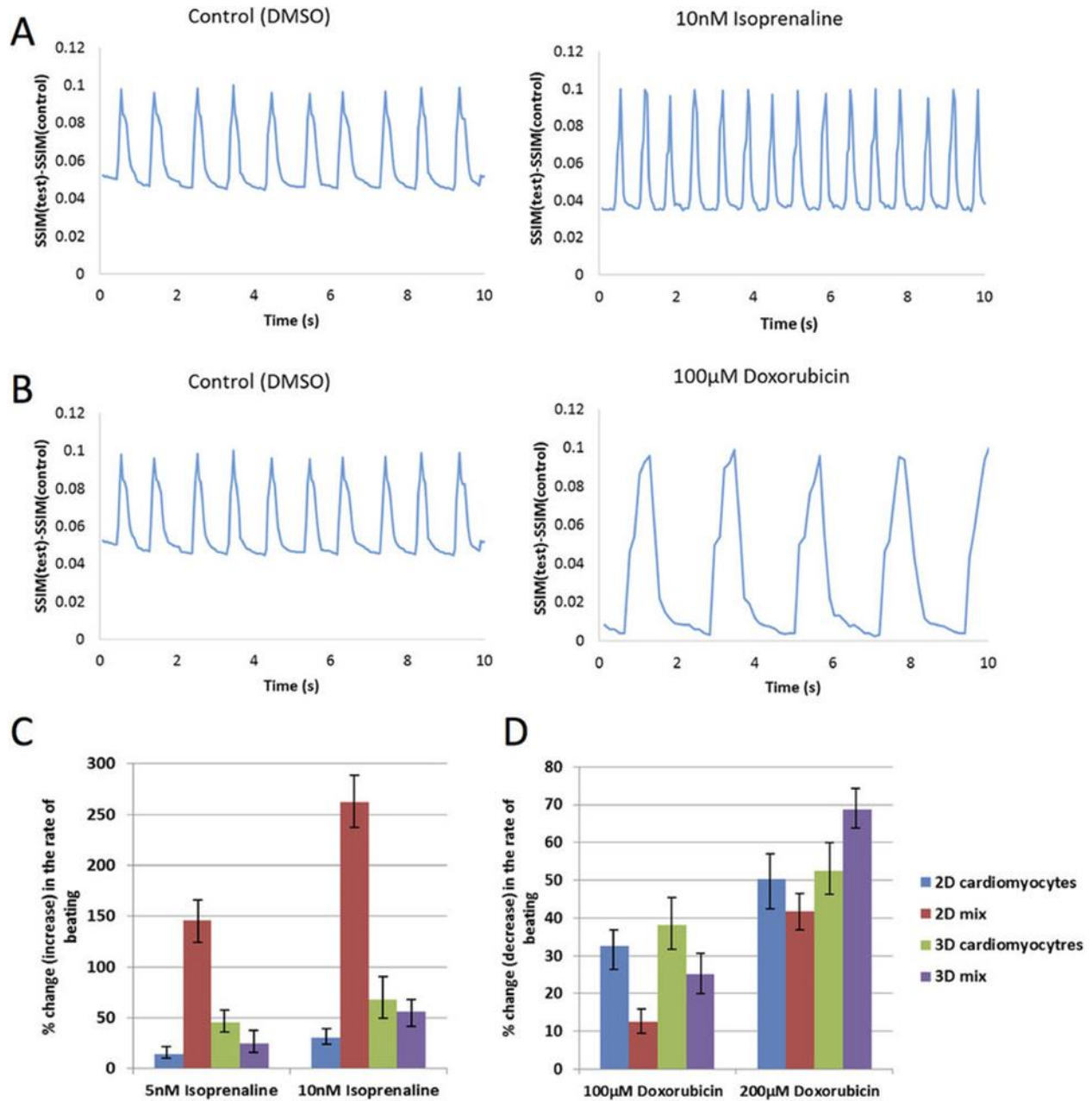


Figure 2.9: Chronotropic effects of cardiac tissues under treatment with varying concentrations of isoprenaline and doxorubicin. A) A representative beating signal for 3D mix tissues. The increase in beating interval was in response to treatment with 10nM isoprenaline. B) A representative beating signal comparisons for 3D mix tissues. The beating interval decreased in response to treatment with 100µM doxorubicin. C) Percentage increase in beating rate for tissues

treated with 5nM and 10nM isoprenaline. **D)** Percentage decrease in beating rate for tissues treated with 100 μ M and 200 μ M doxorubicin. Error bars represent the standard error of the mean (s.e.m). n=20, p<0.05.

The image series were analyzed using ImageJ and a similarity score was assigned. The graph shows the increase in beating frequency for cells treated with isoprenaline and decrease in beating frequency for cells treated with doxorubicin. These results show the scaffold-free cardiac tissues beat spontaneously without external stimulation and react accordingly to known cardiomyocyte drug stimulants.

2.5 Conclusion

In summary, we have used the combination of bio-orthogonal chemistry and cell surface engineering to program the rapid self-assembly of 3 different cell types into a functional 3-dimensional cardiac tissue. This click ligation method requires no polymers or extrinsic scaffold to trap or encapsulate cells. Cardiac tissue requires a high density of cells that are physically in contact in order to generate long range synchronous beating throughout the tissue. Significantly, the tissues generated by the ViaGlue liposome reagents were able to spontaneously beat synchronously throughout the entire tissue, due to high cell density and efficient cell contacts, without the requirement of external electrical stimulation. To evaluate the function of the various constructed cardiac tissues several cardiomyocyte antibody markers and drug toxicity assays were

performed. Furthermore, we observe gradual production of extracellular matrix from the cells soon after tissue assembly via the inter cell click ligation. The ViaGlue strategy is general and capable of assembling a variety of cell types to generate a range of tissues. These tissues may be used for many applications including drug screening and as models for disease and infection as well as eventual cardiac patch in vivo applications. Many different cell types including stem cells may be used with the strategy and the inter cell click ligation is compatible with microfluidic and 3D printing technologies.²³⁻³⁰ We believe the combination of liposome fusion, bio-orthogonal chemistry and cell surface engineering to tailor cell surfaces will have a significant impact on autocrine and paracrine signaling studies and for the development and evaluation of tissues for drug screening and therapeutic organ on a chip based biotechnology applications.

2.6 References

1. Bajaj, P., Schweller, R. M., Khademhosseini, A., West, J. L. & Bashir, R. 3D Biofabrication Strategies for Tissue Engineering and Regenerative Medicine. *Annu. Rev. Biomed. Eng.* **16**, 247–276 (2014).
2. Vunjak-Novakovic, G. et al. Challenges in cardiac tissue engineering. *Tissue Eng. Part B. Rev.* **16**, 169–187 (2010).

Lutolf, M. P. & Hubbell, J. A. Synthetic biomaterials as instructive extracellular microenvironments for morphogenesis in tissue engineering. *Nat. Biotechnol.* **23**, 47–55 (2005).
3. Uygun, B. E. et al. Organ reengineering through development of a transplantable recellularized liver graft using decellularized liver matrix. *Nat. Med.* **16**, 814–820 (2010).
4. Layered long-term co-culture of hepatocytes and endothelial cells on a transwell membrane: toward engineering the liver sinusoid. *Biofabrication* **5**, 045008 (2013).
5. Page, H., Flood, P. & Reynaud, E. G. Three-dimensional tissue cultures: current trends and beyond. *Cell Tissue Res.* **352**, 123–131 (2013).
6. Rustad, K.C., Sorkin, M., Levi, B., Longaker, M.T., and Gurtner, G.C. Strategies for organ level tissue engineering. *Organogenesis.* **6**, 151–157 (2010).
7. Khetani, S. R. & Bhatia, S. N. Microscale culture of human liver cells for drug development. *Nat. Biotechnol.* **26**, 120–126 (2008).
8. Petersen, T.H. et al. Tissue-engineered lungs for in vivo implantation. *Science.* **329**, 538–541. (2010).
9. Groeber, F., Holeiter, M., Hampel, M., Hinderer, S. & Schenke-Layland, K. Skin tissue engineering — In vivo and in vitro applications. *Adv. Drug Deliv. Rev.* **63**, 352–366 (2011).
10. Roger, V. L. et al. Heart disease and stroke statistics--2011 update: a report from the American Heart Association. *Circulation* **123**, e18–e209 (2011).
11. Pereira, G. C. et al. Drug-induced Cardiac Mitochondrial Toxicity and Protection: From Doxorubicin to Carvedilol. *Curr. Pharm. Des.* **17**, 2113–2129 (2011).
12. Emmert, M. Y., Hitchcock, R. W. & Hoerstrup, S. P. Cell therapy, 3D culture systems and tissue engineering for cardiac regeneration. *Adv. Drug Deliv. Rev.* **69-70**, 254–269 (2014).

13. Shachar, M., Tsur-Gang, O., Dvir, T., Leor, J. & Cohen, S. The effect of immobilized RGD peptide in alginate scaffolds on cardiac tissue engineering. *Acta Biomater.* 7, 152–162 (2011).
14. Chen, J. L. et al. Efficacy of hESC-MSCs in knitted silk-collagen scaffold for tendon tissue engineering and their roles. *Biomaterials.* 31--36, 9438–9451 (2010).
15. Eng, D., Caplan, M., Preul, M. & Panitch, A. Hyaluronan scaffolds: a balance between backbone functionalization and bioactivity. *Acta Biomater.* 6, 2407–2414 (2010).
16. Zhang, H., Zhou, L. & Zhang, W. Control of scaffold degradation in tissue engineering: a review. *Tissue Eng. Part B. Rev.* 20, 492–502 (2014).
17. Neuman, R.E., Logan, M.A. The determination of collagen and elastin in tissues. *J Biol Chem.* 2, 549-556 (1950).
18. You, J.-O., Rafat, M., Ye, G. J. C. & Auguste, D. T. Nanoengineering the heart: conductive scaffolds enhance connexin 43 expression. *Nano Lett.* 11, 3643–3648 (2011).
19. Bertozzi, C. R. A decade of bioorthogonal chemistry. *Acc. Chem. Res.* 44, 651–653 (2011).
20. McKay, C. S. & Finn, M. G. Click chemistry in complex mixtures: bioorthogonal bioconjugation. *Chem. Biol.* 21, 1075–1101 (2014).
21. Patterson, D. M., Nazarova, L. A. & Prescher, J. A. Finding the right (bioorthogonal) chemistry. *ACS Chem. Biol.* 9, 592–605 (2014).
22. O'Brien, P. J., Luo, W., Rogozhnikov, D., Chen, J. & Yousaf, M. N. Spheroid and Tissue Assembly via Click Chemistry in Microfluidic Flow. *Bioconjug. Chem.* 26, 1939–1949 (2015).
23. Dutta, D., Pulsipher, A., Luo, W. & Yousaf, M. N. Synthetic chemoselective rewiring of cell surfaces: generation of three-dimensional tissue structures. *J. Am. Chem. Soc.* 133, 8704–8713 (2011).
24. Luo, W., Pulsipher, A., Dutta, D., Lamb, B. M. & Yousaf, M. N. Remote control of tissue interactions via engineered photo-switchable cell surfaces. *Sci. Rep.* 4, 6313 (2014).
25. Park, S., Westcott, N. P., Luo, W., Dutta, D. & Yousaf, M. N. General chemoselective and redox-responsive ligation and release strategy. *Bioconjug. Chem.* 25, 543–551 (2014).
26. Dutta, D., Pulsipher, A., Luo, W., Mak, H. & Yousaf, M. N. Engineering cell surfaces via liposome fusion. *Bioconjug. Chem.* 22, 2423–2433 (2011).

27. Elahipanah, S., Radmanesh, P., Luo, W., O'Brien, P. J., Rogozhnikov, D., & Yousaf, M. N. Rewiring Gram-Negative Bacteria Cell Surfaces with Bio-Orthogonal Chemistry via Liposome Fusion. *Bioconjugate Chem.* 2016. ASAP DOI: 10.1021/acs.bioconjchem.6b00073
28. Luo, W., et al. A Dual Receptor and Reporter for Multi-Modal Cell Surface Engineering. *ACS Chem. Biol.* 10, 2219–2226 (2015)
29. Pulsipher, A., Dutta, D., Luo, W., & Yousaf, M. N. Cell surface engineering by a conjugation and release approach based on the formation and cleavage of oxime linkages upon mild electrochemical oxidation and reduction. *Angew. Chem. Int. Ed.* 53, 9487-9492 (2014).
30. Vuorenpää, H. et al. Novel in vitro cardiovascular constructs composed of vascular-like networks and cardiomyocytes. *In Vitro Cell. Dev. Biol. Anim.* 50, 275–286 (2014).
31. Sehnert, A.J., Huq, A., Weinstein, B.M., Walker, C., Fishman, M., Stainier, D.Y. Cardiac troponin T is essential in sarcomere assembly and cardiac contractility. *Nat Genet.* 1, 106-110 (2002).
32. Michela, P., Velia, V., Aldo, P., Ada, P. Role of connexin 43 in cardiovascular diseases. *Eur J Pharmacol.* 768:71-76 (2015).
33. Pusztaszeri, M.P., Seelentag, W., Bosman, F.T. Immunohistochemical expression of endothelial markers CD31, CD34, von Willebrand factor, and Fli-1 in normal human tissues. *J Histochem Cytochem.* 4, 385-395 (2006).
34. Biela, E., et al. Col-F, a fluorescent probe for ex vivo confocal imaging of collagen and elastin in animal tissues. *Cytometry A.* 6, 533-539 (2013).
35. Aiba, T., Tomaselli, G.F. Electrical remodeling in the failing heart. *Curr Opin Cardiol.* 25, 29-36 (2010).
36. Birgersdotter, A., et al. Three-dimensional culturing of the Hodgkin lymphoma cell-line L1236 induces a HL tissue-like gene expression pattern. *Leukemia & Lymphoma*, 48, 2042-2053 (2007).
37. Wallace, K.B. Doxorubicin-induced cardiac mitochondrionopathy. *Pharmacol Toxicol.* 93,105-115 (2003).
38. Fink, C., Ergün, S., Kralisch, D., Remmers, U., Weil, J., Eschenhagen, T. Chronic stretch of engineered heart tissue induces hypertrophy and functional improvement. *FASEB J.* 14, 669-679 (2000).
39. Stevens, M. M. & George, J. H. Exploring and engineering the cell surface interface. *Science* **310**, 1135–1138 (2005).

Chapter 3

Generation of a Scaffold-Free Three-Dimensional Liver Tissue via a Rapid Cell-to-Cell Click Assembly Process

This work has been published in *Bioconjugate Chemistry*, Volume 27, Pages 1991-1998 in 2016 under the title "Generation of a Scaffold-Free Three-Dimensional Liver Tissue via a Rapid Cell-to-Cell Click Assembly Process." It is reprinted with permission (© American Chemical Society 2016). Rogozhnikov, D.; Luo, W.; Elahipanah, S.; O'Brien, P. J.; Yousaf, M. N. are co-authors of this work.

3.1 Summary

There has been tremendous interest in constructing in vitro liver organ models for a range of fundamental studies of cell signaling, metabolism, and infectious diseases, and as a commercial system to evaluate therapeutic drug discovery prioritization and toxicity. Although there has been progress toward studying two-dimensional hepatic function in vitro, there remain challenging obstacles to generate rapid and efficient scaffold-free three-dimensional multiple cell line co-culture tissue models of liver. Herein, we develop and employ a strategy to induce specific and stable cell–cell contacts among multiple hepatic cell lines to generate 3D tissues through cell-surface engineering based on liposome delivery and fusion to display bio-orthogonal functional groups from cell membranes. We generate, for the first time, a three cell line co-culture 3D liver tissue model by assembling hepatocytes, hepatic endothelial cells, and hepatic stellate cells via a rapid inter-cell click ligation process. We compare and analyze the function of the superior 3D liver tissue chips with 2D co-culture monolayer by assessing mitochondrial metabolic activity and evaluating drug toxicity.

3.2 Introduction

Recent strategies to assemble complex tissues in vitro have revolutionized biomaterial and bioengineering research and are now a central design feature for drug discovery and organ engineering research efforts to improve human health.¹⁻⁵ In particular, the human liver is a complex multicellular organ containing a range of different cell types including hepatocytes as the key parenchymal cells and hepatic sinusoidal endothelial cells (HSEC), hepatic stellate cells (HSC), and Kupffer and pit cells as nonparenchymal cells.⁶⁻⁷ The liver organ is responsible for many diverse functions, including protein, carbohydrate, and lipid metabolism, detoxification of endogenous and exogenous compounds, storage of glucose, production of bile and cholesterol, secretion of albumin and clotting factors, production of urea, and many other vital processes.⁸ Due to its central importance, any liver function impairment may lead to a range of deleterious illnesses and diseases.^{9,10} Furthermore, many therapeutic drugs discovered in cell based assays result in hepatotoxicity in animal trials leading to high failure rates in drug approvals. This directly impacts the tremendous cost associated with drug discovery and may also result in the retrieval of existing drugs from the pharmaceutical market due to liver toxicity.¹¹⁻¹²

Despite the critical significance of establishing in vitro liver tissue models, many challenges limit the exploration and development of the field of liver tissue engineering.¹³ For example, in order to evaluate liver toxicity of drug molecules before animal studies or clinical trials, a functional liver tissue model system established in the laboratory would be highly desirable to assign drug priority.¹⁴ However, for in vitro models, it is very difficult to maintain hepatocyte cells, which rapidly lose liver-specific functions and stop growth under in vitro conditions.¹⁵ In order to address this severe cell culture limitation, many liver model systems

containing co-cultures of parenchymal hepatocytes with other nonparenchymal cells have been investigated.¹⁶ The current state of the art for 2D liver tissue is based on co-culturing nonparenchymal cells with hepatocytes in specific ratios or patterns.¹⁷ Pioneering research discovered that hepatocytes could survive and maintain liver-specific functions for much longer periods when surrounded by certain (maintenance) cell lines.¹⁸ These artificial co-culture systems have greatly expanded the range of liver studies possible and as an in vitro drug screening platform.¹⁹

While two-dimensional co-cultured hepatocytes were used in various drug analyses to help researchers estimate liver function and drug responses, most of these systems remain as traditional cell monolayer systems (two-dimensional systems).¹⁴ The two-dimensional tissue on a chip systems have advanced in vitro liver model systems, but there remain many challenges to generating appropriate functional three-dimensional in vitro tissue models with more than two liver specific cell types. These 3D co-culture systems would be better mimics of real liver tissue and may expand liver cell viral and toxicity studies, which in turn may lead to potential new liver organ assays and functional liver construction.

To achieve 3D cell culture and tissue construction, a variety of synthetic scaffolds were developed to support cell adhesion and growth and to study cell behavior in 3D. These scaffolds usually contain synthetic polymers such as poly(ϵ -caprolactone) (PCL), poly(L-lactic acid) (PLLA), polyglycolic acid (PGA), and poly(lactic-*co*-glycolic acid) (PLGA) or biological materials such as collagen, gelatin, chitosan, alginate, and agarose.^{20,21} While synthetic scaffolds were widely studied to support cell proliferation and construct 3D tissues, many limitations remained for cell based research and applications, including the inherent stability of the

scaffolds, toxicity of degradation byproducts, potential inflammation and immune responses, interference with cell–cell interactions, duration for cell saturation in the scaffold, and unpredictable impact on signaling pathways.^{22,23} Although some scaffolds are biocompatible and capable of mimicking certain features of the extracellular matrix, their long-term safety and side effects are still unclear. Therefore, scaffold-free tissues may present an alternative and complementary system for future applications in tissue engineering and regenerative medicine. Herein, we introduce a scaffold-free platform system to generate rapid, efficient, and controlled multiple cell type co-culture cell assemblies of 3D liver tissues. The strategy relies on mildly rewiring cell surfaces in order to click cells together to form stable complex structures without the use of polymer scaffolds or encapsulating gel materials.²⁴ This system is based on integrating a universal cell surface engineering method to install chemoselective and bioorthogonal lipid-like groups onto cell membranes to which interfacial click reactions among different cell type membranes can be induced.²⁵ Upon this multivalent interfacial ligation, cells can be clicked together and thus result in rapid cell–cell assembly with high cell economy. With simple manipulation, cell orientation and positioning can be potentially achieved to construct multicellular tissues approaching the complexity of organs.²⁶

3.3 Experimental

3.3.1 Tissue Culture

Immortalized human hepatocytes Fa2N-4 were obtained from Xenotech, KS. The cells were thawed and cultured on collagen I-coated plates in multifunction enhancing (MFE) plating medium containing 10% newborn calf serum (Xenotech, KS), and 1% penicillin/streptomycin

solution (Sigma). At 24 h upon plating, the medium was replaced with MFE serum-free support medium containing component A. The medium was replaced every 48 h. The cells were passaged upon reaching confluence (every 3–4 days).

Primary human hepatic stellate cells (HSC) were obtained from ScienCell, CA. The cells were cultured on poly(L-lysine)-coated plates in stellate cell medium (SteCM) consisting of 500 mL basal medium, 5 mL of stellate cell growth supplements (SteCGS), 10 mL of fetal bovine serum (FBS), and 5 mL of penicillin/streptomycin solution. The cells were passaged upon reaching 95% confluence. The medium was changed every 48 h.

Primary human hepatic sinusoidal endothelial cells (HSEC) and their medium were purchased from ScienCell, CA. The cells were cultured on fibronectin-coated plastic plates in endothelial cell medium (ECM) consisting of 500 mL of basal medium, 5 mL of endothelial cell growth supplement (ECGS), 25 mL FBS, and 5 mL penicillin streptomycin solution. The cells were passaged upon reaching 95% confluence (every 2–3 days) and the medium was changed every 48 h.

All cells were maintained at 37 °C, 5% CO₂.

3.3.2 Preparation of Liposomes

To prepare oxyamine and ketone-tethered liposomes, chloroform solutions of palmitoyl-oleoylphosphatidylcholine (POPC) and 1,2 dioleoyl-3-trimethylammonium-propane (DOTAP) were mixed with *O*-dodecyloxyamine (for oxyamine-tethered liposomes) or dodecanone (for ketone-tethered liposomes) on the following ratios: POPC (430 µL, 10 mg/mL in CHCl₃ at 86 mol %); DOTAP (10 µL, 10 mg/mL in CHCl₃ at 2 mol %); and *O*-dodecyloxyamine or dodecanone

(60 μ L, 10 mM in CHCl_3 at 12 mol %). The mixtures of lipids were thoroughly dried and then resuspended in 3 mL of phosphate-buffered saline (PBS). The suspension was then sonicated with a tip sonicator for 20 min until it was clear.

3.3.3 Liver Tissue Assembly

Prior to tissue assembly the cells were allowed to reach 85–95% confluence. Cells were then treated with liposome solution (50 μ L of liposomes/1 mL of medium) and incubated at 37 °C for 4 h. The medium was discarded and the cells were washed with PBS twice. The ketone- and oxyamine-tethered cells were removed from the plate with 0.25% trypsin and centrifuged at 800 rpm. The medium was discarded and the oxyamine- and ketone-labeled hepatocytes, HSC and HSEC, were mixed in a small volume of medium (2×10^6 cells/mL). Small drops of concentrated resuspended cell solutions were then placed in 12-well (3.7 cm²) collagen I-coated plates and given a slight shake to induce cells to aggregate and assemble. Each mixed (co-culture) 2D or 3D sample contained 1×10^5 of Fa2N-4 hepatocytes, 1×10^5 of HSEC and 5×10^4 of HSC. Each 2D and 3D hepatocyte-only culture contained 1×10^5 of Fa2N-4 hepatocytes. The cells were then incubated at 37 °C and 5% CO₂ for 16 h to achieve full spreading of cells in the tissues. Upon spreading of cells, fresh MFE plating medium was added into the plates. After 24 h, the medium was exchanged with a 1:1 mixture of MFE support medium and endothelial cell medium (ECM). Cells in the control samples were treated with nonfunctionalized liposomes.

3.3.4 Fluorescent Staining for Collagen and Elastin in 2D and 3D Assemblies

To visualize the secretion of ECM by tissues over time, the cells were stained with the green fluorescent probe Col-F (Immunochemistry Technologies, MN), which binds collagen and elastin. A 20 mM stock solution of Col-F reagent in DMSO was prepared. The stock solution

was dissolved in the medium to give a final 20 μM concentration. The tissues were treated with the medium containing 20 μM of Col-F reagent and incubated for 1 h at 37 °C. The medium was removed and the cells were washed twice with PBS. The cells were then fixed with 10% formalin for 15 min and visualized via fluorescent microscopy with excitation of 488 nm and emission of 520 nm.

3.3.5 Immunohistochemistry and Confocal Microscopy

Prior to tissue assembly cells were incubated in serum-free medium containing fluorescent live stain (Life Technologies). Fa2N-4 hepatocytes, HSEC, and HSC were treated with 25 μM CellTracker Blue CMAC (7-amino-4-chloromethylcoumarin), 25 μM CellTracker Green CMFDA (5-chloromethylfluorescein diacetate), and 25 μM CellTracker Red CMTPX, respectively. The cells were incubated for 45 min, after which they were washed thoroughly with PBS and incubated in serum-free medium for an additional 45 min. Cells were then assembled into 3D tissues and incubated for 24 h. Subsequently, the tissues were fixed with 10% formalin for 15 min and visualized with LSM-700 (Zeiss) confocal microscope.

3.3.6 Activation of Cytochrome P450 3A4

To induce cytochrome P450 3A4, the 3D tissue samples were incubated in MFE support medium containing 10 μM Rifampin (Sigma) for 72 h at 37 °C, 5% CO_2 . The control samples were treated with DMSO vehicle only for calculation of fold activation. The medium was changed every 24 h. The samples were analyzed via P450-Glo CYP3A4 Assay Kit (Luciferin-IPA) (Promega) by using the manufacturer's instructions for the nonlytic cycle. The sample's medium was exchanged with fresh MFE support medium containing 3 μM Luciferin-IPA and the samples were incubated for 50 min. 50 μL of medium was then transferred into a white 96-well plate. 50 μL of the detection reagent was then added into each well. The samples were covered

with aluminum foil and incubated for 20 min at room temperature. The luminescence was read with a Biotek Synergy Multidetector Plate Reader (Biotek).

3.3.7 Albumin Analysis

Culture medium was collected from the various samples and the albumin content was measured via Human Albumin Pincer Assay kit (Mediomics). New medium (1:1 MFE support medium and endothelial cell medium (ECM)) was added 24 h prior to collection for albumin quantification.

3.3.8 Toxicity Assays

Liver tissues were incubated with 10 μ M troglitazone, 150 μ M rosiglitazone, or 7.5 μ M cyclophosphamide dissolved in MFE support medium for 16 h. The control samples were treated with DMSO vehicle. Subsequently, cell viability was analyzed by (3-(4,5-dimethylthiazol-2-yl)-2,5-diphenyl tetrazolium bromide (MTT) assay (Sigma), where the tetrazolium ring is cleaved by mitochondrial dehydrogenase enzymes. The samples were then incubated in DMEM phenol red-free medium containing MTT reagent for 1 h resulting in production of a purple precipitate which was subsequently dissolved in a 1:1 solution of isopropanol and DMSO. The absorbance was measured at 570 nm using a Synergy Biotek assay device. The data was analyzed via Student T test analysis by comparing two groups of data: 3D and 2D monocultures as well as 3D and 2D co-cultures.

3.4 Results and Discussion

As shown in **Figure 3.1**, parenchymal (hepatocytes) and nonparenchymal (stellate and endothelial) liver cells can be surface-engineered via functionalized liposomes presenting ketone or oxyamine groups. After cell surface engineering, these ketone or oxyamine-tailored cells can

be chemoselectively ligated together through interfacial multivalent oxime bonding. The oxime conjugation is stable, bio-orthogonal, and instantaneous through polyvalency under physiological conditions.²⁷⁻³³ Moreover, it does not require any catalyst or produce any toxic side product.

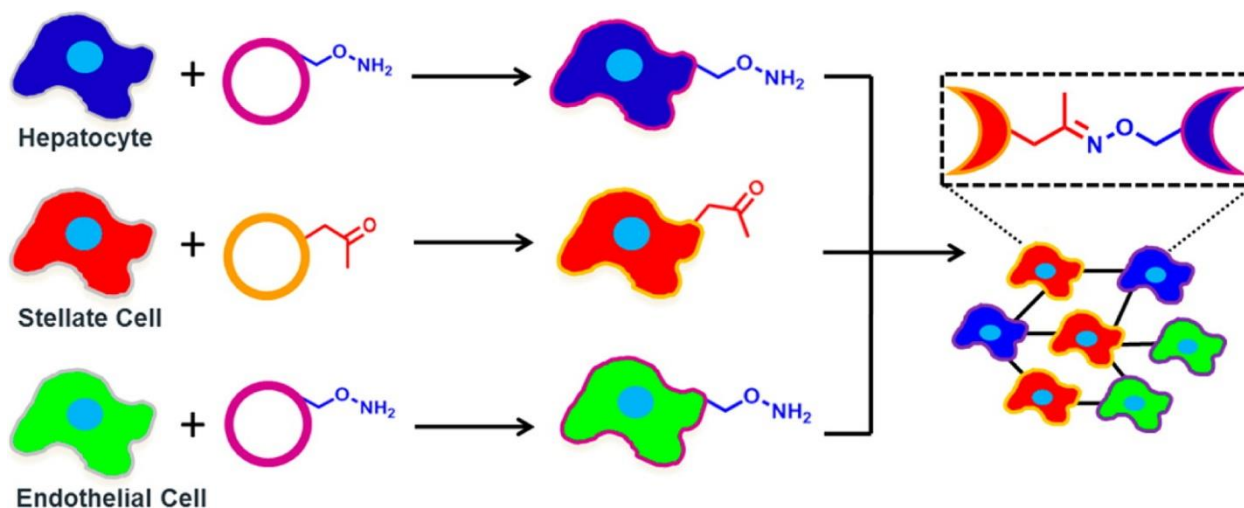


Figure 3.1. General schematic process of engineering cell surfaces with bio-orthogonal chemistry groups for the programmable assembly of multiple cell lines into complex coculture spheroids and tissues. The bio-orthogonal groups were delivered to parenchymal and nonparenchymal liver cells via a straightforward liposome fusion strategy. The cells were surface-engineered to present oxyamine and ketone functional groups. The tailored cells rapidly assemble on demand through an interfacial oxime ligation.

These velcro-like features on the cell surface allow for the installation of only minimal amounts (several thousand) of ketone or oxyamine groups onto cells surfaces to initiate the multivalent oxime conjugation, while ensuring no cytotoxic impact on cells. Previous studies have shown that the liposome fusion delivery of cargo and bio-orthogonal lipids is a transient transfection that helps to initiate the cell-to-cell assembly process.²⁴⁻³⁹ Over time, the cells proliferate and dilute the bio-orthogonal lipids; however, during this time period the cells excrete new

extracellular matrix which then holds the assemblies and eventually tissues together with high cell density.⁴⁰

Based on the cell surface engineering method, human immortalized hepatocytes Fa2N-4, human hepatic stellate cells (HSC), and human hepatic sinusoidal endothelial cells (HSEC) were surface-engineered to present oxyamine or ketone molecules, respectively. Fa2N-4 hepatocytes are noncancerous and widely used in liver model systems due to their ease of maintenance and similar expression profile of liver-specific functions.⁴¹ As shown in **Figure 3.2**, through the interfacial oxime conjugation between oxyamine and ketone, these surface-engineered liver cells,

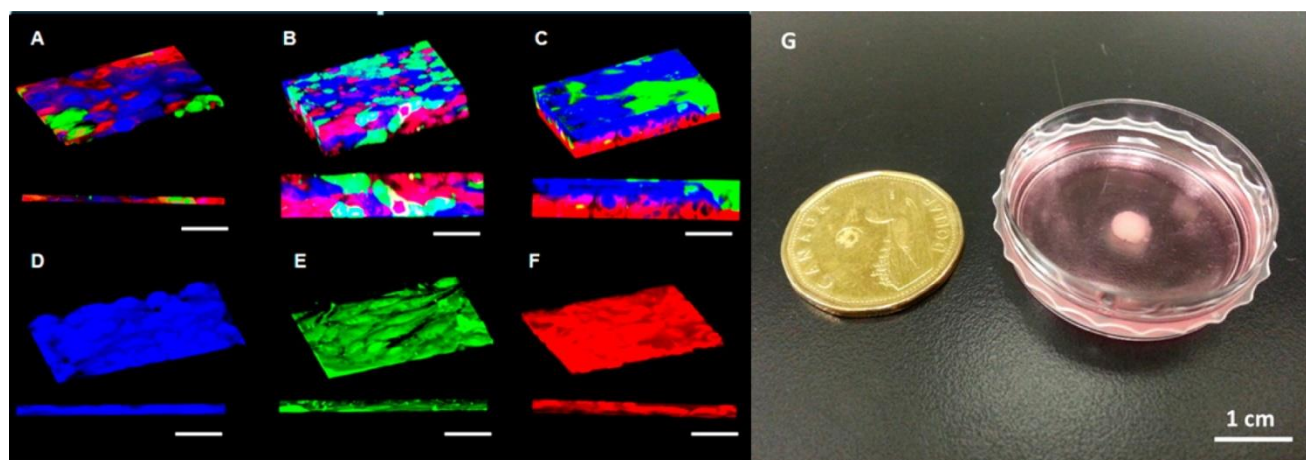


Figure 3.2. Fluorescent images and digital photograph of single layer and three-dimensional liver tissue. (A) 3D and sideview confocal image of a three cell type co-culture as a single layer. The cells do not have bio-orthogonal groups and therefore only form a mixed monolayer. (B) Confocal image of three-dimensional tissue containing the three cells types engineered with ketone and oxyamine groups via liposome fusion. The three cell types formed mixed multilayers. (C) Confocal images of surface-engineered liver tissue assembly with orientation control. Stellate cells (red) were at the bottom, and mixed hepatocytes (blue) and endothelial cells (green) were on the top. Hepatocytes, hepatic endothelial cells, and hepatic stellate cells were live-stained as blue (D), green (E), and red (F), respectively. (D–F) show monolayers of the individual cells used to construct the liver tissue. Scale bar (A–F) represents 50 μm . (G) Digital camera photograph of macroscale liver tissue that was fabricated based on surface-engineered hepatocytes, stellate cells, and hepatic endothelial cells.

when mixed, rapidly assemble into 3D tissue on demand.

To easily distinguish among the three cell types in co-culture, hepatocytes, hepatic endothelial cells, and hepatic stellate cells were live-stained as blue, green, and red with vital dyes, respectively. Without the surface engineering process, mixing the three cell types only resulted in a 2D monolayer (**Figure 3.2A**). In contrast, 3D multilayer liver tissues were easily and rapidly constructed when the three bio-orthogonal cell surface engineered cells were mixed (**Figure 3.2B**). Due to the interfacial ligation, the surface-engineered cells may also be oriented depending on the manner of sequential addition. For example, stellate cells (red) were seeded first to form a bottom layer to which mixed hepatocytes (blue) and endothelial cells (green) were seeded to form an oriented multilayer structure (**Figure 3.2C**). Without the surface engineering procedure the cells only formed 2D monolayers (**Figure 3.2D–F**). This controllable cell assembly and orientation system can only occur with surface-engineered cells. This unique system provides researchers the opportunity for truly scaffold-free construction of any tissue in a range of orientations. Furthermore, the cell ligation assembly method allows for large-scale tissues to be generated (**Figure 3.2G**) rapidly with efficient cell economy. We found the assembled tissues were stable for many weeks with no change in liver specific functions. Future studies combined with 3D printing technology may afford complex tissues approaching the complexity of organs. As a representative example shown in **Figure 3.2G**, a macroscale liver tissue was constructed in 4 h through the efficient bio-orthogonal tissue click method.

To demonstrate that the co-culture assemblies excrete their own extracellular matrix (ECM) after initial adhesion through the interfacial click ligation method we examined over time the production of collagen and elastin. **Figure 3.3** shows fluorescent images of ECM production

over time for 2D and 3D co-culture assemblies of the three cell lines. The cell nuclei were stained blue with DAPI and the secretion of ECM is visualized over time as green through fluorescent small molecule Col-F staining of collagen and elastin. It is clear that the initial cell-to-cell adhesion process is rapidly induced through oxime ligation which is then re-enforced over time through the production of ECM.

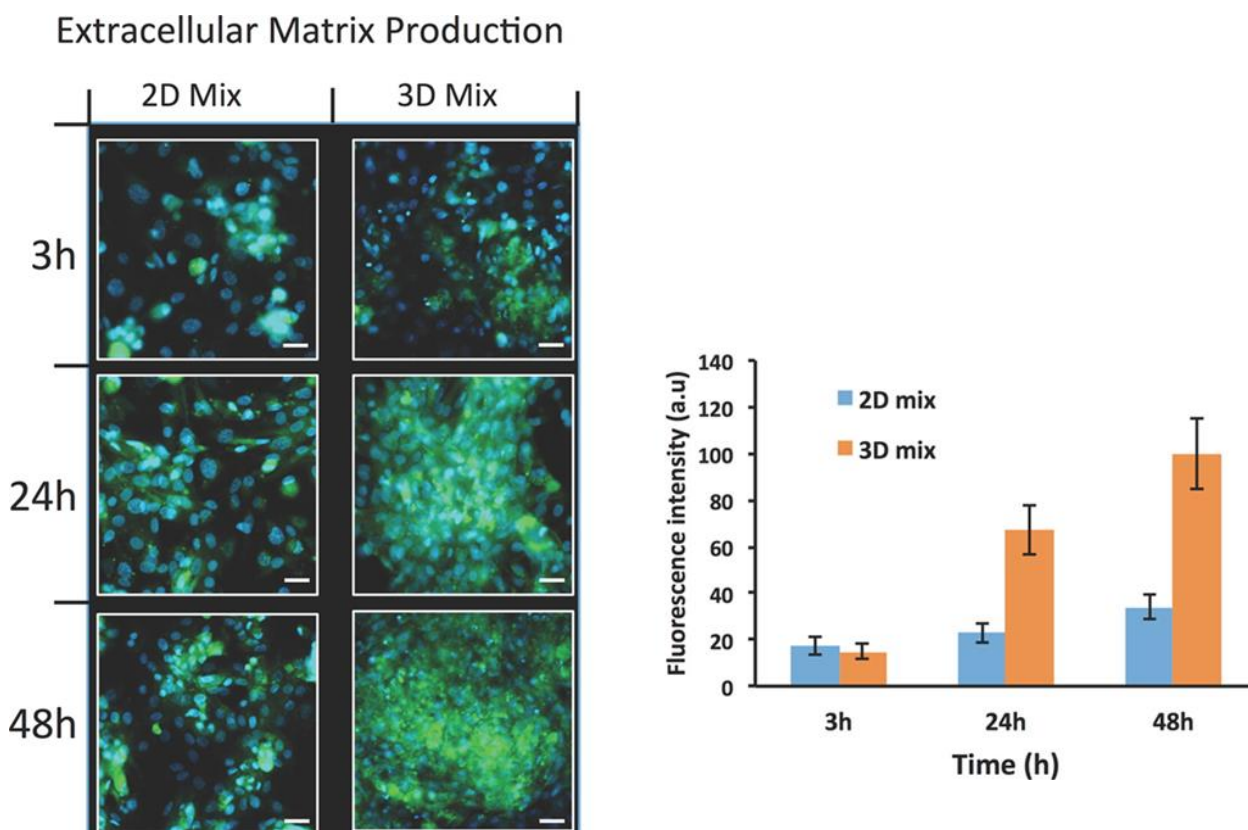


Figure 3.3. Fluorescent image comparisons of extracellular matrix (ECM) production over time after two-dimensional co-culture monolayer and three-dimension multilayer tissue assembly. (Left) Nuclei of the three cell lines are stained blue and the production of ECM is stained green with a small molecule probe for collagen and elastin. After initial rapid 3D cell assembly via bio-orthogonal ligation, the cells soon excrete extracellular matrix to further support cell adhesion. Scale bar = 40 μm . **(Right)** Secretion of extracellular matrix over time by 2D monolayers and 3D tissues of mixed cells. Relative fluorescent intensity produced by Col-F staining of collagen and elastin was measured at 3, 24, and 48 h and expressed in arbitrary units (a.u). $n = 15$, $p < 0.05$. All fluorescent intensity images were relative to the 48 h time point image (assigned 100 arbitrary units).

To further demonstrate the utility and scope of the system, four representative liver tissues were fabricated and then analyzed and compared for various liver specific functions (**Figure 3.4A**).

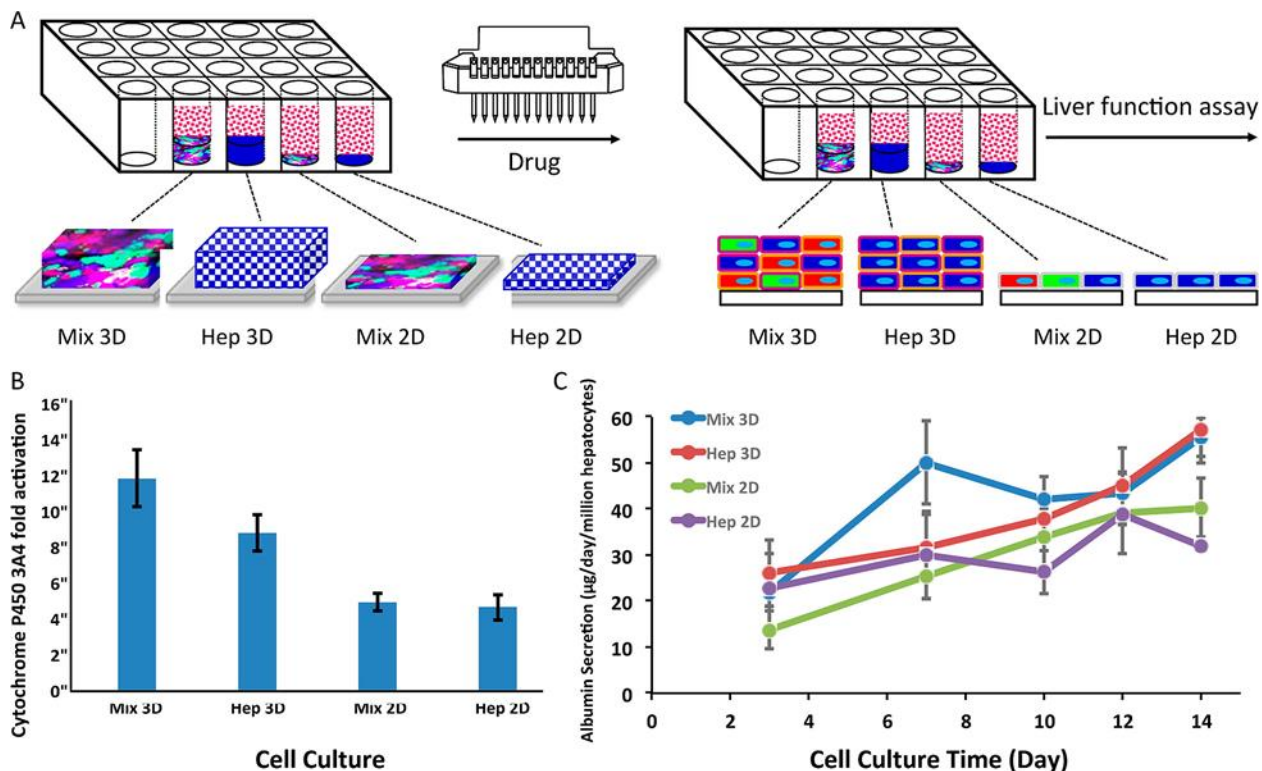


Figure 3.4. Fabrication and analysis of various types of liver chips generated via an intercell bio-orthogonal ligation strategy. (A) Schematic of different types of liver chips for liver function analysis. (B) Study of cytochrome P450 3A 4-fold activation in different liver tissues treated with 10 μ M rifampin over 72 h. (C) Rates of albumin secretion by different liver tissues over 14 days. Error bars represent standard error of the mean.

As a comparison, 3D co-culture liver tissue (Mix 3D – containing all three cell lines), 3D hepatocyte liver tissue (Hep 3D – containing only the hepatocyte cell line), 2D co-culture liver tissue (Mix 2D – containing all 3 cell types, and 2D hepatocytes liver tissue (Hep 2D – containing only hepatocyte cell line) were studied for enzyme activity of cytochrome P450

3A4—a well-known enzyme responsible for drug metabolism in hepatocytes (**Figure 3.4B**).⁴² These liver tissues were treated with rifampin, a common cytochrome p450 3A4 activator, for 72 h. It was observed that the 3D co-culture liver chip (Mix 3D) showed highest activation (~4-fold), and 2D hepatocytes tissue (Hep 2D) showed the lowest activation. It is well-known that the albumin secretion is an important liver-specific function and therefore we performed an albumin secretion assay over 14 days. According to the results from the assays, 3D coculture (Mix 3D) and 3D hepatocyte (Hep 3D) liver tissues showed excellent liver function over 14 days. These results provide clear evidence that the scaffold-free 3D liver tissue system has tremendous potential in liver tissue engineering and liver on a chip fabrication and applications.

Liver toxicity is one of the primary reasons for withdrawal of drugs from the market as well as from lengthy and expensive clinical trials.¹⁴ Therefore, drug screening of model livers or liver chips before clinical trials is considered a critical step during the evaluation and prioritization of drug candidates. In order to highlight the potential of the tissue chip system described for drug screening application, several representative drugs were tested on the various liver tissue chips fabricated (**Figure 3.5**). It has been shown that cellular interactions between hepatocytes and other nonparenchymal cells such as HSC and HSEC modulate the physiological response of liver to drugs in 2D monolayer coculture systems. Thus, when modeling the drug response in vitro it is important to account for interactions of parenchymal and nonparenchymal cells in a complex 3D tissue environment. In this work, we compared the responses of four different liver tissue chips to the treatments with common hepatotoxic compounds including troglitazone, rosiglitazone, and cyclophosphamide. These various liver chips were treated with 10 μ M troglitazone, 150 μ M rosiglitazone, or 7.5 mM cyclophosphamide, respectively, over 16 h to screen for acute liver toxicity (**Figure 3.5B–D**). To evaluate the responses, a standard MTT

assay for analyzing mitochondrial activity was performed after 16 h drug treatment. It was found that the 3D coculture liver chip showed the highest mitochondrial activity in response to these drugs while 2D hepatocytes showed the lowest mitochondrial activity. These results further support that 3D cocultured liver tissue containing parenchymal and nonparenchymal liver cells displayed the best liver function and highest resistance to drug toxicity.

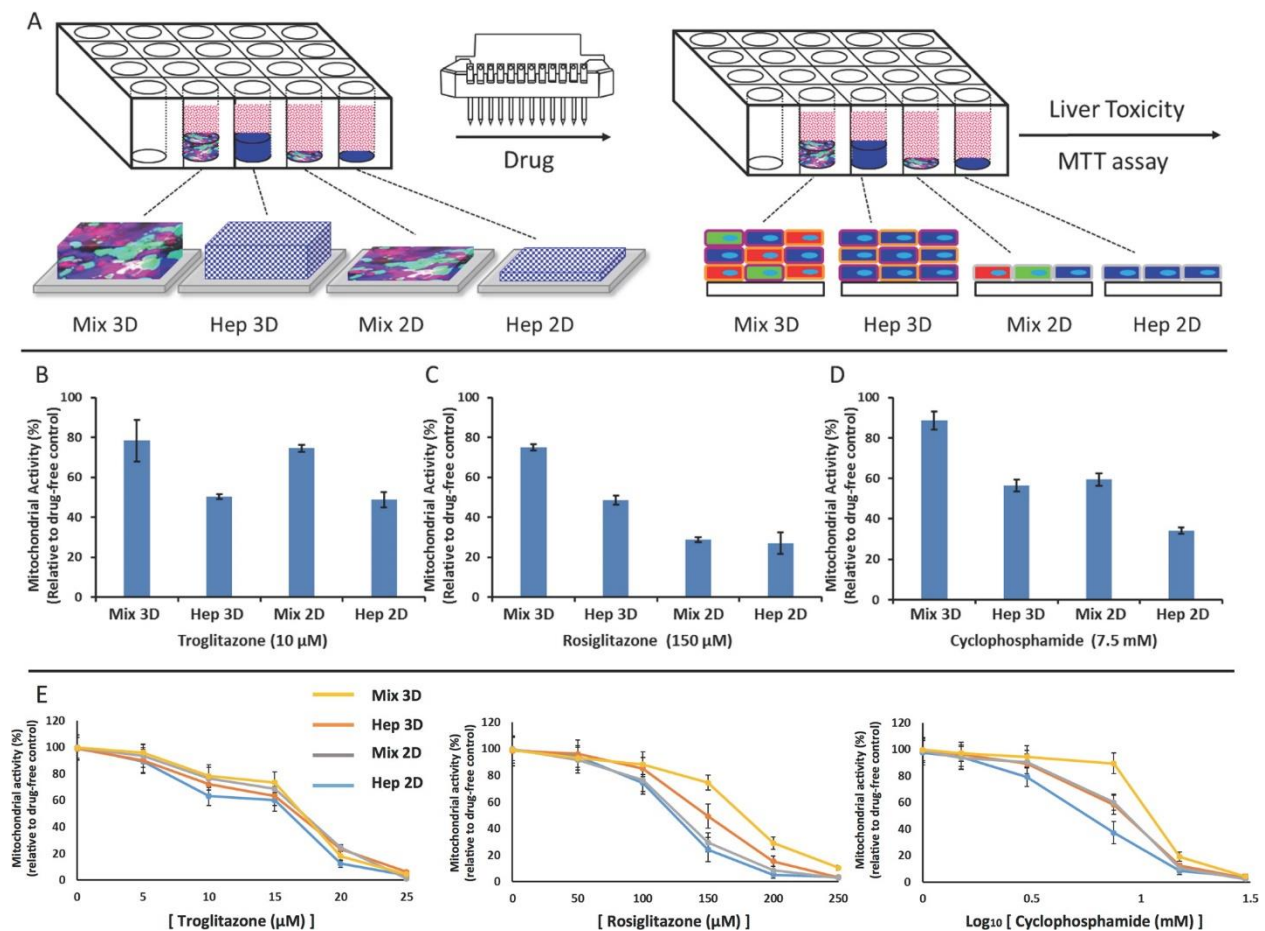


Figure 3.5. Study of mitochondrial activity for evaluation of liver toxicity in different types of liver constructed chips. (A) Drug screening of fabricated liver chips based on MTT assay after treating tissues for 16 h with (B) 10 μ M troglitazone, (C) 150 μ M rosiglitazone, and (D) 7.5 mM cyclophosphamide. (E) Plots of MTT assay for a range of drug concentrations for various tissue constructs.

3.5 Conclusion

In this report, we established for the first time a scaffold-free 3D tissue construction system based on a straightforward bio-orthogonal cell surface engineering tissue click ligation and applied it to liver fabrication and study. Based on this strategy we were able to rapidly construct a range of complex 3D liver tissues containing multiple parenchymal hepatocytes and nonparenchymal liver cell lines and evaluate their ability to recapitulate liver function through a variety of metabolic and drug assays. The 3D coculture liver tissue showed similar function to a real liver organ, and expressed excellent liver-specific functions. Furthermore, the 3D liver chip fabricated provides a new platform to generate a wide range of complex tissues with multiple cell types for a variety of future drug screening and tissue specific assays. The method can be used to generate a range of length scales of oriented 3D cocultures and multilayer tissues with many cell type components. The bioorthogonal ligation between cells initiates the assembly process, which is then further enhanced (held together) over time by the production of extracellular matrix. This strategy is also amenable to bioprinting and microfluidic methods to assemble stable spheroids and tissues in flow without post-encapsulation materials and may be combined with 3D printing and biodegradable polymers for the generation of many complex tissues.⁴³⁻⁴⁷ Due to the efficient cell assembly (cell economy) process this method in combination with polymer strategies may allow for filling of polymer molds or decellularized scaffolds rapidly for bioreactor applications since the cell types attach to each other and the polymer to rapidly generate thick tissues in a range of length scales. Finally, many complex thick tissues may be generated in 3D for organ on a chip type drug screens or viral assay screens, or as model systems for paracrine and autocrine signaling.

3.6 References

1. Friedman, S. L. Molecular Regulation of Hepatic Fibrosis, an Integrated Cellular Response to Tissue Injury. *J. Biol. Chem.* **275**, 2247–2250 (2000).
2. Lutolf, M. P. & Hubbell, J. A. Synthetic biomaterials as instructive extracellular microenvironments for morphogenesis in tissue engineering. *Nat. Biotechnol.* **23**, 47–55 (2005).
3. Groeber, F., Holeiter, M., Hampel, M., Hinderer, S. & Schenke-Layland, K. Skin tissue engineering — In vivo and in vitro applications. *Adv. Drug Deliv. Rev.* **63**, 352–366 (2011).
4. Bhatia, S. N., Underhill, G. H., Zaret, K. S. & Fox, I. J. Cell and tissue engineering for liver disease. *Sci. Transl. Med.* **6**, 245sr2-245sr2 (2014).
5. Vunjak-Novakovic, G. *et al.* Challenges in cardiac tissue engineering. *Tissue Eng. Part B. Rev.* **16**, 169–87 (2010).
6. Murphy, S. V & Atala, A. 3D bioprinting of tissues and organs. *Nat. Biotechnol.* **32**, 773–785 (2014).
7. Crispe, I. N. The Liver as a Lymphoid Organ. *Annu. Rev. Immunol.* **27**, 147–163 (2009).
8. Godoy, P. *et al.* Recent advances in 2D and 3D in vitro systems using primary hepatocytes, alternative hepatocyte sources and non-parenchymal liver cells and their use in investigating mechanisms of hepatotoxicity, cell signaling and ADME. *Arch. Toxicol.* **87**, 1315–530 (2013).
9. Llovet, J. M., Burroughs, A. & Bruix, J. Hepatocellular carcinoma. *Lancet* **362**, 1907–17 (2003).
10. Bataller, R. & Brenner, D. A. Liver fibrosis. *J. Clin. Invest.* **115**, 209–218 (2005).
11. Begriche, K., Massart, J., Robin, M.-A., Borgne-Sanchez, A. & Fromenty, B. Drug-induced toxicity on mitochondria and lipid metabolism: mechanistic diversity and deleterious consequences for the liver. *J. Hepatol.* **54**, 773–94 (2011).
12. Shen, C., Meng, Q. & Zhang, G. Species-specific toxicity of troglitazone on rats and human by gel entrapped hepatocytes. *Toxicol. Appl. Pharmacol.* **258**, 19–25 (2012).

13. Soldatow, V. Y., LeCluyse, E. L., Griffith, L. G. & Rusyn, I. In vitro models for liver toxicity testing. *Toxicol. Res.* **2**, 23–39 (2013).
14. Khetani, S. R. & Bhatia, S. N. Microscale culture of human liver cells for drug development. *Nat. Biotechnol.* **26**, 120–6 (2008).
15. Krause, P., Saghatolislam, F., Koenig, S., Unthan-Fechner, K. & Probst, I. Maintaining hepatocyte differentiation in vitro through co-culture with hepatic stellate cells. *In Vitro Cell. Dev. Biol. Anim.* **45**, 205–12 (2009).
16. Kim, K., Ohashi, K., Utoh, R., Kano, K. & Okano, T. Preserved liver-specific functions of hepatocytes in 3D co-culture with endothelial cell sheets. *Biomaterials* **33**, 1406–13 (2012).
17. Ho, C.-T. *et al.* Liver-cell patterning lab chip: mimicking the morphology of liver lobule tissue. *Lab Chip* **13**, 3578–87 (2013).
18. Bhatia, S. N., Yarmush, M. L. & Toner, M. Controlling cell interactions by micropatterning in co-cultures: hepatocytes and 3T3 fibroblasts. *J. Biomed. Mater. Res.* **34**, 189–99 (1997).
19. Kang, Y. B. (Abraham), Rawat, S., Cirillo, J., Bouchard, M. & Noh, H. (Moses). Layered long-term co-culture of hepatocytes and endothelial cells on a transwell membrane: toward engineering the liver sinusoid. *Biofabrication* **5**, 45008 (2013).
20. Uygun, B. E. *et al.* Organ reengineering through development of a transplantable recellularized liver graft using decellularized liver matrix. *Nat. Med.* **16**, 814–20 (2010).
21. Yoon No, D., Lee, K.-H., Lee, J. & Lee, S.-H. 3D liver models on a microplatform: well-defined culture, engineering of liver tissue and liver-on-a-chip. *Lab Chip* **15**, 3822–37 (2015).
22. Feng, Z.-Q. *et al.* The effect of nanofibrous galactosylated chitosan scaffolds on the formation of rat primary hepatocyte aggregates and the maintenance of liver function. *Biomaterials* **30**, 2753–63 (2009).
23. Hammond, J. S. *et al.* Scaffolds containing growth factors and extracellular matrix induce hepatocyte proliferation and cell migration in normal and regenerating rat liver. *J. Hepatol.* **54**, 279–87 (2011).
24. Dutta, D., Pulsipher, A., Luo, W. & Yousaf, M. N. Synthetic chemoselective rewiring of cell surfaces: generation of three-dimensional tissue structures. *J. Am. Chem. Soc.* **133**, 8704–13 (2011).
25. Dutta, D., Pulsipher, A., Luo, W., Mak, H. & Yousaf, M. N. Engineering cell surfaces via liposome fusion. *Bioconjug. Chem.* **22**, 2423–33 (2011).

26. Luo, W., Pulsipher, A., Dutta, D., Lamb, B. M. & Yousaf, M. N. Remote control of tissue interactions via engineered photo-switchable cell surfaces. *Sci. Rep.* **4**, 6313 (2014).
27. Bertozzi, C. R. A decade of bioorthogonal chemistry. *Acc. Chem. Res.* **44**, 651–3 (2011).
28. McKay, C. S. & Finn, M. G. Click chemistry in complex mixtures: bioorthogonal bioconjugation. *Chem. Biol.* **21**, 1075–101 (2014).
29. Dieterich, D. C. *et al.* Labeling, detection and identification of newly synthesized proteomes with bioorthogonal non-canonical amino-acid tagging. *Nat. Protoc.* **2**, 532–40 (2007).
30. Patterson, D. M., Nazarova, L. A. & Prescher, J. A. Finding the right (bioorthogonal) chemistry. *ACS Chem. Biol.* **9**, 592–605 (2014).
21. Rashidian, M., Song, J. M., Pricer, R. E. & Distefano, M. D. Chemoenzymatic reversible immobilization and labeling of proteins without prior purification. *J. Am. Chem. Soc.* **134**, 8455–67 (2012).
32. Park, S., Westcott, N. P., Luo, W., Dutta, D. & Yousaf, M. N. General chemoselective and redox-responsive ligation and release strategy. *Bioconjug. Chem.* **25**, 543–51 (2014).
33. Pulsipher, A., Dutta, D., Luo, W. & Yousaf, M. N. Cell-Surface Engineering by a Conjugation-and-Release Approach Based on the Formation and Cleavage of Oxime Linkages upon Mild Electrochemical Oxidation and Reduction. *Angew. Chemie Int. Ed.* **53**, 9487–9492 (2014).
34. Torchilin, V. P. Recent advances with liposomes as pharmaceutical carriers. *Nat. Rev. Drug Discov.* **4**, 145–160 (2005).
35. Csiszár, A. *et al.* Novel Fusogenic Liposomes for Fluorescent Cell Labeling and Membrane Modification. *Bioconjug. Chem.* **21**, 537–543 (2010).
36. Chen, Y.-F., Sun, T.-L., Sun, Y. & Huang, H. W. Interaction of Daptomycin with Lipid Bilayers: A Lipid Extracting Effect. *Biochemistry* **53**, 5384–5392 (2014).
37. Chan, Y.-H. M. & Boxer, S. G. Model membrane systems and their applications. *Curr. Opin. Chem. Biol.* **11**, 581–587 (2007).
38. Nicolson, G. L. The Fluid—Mosaic Model of Membrane Structure: Still relevant to understanding the structure, function and dynamics of biological membranes after more than 40years. *Biochim. Biophys. Acta - Biomembr.* **1838**, 1451–1466 (2014).
39. O'Brien, P. J., Luo, W., Rogozhnikov, D., Chen, J. & Yousaf, M. N. Spheroid and Tissue Assembly via Click Chemistry in Microfluidic Flow. *Bioconjug. Chem.* **26**, 1939–1949 (2015).

40. Luo, W. *et al.* A Dual Receptor and Reporter for Multi-Modal Cell Surface Engineering. *ACS Chem. Biol.* **10**, 2219–2226 (2015).
41. Hariparsad, N., Carr, B. A., Evers, R. & Chu, X. Comparison of Immortalized Fa2N-4 Cells and Human Hepatocytes as in Vitro Models for Cytochrome P450 Induction. *Drug Metab. Dispos.* **36**, 1046–1055 (2008).
42. Guillouzo, A. & Guguen-Guillouzo, C. Evolving concepts in liver tissue modeling and implications for *in vitro* toxicology. *Expert Opin. Drug Metab. Toxicol.* **4**, 1279–1294 (2008).
43. Stevens, M. M. Exploring and Engineering the Cell Surface Interface. *Science (80-.)*. **310**, 1135–1138 (2005).
44. Gartner, Z. J. & Bertozzi, C. R. Programmed assembly of 3-dimensional microtissues with defined cellular connectivity. *Proc. Natl. Acad. Sci.* **106**, 4606–4610 (2009).
45. Kelm, J. M. *et al.* A novel concept for scaffold-free vessel tissue engineering: Self-assembly of microtissue building blocks. *J. Biotechnol.* **148**, 46–55 (2010).
46. Gou, M. *et al.* Bio-inspired detoxification using 3D-printed hydrogel nanocomposites. *Nat. Commun.* **5**, (2014).
47. Zorlutuna, P. *et al.* Microfabricated Biomaterials for Engineering 3D Tissues. *Adv. Mater.* **24**, 1782–1804 (2012).

Chapter 4

Cell Polymerization via a Biocompatible Crosslinker

4.1 Summary

The crosslinker is a small molecule which is used to chemically link synthetic polymer threads or biomolecules into a complex superstructure with distinct properties. Molecules that are currently used today as crosslinking agents include divinyl and multivinyl agents that work via radical polymerization, cysteine amino acids which produce disulfide linkages, as well as metal ions which establish connections with monomers by forming ionic bonds. In this work, we created a di-functional bio-orthogonal dioxyamine crosslinker which was used to assemble cells into complex 3D tissues. The GFP- and RFP- expressing fibroblasts were surface engineered to present ketone functionalities via liposome fusion and crosslinked with the dioxyamine crosslinker into 3D spheroids. The technology was also used to assemble hepatocytes, stellate cells and endothelial cells into a functional liver tissue for the drug toxicity studies. Unlike previously used technologies, this novel method is scaffold free and does not rely on the use of exogenous polymer materials to support the cell mass.

4.2 Introduction

Cross-link has been used as a general term in both synthetic polymer science and biological science to describe covalent or ionic bonding between different polymer chains, including synthetic polymers and natural polymers like proteins. By cross-linking polymer chains via a cross-linking agent, also called a cross-linker, a polymer network and even a macromolecule with infinite molecular weight can be obtained, thus modified physical and chemical properties as well as a variety of important applications may be achieved.¹⁻³

In polymer science, a cross-linker is usually a divinyl or multivinyl agent, through which radical polymerization or copolymerization of vinyl monomers can be extended to a cross-linked network. To date, radical polymerization and cross-linking is still the main stream in conventional the polymer system, and nearly 50% of all commercial synthetic polymers are produced via conventional radical polymerization and cross-linking.^{1,4-6} By simply adjusting the conditions of cross-linking, physical and chemical properties of polymers can be modified significantly, and various polymers can be produced on demand.⁷⁻⁹ Thus, divinyl and multivinyl cross-linkers have been considered crucial components to polymer science and industry.^{10,11}

In biological science, non-vinyl cross-linking compounds containing two reactive functionalities is also widely used and have played an important role in a range of biological applications.¹²⁻¹⁴ For instance, chemical cross-linking of proteins via a bifunctional cross-linker is very important in the stabilization and analysis of the native molecular structures of proteins, enzymes and oligopeptides.¹⁵⁻¹⁸ Another example is the bifunctional alkylator, also known as DNA cross-linker, which has been used as an important class of cancer chemotherapeutic regimens.¹⁹

Moreover, there are many other types of cross-linkers such as metal ions,²⁰⁻²³ proteins with two or multiple binding specificities,²⁴⁻²⁷ etc.

While cross-linkers and cross-linking systems have been broadly used in many fields like polymer, biology, biomaterial, and even nanomaterial,²⁸⁻³¹ the concept and application are still limited to the construction of a material network from chemical monomers. For the first time live cells have been considered monomers in the construction of 3D tissue networks, thus enabling the ability to control cell assembly and tissue construction for a range of important applications such as regenerative medicine, tissue engineering, and organ transplantation.

To date, 3D cell culture and tissue construction still rely heavily on 3D matrices such as collagen, gelatin, alginate, and agarose hydrogels, as well as other porous polymer scaffolds and decellularized organ scaffolds. However, there are many challenges associated with the use of 3D matrices for cell based research and applications, including the stability of scaffolds, toxicity of degradation products, potential inflammation and immune responses, interference with cell-cell interaction, and unpredictable impacts on signaling pathways.³² Moreover, despite the fact that some biocompatible scaffolds can mimic the extracellular matrix and allow cells to adhere and proliferate, these man-made environments are still not ideal for making applicable tissues and organs. Therefore, scaffold-free tissue construction methodology would be of central importance to future applications in tissue engineering and regenerative medicine.

Herein, we developed a new cross-linking system as well as a new technique based on the cross-linking of surface-engineered cellular “monomers”. This new, innovative system has been demonstrated to be applicable to a variety of biological studies, and is also expected to expand to applications in nanomaterials, micro-size materials and micro-size biological units under the condition that they can be surface-tailored to present certain functionalities which are clickable to

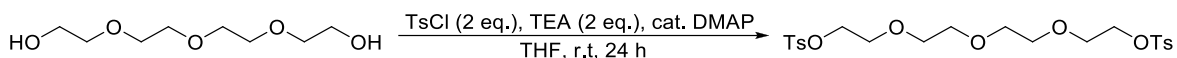
specific cross-linkers. In particular, a bioorthogonal oxime chemistry was introduced into our system for cross-linking ketone-tailored cells via a dioxyamine cross-linker. Oxime conjugation between an oxyamine and ketone is well known to be efficient and bioorthogonal under physiological conditions.³³⁻³⁶ By installing ketone functionality onto the cell surface through a universal surface engineering method,³⁷⁻⁴⁰ any type of cell can be assembled together by a poly(ethylene glycol)- or oligo(ethylene glycol)-based dioxyamine cross-linker.

In this work, it is the first time that a biocompatible difunctional cross-linker was integrated with a recently developed cell surface engineering method for cross-linking live cells and achieving controllable cell assembly and 3D tissue construction. Based on this novel system, scaffold-free tissue construction can be easily achieved.

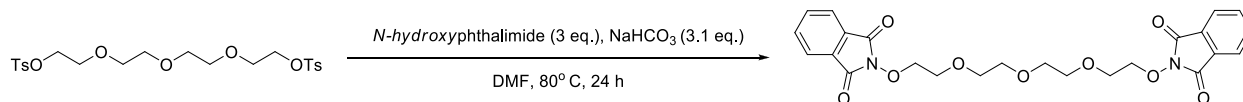
4.3 Experimental

All chemical reagents were obtained from Sigma-Aldrich and Fisher Scientific. *O*-Dodecyloxyamine was synthesized as previously reported.³⁷ 1-palmitoyl-2-oleoyl-sn-glycero-3-phosphocholine (POPC) and 1,2-dioleoyl-3-trimethylammonium-propane (DOTAP) were purchased from Avanti Polar Lipids (Alabaster, AL). 3T3 Swiss Abino Fibroblasts were purchased from ATCC. RFP Expressing Human Neonatal Dermal Fibroblasts (RFP-HNDFs) were purchased from Olaf Pharmaceuticals. NIH3T3/GFP cell line was purchased from Cell Biolabs, Inc. These cell lines were transferred by Cedarlane labs (Burlington, Canada). Immortalized human hepatocytes Fa2N-4 (cells that were transformed with the SV-40 large T antigen), were obtained from Xenotech, KS. Primary human hepatic stellate cells (STeC) were obtained from Sciencell, CA. Primary human hepatic sinusoidal endothelial cells (EC) and their medium were purchased from Sciencell, CA.

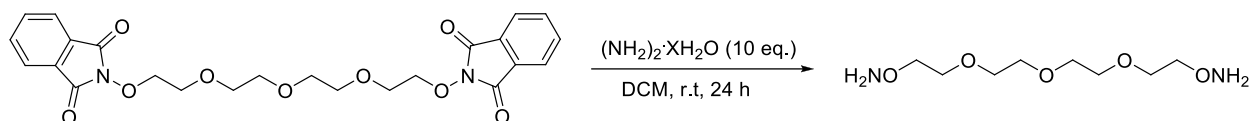
4.3.1 Synthesis of Dioxyamine Crosslinker



To a round bottom flask equipped with a stir bar was added TEG (1 eq.) in THF. To this solution was added Et₃N (2 eq.) and a catalytic amount of DMAP. To this mixture a solution of 4-toluenesulfonyl chloride (2 eq.) in THF was added to the reaction mixture and the reaction was allowed to proceed for 24 h. The reaction mixture was then filtered and concentrated *in vacuo* to remove THF. The resulting residue was then diluted with DCM and the mixture was washed with a saturated aqueous solution of ammonium chloride and the aqueous phase was separated. The organic phase was washed with brine, dried using magnesium sulfate and concentrated *in vacuo*. The crude product was purified by flash column chromatography (hexanes: EtOAc, 1:1) to yield the product as a clear oil.



To a round bottom flask equipped with a stir bar was added *N*-hydroxyphthalimide (2 eq.) and NaHCO₃ (2 eq.) in DMF. This mixture was stirred at 80°C for 1 h, until turning dark brown. A solution of tosylated TEG (1 eq.) in DMF was added dropwise and the reaction was allowed to proceed for 24 h at 80°C. Upon completion, the reaction mixture was filtered and concentrated *in vacuo* to remove DMF. The product was washed with DCM and saturated ammonium chloride and the aqueous phase was separated. The organic phase was washed with brine, dried using magnesium sulfate and concentrated *in vacuo*. The crude product was purified by flash column chromatography (hexanes: EtOAc, 1:1) to yield a clear oil product.



To a round bottom flask equipped with a stir bar was added the phthalate (1 eq.) in DCM. To this solution was added hydrazine hydrate (10 eq.) dropwise and the reaction was allowed to proceed for 24 h at r.t. Upon completion, the excess hydrazine was washed with water and the aqueous phase separated. The organic phase was washed with brine, dried using magnesium sulfate and concentrated *in vacuo* to yield the product as a pale yellow oil.

4.3.2 Preparation of Functionalized Liposomes

Liposomes were prepared as previously reported. The ligand to be incorporated into the liposome was added to CHCl_3 to make a 10 mM solution. To 60 μL of this solution was added 430 μL of POPC solution (10 mg/mL) and 10 μL of DOTAP solution (10 mg/mL). This mixture was then concentrated *in vacuo* to remove CHCl_3 . To the thoroughly dried mixture was added 3 mL PBS to make a 1.5 mg/mL suspension, which was then sonicated by tip sonicator for 20 min to make a clear liposome solution.

4.3.3 Cell Culture

3T3 Swiss Abino Fibroblasts, RFP Expressing Human Neonatal Dermal Fibroblasts, and C3H/10T1/2 cells were cultured in Dulbecco's modified Eagle medium (DMEM) with 10% fetal bovine serum (FBS) and 1% penicillin/streptomycin. NIH3T3/GFP cells were cultured in DMEM containing 10% FBS, 0.1 mM MEM Non-Essential Amino Acids, 2 mM L-glutamine, 10 $\mu\text{g}/\text{mL}$ Blastidicin, and 1% penicillin/streptomycin. Immortalized human hepatocytes Fa2N-4 were cultured on collagen I-coated plates in multifunction enhancing (MFE) plating medium containing

10% newborn calf serum (Xenotech, KS), and 1% penicillin/streptomycin solution. At 24h upon plating, the medium was replaced with MFE serum-free support medium containing component A. The medium was replaced every 48h. The cells were passaged upon reaching confluence (every 3-4 days). Primary human hepatic stellate cells (STeC) were cultured on poly-L-lysine-coated plates in stellate cell medium (SteCM) consisting of 500ml basal medium containing 5ml of stellate cell growth supplements (SteCGS), 10ml of fetal bovine serum (FBS) and 5ml of penicillin/streptomycin solution. The cells were passaged upon reaching confluence. The medium was changed every 48h. Primary human hepatic sinusoidal endothelial cells (EC) were cultured on fibronectin-coated plastic plates in endothelial cell medium (ECM) containing 5ml of endothelial cell growth supplement (ECGS), 25ml FBS and 5ml penicillin streptomycin solution in 500ml of basal medium. The cells were passaged upon reaching confluence (every 2-3 days) and the medium was changed every 48h. All these cells were incubated at 37°C in a humidified atmosphere of 5% CO₂, and released from tissue culture plates using 0.05% trypsin in 0.53 mM EDTA.

4.3.4 Cell Surface Engineering via Liposome Fusion

To fresh cell media was added 5% volume of functionalizing liposome solution. The cells were maintained in this media for 4h before exchanging the media.

4.3.5 Cell – Cell Crosslinking

To a ketone functionalized cell suspension was added 5% volume of 100 mM oxyamine crosslinking solution to reach a final concentration of 5 mM. Cells were maintained in this media

for 30 min, and then pipetted onto glass substrates for imaging or further maintenance. A control sample was also prepared using cells bearing no functionality.

4.3.6 Confocal Microscopy

The cell samples for confocal microscopy were fixed with formaldehyde (3.2% in PBS) for 20 min, rinsed with PBS, and then secured in fluorescence mounting medium (Dako, Carpinteria, CA, USA), which enhances the visualization of cells when viewed under a fluorescent microscope, with a thin glass cover slip. The mounted samples were imaged by Zeiss LSM 700 laser scanning confocal microscope and analyzed by ZEN 2000 imaging software.

4.3.7 Liver Tissue Assembly

Prior to tissue assembly the cells were allowed to reach 90-100% confluence. After that, all cells were treated with ketone liposome solution (50 μ l of liposomes/1ml of medium) and incubated at 37°C for 4h. The medium was discarded and the cells were washed with PBS twice. Following that, the ketone- and oxyamine-tethered cells were removed from the plate with 0.25% trypsin and centrifuged down at 800rpm. The medium was discarded and ketone-labeled hepatocytes, stellate cells and endothelia cells were mixed with crosslinker solution for 30 min, before placed on 12-well (3.7cm²) collagen I-coated plates and given a slight shake to induce cells assembly. Each mixed (co-culture) 2D or 3D sample contained $\sim 1 \times 10^5$ of Fa2N-4 hepatocytes, $\sim 1 \times 10^5$ of HSEC and $\sim 5 \times 10^4$ of HSC. Each 2D and 3D hepatocyte-only culture contained $\sim 1 \times 10^5$ of Fa2N-4 hepatocytes. The cells were then incubated at 37°C and 5% CO₂ for 16h to achieve full spreading of cells in the tissues. Upon spreading of cells, fresh MFE plating medium was added onto the plates. After 24h, the medium was replaced with 1:1 mixture of MFE support medium and ECM.

4.3.8 Immunohistochemistry and Confocal Microscopy

Prior to tissue assembly cells were incubated in serum-free medium containing fluorescent live stain (Life Technologies). Fa2N-4 hepatocytes, endothelia cells, and stellate cells were treated with 25 μ M CellTracker™ Blue CMAC (7-amino-4-chloromethylcoumarin), 25 μ M CellTracker™ Green CMFDA (5-chloromethylfluorescein diacetate), and 25 μ M CellTracker Red CMTPX respectively. The cells were incubated for 45min, after which they were washed thoroughly with PBS and incubated in serum-free medium for another 45min. Following that, the cells were assembled into 3D tissues and incubated for 24h. Subsequently, the tissues were fixed with 10% formalin for 30min and visualized with LSM-700 (Zeiss) confocal microscope.

4.3.9 Activation of Cytochrome P450 3A4

To induce cytochrome P450 3A4, the 3D tissue samples were incubated in MFE support medium containing 10 μ M Rifampin (Sigma) for 72h at 37°C, 5% CO₂. The control samples were treated with DMSO vehicle only for calculation of fold activation. The medium was changed every 24h. The samples were analyzed via P450-Glo™ CYP3A4 Assay Kit (Luciferin-IPA) (Promega) by using the manufacturer's instructions for the non-lytic cycle. The sample's medium was replaced with fresh MFE support medium containing 3 μ M Luciferin-IPA and the samples were incubated for 50min. Following that, 50 μ l of medium was transferred into white 96-well plate. After that, 50 μ L of the detection reagent was added into each well. The samples were covered with the aluminum foil and incubated for 20 min at room temperature. The lumiscence was read using Biotek Synergy Multi-detection Plate Reader.

4.3.10 Albumin Analysis of Liver Tissues

Liver tissues were maintained for 14 days before culture medium was collected from the samples. The albumin content was measured via Human Albumin Pincer Assay kit (Mediomics). New medium (1:1 MFE support medium and ECM) was added 24h prior to collecting it for albumin quantification.

4.3.11 Liver Toxicity Assays

Liver tissues were incubated with 7.5 μ M Cyclophosphamide dissolved in MFE support medium for 16h. The control samples were treated with DMSO vehicle. Subsequently, the cell viability was analyzed by (3-(4,5-dimethylthiazol-2-yl)-2,5-diphenyl tetrazolium bromide (MTT) assay (Sigma), where the tetrazolium ring is cleaved by mitochondrial dehydrogenase enzymes. The samples were incubated in DMEM phenol red-free medium containing MTT reagent for 1h resulting in production of a purple precipitate which was subsequently dissolved in 1:1 solution of isopropanol and DMSO. The absorbance was measured at 570nm using Synergy Biotek device.

4.4 Results and discussion

As shown in Figure 1, a lipid-like molecule (dodecanone) was mixed with a neutral lipid, 1-palmitoyl-2-oleoyl-*sn*-glycero-3-phosphocholine (POPC), and a cationic lipid, 1,2-dioleoyl-3-trimethylammonium-propane (DOTAP), in order to make a functionalized liposome, which was then used for cell surface engineering (**Figure 1A**). After cells were engineered with the lipid-like molecule (2-dodecanone) to present a functional group (ketone) on cell membrane, the specially designed cross-linker (dioxyamine) can then chemoselectively react with the functional groups (ketone) on cells surfaces. Although any bioorthogonal molecular recognition pair can be integrated into this universal surface engineering and cross-linking system, a low-toxicity and water-soluble ethylene glycol based dioxyamine was used as the cross-linker in this work, while a ketone group was introduced to cell surface as the chemoselective recognition group. Oxime conjugation between an oxyamine and ketone is well known as bioorthogonal, stable and efficient under physiological conditions. Based on our cell surface engineering system, there are only a small amount (several thousand) of functional groups (ketones) present on each cell membrane.¹⁵ This means that ketone molecules were so dispersed on cell surface that the distance between any two ketone molecules can be considered infinitely large compared to the molecular length of the cross-linker, thus the chance of one dioxyamine quenched by two ketones on the same cell surface is negligible. With excess dioxyamine cross-linker in cell suspension, multivalent oxime bonding between dioxyamine cross-linkers and ketones among different cells can be achieved, and various cells can be cross-linked and assembled into spheroids and microtissues due to the interfacial oxime conjugation (**Figure 1B**). When different cell lines were surface-engineered with ketones and mixed in presence of dioxyamine cross-linker, multicellular cross-linking and three-dimensional (3D) co-culture tissue can be constructed on demand (**Figure 1C**).

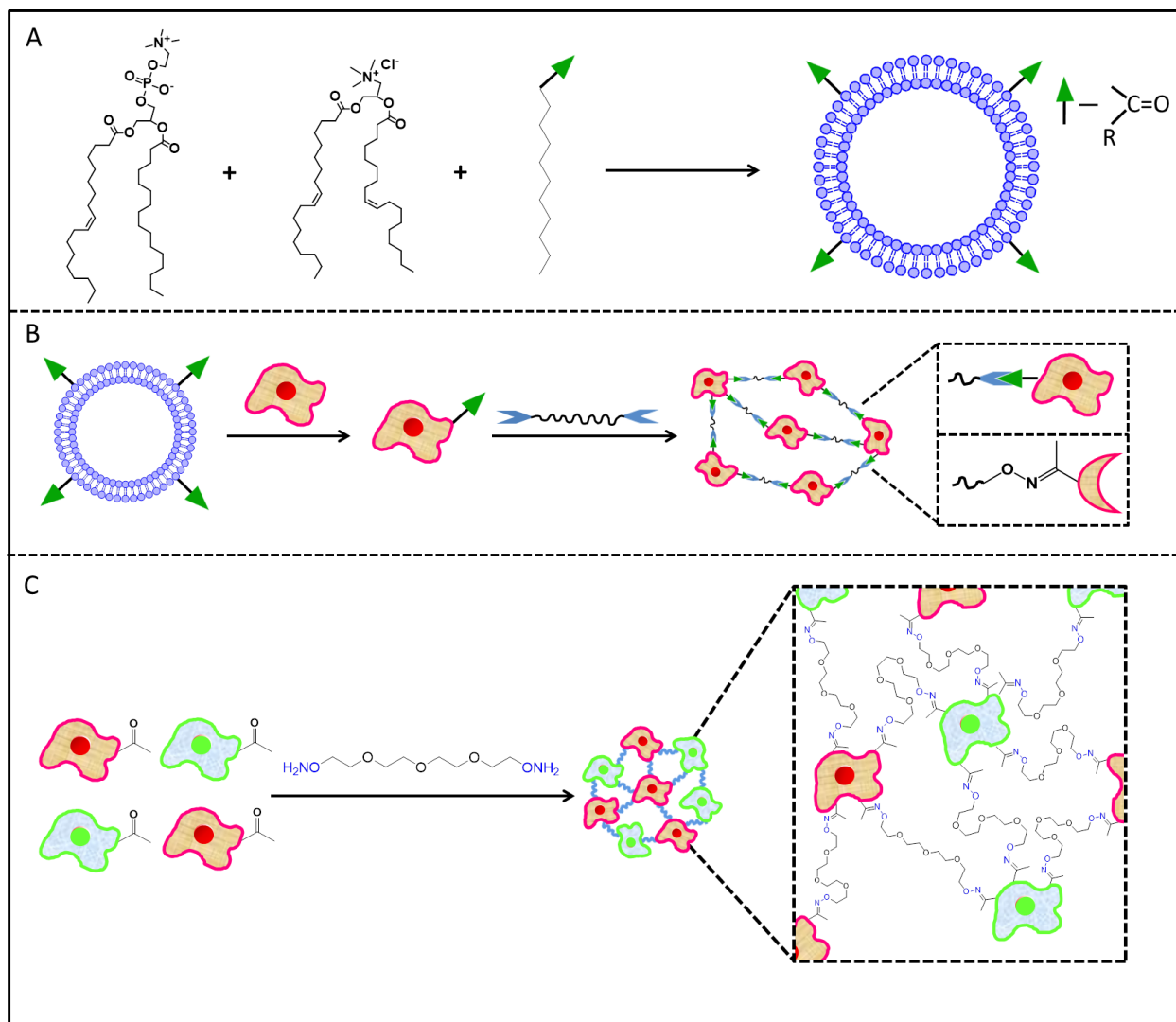


Figure 4.1. Schematic of cell surface engineering and cross-linking surface-engineered cells. (A) Liposome formation. Functionalized liposomes were made from POPC, DOTAP, and lipid-like molecule with functionalized group (ketone). (B) Cell surface engineering and cell cross-linking. Functionalized Liposomes were fused to cells to engineer cells surface to present functional group (ketone), which can then react with a specially designed cross-linker with chemoselective reacting group (oxyamine), to form a stable chemical bonding (oxime). Based on this interfacial chemoselective oxime conjugation, which is very efficient and stable under physiological condition, surface-engineered cells can be easily clicked and assembled to form clusters and microtissues. (C) By integrating cell surface engineering and crosslinking strategies, various ketone-labelled cell lines can be assembled together by the dioxyamine cross-linker to construct multicellular co-culture systems and three-dimensional (3D) tissues on demand.

To test the integrated surface engineering and crosslinking system, different cell lines were incorporated into this work as shown in **Figure 4.2**. As a representative study, RFP expressing human neonatal dermal fibroblasts (RFP-HNDFs) were surface-engineered with ketone groups, which efficiently react with an oxyamine group when a dioxyamine cross-linker was introduced to the cell suspension. After multivalent oxime bonding among different cell membranes, RFP-HNDFs were locked together and cell spheroids were observed in a short period of time (15 min). In comparison, control experiment with the same condition but no cross-linker involved showed no spheroids (**Figure 4.2A**). In another representative study, GFP expressing NIH3T3 (GFP-NIH3T3) cells were also surface-engineered with ketone molecules by the same method. After mixing the ketone-tailored GFP-NIH3T3 cells with dioxyamine cross-linker, GFP-NIH3T3 spheroids can be observed in 15 min, while no spheroid was found in the control experiment in the absence of cross-linker. In order to further test our system for future tissue engineering application and tissue construction purpose, which requires assembly of multiple cell lines to build up multicellular co-culture system, RFP-HNDFs and GFP-NIH3T3 cells were both surface-engineered and then incorporated into the cross-linking system to achieve co-cultured microtissue as shown in **Figure 4.2C**. In a common co-culture system, different cell lines usually have the tendency to exclude other cell populations and find their own population. This phenomenon leads to uncontrollable cell separation in a normal co-culture system. However, our cross-linking system allows different cell populations to be efficiently locked together and well connected on demand. This important merit provides a great opportunity for studying controllable cell-cell contact as well as intercellular interaction between different cell populations. To further exhibit the potential of this powerful strategy, a representative application in liver tissue engineering was performed in this work.

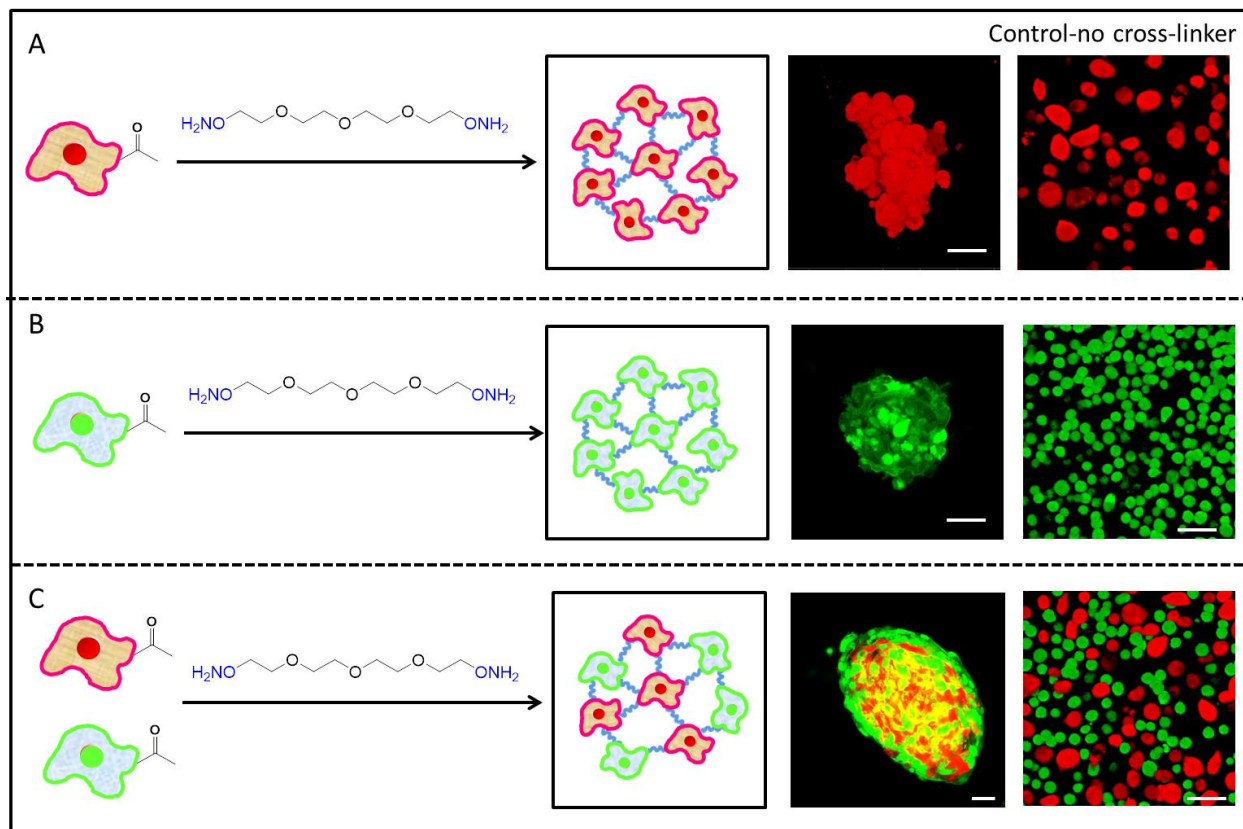


Figure 4.2. Schematic and fluorescent microscopy showing cross-linking and assembly of surface-engineered cells. (A) Ketone-tailored RFP expressing human neonatal dermal fibroblasts (RFP-HNDFs) were assembled by the dioxamine cross-linker to form RFP-HNDFs spheroid microtissue. Control treated with the same conditions except cross-linker resulted in regular cell culture. (B) Ketone-tailored GFP expressing NIH3T3 (GFP-NIH3T3) cells were assembled by the dioxamine cross-linker to form GFP-NIH3T3 spheroid microtissue. Control without cross-linker showed regular cell culture. (C) Mixing surface-engineered RFP-HNDFs and GFP-NIH3T3 with the cross-linker resulted in co-culture spheroid microtissue, while control without cross-linker showed random cells mixture.

The liver is one of the most important organs in the human body and has over 500 functions including the metabolism of proteins, carbohydrates, and lipids; detoxification of endogenous and exogenous compounds; the production of bile for digestion; and secretion of many serum proteins (i.e. albumin, coagulation factors). Despite significant efforts devoted to liver tissue study and engineering, the liver tissue remains one of the most difficult tissues to reconstruct and analyze in

the laboratory. The main reason is that hepatocytes are very difficult to maintain and rapidly lose liver-specific functions under *in vitro* conditions. The most common method for the maintenance of liver functionality and to allow for hepatocytes to survive longer, coculture systems are fabricated or 3D tissue/scaffold hybrids are constructed to provide the specific cell-cell contact hepatocytes require. While various methodologies were developed for better maintenance of hepatocytes and certain functions, construction of scaffold free 3D liver tissue remains challenging.

In this work, 3D liver tissue was constructed via the integrated crosslinking and surface engineering system as another representative application. Through surface engineering liver cells such as hepatocytes, stellate cells, and endothelial cells, ketone functionality can be installed onto the cell membranes to allow for an interfacial oxime reaction with a dioxyamine cross-linker in physiological conditions. In particular, 3D multilayer tissue can be constructed by mixing three ketone-engineered liver cell lines with the bioxyamine cross-linker, while 2D monolayers can be obtained without a cross-linker (**Figure 4.3A**). By altering the conditions of the crosslinking system, various cell assembly and tissue constructions can be achieved. For instance, multicellular spheroids can be made by coculturing three engineered cell lines in the presence of a crosslinker for 20 min (**Figure 4.3B**). More importantly, 3D multilayer hepatocytes (**Figure 4.3C**) and 3D multilayer coculture liver tissues (**Figure 4.3D**) were constructed on demand. Without incorporating the integrated cross-linking system, only a 2D monolayer was obtained (**Figure 4.3E**). It was observed that the liver tissue constructed by the cross-linking system can survive and maintain liver specific functionality for several weeks (data not shown here). This merit is of central importance to potential liver chip fabrication and drug analysis.

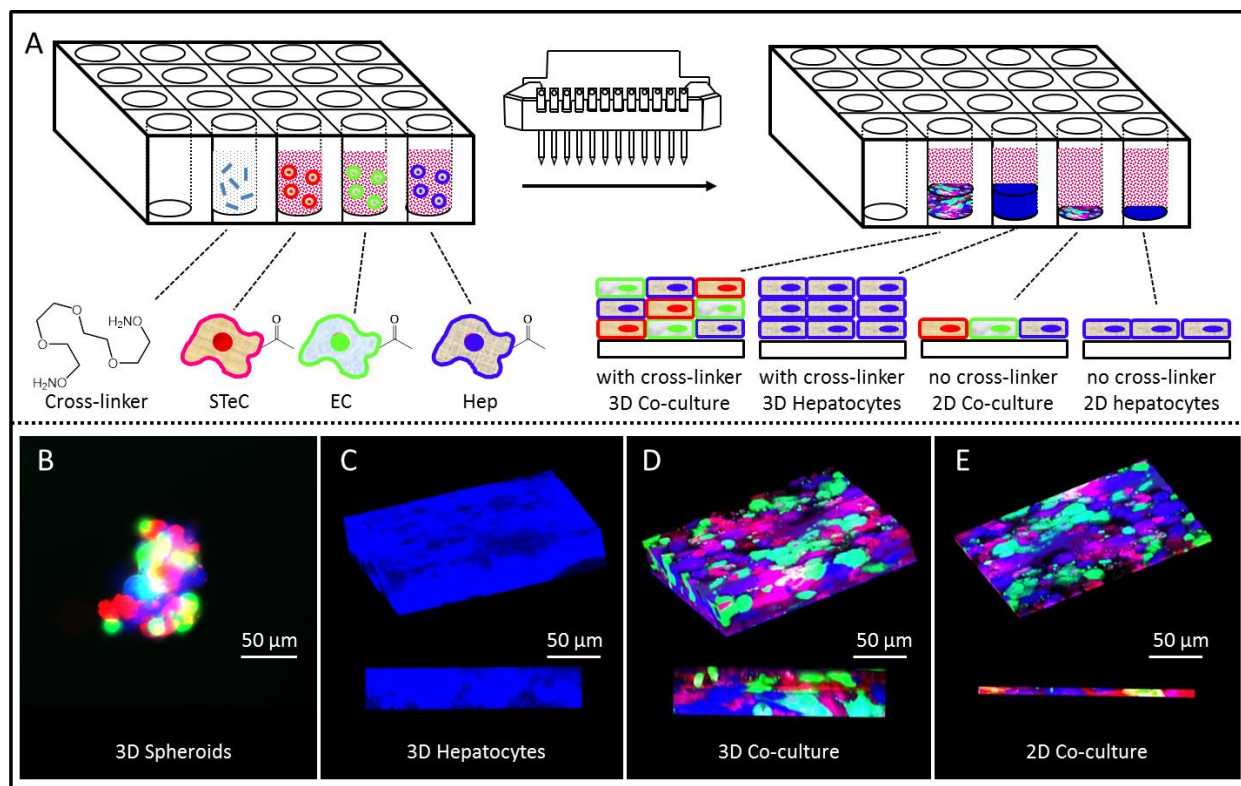


Figure 4.3. Constructing model 3D liver tissue by the integrated surface engineering and cross-linking system. (A) Surface-engineered liver cell lines including hepatocytes (Hep), stellate cells (STeC), and endothelial cells (EC), were assembled together by the cross-linker to form a 3D co-culture multilayer tissue. Control without cross-linker resulted in 2D monolayer. (B) Overlay fluorescent micrograph of liver spheroid microtissue. (C) Confocal microscopy images (3D view and side view) of multilayer 3D hepatocytes, made by mixing surface-engineered hepatocytes with cross-linker. (D) Confocal microscopy images of multilayer 3D co-culture tissue, made by mixing three surface-engineered liver cell lines with a cross-linker. (E) Confocal images of 2D monolayer, made by mixing three surface-engineered liver cell lines but without cross-linker. Hepatocytes (Hep), stellate cells (STeC), and endothelial cells (EC) were live stained with blue, red, and green respectively. Scale bars represent 50 μm .

Since the 3D multilayer live tissue can be easily fabricated on demand, a further exploration was performed to evaluate and demonstrate the potential applicability of our system in liver chip studies. To make a parallel comparison, standard liver assay and drug toxicity tests were performed simultaneously based on various liver tissues, including a 2D coculture monolayer, 3D coculture multilayer, 2D hepatocytes monolayer, and 3D hepatocytes multilayer (**Figure 4.4**). With the same amount of cells involved in all the liver chips, different levels of albumin expression and drug

resistance were recorded. It was found that the 3D multilayer liver chips are far superior to the 2D monolayer liver chips comparing the albumin expression, which is a well-known liver-specific function. Moreover, the 3D multilayer coculture liver chip is superior to others comparing the drug resistance (cyclophosphamide, 7.5 mM). Therefore, based on this study, it can be concluded that the 3D coculture multilayer liver chip is superior at both albumin expression and drug resistance. This preliminary result showed a great potential of the 3D coculture liver chip as future candidate of liver-specific functions and drugs screening.

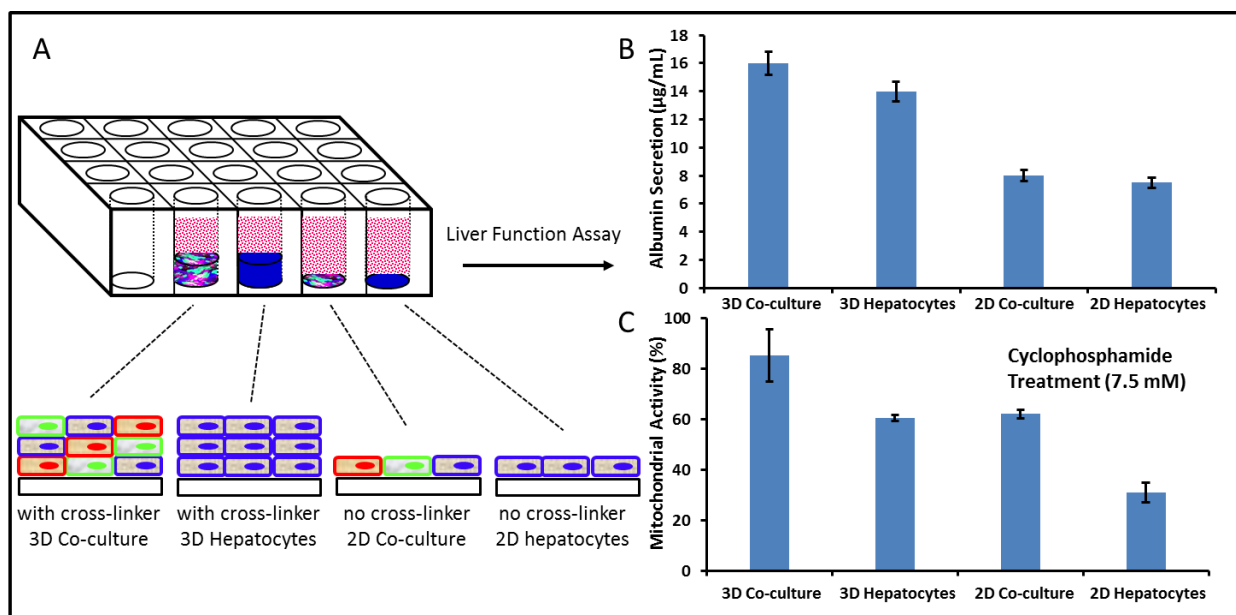


Figure 4.4. Constructed model 3D liver tissue for liver chip assay application. (A) Liver microtissues were constructed by the integrated surface engineering and cross-linking system, and applied as liver chip for the liver assay study and drug analysis. (B) Albumin assay was performed and analyzed based on the constructed liver chips. (C) Liver toxicity test of Cyclophosphamide (7.5 mM) was performed and analyzed based on the constructed liver chips.

4.5 Conclusion

In this work, a scaffold-free tissue assembly method has been developed by integrating a cell surface engineering strategy with a novel cell cross-linking method. Based on this surface engineering strategy, many different cell lines can be tailored with specific functionalities allowing for interfacial conjugation with corresponding cross-linkers to achieve efficient cell-cell assembly and tissue construction. In this work, ketone-tailored cells and a low-toxicity tetra(ethylene glycol)-based dioxyamine crosslinker were introduced as a demonstration of this universal methodology. Due to the efficient bioorthogonal conjugation between ketone and oxyamine, a variety of ketone-tailored cells were cross-linked via the dioxyamine cross-linker, resulting in multicellular tissue formation on demand. As a representative application of this integrated system, three major liver cells were surface-engineered and cross-linked to form 3D liver tissue, which was then used as a 3D liver chip for a liver function assay and drug analysis. This integrated cell surface engineering and cross-linking methodology provides us with an incredible opportunity for the efficient and controllable assembly of any cell lines, and can open the doors for a range of future applications in tissue engineering, regenerative medicine, and organ transplantation.

4.6 References

1. Matyjaszewski, K. (Krzysztof), Gnanou, Y., Leibler, L. & Wiley InterScience (Online service). *Macromolecular engineering : precise synthesis, materials properties, applications*. (Wiley-VCH, 2007).
2. Li, B. *et al.* A New Strategy to Microporous Polymers: Knitting Rigid Aromatic Building Blocks by External Cross-Linker. *Macromolecules* **44**, 2410–2414 (2011).
3. Nicolaÿ, R., Kamada, J., Van Wassen, A. & Matyjaszewski, K. Responsive Gels Based on a Dynamic Covalent Trithiocarbonate Cross-Linker. *Macromolecules* **43**, 4355–4361 (2010).
4. Braunecker, W. A. & Matyjaszewski, K. Controlled/living radical polymerization: Features, developments, and perspectives. *Prog. Polym. Sci.* **32**, 93–146 (2007).
5. Le Droumaguet, B. & Nicolas, J. Recent advances in the design of bioconjugates from controlled/living radical polymerization. *Polym. Chem.* **1**, 563 (2010).
6. Chu, D. S. H. *et al.* Application of Living Free Radical Polymerization for Nucleic Acid Delivery. *Acc. Chem. Res.* **45**, 1089–1099 (2012).
7. Bispo, M., Guillon, D., Donnio, B. & Finkelmann, H. Main-Chain Liquid Crystalline Elastomers: Monomer and Cross-Linker Molecular Control of the Thermotropic and Elastic Properties. *Macromolecules* **41**, 3098–3108 (2008).
8. Hennink, W. . & van Nostrum, C. . Novel crosslinking methods to design hydrogels. *Adv. Drug Deliv. Rev.* **54**, 13–36 (2002).
9. Kharkar, P. M., Kiick, K. L. & Kloxin, A. M. Designing degradable hydrogels for orthogonal control of cell microenvironments. *Chem. Soc. Rev.* **42**, 7335–7372 (2013).
10. Gao, H. & Matyjaszewski, K. Synthesis of functional polymers with controlled architecture by CRP of monomers in the presence of cross-linkers: From stars to gels. *Prog. Polym. Sci.* **34**, 317–350 (2009).
11. Kushner, A. M., Gabuchian, V., Johnson, E. G. & Guan, Z. Biomimetic Design of Reversibly Unfolding Cross-Linker to Enhance Mechanical Properties of 3D Network Polymers. *J. Am. Chem. Soc.* **129**, 14110–14111 (2007).
12. Paramelle, D., Miralles, G., Subra, G. & Martinez, J. Chemical cross-linkers for protein structure studies by mass spectrometry. *Proteomics* **13**, 438–456 (2013).

13. Haney, C. M. & Horne, W. S. Dynamic covalent side-chain cross-links via intermolecular oxime or hydrazone formation from bifunctional peptides and simple organic linkers. *J. Pept. Sci.* **20**, 108–114 (2014).
14. Sinz, A. Divide and conquer: cleavable cross-linkers to study protein conformation and protein–protein interactions. *Anal. Bioanal. Chem.* **409**, 33–44 (2017).
15. Kluger, R. & Alagic, A. Chemical cross-linking and protein–protein interactions—a review with illustrative protocols. *Bioorg. Chem.* **32**, 451–472 (2004).
16. Buskas, T., Li, Y. & Boons, G.-J. The Immunogenicity of the Tumor-Associated Antigen Lewisy May Be Suppressed by a Bifunctional Cross-Linker Required for Coupling to a Carrier Protein. *Chem. - A Eur. J.* **10**, 3517–3524 (2004).
17. Lévesque, S. G. & Shoichet, M. S. Synthesis of Enzyme-Degradable, Peptide-Cross-Linked Dextran Hydrogels. *Bioconjug. Chem.* **18**, 874–885 (2007).
18. Vanderhooft, J. L., Mann, B. K. & Prestwich, G. D. Synthesis and Characterization of Novel Thiol-Reactive Poly(ethylene glycol) Cross-Linkers for Extracellular-Matrix-Mimetic Biomaterials. *Biomacromolecules* **8**, 2883–2889 (2007).
19. Shen, X. & Li, L. Mutagenic repair of DNA interstrand crosslinks. *Environ. Mol. Mutagen.* NA-NA (2010). doi:10.1002/em.20558
20. Micklitsch, C. M. *et al.* Zinc-Triggered Hydrogelation of a Self-Assembling β -Hairpin Peptide. *Angew. Chemie Int. Ed.* **50**, 1577–1579 (2011).
21. Lux, J. *et al.* Metal chelating crosslinkers form nanogels with high chelation stability. *J. Mater. Chem. B* **1**, 6359 (2013).
22. Smith, S. J., Du, K., Radford, R. J. & Tezcan, F. A. Functional, metal-based crosslinkers for α -helix induction in short peptides. *Chem. Sci.* **4**, 3740 (2013).
23. Pasqui, D., Atrei, A., Giani, G., De Cagna, M. & Barbucci, R. Metal oxide nanoparticles as cross-linkers in polymeric hybrid hydrogels. *Mater. Lett.* **65**, 392–395 (2011).
24. Cao, Y. & Suresh, M. R. Bispecific Antibodies as Novel Bioconjugates. *Bioconjug. Chem.* **9**, 635–644 (1998).
25. Wang, H., Shi, Y., Wang, L. & Yang, Z. Recombinant proteins as cross-linkers for hydrogelations. *Chem. Soc. Rev.* **42**, 891–901 (2013).
26. Lorand, L. & Graham, R. M. Transglutaminases: crosslinking enzymes with pleiotropic functions. *Nat. Rev. Mol. Cell Biol.* **4**, 140–156 (2003).

27. Lutolf, M. P. *et al.* Synthetic matrix metalloproteinase-sensitive hydrogels for the conduction of tissue regeneration: Engineering cell-invasion characteristics. *Proc. Natl. Acad. Sci.* **100**, 5413–5418 (2003).
28. Bigi, A., Cojazzi, G., Panzavolta, S., Roveri, N. & Rubini, K. Stabilization of gelatin films by crosslinking with genipin. *Biomaterials* **23**, 4827–4832 (2002).
29. Khetan, S. *et al.* Degradation-mediated cellular traction directs stem cell fate in covalently crosslinked three-dimensional hydrogels. *Nat. Mater.* **12**, 458–465 (2013).
30. Ifkovits, J. L. & Burdick, J. A. Review: Photopolymerizable and Degradable Biomaterials for Tissue Engineering Applications. *Tissue Eng.* **13**, 2369–2385 (2007).
31. Mann, B. K., Gobin, A. S., Tsai, A. T., Schmedlen, R. H. & West, J. L. Smooth muscle cell growth in photopolymerized hydrogels with cell adhesive and proteolytically degradable domains: synthetic ECM analogs for tissue engineering. *Biomaterials* **22**, 3045–3051 (2001).
32. Luo, W. *et al.* A Dual Receptor and Reporter for Multi-Modal Cell Surface Engineering. *ACS Chem. Biol.* **10**, 2219–2226 (2015).
33. Norotte, C., Marga, F. S., Niklason, L. E. & Forgacs, G. Scaffold-free vascular tissue engineering using bioprinting. *Biomaterials* **30**, 5910–5917 (2009).
34. Elahipanah, S. *et al.* Rewiring Gram-Negative Bacteria Cell Surfaces with Bio-Orthogonal Chemistry via Liposome Fusion. *Bioconjug. Chem.* **27**, 1082–1089 (2016).
35. Elahipanah, S., O’Brien, P. J., Rogozhnikov, D. & Yousaf, M. N. General Dialdehyde Click Chemistry for Amine Bioconjugation. *Bioconjug. Chem.* **28**, 1422–1433 (2017).
36. O’Brien, P. J., Elahipanah, S., Rogozhnikov, D. & Yousaf, M. N. Bio-Orthogonal Mediated Nucleic Acid Transfection of Cells via Cell Surface Engineering. *ACS Cent. Sci.* **3**, 489–500 (2017).
37. Dutta, D., Pulsipher, A., Luo, W., Mak, H. & Yousaf, M. N. Engineering Cell Surfaces via Liposome Fusion. *Bioconjug. Chem.* **22**, 2423–2433 (2011).
38. Dutta, D., Pulsipher, A., Luo, W. & Yousaf, M. N. Synthetic Chemoselective Rewiring of Cell Surfaces: Generation of Three-Dimensional Tissue Structures. *J. Am. Chem. Soc.* **133**, 8704–8713 (2011).
39. Rogozhnikov, D., O’Brien, P. J., Elahipanah, S. & Yousaf, M. N. Scaffold Free Bio-orthogonal Assembly of 3-Dimensional Cardiac Tissue via Cell Surface Engineering. *Sci. Rep.* **6**, 39806 (2016).

Chapter 5

Assembly of Cells into 3D Tissues via Bio-orthogonal Chemistry and Preferential Differentiation of Stem Cells in Co-cultures with Controlled Cell Orientations.

5.1 Summary

In vivo, cells exist in a complex environment where they interact with other cell types via cytokines and physical contact. It is important to recapitulate the natural 3D structure of tissue for use in organ transplantation, biological modeling and drug screening. For the successful formation of 3D tissue *ex vivo*, one requires a method for the assembly of cells from different cell types into multilayers with controlled orientation. The technology must be selective, non-cytotoxic, applicable under physiological conditions and inexpensive. Here, we introduce a method which is based on bio-orthogonal oxime chemistry. In this study, we tailored cell membranes with oxyamine- and ketone-functionalized lipids which were delivered onto cell membranes via liposome fusion. The cells with functionalized cell surfaces were mixed in a small volume and the functional groups on cell membranes clicked with each other producing a covalent oxime bond, resulting in cell assembly. The oxime click-chemistry method can be used to assemble cells from different cell types into 3D co-cultures with variable thickness, cell composition and orientation within the co-culture.

In this project we applied the oxime click-chemistry method to assemble cells into different 3D co-cultures to study stem cell differentiation. Two types of stem cells, hMSC and C310T1/2, were assembled into 3D structures with different orientations and treated with adipogenic or osteogenic factors to induce differentiation. The orientation of the cells in the co-culture influenced the rate of stem cell differentiation and choice of lineage.

5.2 Introduction

Cell behaviour is determined by multiple factors such as hormones, cytokines and physical interactions between cells in a complex three-dimensional (3D) environment¹⁻⁴. The interplay of these signals results in coordinated cell behaviours such as migration, differentiation and apoptosis⁵⁻⁷. Therefore, developing *in vitro* systems capable of recapitulating the natural interactions between cells is important for further advancement in medicine, pharmaceutical science and fundamental biology⁸⁻¹⁰. Traditional tissue culture methods involve culturing cells in monolayers on various substrates. *In vivo*, however, cells form complex 3D tissues composed of multiple cell layers¹¹. Formation of tissues *in vitro* requires the assembly of different cell types into organized 3D structures with defined orientations. This co-culture system must also enable intercellular communication and the formation of cell-cell junctions, which is challenging¹²⁻¹⁴. In recent years, numerous attempts have been made to construct 3D tissues using materials such as hydrogels, polymers and components of the extracellular matrix¹⁵⁻¹⁸. The major limitation of these technologies is that the material, which works as a scaffold, occupies space within the tissue and creates a physical barrier between the cells. As a result, instead of forming cell-cell junctions, the cells attach to the scaffold material, hampering physical and cytochemical signaling¹⁹. Therefore, a new strategy is needed to assemble cells into multi-layers with a controlled 3D orientation while maintaining effective intercellular communication. The method must be inexpensive, precise and non-cytotoxic. It has to utilize a minimal amount of material, be general for a range of cell types, be simple and quick and allow scaling for mass production.

Our group has developed a methodology which is based on bio-orthogonal lipids delivered onto cell surfaces via liposome fusion (**Figure 5.1**). A reaction between two functional groups, an oxyamine and a ketone, results in the formation of an oxime bond. The reaction is

quick, chemoselective, non-cytotoxic and occurs under physiological conditions (37°C, pH 7).²⁰⁻
²⁴ Cells with engineered cell membranes can be mixed together and the functional groups on the membranes will react and form a strong covalent bond, thus attaching these cells together. Using bio-orthogonal click chemistry it is possible to click-assemble cells into 3D structures with controlled orientations.²⁵ These multilayers can be used for two different purposes: to study cellular behavior in 3D as well as to construct functional tissues for transplantation and drug testing.^{26,27}

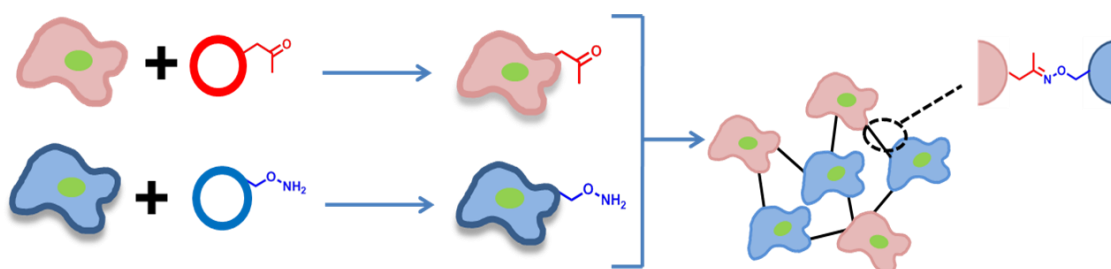


Figure 5.1: The schematic representation of cell surface engineering and the bio-orthogonal reaction between oxamine and ketone functionalities. The delivery of bio-orthogonal ketone and oxamine groups onto cell surfaces is accomplished via liposome fusion and results in the formation of two differently labeled cell populations. When the ketone- and oxamine-tethered cells are brought into contact, oxamine and ketone groups click with each other, producing a stable oxime bond and resulting in cell assembly.

Here in, we developed a scaffold-free system to assemble stem cells into 3D co-cultures with controlled orientation and studied stem cell differentiation in 3D co-culture.

Human mesenchymal stem cells (hMSC) are very important tool of regenerative medicine.²⁸⁻³⁰ These stem cells are multipotent and are capable of differentiating into three major lineages: adipogenic (fat), osteogenic (bone), and chondrogenic (connective tissue).³¹ The ability to be transformed into different cell types, makes hMSC useful for the development of artificial tissues and organs. The goal of this project is to assemble two different types of stem cells:

mouse embryonic fibroblasts (C3H 10T1/2) and human mesenchymal stem cells into 3D co-cultures with different orientations and to study how the orientation of stem cells in co-culture affects the rate of their differentiation as well as the lineage into which these cells differentiate.

5.3 Experimental

5.3.1 Tissue Culture

Human mesenchymal stem cells (hMSC) were obtained from Lonza (Bazel, Switzerland). Mouse embryonic fibroblasts (C3H10T1/2) were obtained from Prof. McDermott's group. The cells were cultured in high-glucose (4500 mg/L) Dulbecco's Modified Eagle's Medium (DMEM) with 10% fetal bovine serum (FBS), 1% penicillin/streptomycin solution at 37°C and 5% CO₂.

To passage the cells, the medium was removed and the cells were washed twice with phosphate buffered saline (PBS). After that, the cells were treated with 0.25% Trypsin-EDTA for 3 min, followed by the neutralization of the Trypsin solution with two volumes of medium. The cells were centrifuged at 800 rpm for 5 min, and the cell pellet was re-suspended with DMEM and passaged onto new plates. All experiments involving hMSC were conducted with cells at passage 4.

5.3.2 Formation of Liposomes

To form oxyamine- and ketone-tethered LUVs, chloroform solutions of palmitoyl-oleoyl phosphatidylcholine (POPC); 1,2-dioleoyl-3-trimethylammonium-propane (DOTAP); dodecanone (for ketone-containing liposomes); and *O*-dodecyloxyamine (for oxyamine-

containing liposomes) were mixed as follows: POPC (430 μL , 10 mg/mL in CHCl_3 at 86 mol %); DOTAP (10 μL , 10 mg/mL in CHCl_3 at 2 mol %); and *O*-dodecylamine or dodecanone (60 μL , 10 mM in CHCl_3 at 12 mol %). The samples were air-dried for 18 h and then re-suspended in 3 mL of PBS (pH 7.4). The mixture of lipids was then sonicated with a tip sonicator for 20 min until the solution was clear.

5.3.3 Formation of Cell Multi-layers

Prior to the formation of cell multi-layers, both hMSC and 10T1/2 cells for both the top and the bottom layers were cultured to 95–100% confluence.

Liposomes were mixed with DMEM in the following proportions: 50 μL of liposome solution per 1 mL of medium. The cells were incubated with the liposomes for 4 h at 37°C. After that, the medium was removed and the cells were washed twice with PBS. Following that, the oxyamine-labeled cells were removed from the plate with 0.25% trypsin and centrifuged down at 800 rpm, the medium was decanted and the cells were re-suspended with 3 mL of fresh medium and added to the plate containing ketone-labeled cells. The average concentration of cells seeded as the second layer was 1.5×10^5 cells per 1 mL of medium.

5.3.4 Adipogenic Differentiation

hMSC and 10T1/2 cells (monolayers, multi-layers and spheroids) were induced with DMEM (Sigma), containing 4500 $\mu\text{g}/\text{mL}$ of glucose 10% FBS, 1 μM dexamethasone (DEX) and 500 μM 3-isobutyl-1-methylxanthine (IBMX) and 1 $\mu\text{g}/\text{mL}$ insulin for 7 days at 37°C, 5% CO_2 . After that, the cells were cultured for 11 more days in DMEM containing 4500 $\mu\text{g}/\text{mL}$ of

glucose; 10% FBS; 1% penicillin-streptomycin; and 1 $\mu\text{g}/\text{mL}$ insulin at 37°C, 5% CO₂. The medium was changed every 3-4 days. The samples were run in triplicates.

5.3.5 Preferential Differentiation

For the first 7 days, monolayers and multi-layers and spheroids of hMSC and 10T1/2 cells were in the medium containing 4500 $\mu\text{g}/\text{mL}$ of glucose, 10% FBS and the following combination of adipogenic and osteogenic inducing factors: 1 μM DEX and 500 μM IBMX, 1 $\mu\text{g}/\text{mL}$ insulin, 10mM β -Glycerophosphate and 0.05mM L-ascorbic acid-2-phosphate at 37°C, 5% CO₂. After that, the medium was changed to DMEM containing 4500 $\mu\text{g}/\text{mL}$ of glucose, 10% FBS, 100 nM DEX and 500 μM IBMX, 1 $\mu\text{g}/\text{mL}$ insulin, 10mM β -Glycerophosphate and 0.05mM L-ascorbic acid-2-phosphate and the cells were cultured for 11 more days at 37°C, 5% CO₂. The samples were run in triplicates.

5.3.6 Immunohistochemistry

Adipogenic differentiation was characterized with staining by Oil Red O solution. The working solution of Oil Red O was prepared as follows: dry Oil Red O powder was dissolved in 99.5% isopropanol to give a 3% stock solution (w/v). The stock solution was suction-filtered through a paper filter and the working solution was prepared by diluting 3 volume parts of the filtered stock solution with 2 parts of distilled water. After the 3D co-culture and adipogenic differentiation, hMSC and 10T1/2 cells were fixed with 3.8% formaldehyde for 15 min, then washed twice with PBS, once with water and once with 60% isopropanol (3–5 min). After that, the cells were stained with the working solution of Oil Red O stain (15 min), rinsed with water,

stained with Harris Hemotoxylin dye for 3 min, washed with water again and visualized with the light microscope.

Osteogenic differentiation was characterized with Alizarin Red S staining. The cells were fixed with 10% formaldehyde for 20 min, rinsed with distilled water and incubated for 15 min in 2% (w/v) solution of Alizarin Red S at pH 4.2. Then, the samples were washed twice with distilled water and visualized under the inverted light microscope.

5.3.7 Cell Viability Assay

The medium was decanted and the cells were washed twice with PBS. After that, the cells were incubated in a 0.4% solution of Trypan Blue (Sigma) for 2 min. The samples were subsequently washed twice with PBS and visualized under the light microscope.

5.3.8 Statistical Analysis

Following differentiation, the cells were stained and the images of the cells were taken with the bright field microscope. The degree of adipogenic and osteogenic differentiation was assessed using Image J. The program calculated the number of red pixels in the image. The number of red pixels was divided by the total number of pixels in the picture. The ratios were compared between the co-culture types. 10 images were taken per sample and there were 3 samples in each category. The data were analyzed and graphed as a three-dimensional plot using Microsoft Excel 2010 software. The co-culture type with the highest level of differentiation was set to 100% and the data from other categories were adjusted relative to this value.

5.3.9 Confocal Microscopy

The cells were fixed with 3.8% formaldehyde for 15 min, followed by permeation with 0.1% Triton X for 30 min. After that, the cells were incubated for 2 h in the PBS mixture of the following dyes: 1 $\mu\text{g/mL}$ phalloidin-TRITC (actin) and 0.3 $\mu\text{g/mL}$ DAPI (nucleus). Cell multi-layers were visualized with a Zeiss LSM-700 confocal microscope. The data were recorded and analyzed using ZEN software. On average, 50 images were taken to produce each 3D representation. The average exposure times were 400 ms for DAPI and 1200 ms for TRITC stains.

5.3.10 RT-PCR

Following adipogenic differentiation, the total RNA was extracted from the cells using RNeasy[®] kit (Qiagen). A total of 1 μg of total RNA was converted into cDNA using random primers and AMV reverse transcriptase in GoScript Transcription System (Promega). Following that, the cDNA was amplified using Hot Start Taq DNA Polymerase kit (New England Biolabs) using markers for 3 genes (Lp1, PPAR γ 2, β 2mg). The following primers were used:

PPAR γ 2 (sense 5-GCTGTTATGGGTGAAACTCTG-3, antisense (5ATAAGGTGGAGATGCAGGCTC-3),

Lpl (sense 5-GAGATTTCTCTGTATGGCACC-3, antisense 5-CTGCAAATGAGACACTTTCTC-3'),

β 2mg (sense 5-ACCCCACTGAAAAAGATGA-3, antisense 5-GCATCTTCAAACCTCCATGAT-3)

The annealing temperatures for the primers are 55, 52 and 53°C respectively. The time for each amplification cycle was 1 min and 30 cycles in total were performed. The products were resolved via agarose gel electrophoresis β 2mg at 1.5% agarose concentration. The transcript sizes are as follows: 351bp (PPAR γ 2), 276bp (Lpl) and 116bp (β 2mg) respectively.

5.4 Results and Discussion

The objective of this study was to generate 3D co-culture systems of hMSC and C3H 10T1/2 cells with different cell orientations and then to study how the orientation of stem cells in the co-culture influences their differentiation. To form 3D multilayers the stem cells were first cultured in mono-layers and then treated with ketone- or oxyamine-tethered liposomes (**Figure 5.2**). After that, the cells with engineered membranes were seeded onto the oxyamine- or ketone-functionalized cell monolayers forming a multilayer.

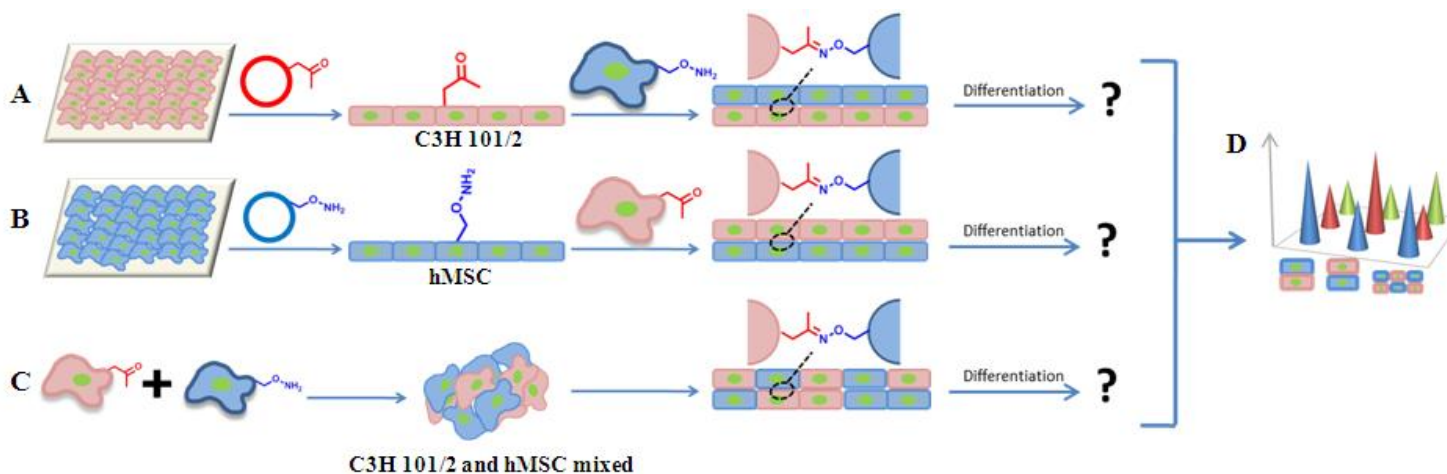


Figure 5.2: Schematic representation of 3D co-cultures of C3H 10T1/2 and hMSC generated via liposome fusion technology. Control of cell orientation via bio-orthogonal chemistry. **A)** A monolayer of C3H10T1/2 was treated with ketone-tethered liposomes to produce a ketone-labeled cell monolayer which is seeded with oxyamine-labeled hMSC to produce a cell multilayer with controlled orientation. **B)** A monolayer of hMSC was treated with oxyamine-tethered liposomes to produce an oxyamine-labeled hMSC which was subsequently seeded with ketone-tethered cells C3H 10T1/2 to produce a multilayer with a reversed orientation. **C)** Ketone- and oxyamine-tethered C3H 10T1/2 and hMSC were mixed together and seeded onto a substrate. **D)** All co-culture types were treated with adipogenic factors for 18 days and the percentage of differentiated cells was measured at different points in time to produce a 3D plot (the percentage of differentiated cells vs. co-culture type vs time).

Alternatively, a co-culture of mixed hMSC and C3H 10T1/2 cells with controlled cell orientation can be produced. The functionality of bio-orthogonal chemistry was demonstrated with GFP- and RFP-transfected NIH3T3 fibroblasts which were arranged into 3D structures (**Figure 5.3**).

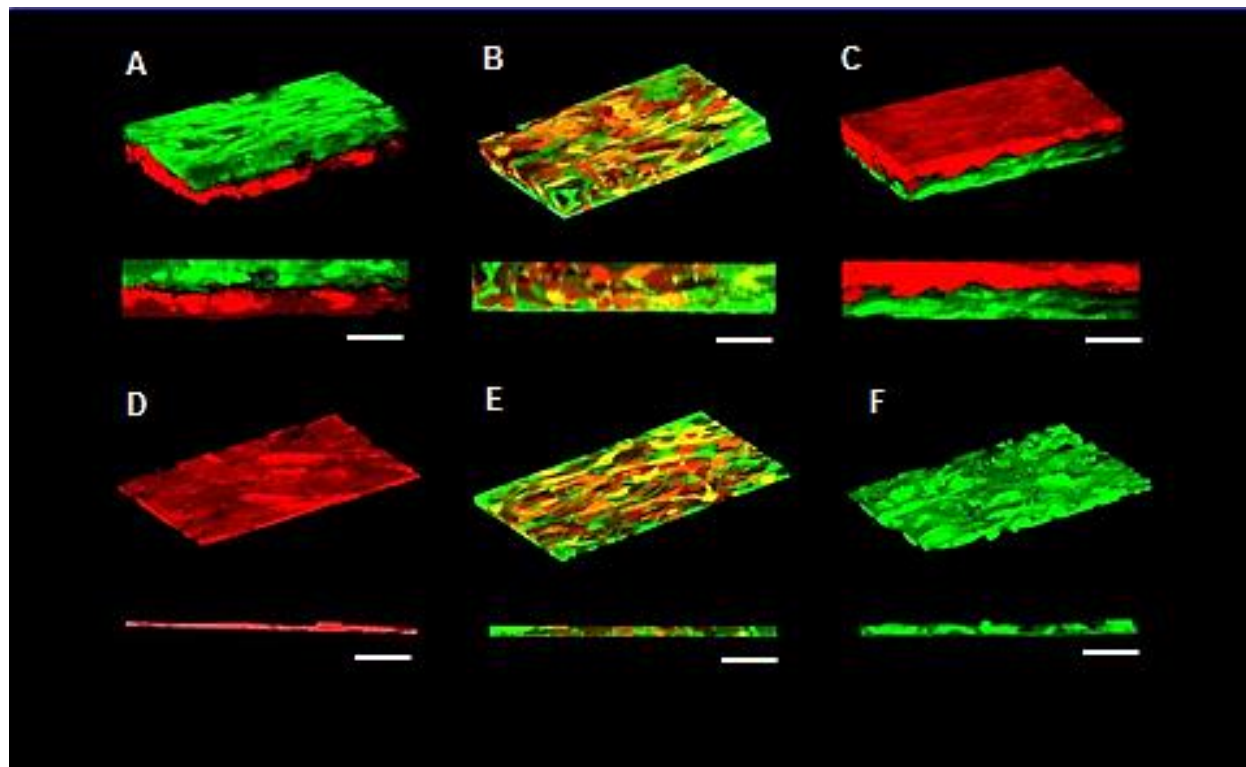


Figure 5.3: Control of orientation and thickness of cell multilayers via bio-orthogonal chemistry. Formation of cell zones with controlled orientation **A**) RFP expressing NIH3T3 cells transfected with functionalized (ketone and oxyamine) liposomes seeded with GFP-expressing NIH3T3 cells transfected with functionalized liposomes. **B**) Ketone-tethered RFP cells mixed with oxyamine-tethered GFP cells. **C**) Functionalized GFP cells seeded with functionalized RFP cells. RFP (**E**), GFP and RFP (**F**) or GFP (**G**) monolayers treated with non-functionalized liposome and seeded with fluorescent GFP or RFP cells treated with a ketone- or oxyamine-tethered liposomes. The scale bar is 50 μm .

GFP and RFP cells treated with functionalized (ketone and oxyamine) liposomes could be arranged into 3D structures with thick green and red zones. The structures contain an average of three cell layers per zone, with a total of six cell layers. The thickness of these multilayers is $\sim 50 \mu\text{m}$. GFP and RFP cells treated with liposomes containing no oxyamine or ketone groups (non-functionalized liposomes) did not form 3D structures and remained as monolayers with an

average thickness of 10 μm . Therefore, cell multilayers can only form if ketone and oxyamine groups are present on the cell surfaces.

Using bio-orthogonal chemistry we can form co-culture systems with C3H 10T1/2 cells and hMSC stem cells with different orientations. The cells treated with oxyamine and ketone liposomes formed multilayers, while the cells treated with no liposome or non-functionalized liposome did not generate multilayers. Upon formation of multilayers, the cells were treated with adipogenic differentiation factors to observe which co-culture differentiates into adipocytes (the fat cells) the fastest (**Figure 5.4**). The cells were treated for 18 days and the adipocytes were stained with Oil Red O.

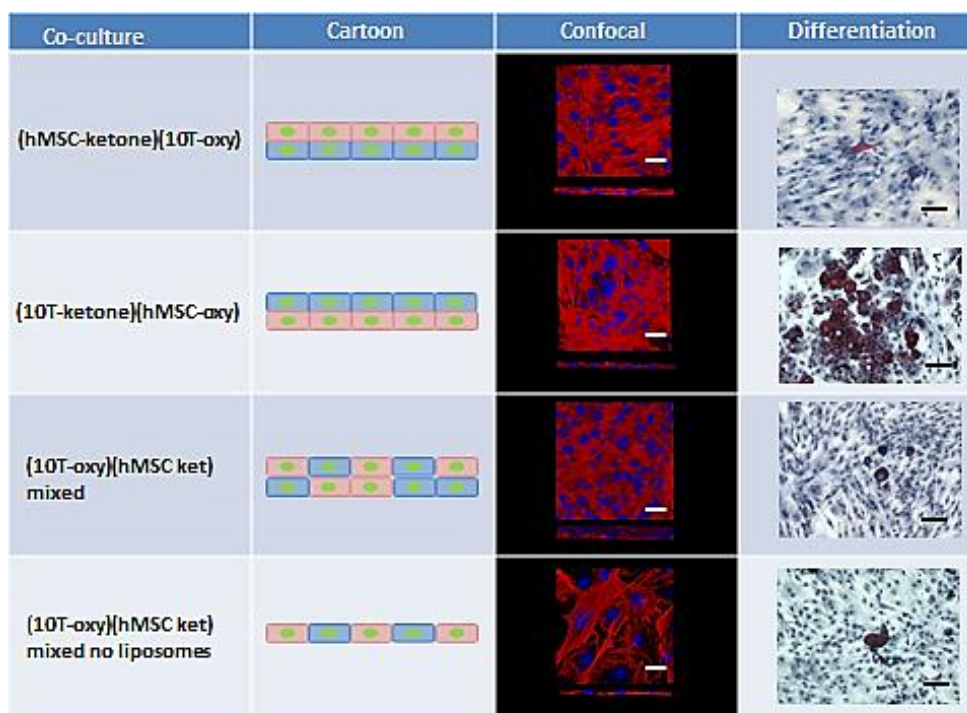


Figure 5.4: Multilayers of co-culture of human mesenchymal stem cells (hMSC) with murine (mouse) C3H10T1/2 fibroblasts and their adipogenic differentiation (visualized with Oil Red O staining). The table contains the schematic representation of the multiple 3D co-culture types of hMSC and C3H10T1/2 cells with controlled orientations (**column 2**), confocal images of cell multilayers (top and side views), Phalloidin TRITC (red)-actin, DAPI (blue)-nucleus (**column 3**) and the results of orientation-based adipogenic differentiation on day 18. Adipogenic Oil Red O staining of differentiated hMSC and C3H10T1/2 cells was visualized under the light microscope (**column 4**). The scale bar is 50 μm .


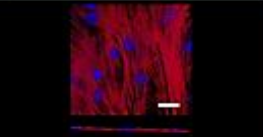
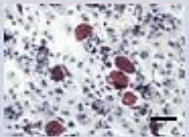

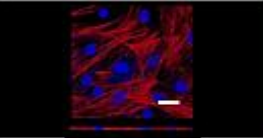
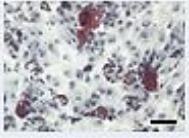

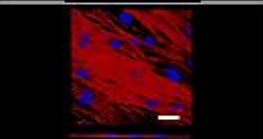
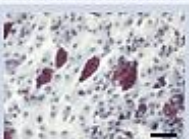
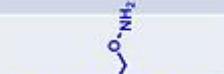
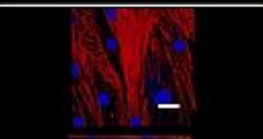
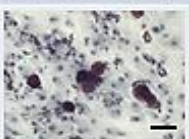

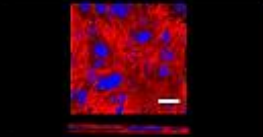
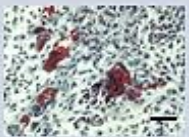

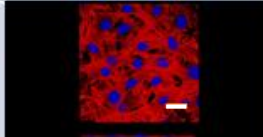
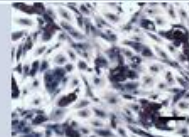

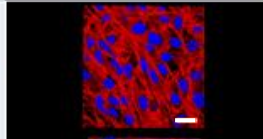
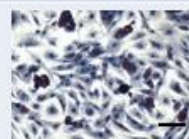

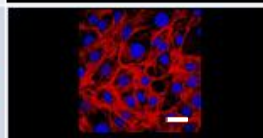
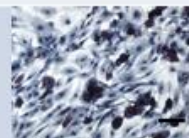
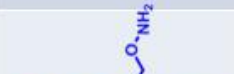
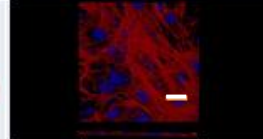
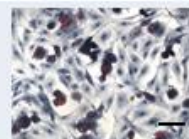

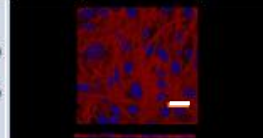
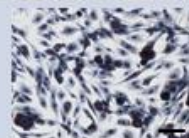
Co-culture	Cartoon	Confocal	Differentiation
hMSC no liposome			
Non-functionalized liposome			
hMSC liposome ketone			
hMSC liposome oxyamine			
hMSCx2			
10T1/2 no liposome			
10T1/2 non-functionalized liposome			
10T1/2 liposome ketone			
10T1/2 liposome oxyamine			
10T1/2x2			

Figure 5.4 (continued): Multilayers of co-culture of human mesenchymal stem cells (hMSC) with murine (mouse) C3H10T1/2 fibroblasts and their adipogenic differentiation (visualized with Oil Red O staining). The table contains the schematic representation of the multiple 3D co-culture types of hMSC and C3H10T1/2 cells with controlled orientations (**column 2**), confocal images of cell multilayers (top and side views), Phalloidin TRITC (red)-actin, DAPI (blue)-nucleus (**column 3**) and the results of orientation-based adipogenic differentiation on day 18. Adipogenic Oil Red O staining of differentiated hMSC and C3H10T1/2 cells is visualized under the light microscope (**column 4**). The scale bar is 50 μ m.

The average thickness of the cell bilayers was 12 μm , monolayer 7 μm , mixed 4–5 cell layers (25 μm). The orientation of cells in a multilayer influences stem cell differentiation. With oxime click-chemistry it is possible to control co-culture orientation and, to some extent, the thickness of cell zones in the multilayers.

To further confirm adipogenic differentiation, we checked the stem cells for expression of PPAR γ 2 and Lpl, the adipogenic genetic markers,³² as well as β 2mg – a control marker expressed in all human cells.³³ The RT-PCR analysis confirmed the expression of these markers in adipogenically-induced cultures.

The results of the differentiation experiment are summarized as a 3D plot (**Figure 5.5**). This plot shows a difference in the rate of stem cell differentiation depending on orientation.

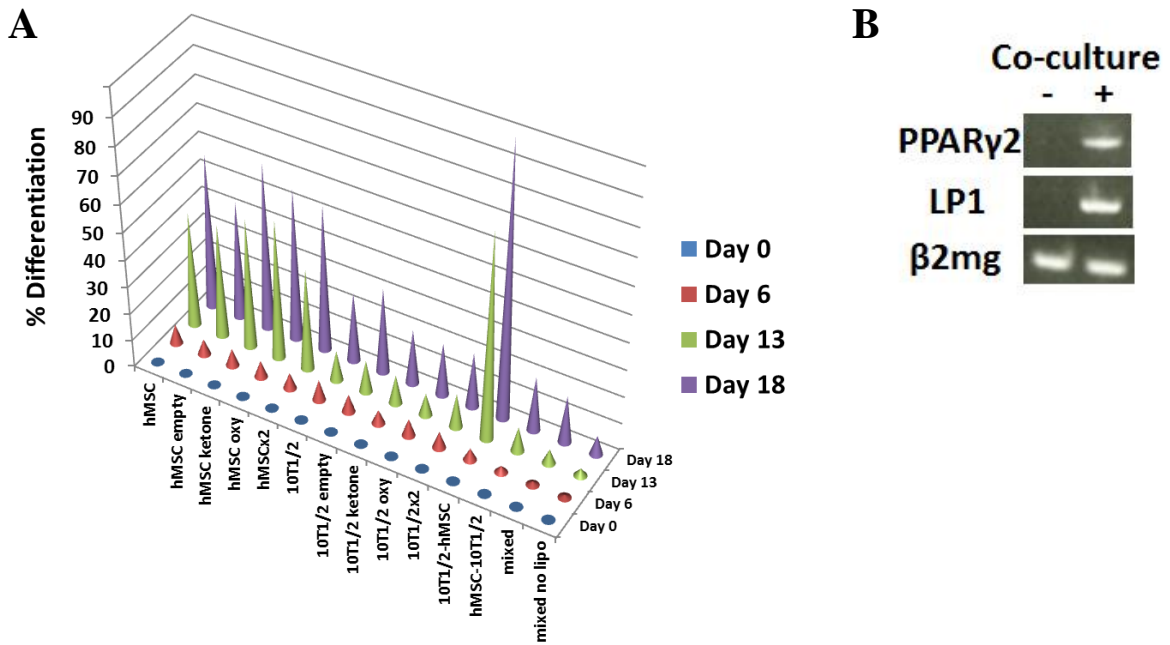


Figure 5.5: 3D plot describing the rate of adipogenic differentiation based on stem cell orientation. (A) The x-axis is the co-culture orientation, the y-axis is the time points at which the adipogenic differentiation was measured (Days 0, 6, 13 and 18), and the z-axis represents the percentage differentiation, with the most profound differentiation adjusted to 100%. $n=3$. Average SEM= $\pm 4.2\%$. $P<0.05$ (B) The RT-PCR of hMSC on day 18, depicting the expression of adipogenic markers (PPAR γ 2, LPL) and the loading control marker β 2mg in cells treated with adipogenic differentiation media (+) and the control group treated with standard media (DMEM) only (-).

Out of all the orientations, the co-culture system with 10T1/2 cells on the bottom and hMSC cells at the top differentiates the fastest. The process of liposome fusion does not affect the rate of adipogenic differentiation, as can be seen from the graph, where the percent of differentiated hMSC and 10T1/2 cells does not vary regardless of whether they were treated with a non-functionalized liposome or no liposome at all.

These data are the first to show that the oriented tissue microenvironment influences the rate of stem cell differentiation. These studies would not be possible without quick and controlled cell assembly to form multi-layers of various orientations.

Physical and cytochemical interactions between cells are of great importance to biology and medicine. Understanding how a microenvironment created by physical and cytochemical interactions between cells influences stem cell fate (direction of stem cell differentiation) is highly relevant for multiple fields such as biology, bio-engineering and health care.¹⁹ Therefore, the development of methods to direct stem cell differentiation is of major biotechnological and medical interest. One of the interesting questions to answer is: Do stem cells alter the direction of their differentiation depending on orientation in co-culture? To study the potential dependence of stem cell fate on orientation in co-culture, we compared co-culture multilayers of two different types of stem cells (hMSC and C3H10T1/2) with different orientations to observe the difference in cell fate (**Figure 5.6**). In this experiment, the cells were provided a general media containing the growth factors required for both adipogenic and osteogenic differentiation, thus the cells were given the option to choose or not to choose a particular lineage. The cells can differentiate into adipocytes, osteoblasts or both or not differentiate at all.

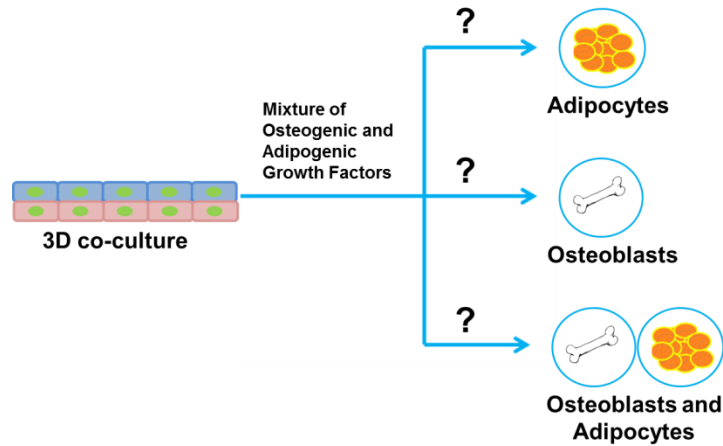


Figure 5.6: Schematic representation of the experiment involving a choice of cell lineage. Co-cultures with different orientations of hMSC and C3H 10T1/2 cells were treated for 18 days with a combination of adipogenic and osteogenic growth factors. The cells, therefore, can differentiate into adipocytes or osteoblasts or into a mixture of both.

The treatment was continued for 18 days, after which the cells were stained for the presence of adipocytes and osteoblasts and the relative quantities of both adipocytes and osteoblasts were assessed (**Figure 5.7**).

Co-culture	Cartoon	Adipogenic Control	Adipogenic	Osteogenic Control	Osteogenic
10T1/2-hMSC					
hMSC-10T1/2					
hMSC-10T1/2 mixed no lipo					
hMSC-10T1/2 mixed lipo					
hMSC no choice media					

Figure 5.7: The orientation of stem cells in co-culture influences their lineage preference. The cells are incubated in the DMEM for 18 days containing growth factors for both adipogenic and osteogenic differentiation. **Column 2:** Schematic representation of a co-culture orientation. **Column 3:** Oil Red O staining of co-culture incubated in DMEM only. **Column 4:** Co-culture treated with adipogenic and osteogenic factors and stained for the presence of adipocytes with Oil Red O. **Column 5:** The co-cultures were treated with standard media (DMEM) for 18 days and stained for the presence of osteoblasts with Alizarin S Red. **Column 6:** The co-cultures were treated with the medium containing adipogenic and osteogenic growth factors and stained for the presence for osteoblasts with Alizarin S Red. n=3.

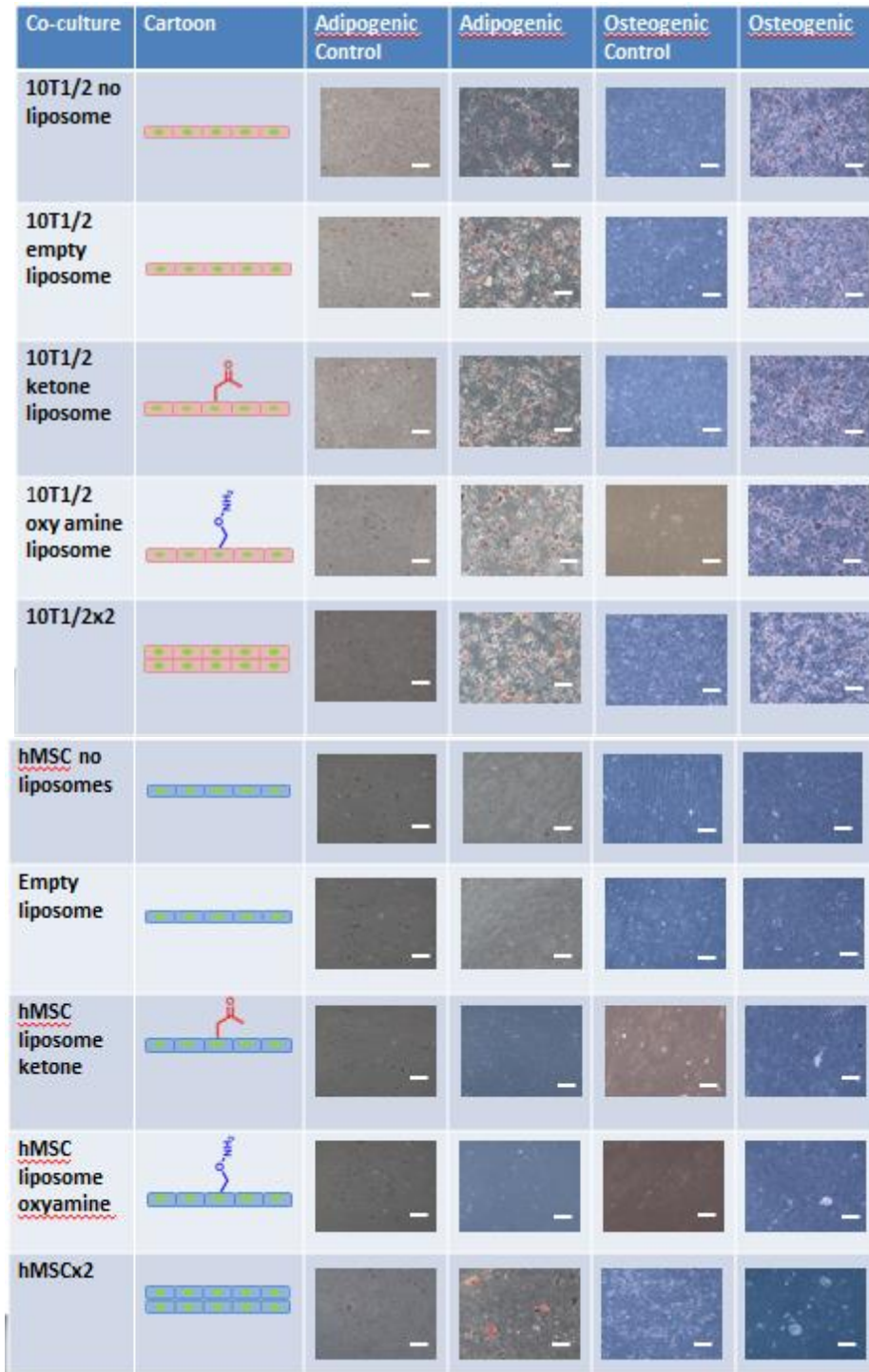


Figure 5.7 continued: The orientation of stem cells in co-culture influences their lineage preference. The cells are incubated in the DMEM, containing growth factors for both adipogenic and osteogenic differentiation, for 18 days. **Column 2:** The schematic representation of a co-culture orientation. **Column 3:** Oil Red O staining of co-culture incubated in DMEM only. **Column 4:** Co-culture treated with adipogenic and osteogenic factors and stained for presence of adipocytes with Oil Red O. **Column 5:** The co-cultures were treated with the standard media (DMEM) for 18 days and stained for the presence of osteoblasts with Alizarin S Red. **Column 6:** The co-cultures were treated with the medium containing adipogenic and osteogenic growth factors and stained for the presence for osteoblasts with Alizarin S Red. n=3.

Depending on the orientation in co-culture, some co-cultures differentiated into adipocytes, some into osteoblasts and some into both, while some did not differentiate at all. The results of the experiment are summarized in **Figure 5.8**.

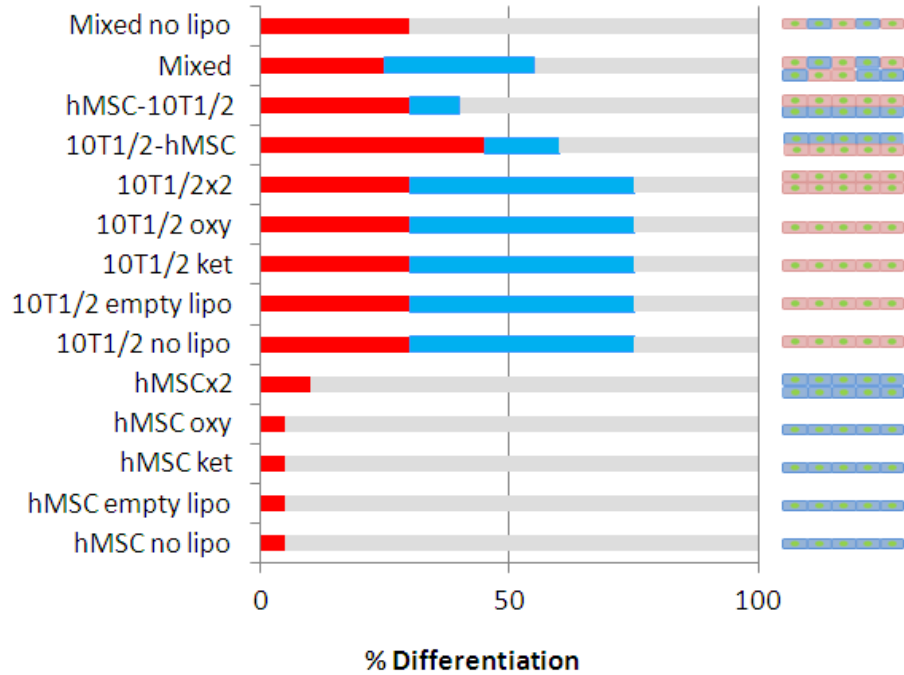


Figure 5.8: Plot describing the differentiation of co-cultures with different cell orientations into adipocytes and osteoblasts after 18 days of incubation in media containing both adipogenic and osteogenic growth factors. The red regions of the graph represent the percentage of adipocytes in the co-culture, blue osteogenic differentiation and grey no differentiation. n=3. P<0.05 Average SEM= ±6.3%.

From the graph it can be seen that most co-cultures produced a mix of adipocytes and osteoblasts with some cells remaining undifferentiated. In mixed co-cultures of 10T1/2 and hMSC, the monolayers of the differentiated cells chose only the adipogenic lineage, while in the multi-layers, these cells produced an almost equal mix of adipocytes and osteoblasts. In co-cultures with layered orientations of 10T1/2 and hMSC, when hMSC are at the top and 10T1/2 are on the bottom, more cells differentiated into adipocytes, while in the co-culture with reversed orientation, there was less adipogenic differentiation and a similar level of osteogenic differentiation. In both monolayer and multi-layer cultures of hMSC, there was a very small

amount of adipogenic differentiation observed with no osteogenic differentiation at all. Between all the 10T1/2 cultures, the amount of differentiation was the same (with about 60% of all differentiated cells going into the osteogenic and 40% into the adipogenic lineage). These data demonstrate that the choice of lineage depends on stem cell orientation. Recent studies conducted on stem cell differentiation have shown that the rate of stem cell differentiation as well as the choice of lineage are influenced by the surface on which these cells grow^{20,21}. In this experiment, there are two surfaces, one is the plastic substrate on which the cells grow, and the other is the membrane of the cell above. We hypothesized that the difference in the rate of differentiation as well as the choice of lineage are due to physical forces such surface tension (the hard surface of the culture plate vs. the soft surface of the bottom cell layer) as well as signaling between the cell lines. The dependence of cell lineage choice on cell orientation in co-culture needs to be further investigated using contemporary genomic and proteomic methods, and the ability to generate co-cultures with controlled orientation is critical for these new types of studies.

5.5 Conclusion

Bio-orthogonal chemistry is a powerful tool which allows for the assembly of cells into 3D structures. It is simple and reliable and works with multiple cell types. Here it was demonstrated how this method can be used to study the differentiation of stem cells in a 3D microenvironment. It showed that hMSC and C3H10T1/2 co-cultures differentiate at different rates as well as into different lineages if given a choice to do so, and their fate depends on orientation of these cells inside the co-culture. Our technique is versatile and can be used for different types. This is the first scaffold-free method used to create 3D stem cell co-culture models.

5.6 References

1. Cukierman, E., Pankov, R., Stevens, D. R. & Yamada, K. M. Taking Cell-Matrix Adhesions to the Third Dimension. *Science* (80-.). **294**, (2001).
2. Salamanna, F. *et al.* A Human 3D In Vitro Model to Assess the Relationship Between Osteoporosis and Dissemination to Bone of Breast Cancer Tumor Cells. *J. Cell. Physiol.* **232**, 1826–1834 (2017).
3. Griffith, L. G. & Swartz, M. A. Capturing complex 3D tissue physiology in vitro. *Nat. Rev. Mol. Cell Biol.* **7**, 211–224 (2006).
4. Albrecht, D. R., Underhill, G. H., Wassermann, T. B., Sah, R. L. & Bhatia, S. N. Probing the role of multicellular organization in three-dimensional microenvironments. *Nat. Methods* **3**, 369–375 (2006).
5. Discher, D. E., Mooney, D. J. & Zandstra, P. W. Growth Factors, Matrices, and Forces Combine and Control Stem Cells. *Science* (80-.). **324**, 1673–1677 (2009).
6. Schekman, R. W., Goldstein, L. B. & Lehmann, R. *Annual review of cell and developmental biology : volume 26, 2010.* (Annual Reviews, 2010).
7. Weber, P. *et al.* Monitoring of Apoptosis in 3D Cell Cultures by FRET and Light Sheet Fluorescence Microscopy. *Int. J. Mol. Sci.* **16**, 5375–5385 (2015).
8. Fischbach, C. *et al.* Engineering tumors with 3D scaffolds. *Nat. Methods* **4**, 855–860 (2007).
9. Kimlin, L., Kassis, J. & Virador, V. 3D *in vitro* tissue models and their potential for drug screening. *Expert Opin. Drug Discov.* **8**, 1455–1466 (2013).
10. Pathak, A. & Kumar, S. Independent regulation of tumor cell migration by matrix stiffness and confinement. *Proc. Natl. Acad. Sci.* **109**, 10334–10339 (2012).
11. Shen, L. Tight junctions on the move: molecular mechanisms for epithelial barrier regulation. *Ann. N. Y. Acad. Sci.* **1258**, 9–18 (2012).
12. Harris, T. J. C. & Tepass, U. Adherens junctions: from molecules to morphogenesis. *Nat. Rev. Mol. Cell Biol.* **11**, 502–514 (2010).
13. Mammoto, T. & Ingber, D. E. Mechanical control of tissue and organ development. *Development* **137**, 1407–1420 (2010).
14. Tambe, D. T. *et al.* Collective cell guidance by cooperative intercellular forces. *Nat. Mater.* **10**, 469–475 (2011).

15. Lu, T.-Y. *et al.* Repopulation of decellularized mouse heart with human induced pluripotent stem cell-derived cardiovascular progenitor cells. *Nat. Commun.* **4**, (2013).
16. Xu, T. *et al.* Complex heterogeneous tissue constructs containing multiple cell types prepared by inkjet printing technology. *Biomaterials* **34**, 130–139 (2013).
17. Song, J. J. *et al.* Regeneration and experimental orthotopic transplantation of a bioengineered kidney. *Nat. Med.* **19**, 646–651 (2013).
18. Sun, H. *et al.* Osteogenic differentiation of human amniotic fluid-derived stem cells induced by bone morphogenetic protein-7 and enhanced by nanofibrous scaffolds. *Biomaterials* **31**, 1133–1139 (2010).
19. Yang, S., Leong, K.-F., Du, Z. & Chua, C.-K. The Design of Scaffolds for Use in Tissue Engineering. Part I. Traditional Factors. *Tissue Eng.* **7**, 679–689 (2001).
20. Park, S. & Yousaf, M. N. An Interfacial Oxime Reaction To Immobilize Ligands and Cells in Patterns and Gradients to Photoactive Surfaces. *Langmuir* **24**, 6201–6207 (2008).
21. Dutta, D., Pulsipher, A., Luo, W. & Yousaf, M. N. Synthetic Chemoselective Rewiring of Cell Surfaces: Generation of Three-Dimensional Tissue Structures. *J. Am. Chem. Soc.* **133**, 8704–8713 (2011).
22. Elahipanah, S. *et al.* Rewiring Gram-Negative Bacteria Cell Surfaces with Bio-Orthogonal Chemistry via Liposome Fusion. *Bioconjug. Chem.* **27**, 1082–1089 (2016).
23. Rogozhnikov, D., O'Brien, P. J., Elahipanah, S. & Yousaf, M. N. Scaffold Free Bio-orthogonal Assembly of 3-Dimensional Cardiac Tissue via Cell Surface Engineering. *Sci. Rep.* **6**, 39806 (2016).
24. O'Brien, P. J., Elahipanah, S., Rogozhnikov, D. & Yousaf, M. N. Bio-Orthogonal Mediated Nucleic Acid Transfection of Cells via Cell Surface Engineering. *ACS Cent. Sci.* **3**, 489–500 (2017).
25. Rogozhnikov, D., Luo, W., Elahipanah, S., O'Brien, P. J. & Yousaf, M. N. Generation of a Scaffold-Free Three-Dimensional Liver Tissue via a Rapid Cell-to-Cell Click Assembly Process. *Bioconjug. Chem.* **27**, 1991–1998 (2016).
26. Tian, H. *et al.* Myogenic differentiation of human bone marrow mesenchymal stem cells on a 3D nano fibrous scaffold for bladder tissue engineering. *Biomaterials* **31**, 870–877 (2010).
27. Lam, C. R. I. *et al.* A 3D Biomimetic Model of Tissue Stiffness Interface for Cancer Drug Testing. *Mol. Pharm.* **11**, 2016–2021 (2014).

28. Murphy, M. B., Moncivais, K. & Caplan, A. I. Mesenchymal stem cells: environmentally responsive therapeutics for regenerative medicine. *Exp. Mol. Med.* **45**, e54 (2013).
29. Richardson, S. M. *et al.* Mesenchymal stem cells in regenerative medicine: Opportunities and challenges for articular cartilage and intervertebral disc tissue engineering. *J. Cell. Physiol.* **222**, 23–32 (2010).
30. Hilfiker, A., Kasper, C., Hass, R. & Haverich, A. Mesenchymal stem cells and progenitor cells in connective tissue engineering and regenerative medicine: is there a future for transplantation? *Langenbeck's Arch. Surg.* **396**, 489–497 (2011).
31. Steward, A. J. & Kelly, D. J. Mechanical regulation of mesenchymal stem cell differentiation. *J. Anat.* **227**, 717–731 (2015).
32. Tontonoz, P. & Spiegelman, B. M. Fat and Beyond: The Diverse Biology of PPAR γ . *Annu. Rev. Biochem.* **77**, 289–312 (2008).
33. Ban, T., Yamaguchi, K. & Goto, Y. Direct Observation of Amyloid Fibril Growth, Propagation, and Adaptation. *Acc. Chem. Res.* **39**, 663–670 (2006).

Chapter 6

Spheroid and Tissue Assembly via Click Chemistry in Microfluidic Flow

Parts of this work have been published in *Bioconjugate Chemistry*, Volume 26, Pages 1939-1949 in 2015 under the title "Spheroid and Tissue Assembly via Click Chemistry in Microfluidic Flow" This work was reprinted with permission (© American Chemical Society 2015). O'Brien, P. J., Luo, W., **Rogozhnikov, D.**, Chen, J. & Yousaf, M. N are co-authors of this work.

6.1 Summary

Three-dimensional co-cultures are important tools that can be used to study cell behavior *in vitro*, model cancer progression and analyze the potential toxic effect of drug candidates. Modern methods used to generate complex 3D tissues utilize natural or polymer scaffolds to support the cell mass. Such approaches, although beneficial for applications where tensile strength is required, have a range of limitations which include low cell density, obstruction of intercellular connection and accumulation of degradation byproducts. Herein, we show a new strategy to rapidly and efficiently assemble 3D tissues via microfluidic flow without the use of polymers or biological scaffolds. The system relies on bio-orthogonal click chemistry, microfluidics and cell surface engineering. Simple bio-orthogonal lipids are synthesized and delivered onto cell membranes via liposome fusion. The reaction between the bio-orthogonal molecules is quick and specific which enables rapid cell assembly in flow. We demonstrate the efficiency of our method by assembling different types of spheroids and oriented 3D tissues in flow.

6.2 Introduction

Three dimensional co-culture systems have become an increasingly popular technology in the fields of transplantation, disease modeling and drug testing.¹⁻⁸ The most recent methods to produce 3D tissues are based on either additive technologies such as 3D printing and electrospinning to build 3D scaffolds or on production of organoids through stem cell technology.⁹⁻¹³ Both methods are relatively slow and require hours or even days to manufacture a functional tissue. To address this issue, rapid technologies such as microfluidics are being developed.

Microfluidics is the modern method of microfabrication which is used extensively in the fields of analytical chemistry nanotechnology and microelectronics.^{14,15} The core principle of microfluidics is based on the physical phenomenon of laminar flow.¹⁶ Unlike in turbulent flow, where the fluids undergo irregular fluctuation and mixing with constant changes in flow direction and speed, in laminar flow fluids move in parallel layers with no mixing between the layers.¹⁷ In this orderly flow, molecules present in flowing solution migrate between the parallel layers via diffusion. To achieve laminar flow several important parameters must be controlled. These are the flow rate, width of the micro-channel as well as the viscosity of the flowing solution.¹⁸ To prevent the turbulent flow which has a large shear force, the width of the flow channel is optimized to be between 50-300 μm . The flow rate of solution is usually adjusted to be within the range of 0.1-2 $\mu\text{L}/\text{min}$. This orderly laminar flow reduces the sheer force which exists in a turbulent flow, enabling the use of microfluidics for such delicate processes as cell sorting, disease diagnostics as well as genomic analysis.¹⁹⁻²¹

The use of microfluidics for generation 3D tissues is still in early development. Technologies used today for tissue assembly via microfluidic flow rely on use of exogenous polymer materials or extracellular matrix proteins to make cells “sticky” and promote 3D cell assembly.²²⁻²⁴ Such approach relies on encapsulation of cells, thus isolating them from contact with neighboring cells and the environment. In these experiments single cells are flown within the microchannel together with charged collagen or polymer monomers resulting in formation of solid polymer-cell complexes. Tissues that are obtained in these experiments, although durable due to presence of elastic materials have relatively low cell density, a factor which is crucial for manufacturing of cell-dense tissues such as cardiac tissue. Biodegradation of exogenous polymers also presents a problem due to accumulation of degradation byproducts which may potentially induce an immunological response if transplanted into the body.²⁵⁻²⁷

Therefore, a general method to rapidly assemble cells with sufficient cell economy would stimulate the emergence of new technological platforms for therapeutic drug screening, regenerative medicine as well as *in vitro* modeling systems to simulate disease progression. This method should be inexpensive, scaffold-free and applicable for different cell types.

Herein we introduce a new scaffold-free bio-orthogonal click chemistry method based on ligation between two functional groups, an oxyamine and a ketone to form a covalent oxime bond. The reaction is chemoselective, occurs under physiological conditions and is non-cytotoxic. An exceptional selectivity of this reaction enables rapid cell assembly without the use of exogenous scaffolds promoting formation of tissues with high cell density. To deliver oxyamine and ketone moieties onto cell surface liposomal delivery vesicles are used. Liposomes are commonly used for drug encapsulation and delivery. Here, we use bio-orthogonal liposomes to engineer the cell surfaces and assemble cells into 3D tissues in flow.

6.3 Experimental

O-Dodecyloxyamine-tetra(ethylene)glycol was synthesized as previously described.(25, 26) 1-Palmitoyl-2-oleoyl-*sn*-glycero-3-phosphocholine (POPC) and 1,2-dioleoyl-3-trimethylammonium-propane (DOTAP) were purchased from Avanti Polar Lipids (Alabaster, AL). All other chemicals were obtained from Sigma-Aldrich or Fisher Scientific. 3T3 Swiss albino mouse fibroblasts, C3H/10T1/2 mouse embryonic fibroblast cells, RFP Expressing Human Neonatal Dermal Fibroblasts, and GFP expressing NIH3T3 cells were obtained from ATCC. Human mesenchymal stem cell (hMSC), hMSC basic, growth, and differentiation media were obtained from Lonza.

6.3.1 Cell Culture

C3H/10T1/2 were cultured in Petri dishes at 37 °C and 5% CO₂ with DMEM media containing 10% fetal bovine serum (FBS) and 1% penicillin/streptomycin (P/S). RFP Expressing Human Neonatal Dermal Fibroblasts (RFP) were maintained in DMEM containing 10% FBS and 1% P/S. The cell cultures used for experiments were between 3 and 8 passages. GFP expressing NIH3T3 (GFP) cells were cultured in DMEM (high glucose), with 10% FBS, 0.1 mM MEM Non-Essential Amino Acids, 2 mM l-glutamine, 1% P/S, and 10 µg/mL Blasticidin. 3T3 Swiss albino mouse fibroblasts were cultured in Dulbecco's Modified Eagle Medium (Gibco) containing 10% FBS and 1% penicillin/streptomycin at 37 °C in 5% CO₂. hMSCs were cultured in growth media at 37 °C in 5% CO₂. Adipogenic differentiation was induced by adipogenic induction medium and kept by induction/maintenance cycles as described in the Lonza protocol. Osteogenic differentiation was induced by osteogenic induction medium provided by Lonza.

6.3.2 Microfluidic Device Fabrication and Design

The microchannel was designed with a simple Y-shape, where cell suspensions are brought together in the Y-joint mixing zone. In order to make a simple, cheap, and robust device, PMMA blocks were used as the device substrate. The experimental device was fabricated using laser ablation to etch PMMA blocks (1/8 in thickness, 1.25 in length, and 1.42 in width). The PMMA channels were laser etched using Versalaser 2.30 with a CO₂ laser at 14.25 W power to produce parabolic channels with a measured base width of 170 μm , a peak height of 200 μm , and a channel length of 1.5 cm. The fluid inlet connections were fabricated using 406 μm (0.016 in) OD stainless steel capillary tubes with an 203 μm (0.008 in) ID and a length of 2.0 cm, which were embedded into the PMMA blocks using thermal heating to be in line with the channel flowaxes, while the fluid outlet capillary was cut to 2.0 cm and embedded by thermal heating and pressure similarly to the fluid inlets and allowed to cool. The top block of PMMA is used to cap the channel through thermal bonding with the etched bottom block in a convection oven for 2 h at 275 °C and allowed to cool completely to room temperature over 2 h under pressure. Once cooled, the fluid connections are finished by slipping PEEK tubing (ID 203 μm /0.008 in) over the metal capillary and sealed using epoxy resin (3M). Finally, high pressure HPLC 1 mL Luer lock glass syringes (Hamilton) are connected to the PEEK tubing using finger tight female Luer fittings (UpChurch Scientific).

6.3.3 Liposome Formation and Formulation

To prepare liposomes bearing ketone or oxyamine functionalities, 60 μL 2-dodecanone-tetra(ethylene)glycol (10 mM in CHCl₃) or *O*-dodecyloxyamine-tetra(ethylene)glycol (10 mM in

CHCl₃) was mixed with 430 μ L POPC (10 mg/mL in CHCl₃) and 10 μ L of DOTAP (10 mg/mL in CHCl₃), and then thoroughly dried via N₂. After the CHCl₃ was evaporated, the lipid mixture was suspended in 3 mL of PBS, followed by tip sonication for 15 min until the suspension became clear.

6.3.4 Cell Surface Modification Using Liposome Fusion

Once cells reach 90% confluency, 5% (v/v) liposomes (ketone or oxyamine bearing liposomes) were added to the cell culture media, and incubated with cells at 37 °C and 5% CO₂ for 1 h to create ketone- or oxyamine-tailored cells.

6.3.5 General Method for Spheroid Generation in Microfluidic Device

GFP NIH 3T3 and RFP HNDP cells were grown to approximately 90% confluency and then treated with oxyamine and ketone bearing liposomes, respectively, using the standard protocol. Once the cells were surface engineered, they were washed 3 times with PBS and then detached using 0.25% trypsin/EDTA at 37 °C and 5% CO₂. Once the cells were detached and neutralized by DMEM media (10% FBS), cell suspensions were transferred to separate 15 mL centrifuge tubes and centrifuged down at 800 rpm for 5 min. The supernatant was discarded and the remaining pellet was resuspended in DMEM media to reach a final concentration of 4×10^6 /mL. Once the ketone and oxyamine-tailored cell suspensions were ready, 250 μ L of each cell suspension was immediately loaded into separate sterilized 1 mL gastight Luer lock Hamilton gas chromatography syringes. The connection tubing and microfluidic device were sterilized by passing 1 mL 70% ethanol solution, followed by 1 mL of PBS buffer. Once sterilized, the loaded syringes were finger tightened onto male Luer connections and placed onto a Harvard 11 PLUS

syringe pump. The flow rate was set to 8 $\mu\text{L}/\text{min}$ for 5 min to purge air bubbles from the system, then reduced to 0.4 $\mu\text{L}/\text{min}$ for 5 min, where the fluid was discarded and subsequent eluent was collected onto 1 cm^2 glass slides. The 1 cm^2 glass slides were prepared in advance and sterilized by sonication in 70% ethanol solution for 30 min. The microfluidic experiments typically lasted around 45 min. After experiments were done, the collecting slides were transferred to tissue culture plates and incubated at 37 °C and 5% CO_2 for 25 min. The cells on the slides were then fixed by 3.8% formaldehyde solution for 15 min, followed with gentle washing with PBS. The cell samples were observed and imaged using a Nikon Eclipse TE2000-U Fluorescence Microscope.

6.3.6 Engineered Spheroid Growth Kinetics Using Microfluidics

C3H/10T1/2 cells were cultured to approximately 90% confluency and engineered using standard conditions. Once the cells were detached, the suspension would be diluted using serum containing growth medium to obtain different cell densities; 250 μL of each cell suspension was immediately loaded into separate sterilized 1 mL gastight Luer lock Hamilton gas chromatography syringes. The connection tubing and microfluidic device were sterilized by passing 1 mL 70% ethanol solution, followed by 1 mL of PBS buffer. The loaded syringes were then finger tightened onto male Luer connections and placed onto a Harvard 11 PLUS syringe pump. The flow rate is set to 8 $\mu\text{L}/\text{min}$ for 5 min to purge air bubbles from the system, then the flow rate was lower to the experimental flow rate (0.2–0.6 $\mu\text{L}/\text{min}$) for 5 min to discard enough fluid before collecting cell clusters. Live cell images were obtained in situ at 10 \times magnification using an Olympus CKX41 microscope to record the size and growth of the clusters. The images of cell clusters were recorded at 0 mm, 7.5 mm, and 15.0 mm of the

microfluidic channel to collect data of cluster size, while the flow rate and the cell density were changed to study the relationship between microtissue generation and microfluidic flow conditions as shown in the 3D plot.

6.3.7 Confocal Microscopy of RFP/GFP 3D Coculture Microtissues

To obtain confocal images of coculture microtissues, GFP and RFP cells were grown to approximately 95% confluency and treated with oxyamine and ketone bearing liposomes, respectively, using our standard protocol. Engineered cells ($250\ \mu\text{L}$, $2 \times 10^6/\text{mL}$) were immediately loaded into separate sterilized 1 mL gastight Luer lock Hamilton gas chromatography syringes, which were finger tightened onto male Luer connections and placed onto a Harvard 11 PLUS syringe pump. The flow rate was set to $8\ \mu\text{L}/\text{min}$ for 5 min to purge air bubbles from the system, and then reduced to $0.4\ \mu\text{L}/\text{min}$ for 5 min. After that, collection of cells was started. Flow experiments were performed for 3 h, before the collecting slides were transferred to tissue culture plates and incubated at $37\ ^\circ\text{C}$ and 5% CO_2 . After culturing the cell clusters for 12 h, cell samples were fixed with 3.8% formaldehyde, washed with PBS, and mounted onto thin glass slides with Light Diagnostics Mounting Fluid (Millipore) for 3D confocal microscopy using a Zeiss LSM 700.

6.3.8 Confocal Microscopy of Three-Cell Lines (Red/Green/Blue) Microtissues

To generate three-cell line microtissues and observe by confocal microscopy, oxyamine engineered C3H/10T1/2 cells were treated with 0.3% v/v of CellTracker Blue CMAC (Life Technologies) for 45 min, and then mixed with ketone engineered GFP cells and RFP cells. Blue-stained C3H/10T1/2 cells presenting oxyamine ($4 \times 10^6/\text{mL}$) were loaded into a 1 mL Hamilton glass syringe, while ketone engineered GFP cells ($2 \times 10^6/\text{mL}$) and ketone engineered

RFP cells (2×10^6 /mL) were loaded into another 1 mL Hamilton glass syringe. The two syringes were connected to the microfluidic device and flow rate was controlled at 0.4 μ L/min. Cell clusters were dispensed onto 1 cm² glass slides for 45 min and then incubated in tissue culture plates for 12 h at 37 °C with 5% CO₂. Cell samples were fixed with 3.8% formaldehyde, washed with PBS, and mounted onto thin glass slides with Light Diagnostics Mounting Fluid (Millipore) for 3D confocal microscopy using a Zeiss LSM 700.

6.3.9 3D Coculture Multilayers of HMSCs and 3T3 Fibroblasts

HMSCs and 3T3 fibroblasts were surface engineered with ketone and oxyamine liposomes, respectively. 3T3 fibroblasts presenting oxyamines were then trypsinized and added (1×10^5 cells/mL) to the hMSCs. These cells were cocultured in adipogenic, fibroblast, and osteoblast induction and maintenance media, resulting in the 3D multilayered, tissue-like structures of adipocytes, fibroblasts, osteoblasts, and 3T3 fibroblasts. After differentiation, the 3D coculture was fixed with formaldehyde (4% in PBS, 30 min). Substrates were then immersed in a solution containing water and 60% isopropyl alcohol (3–5 min), followed by staining with Oil Red O (5 min) and Harris Hemotoxylin (1 min). Substrates were visualized by phase contrast microscopy using a Zeiss inverted microscope. The substrates for fibroblast differentiation were fixed with formaldehyde and permeated with 0.1% Triton X-100. Monoclonal antibody of collagen I was applied for 1 h, and then incubated with secondary antibody anti-mouse IgG (FITC conjugate) for 30 min, followed by DAPI for 30 min for nucleus staining (reagents from Fisher Scientific). The substrates for osteogenic differentiation were stained with sigma Alkaline Phosphatase (ALP) kit (sigma kit 85).

6.3.10 Collagen Based RFP and GFP Tissue Formation

To make macro-size (2×2 cm²) robust tissue, collagen was introduced. Oxyamine tailored GFP cells (2 mL, 4×10^6 /mL) and ketone tailored RFP cells (2 mL, 4×10^6 /mL) were loaded into the microfluidic device to generate RFP/GFP microtissue. The flow rate was set to 8 μ L/min for 5 min to purge air bubbles from the system, and then reduced to 0.4 μ L/min for 5 min. After that, collection of cells was started. The cell clusters were collected onto a 2×2 cm² slide loaded with liquid collagen solution. After collection, the collagen/cell hybrid was transferred to a tissue culture plate and incubated at 37 °C and 5% CO₂ for 30 min to allow the collagen solution to solidify. Cell culture media were then added and the collagen/cell hybrid tissue was incubated for 12 h before being peeled off the glass slide. The collagen supported macro-tissue was then fixed with 3.8% formaldehyde, washed with PBS, and mounted onto thin glass slides with Light Diagnostics Mounting Fluid (Millipore) for 3D confocal microscopy using a Zeiss LSM 700.

6.3.11 3D Oriented Coculture Multilayers (RFP-GFP-RFP, thin)

Microscope glass coverslips were cut into small pieces in advance and put into a 96-well microplate. RFP cells were grown on the slips in the microplate until 95% confluency was reached. Through standard liposome treatment, the RFP cells were surface engineered to present ketone group. GFP cells presenting oxyamine (200 μ L, 5×10^5 /mL) were then loaded by standard microfluidics procedure onto the ketone tailored RFP cells, and then cultured for 12 h. After removing most media, ketone tailored RFP cells (200 μ L, 5×10^5 /mL) were loaded onto 1 cm² glass slides by microfluidics, and cultured for 6 h. The slides were then gently picked up and fixed in 3.8% formaldehyde, washed with PBS, and mounted onto thin glass slides with

Light Diagnostics Mounting Fluid (Millipore) for 3D confocal microscopy using a Zeiss LSM 700.

6.3.12 3D Oriented Coculture Multizones (RFP-GFP-RFP, thick)

Microscope glass coverslips were cut into small pieces in advance and put into a 96-well microplate. Ketone tailored RFP cells (150 μ L, 1×10^6 /mL) and oxyamine tailored RFP cells (150 μ L, 1×10^6 /mL) were loaded by standard microfluidics procedure onto the coverslips in the microplate, and cultured for 12 h. After removing most media, ketone tailored GFP cells (150 μ L, 1×10^6 /mL) and oxyamine tailored GFP cells (150 μ L, 1×10^6 /mL) were loaded by microfluidics onto the RFP cells, and then cultured for 12 h. After removing most media, ketone tailored RFP cells (150 μ L, 1×10^6 /mL) and oxyamine tailored RFP cells (150 μ L, 1×10^6 /mL) were loaded by microfluidics again, and cultured for 6 h. The slides inside the microplate were then gently picked up and fixed in 3.8% formaldehyde, washed with PBS, and mounted onto thin glass slides with Light Diagnostics Mounting Fluid (Millipore) for 3D confocal microscopy using a Zeiss LSM 700.

6.3.13 Oxime Bond Formation (Synthesis of 2-(Propan-2-ylideneaminoxy)acetic acid)

To a 10 mL flask with magnetic stir bar, 1.1 mmol, 91.03g/mol, 100 mg) of *o*-(carboxymethyl)hydroxylamine hemihydrochloride was added and purged with argon gas. Freshly distilled acetone (3 mL) was then added by syringe and stirred at room temperature for 4 h. Excess acetone was removed by rotary evaporator to give (140 mg, 131.06 g/mol, 99%) conversion to the oxime product 2-(propan-2-ylideneaminoxy)acetic acid as a white solid. ¹H

NMR (D₂O, 300 MHz): δ 4.45 (s, 2H), 1.85 (s, 3H), 1.79 (s, 3H); ¹³C NMR (D₂O, 400 MHz): δ 175.45, 160.82, 69.81, 20.61, 15.31.

6.3.14 Oxime Hydrolysis Analysis

Oxime hydrolysis experiments were conducted by adding 1.5 mg (11 μ mol) of 2-(propan-2-ylideneaminoxy)acetic acid into five separate scintillation vials, followed by preparation of 0.1 M buffered D₂O solutions using pyridine (pH 11.0), sodium bicarbonate (pH 8.0), PBS (pH 7.4), sodium carbonate (pH 5.0), and sodium formate (pH 3.0), respectively. Once the five separate samples of 2-(propan-2-ylideneaminoxy)acetic acid were dissolved in 0.5 mL of the different pH buffered D₂O solutions, their respective NMR spectra were taken (ns = 8). Data was gathered initially at 3 h intervals, followed by once a day, then once a week to determine the rate of hydrolysis of the starting material.

6.3.15 Oxime Formation Kinetics Conditions

Pseudo-first-order rate experiments were conducted using ¹H NMR (300 MHz) spectroscopy. These experiments were performed in typical NMR tubes by dissolving methoxyamine hydrochloride (1.5 mg, 83.52 g/mol, 18 μ mol) and freshly distilled acetone (150 μ L, distilled over dririte) in 0.25 mL PBS buffered D₂O (pH 7.4) at 37.0 °C, respectively. The two solutions were quickly mixed together in the NMR tube and placed into the spectrometer, and the first time point was immediately taken, with subsequent data points taken every 40 s. This experiment was repeated using 2-(propan-2-ylideneaminoxy)acetic acid (11 mg, 109.30 g/mol, 11 μ mol) dissolved in 0.25 mL PBS buffered D₂O (pH 7.4) in a NMR tube at 37.0 °C, and freshly distilled acetone was added into 0.25 mL PBS buffered D₂O (pH 7.4) and warmed to 37.0 °C. The two

solutions were then mixed in a NMR tube followed by placement into a spectrometer and the first time point was immediately taken, with subsequent data points taken every 40 s.

6.3.16 Stem Cell Differentiation in Coculture. RT-PCR Analysis

Human mesenchymal stem cells (hMSCs) were induced to differentiate for 2 weeks. Total RNA was then extracted by RNA isolation kits (Qiagen). 1 µg of total RNA was converted to cDNA using AMV reverse transcriptase and random hexamer primers (Promega). The resulting cDNA was used in PCR with the following primer, LPL (sense 5'-GAG ATT TCT CTG TAT GGC ACC-3', antisense 5'-CTG CAA ATG AGA CAC TTT CTC-3'), PPAR γ 2 (sense 5'-GCT GTT ATG GGT GAA ACT CTG-3', antisense 5'-ATA AGG TGG AGA TGC AGG CTC-3'), Collagen I (sense 5'-TGC TGG CCA ACC ATG CCT CT-3', antisense 5'-TTG CAC AAT GCT CTG ATC-3'), Collagen II (sense 5'-ATG ACA ACC TGG CTC CCA AC-3', antisense 5'-GCC CTA TGT CCA CAC CGA-3'), RUNX2 (sense 5'-GAT GAC ACT GCC ACC TCT GAC TT-3', antisense 5'-CCC CCC GGC ACC ATG GGA AAC TG-3'), ALPL (sense 5'-CCA TTC CCA CGT CTT CAC ATT-3', antisense 5'-GAG GGC CAG CGC GAG CAG CAG GG-3'), at annealing temperatures of 52 °C, 55 °C, 53 °C, 57 °C, 61 °C, 66 °C, respectively. Amplification reactions were carried out for 1 min through 30 cycles, and the reaction products were subjected to 1% agarose gel electrophoresis. The reaction products are 276bp (Lpl), 351bp (PPAR γ 2), 489bp (Collagen I), 359bp (Collagen II), 362bp (RUNX2), and 418bp (ALPL), respectively.

6.3.17 Bubble Fusion via Oxime Chemistry

Commercially available soap bubble toys were obtained from Crayola. Control experiment was performed by directly using the commercial soap solutions for blowing and merging bubbles — resulting in no fusion—only bubble adhesion. A second experiment was performed based on the

same soap solutions but doped with 5% *O*-dodecyloxyamine and 5% 2-dodecanone, respectively—resulting in bubble fusion via an interfacial oxime ligation.

6.3.18 Spheroid Assembly

Microfluidic device was mounted on a Zeiss AXIO Observer Inverted Fluorescence Microscope. Ketone engineered GFP cells ($2 \times 10^6/\text{mL}$) and oxyamine engineered GFP cells ($2 \times 10^6/\text{mL}$) were prepared in PBS and loaded into the Hamilton glass syringes separately. The two syringes were connected to the microfluidic device and flow rate was controlled at $0.4 \mu\text{L}/\text{min}$. Live recording of the two cell populations flowed through the microfluidic channels were taken automatically by the microscope. Control experiment was identical but without liposome fusion of bio-orthogonal groups to the cells. This resulted in only single cells floating through the channel and no spheroid assemblies observed.

6.4 Results and Discussion

To rewire cell surfaces with bio-orthogonal moieties that function as a chemical Velcro, two types of liposomes were synthesized. **Figure 6.1** describes the general cell surface engineering strategy used to tether cells with bio-orthogonal chemical groups. Oxyamine- (**4**) or ketone- (**3**) functionalized lipids were incorporated into liposomes along with naturally occurring neutral POPC (**1**) and the positively charged DOTAP (**2**) background lipid molecules. Cells (**7,8**) were treated with either ketone (**5**) or oxyamine (**6**) containing liposomes for 1h at 37°C to deliver the functional groups onto cell surfaces. Two populations of cells with complimentary bio-orthogonal moieties (**9,10**) were mixed resulting in contact between the cells triggering a reaction

between oxyamine and ketone moieties present on cell surfaces resulting in the formation of a strong covalent oxime bond with the subsequent cell assembly.

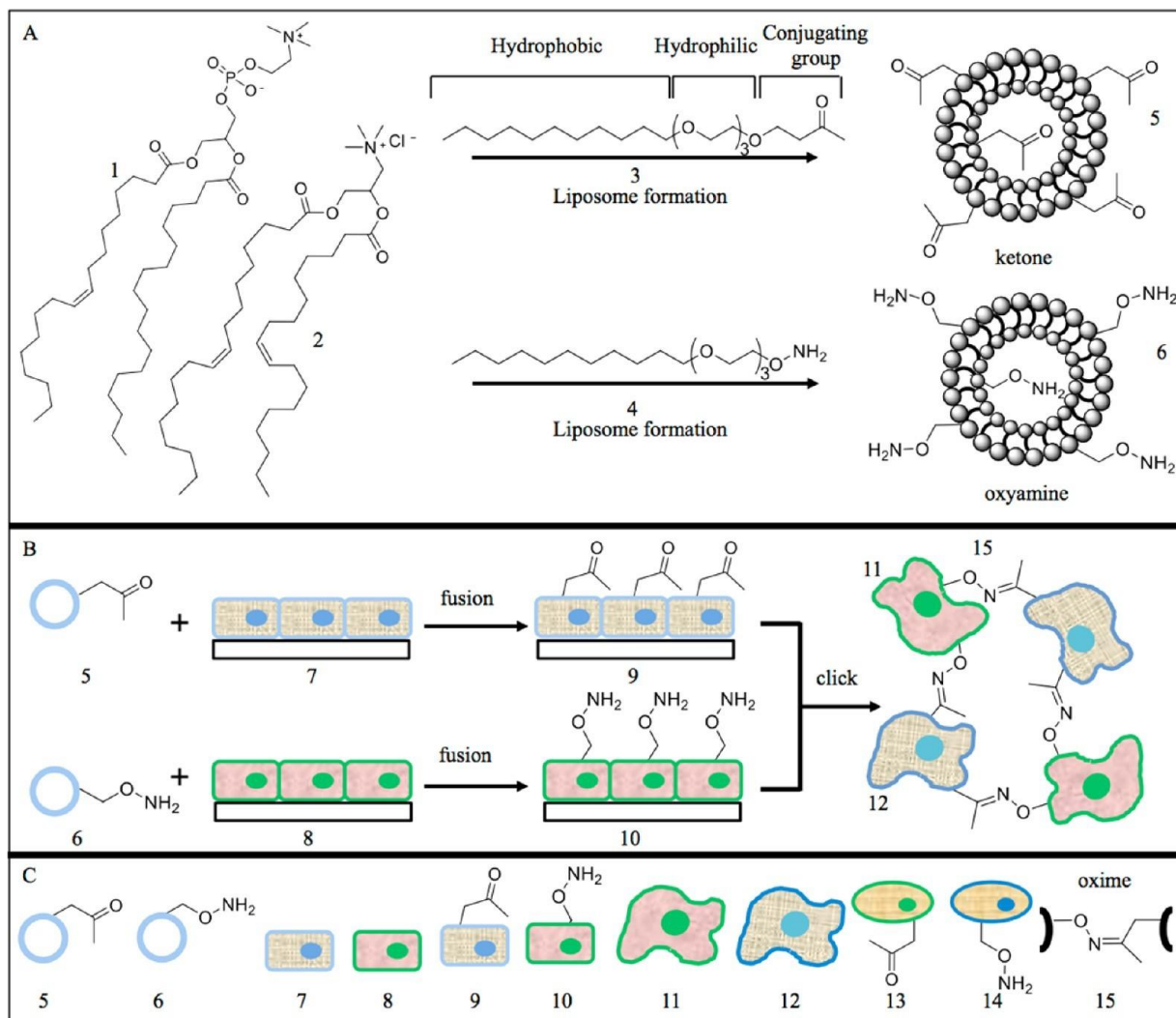


Figure 6.1. Schematic describing the cell surface tailoring strategy to generate complex coculture tissue assemblies. The combination of bio-orthogonal lipids, liposome formation, and liposome fusion result in the generation of engineered cell surfaces that can subsequently be assembled through an interfacial click reaction. **(A)** Bio-orthogonal liposomes are formed by mixing POPC (**1**), DOTAP (**2**), and either a ketone (**3**) or oxyamine (**4**) terminated lipid-like molecules. **(B)** Cell surfaces (**7**) and (**8**) were engineered to present ketones or oxyamines via liposome fusion and delivery. The tailored cells (**9**) and (**10**) were then mixed and formed rapid assemblies (**11**) via the bio-orthogonal oxime (**15**) click ligation. **(C)** List of liposomes, cells, and tailored cells used in the study. (**5**) Ketone tailored liposome, (**6**) oxyamine tailored liposome, (**7**) contact inhibited cell line, (**8**) contact inhibited cell line, (**9**) ketone engineered cell line, (**10**) oxyamine engineered cell line, (**11**) spheroid cell line, (**12**) spheroid cell line, (**13**) suspended ketone engineered cell line, (**14**) suspended oxyamine engineered cell line, and (**15**) oxime ligation bond between two membrane surfaces.

This co-culture assembly can be rapidly achieved due to polyvalent oxime chemistry ligation between the cells. As controls, no cell assemblies were generated in cells which were treated with non-functionalized liposomes. As was demonstrated in previous studies, cell viability is not affected by the liposome fusion process. FACS analysis performed in previous studies was used to determine the amount of oxyamine and ketone moieties present on the cell surface. In this cell assembly process, the chemistry is only used to hold cells in place temporarily until they produce their own extracellular matrix and spread forming intact tissues. As cells proliferate, their membrane is renewed and the chemistry is gradually diluted out, but the cells are held together by the intercellular proteins and the extracellular matrix that they secrete.

In order to assemble cells into co-culture spheroids via microfluidics, the click reaction between the oxyamine and ketone on the cell surfaces must be very rapid. In the field of click chemistry there are several bio-orthogonal reactions that are extensively used. These include the copper-catalyzed reaction between alkyne and azide, the ring strain cycloaddition reaction and the Diels-Alders ligation.²⁸ We, however, selected oxime chemistry because it is relatively easy to synthesize oxyamine- and ketone-tethered lipids and incorporate them into liposomes.

Figure 6.2 describes kinetics experiment which was conducted to assess the reaction rate of ligation between the oxyamine and ketone, and stability of the oxime bond under physiological conditions (pH 7, 37 C) The experiment was performed in PBS and the process of oxime formation was monitored in real time via NMR analysis. The reaction was adjusted to be pseudo-1st-order where the concentration of the ketone molecule is significantly greater than the concentration of the oxyamine. The A_i peak at 3.92 ppm (**Figure 6.2A**) represents the oxyamine that is being converted into oxime as the result of the reaction with the ketone (the B_i peak 3.74 ppm). The areas of both peaks add up to 1.00, so it is possible to deduce the concentration of

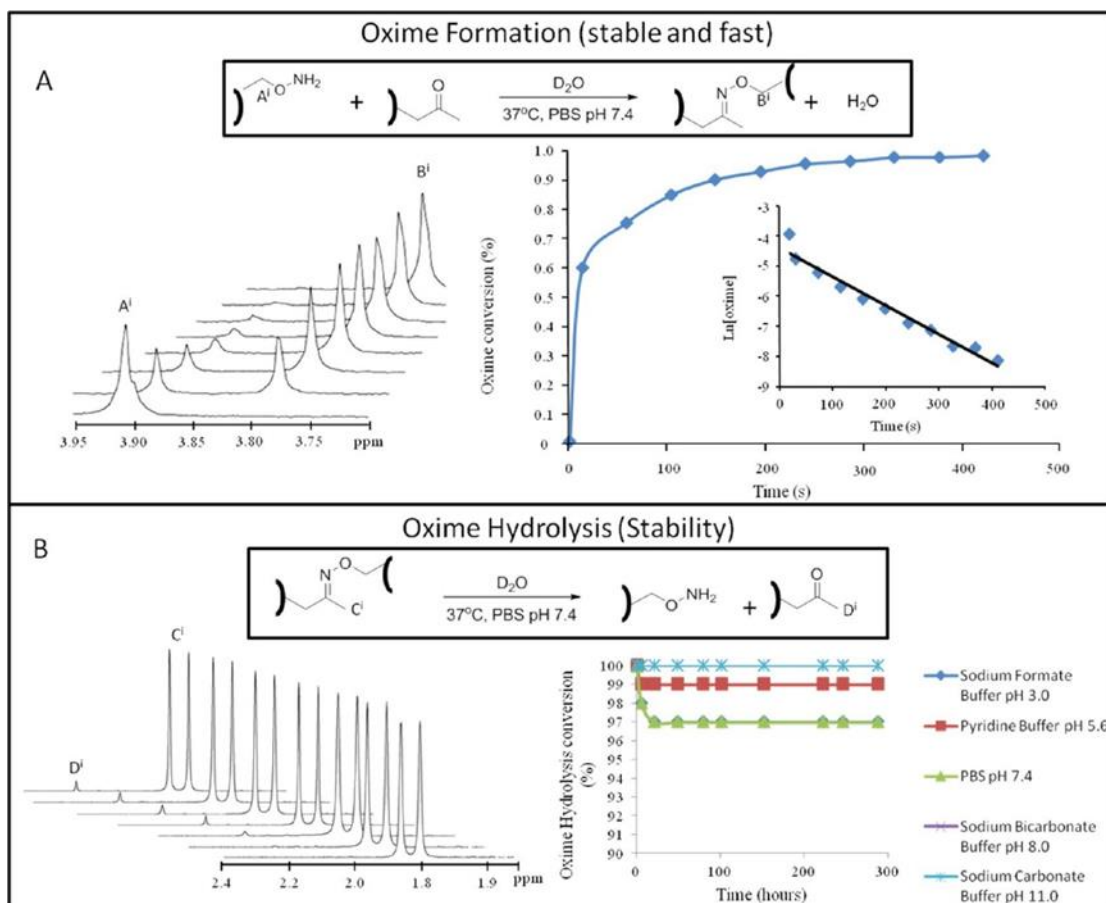


Figure 6.2. NMR study of the kinetics and stability of a bio-orthogonal oxime conjugation reaction under physiological conditions. (A) The reaction of a ketone and oxyamine at physiological conditions (37 °C and pH 7.4) results in the rapid formation of the covalent and a stable oxime bond. ^1H NMR was used to determine the oxime formation kinetics ($k = 0.98 \times 10^{-2} \text{ M s}^{-1}$, $t_{1/2} = 9 \text{ s}$). **(B)** The stability of the oxime bond was studied with ^1H NMR at physiological conditions (pH 3, 5.6, 7.4, 8.0, 11.0). The oxime bond was stable with no hydrolysis after 3 weeks in pH 3.0 and 5.6. At physiological conditions (pH 7.4) there was only 3% hydrolysis over 3 weeks.

oxyamine and oxime at any given time point. The half-life of the oxime formation reaction is 9 s and $k = 0.98 \times 10^{-2} \text{ M s}^{-1}$. However, we surmised that the rate of oxime formation on cell surfaces may be several orders of magnitude faster to multiple oxyamine and ketone moieties being present on the cell surface the ability of the bio-orthogonal lipid molecules to migrate

within the membrane dramatically changing their position and increasing their local concentration density. This polyvalent nature of surface chemistry is what promotes the rapid cell assembly which is necessary for the method to be usable with microfluidics. The stability of oxime was monitored over the course of three weeks in buffer solutions with different pH concentrations. It was demonstrated that oxime bond is stable at physiological conditions since at pH 7.4 and only 3% hydrolysis was observed.

Figure 6.3 shows the general strategy for controlled co-culture spheroid assembly via microfluidic flow. First, monolayers of confluent cells grown in micro-wells are treated with ketone or oxyamine-tethered liposomes. Liposomes fuse with the cell membrane delivering the ketone and oxyamine functionalities onto the cell surface. The cells are detached from the surface via trypsinization and transferred to a Y-joint microfluidic device. The cells are then assembled into coculture spheroids through oxime click chemistry. The sizes of the spheroids are determined by the flow rate, cell concentration, and the length of the assembly chamber. The spheroids are then transferred to a microwell plate where they adhere and form coculture multilayered 3D tissues. As controls, cells without the bio-orthogonal functional groups produce no spheroids upon mixing in the microfluidic channels and result in no 3D assembly (only standard 2D single cell layer sheets are formed).

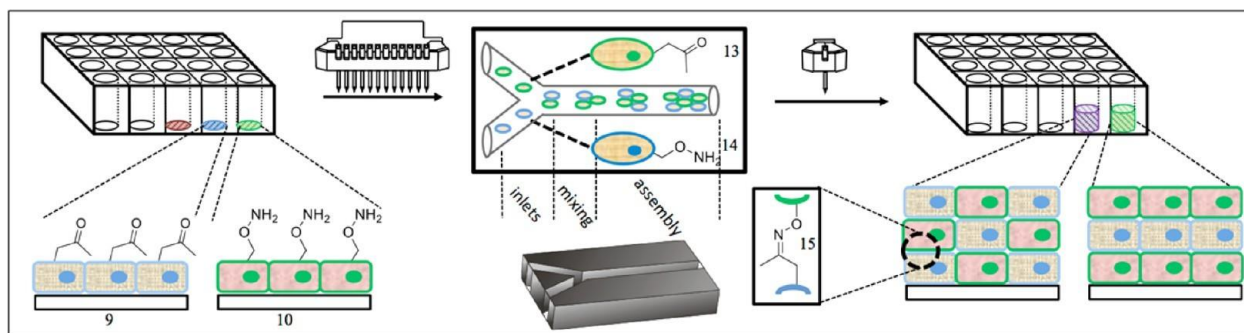


Figure 6.3. Schematic describing the use of microfluidic technology and tailored cell lines to generate multilayer coculture tissues. (Left) Different cell lines are grown in microwell plates to generate 2D contact inhibited monolayers. Liposomes containing either ketone (5) or oxyamines (6) are added to the microwells. The liposomes rapidly fuse to the cells and deliver the functional groups to rapidly produce engineered cell surfaces presenting ketones (9) or oxyamines (10). **(Middle)** The engineered cells are then transferred to a simple microfluidic device. As the cells are flown through the channels they come into contact and assemble into coculture spheroids through oxime click chemistry. The sizes of the spheroids are determined by the flow rate, cell concentration, and the length of the assembly chamber. **(Right)** The spheroids are then transferred to a microwell plate where they adhere and form coculture multilayered 3D tissues. As controls, cells without the bio-orthogonal functional groups produce no spheroids upon mixing in the microfluidic channels and result in no 3D assembly (only standard 2D single cell layer sheets are formed).

The microfluidics device is made using standard PMMA fabrication and contains three parts: two arms and one mixing chamber. The oxyamine-presenting cells are loaded into the first arm, while the ketone-presenting cells are loaded into the second arm. The cells flow through each arm and arrive into the mixing chamber. In the mixing chamber the cells collide, attach to each other instantly due to presence of bio-orthogonal chemistry and form a small spheroid. As the spheroid moves through the chamber, it comes in to contact with other single cells and becomes larger. Finally, the spheroid leaves the microfluidic chamber and attaches to the bottom of the micro-well. Over time the cells secrete ECM and spread forming 3D tissues.^{29,30} This microfluidics-based tissue assembly strategy is an effective method to assemble different types of cells into a complex 3D co-culture which can then be used for various applications such as tumor models as well as in studies focused on autocrine and paracrine signaling.

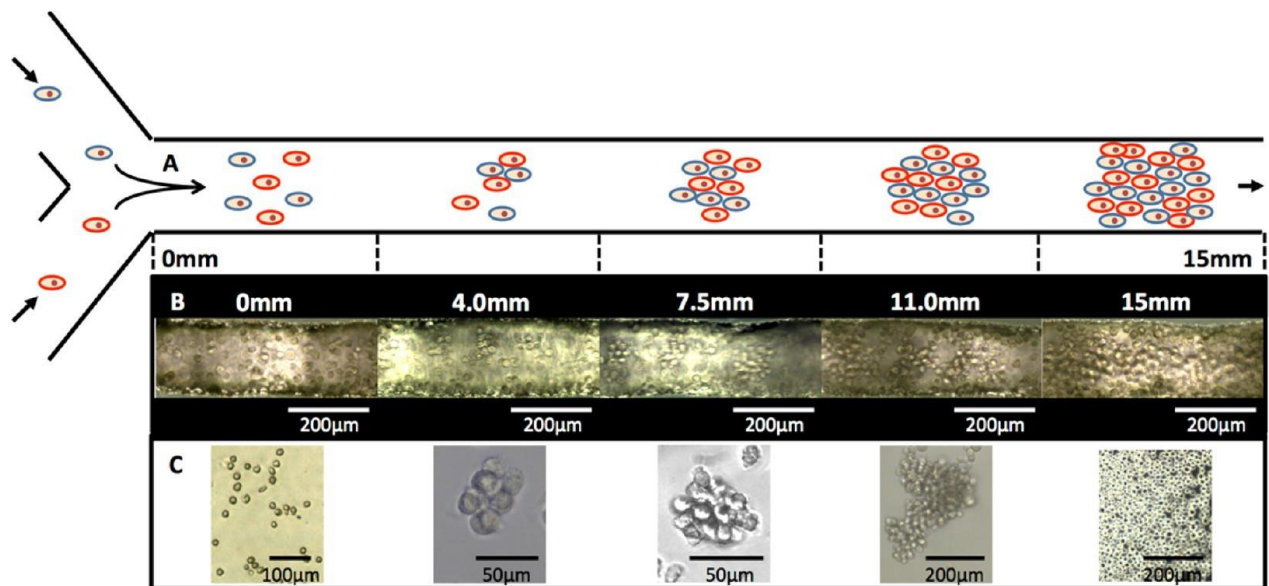


Figure 6.4. Brightfield images of C3H10T1/2 cells at various stages of assembly in the microfluidic channel device. (A) Cartoon of the PMMA microfluidic device showing the flow of cells in the Y joint followed by mixing and assembly at different lengths of the channel. **(B)** Bright field images of representative cell cluster sizes at different flow points along the channel. **(C)** In situ bright field images of cells flowing through the microfluidic device at different flow points. Larger spheroid cell assemblies are produced at longer lengths of the channel.

Control studies clearly indicate that no cell assembly takes place if cells are not functionalized liposomes (**Figure A1**). A sequence of images of growing spheroids as they flow inside the microfluidic channel (**Figure 6.4**).

The size of spheroids generated via microfluidic flow varies with the flow rate and position within the channel. This dependence is demonstrated graphically on Figure 5. The slower the rate of flow, the more time the cells have to collide with each other and form a cluster. The more cells are flown through the channel, the greater the size of the spheroid. It is interesting to note that cells with no chemistry or absence of either oxyamines or ketones on the cell surface formed no clusters. The resulting spheroids were stable and did not require collagen or Matrigel for stabilization. The assembled cells demonstrated good viability as shown on the **Figure 6.5**.

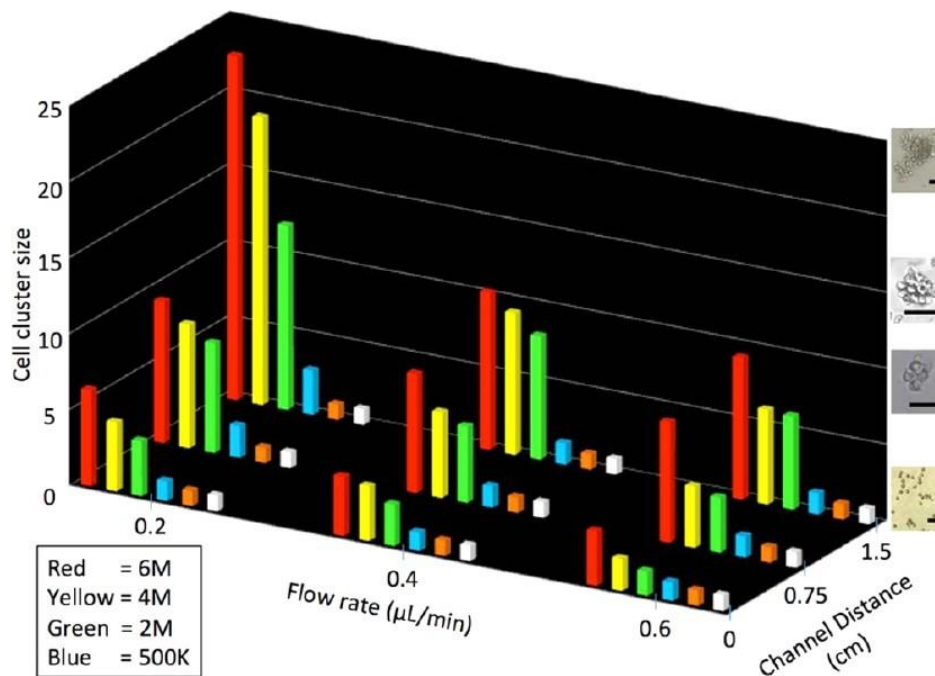


Figure 6.5. 3D plot presenting the relationship between flow rate, channel distance, cell density, and resulting cell cluster size (spheroid) assembled within a microfluidic channel. As the cell density increases and flow rate decreases spheroids assemble at a faster rate. The absence of one (orange) or both (white) surface chemistries results in no spheroid formation. Statistical analysis showed cluster size was within 5% for each condition.

To generate different co-culture spheroids via microfluidic flow, we utilized GFP-expressing (green fluorescent protein) NIH3T3 fibroblasts and RFP-expressing (red fluorescent protein) Dermal Neonatal fibroblast cell lines (**Figure 6.6**). The cells were tailored with ketone and oxyamine functionalities and flown through the microfluidic chamber. **Figure 6.6A** graphically demonstrates the polyvalent nature of surface chemistry. The bio-orthogonal rapid ligation strategy generated different types of co-culture spheroids. Different stoichiometric ratios of GFP and RFP cells were utilized in the primary experiments. For example if the ratio of flown GFP and RFP cells was 1:8, the resulting spheroid where GFP NIH 3T3 cell surrounded by RFP Neonatal Dermal Fibroblast cells (**Figure 6.6C**). If the ratio of GFP and RFP cells was 8:1, the generated spheroids had one RFP-expressing cell surrounded by multiple GFP-expressing cells (**Figure 6.6D**). Three and more types of cells can be assembled into spheroids using our microfluidics method. Figure 6E shows ketone and oxyamine-functionalized GFP, RFP expressing cells combined with C3H10T1\2 stained with CMAC (7-amino-4-chloromethylcoumarin) in 1:1:1 ratio resulting in the formation of a large co-culture spheroid containing three cell types (**Figure 6.6E**). Monoculture spheroids can also be formed via microfluidic strategy. Figure 6F shows a large monoculture spheroid made of ketone and oxyamine-presenting GFP cells. **Figure 6.6H** show a confocal-microscopy image of a spheroid containing an equal number of GFP and RFP cells. Microfluidics tissue assembly enables the formation of different kinds of spheroids with variable size, cell types and cell ratios. The spheroids are fast forming, stable and do not contain exogenous polymer materials. The cells that were not functionalized with ketone and oxyamine functional groups could not be assembled into spheroids.

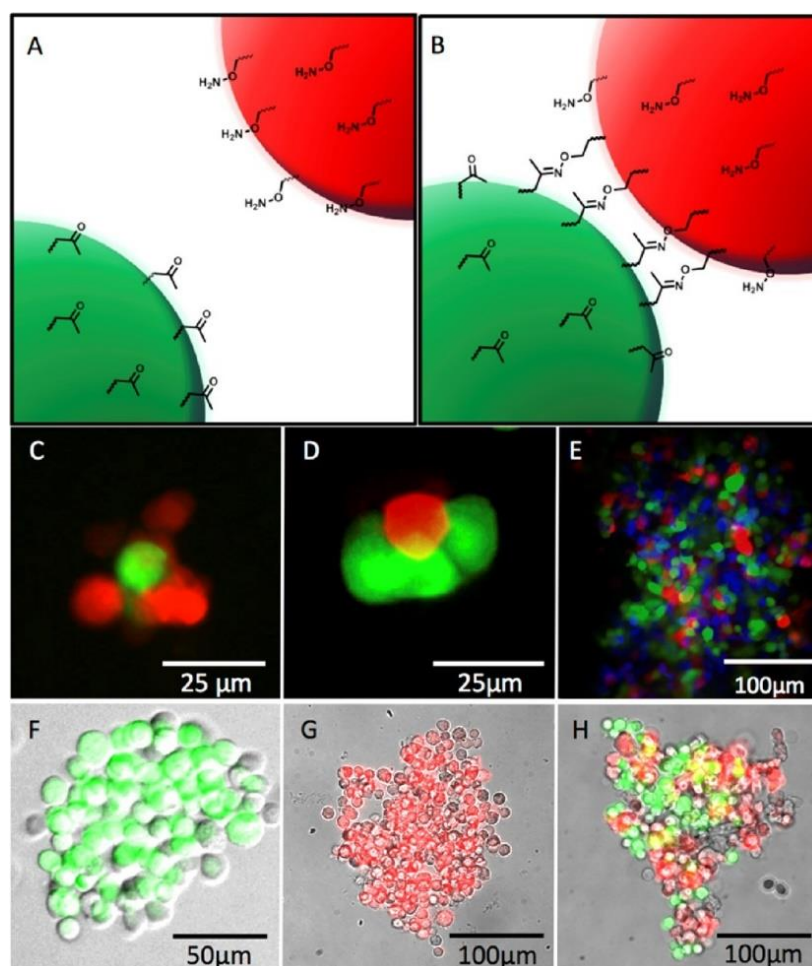


Figure 6.6 Schematic cartoon and fluorescent images of resultant coculture spheroid assembly via click chemistry ligation. (A) Two cell lines engineered with complementary interfacial bio-orthogonal groups where upon contact undergo click oxime ligation (B) resulting in coculture assembly. (C,D) Changing the engineered cell density ratio injected into the microfluidic device results in spheroids with different morphologies. A 1:8 ratio (GFP:RFP) of cells results in a single GFP NIH 3T3 cell surrounded by RFP Neonatal Dermal Fibroblast cells (C). Reversing the ratio to 8:1 (GFP:RFP) results in a single RFP Neonatal Fibroblast cell surrounded by GFP NIH 3T3 cells (D). (E) Fluorescent image of large 3 cell type spheroid, generated by mixing 1:1:1 ratio of GFP:RFP:Blue C3H10T1\2 stained with CMAC (7-amino-4-chloromethylcoumarin) in flow. These third cell tissues were easily generated by engineering GFP and RFP cells with ketones while CMAC stained cells present oxyamine groups. (F) Large spheroid of GFP cells obtained by combining two different populations of GFP cells that present ketone and oxyamine groups. (G) Large spheroid of RFP cells obtained by combining two different populations of RFP cells that present ketone and oxyamine groups. (H) Large spheroid of RFP and GFP cells obtained by flowing a 1:1 ratio of engineered RFP and GFP cells in the microfluidic device. By adjusting the flow rate, cell density, and the ratio of cell density inputs, a range of stoichiometric coculture spheroid assemblies and spheroid sizes could be generated.

In the classical in vitro models cells are grown on flat substrates (i.e Petri dishes) where they form 2D monolayers. The cells in monolayers are contact inhibited and cannot be stacked on top of each other. Therefore such tissue model systems are limited and cannot recapitulate the 3D environment of tissues. Our bio-orthogonal click chemistry technology enables construction of 3D tissues with variable size, thickness, cell composition and cell arrangement. To demonstrate the capacity of our novel tissue assembly methodology, several 3D tissue constructs with variable morphology were assembled. **Figure 6.7 A,B** shows cells that were not functionalized with oxyamine or ketone groups, as the result only 2D cell monolayers were formed. Bio-orthogonal click-chemistry technology enables formation of multilayered tissues with controlled cell orientation. **Figure 6.7 C,D** demonstrates a bilayer of GFP and RFP cells. **Figure 6.7 E,F** shows three layer of GFP and RFP fibroblasts forming three layers. These co-cultures were assembled sequentially, layer by layer via microfluidic flow. The system is flexible and allow for formation of thick tissues with oriented cell zones (**Figure 6.7G, H**). Precise cell deposition achieved via microfluidics allows to position cells exactly into the specific zone. **Figure 6.7 I, J** shows a confocal micrograph of a thick tissue formed via microfluidics by depositing several spheroids on top of each other. As was discussed above, bio-orthogonal chemistry is only used to hold cells together until they secrete their extracellular matrix and spread forming 3D tissues, therefore it is ECM that As cells divide, renew their membrane and the chemistry is diluted out. **Figure 6.7 K,L** shows a 3D co-culture of hMSC cells with fibroblasts differentiating into an adipogenic lineage. Using microfluidics it is possible to flow three or more cell types at once. **Figure 6.7 M,N** shows RFP and GFP-expressing cells tethered with a ketone molecule mixed with oxyamine-tethered blue CMAC-stained cells. Although our methodology is scaffold-free, it

can be used with both ECM and polymer scaffolds. **Figure 6.7 O,P** shows GFP and RFP fibroblasts presenting

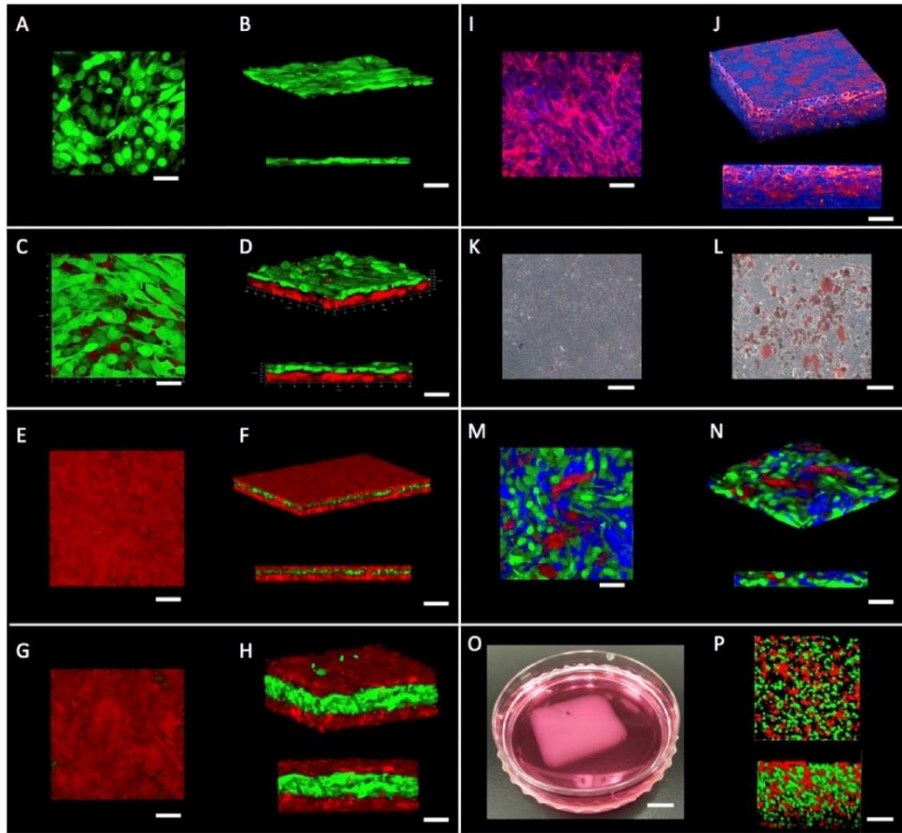
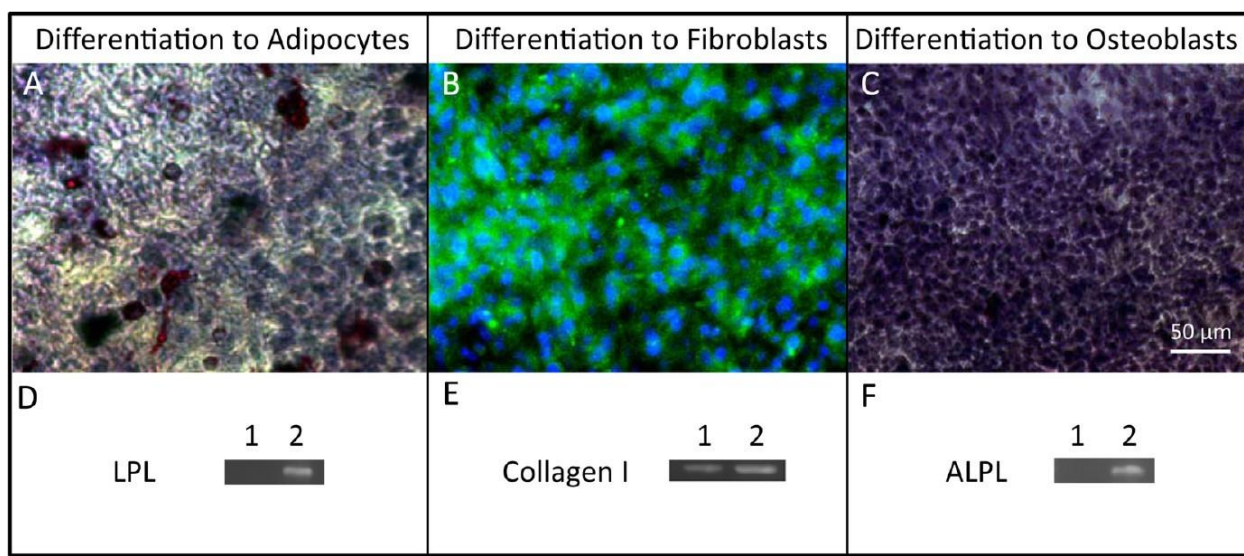


Figure 6.7. Range of confocal and bright-field images of various combinations of GFP NIH 3T3 fibroblasts, RFP neonatal fibroblasts, CMAC live stained C3H10T1/2 pluripotent embryonic fibroblast stem cells. HMSC cells and NIH Swiss 3T3 cells. (A) Top view of a standard contact inhibited single monolayer of GFP NIH 3T3 cells in culture. **(B)** Angled and side view of monolayer showing a thickness of approximately 6 μm . **(C)** Top view image of RFP-GFP bilayer generated by first assembly in microfluidic flow of RFP spheroids followed by deposition onto glass slides to generate RFP multilayer. GFP spheroids were added to this RFP multilayer generated in microfluidic flow. The sequential spheroid and multilayer generation resulted in a bilayer of multilayers of GFP and RFP cells (30 μm thick). **(E,F,G,H)** Image of serial RFP and GFP spheroid assembly in flow followed by sequential deposition resulting in control of coculture orientation multilayers and thickness (**E,F**, 30 μm thick) (**G,H**, 120 μm thick). **(I,J)** Image of TRITC and DAPI stained thick multilayers of Swiss 3T3 fibroblasts (140 μm thick). **(K,L)** Brightfield image of multilayers of HMSC cells mixed with Swiss 3T3 fibroblasts. **(L)** After culturing for 10 days the HMSC cells differentiated to adipocytes in the coculture. **(M,N)** Image of mixed multilayers of 1:1:1 RFP:GFP:Blue C3H10T1/2 cells generated by assembly in flow followed by deposition onto glass slides: The RFP and GFP cells represented ketones and the blue cells represented oxyamines. **(O)** Photograph of a 2 cm \times 2 cm \times 0.5 cm thick collagen tissue containing RFP-ketone and GFP-oxyamine cells. Spheroids of RFP and GFP cells were generated in flow and then mixed with collagen. **(P)** Confocal top and side views of coculture cells in collagen. High cell density within collagen was achieved by the adhesion of large spheroids. The cells adhere to the collagen and to each other, therefore generating high cell density thick tissue instantly.

bio-orthogonal molecules on their cell surfaces mixed with collagen hydrogel to form a 3D tissue. Since the cells are interconnected with oxime chemistry and are also bound to collagen, it is possible to achieve a high cell density and rapidly fill the ECM scaffold.

Three dimensional co-cultures are excellent models to study various biological processes such as cell, migration apoptosis as well as differentiation of stem cells. Using our bio-orthogonal technology in conjunction with microfluidics we generated mixed co-cultures of human mesenchymal stem cells with Swiss 3T3 fibroblasts (**Figure 6.8**).



1 – Day One
2 – Two Weeks

Figure 6.8. Construction of a 3D tissue coculture system via intercell click ligation and application to stem cell differentiation. (A–C) Coculture system of hMSCs/fibroblasts were assembled and then made to differentiate to adipocytes (A), fibroblasts (B), and osteocytes (C) via corresponding induction conditions. Adipocytes, fibroblasts, and osteoblasts were stained red, green, and blue, respectively. Images were taken by 20× phase contrast microscopy. Corresponding gene makers (LPL for adipocytes, Collagen I for fibroblasts, ALPL for osteoblasts) were studied over 2 weeks. (1, day one; 2, 2 weeks) and are represented by the gels as shown in D, E, and F, respectively.

The hMSC cells were mixed with the fibroblasts in 1:1 ratio and the tissues were induced to differentiate into adipocytes, osteoblasts or fibroblasts by treatment with corresponding induction

agents for 2 weeks. The samples were analyzed with reverse transcription PCR on day 1 and week 2 to characterize the expression of the lineage-specific genetic markers. An immunohistochemical analysis was also performed to characterize the lineage specification. This demonstration shows the utility of our technology to produce 3D co-cultures containing various cell types that can be used to study important biological processes such as stem cell differentiation.

6.5 Conclusion

In summary, we have developed a quick and simple method to rewire cell surfaces with bio-orthogonal chemistry and to ligate cells into co-culture spheroids in flow via a fast click reaction between oxyamine and ketone moieties. The bio-orthogonal ligation reaction is quick, specific and occurs under physiological conditions. The oxime bond is stable, resilient to hydrolysis and its formation requires no catalyst. Lipids with bio-orthogonal moieties were synthesized, incorporated into liposomes and delivered onto cell surfaces via liposome fusion producing cells with engineered cell surfaces. Liposome delivery strategy is a well established method to transport molecular cargo inside cells, therefore it is possible to use our technology to simultaneously rewire cell surfaces with the molecule of interest and to deliver cargo such as DNA, RNA or a small molecule into a cell. Our cell surface engineering method allows for the decoration of cell membranes with a wide variety of molecules and nanoscale objects such as metal nanoparticles and fluorescent polymer beads changing properties of cells without modifying their DNA. Multiple cell chemistries can be incorporated into the cellular membrane simultaneously. Microfluidics allows for precise and rapid assembly of spheroids. Since the bio-

orthogonal cell ligation strategy is compatible with a wide variety of cells, it is possible to generate 3D co-cultures containing two or more cell types. The precision of microfluidic technology enables the deposition of cells on top of each other forming complex multilayered tissues of variable thickness. Although no scaffolds are required for cell assembly, our method is compatible for use with biological and polymer materials and can be used in conjunction with modern layer-by-layer deposition methods such as electrospinning and 3D printing.³¹⁻³⁴ The microfluidic tissue assembly method is a versatile platform that can be used to generate 3D tissues for transplantation, drug testing and disease modeling.

6.6 References

1. Gartner, Z. J. & Bertozzi, C. R. Programmed assembly of 3-dimensional microtissues with defined cellular connectivity. *Proc. Natl. Acad. Sci.* **106**, 4606–4610 (2009).
2. Gong, P. *et al.* A Strategy for the Construction of Controlled, Three-Dimensional, Multilayered, Tissue-Like Structures. *Adv. Funct. Mater.* **23**, 42–46 (2013).
3. Matsunaga, Y. T., Morimoto, Y. & Takeuchi, S. Molding Cell Beads for Rapid Construction of Macroscopic 3D Tissue Architecture. *Adv. Mater.* **23**, H90–H94 (2011).
4. Sutherland, R. M. Cell and environment interactions in tumor microregions: the multicell spheroid model. *Science* **240**, 177–84 (1988).
5. Gottfried, E., Kunz-Schughart, L. A., Andreesen, R. & Kreutz, M. Brave Little World: Spheroids as an in vitro Model to Study Tumor-Immune-Cell Interactions. *Cell Cycle* **5**, 691–695 (2006).
6. MacDonald, H. R. & Howell, R. L. The multicellular spheroid as a model tumor allograft. I. Quantitative assessment of spheroid destruction in alloimmune mice. *Transplantation* **25**, 136–40 (1978).
7. Torisawa, Y. *et al.* A multicellular spheroid array to realize spheroid formation, culture, and viability assay on a chip. *Biomaterials* **28**, 559–566 (2007).
8. Tejavibulya, N., Youssef, J., Bao, B., Ferruccio, T.-M. & Morgan, J. R. Directed self-assembly of large scaffold-free multi-cellular honeycomb structures. *Biofabrication* **3**, 34110 (2011).
9. Groeber, F., Holeiter, M., Hampel, M., Hinderer, S. & Schenke-Layland, K. Skin tissue engineering — In vivo and in vitro applications. *Adv. Drug Deliv. Rev.* **63**, 352–366 (2011).
10. Bhatia, S. N., Underhill, G. H., Zaret, K. S. & Fox, I. J. Cell and tissue engineering for liver disease. *Sci. Transl. Med.* **6**, 245sr2-245sr2 (2014).
11. Vunjak-Novakovic, G. *et al.* Challenges in Cardiac Tissue Engineering. *Tissue Eng. Part B Rev.* **16**, 169–187 (2010).
12. Murphy, S. V & Atala, A. 3D bioprinting of tissues and organs. *Nat. Biotechnol.* **32**, 773–785 (2014).

13. Date, S. & Sato, T. Mini-Gut Organoids: Reconstitution of the Stem Cell Niche. *Annu. Rev. Cell Dev. Biol.* **31**, 269–289 (2015).
14. Psaltis, D., Quake, S. R. & Yang, C. Developing optofluidic technology through the fusion of microfluidics and optics. *Nature* **442**, 381–386 (2006).
15. Günther, A. & Jensen, K. F. Multiphase microfluidics: from flow characteristics to chemical and materials synthesis. *Lab Chip* **6**, 1487–1503 (2006).
16. Squires, T. M. & Quake, S. R. Microfluidics: Fluid physics at the nanoliter scale. *Rev. Mod. Phys.* **77**, 977–1026 (2005).
17. Beebe, D. J., Mensing, G. A. & Walker, G. M. Physics and Applications of Microfluidics in Biology. *Annu. Rev. Biomed. Eng.* **4**, 261–286 (2002).
18. Hansen, C. Microfluidics in structural biology: smaller, faster... better. *Curr. Opin. Struct. Biol.* **13**, 538–544 (2003).
19. Shui, L., Bomer, J. G., Jin, M., Carlen, E. T. & van den Berg, A. Microfluidic DNA fragmentation for on-chip genomic analysis. *Nanotechnology* **22**, 494013 (2011).
20. Autebert, J. *et al.* Microfluidic: An innovative tool for efficient cell sorting. *Methods* **57**, 297–307 (2012).
21. Günther, A. & Jensen, K. F. Multiphase microfluidics: from flow characteristics to chemical and materials synthesis. *Lab Chip* **6**, 1487–1503 (2006).
22. Bettinger, C. J. & Borenstein, J. T. Biomaterials-based microfluidics for engineered tissue constructs. *Soft Matter* **6**, 4999 (2010).
23. Dokmeci, M. R. & Khademhosseini, A. Preface to Special Topic: Microfluidics in cell biology and tissue engineering. *Biomicrofluidics* **5**, 22101 (2011).
24. Pierre, J., Oudina, K., Petite, H. & Oddou, C. Microfluidique des milieux poreux : application au génie tissulaire osseux. *La Houille Blanche* 71–77 (2006).
doi:10.1051/lhb:200602008
25. Williams, D. F. On the mechanisms of biocompatibility. *Biomaterials* **29**, 2941–2953 (2008).
26. Kean, T. & Thanou, M. Biodegradation, biodistribution and toxicity of chitosan. *Adv. Drug Deliv. Rev.* **62**, 3–11 (2010).
27. ZIMMERMANN, W. *et al.* Heart muscle engineering: An update on cardiac muscle replacement therapy. *Cardiovasc. Res.* **71**, 419–429 (2006).

28. Patterson, D. M., Nazarova, L. A. & Prescher, J. A. Finding the Right (Bioorthogonal) Chemistry. *ACS Chem. Biol.* **9**, 592–605 (2014).
29. Rogozhnikov, D., Luo, W., Elahipanah, S., O'Brien, P. J. & Yousaf, M. N. Generation of a Scaffold-Free Three-Dimensional Liver Tissue via a Rapid Cell-to-Cell Click Assembly Process. *Bioconjug. Chem.* **27**, 1991–1998 (2016).
30. Rogozhnikov, D., O'Brien, P. J., Elahipanah, S. & Yousaf, M. N. Scaffold Free Bio-orthogonal Assembly of 3-Dimensional Cardiac Tissue via Cell Surface Engineering. *Sci. Rep.* **6**, 39806 (2016).
31. Matthews, J. A., Wnek, G. E., Simpson, D. G. & Bowlin, G. L. Electrospinning of Collagen Nanofibers. *Biomacromolecules* **3**, 232–238 (2002).
32. Bhardwaj, N. & Kundu, S. C. Electrospinning: A fascinating fiber fabrication technique. *Biotechnol. Adv.* **28**, 325–347 (2010).
33. Wu, W., DeConinck, A. & Lewis, J. A. Omnidirectional Printing of 3D Microvascular Networks. *Adv. Mater.* **23**, H178–H183 (2011).
34. Billiet, T., Gevaert, E., De Schryver, T., Cornelissen, M. & Dubruel, P. The 3D printing of gelatin methacrylamide cell-laden tissue-engineered constructs with high cell viability. *Biomaterials* **35**, 49–62 (2014).

Chapter 7

Conclusion and Future Work

In this work I have developed a new scaffold-free method to assemble cells into functional 3D tissues. This unique system combines bio-orthogonal click chemistry, microencapsulation, liposome fusion and cell surface engineering strategies. This novel technique uses no scaffolds or exogenous polymers to support the cell mass. The system exploits a simple ligation reaction between oxyamine and ketone moieties resulting in the formation of a stable covalent oxime bond. The reaction is quick, specific, non-cytotoxic and occurs under physiological conditions. Lipids containing oxyamine and ketone functionalities were synthesized and incorporated into liposomes for delivery onto cell surfaces. Liposomal vesicles are used routinely to transfer molecular cargo inside cells and many modern therapies utilize liposomes for targeted drug delivery.¹ With our technique liposomes were used to engineer cell membranes for the first time. Traditional cell surface modification strategies have relied on the genetic expression of receptor proteins or on metabolic engineering to tether cells to the molecule of interest. Both approaches utilize cellular biochemical pathways which are altered during the process.^{2,3} Liposome delivery, however, works from the outside and does not disrupt the cellular machinery. Although genetic engineering enables changes in properties of the cell membranes via the expression of different surface proteins, the method cannot be used to install non-biological ligands such as small molecules, fluorescent beads or nanoparticles.

Liposome fusion alone or in conjunction with bio-orthogonal chemistry opens the door for new possibilities in cell surface engineering. Using a simple synthetic chemistry, a hydrophobic lipid tail can be attached to a molecule or a nanoscale object, which will allow it to be incorporated into a liposome.⁴ Following membrane fusion, the molecule or the object will be displayed on the cell surface. Cells with rewired membranes can be used for a variety of applications such as fluorescent labeling, cell sorting and tissue engineering.

Bio-orthogonal chemistry combined with a liposomal delivery system allows for the assembly of cells into 3D tissues. Several cell types were combined to produce functional cardiac and liver tissues with variable thickness and layer orientations which were subsequently used to assess drug toxicity. In the future studies these tissues can be transplanted into animal models for treatment of conditions such as liver cirrhosis and ischemic heart disease.^{5,6} Since our system does not employ polymer scaffolds, high cell density can be achieved, which is crucial for cells to establish intercellular connections and promote cell-cell communications in the tissue. In addition, employing our scaffold-free technology will significantly lower the risk of immunological response due to the accumulation of immunologically active byproducts which occurs in the process of scaffold degradation.

3D co-culture systems are powerful tools for *in vitro* modelling and are employed for studying complex biological systems involving interactions between cells from more than one cell type. These interactions take place in important biological processes such as stem cell differentiation, embryonic development and the maturation of lymphocytes. In this work, a complex multilayered co-culture system of hMSC and C3H10T1/2 cells was established and it was demonstrated that the change of cell orientation in the 3D co-culture has an impact on the choice of lineage. In other words, the same cells cultured under the same conditions differentiate into different tissues depending on whether they are positioned on the top or the bottom of the 3D co-culture. Our technology is flexible and enables formation of customized co-culture systems which allows for the modelling of different biological processes.

A future project in which our click chemistry system can be used is in the creation of a model of the blood-brain barrier – a highly-selective semipermeable membrane that separates the central nervous system from the circulating blood. The blood-brain barrier is formed by a single

layer of endothelial cells which are connected by tight junctions. It is permeable to water and gas molecules which can cross it via diffusion, and is impermeable to other lipophilic molecules including most drugs.^{7,8} Overcoming the blood-brain barrier, however, is essential for efficient drug delivery. With our technology, it is possible to simulate the blood-brain barrier by creating a multilayer 3D co-culture of neural cells with endothelial cells. The model can be used to screen the potential drug candidates for their ability to cross the barrier. If successful, the project can lead to the creation of a brain-on-a-chip screening platform.

The bio-orthogonal oxyamine crosslinker is a simple molecule that was used to crosslink ketone-tethered cells resulting in a complex polymer where the monomer subunits are cells. This hybrid polymer-cell system opens new opportunities for polymer modifications and the construction of more complex tissues which would incorporate a wide variety of ligands. Such tissues may also include ketone-tethered nanoparticles, fluorescent beads, or biological molecules such as polysaccharides and could be easily decorated with ligands for different purposes.

7.2 References

1. Eloy, J. O. *et al.* Liposomes as carriers of hydrophilic small molecule drugs: Strategies to enhance encapsulation and delivery. *Colloids Surfaces B Biointerfaces* **123**, 345–363 (2014).
2. Lee, S. *et al.* Chemical Tumor-Targeting of Nanoparticles Based on Metabolic Glycoengineering and Click Chemistry. *ACS Nano* **8**, 2048–2063 (2014).
3. Barrett, D. M., Grupp, S. A. & June, C. H. Chimeric Antigen Receptor– and TCR-Modified T Cells Enter Main Street and Wall Street. *J. Immunol.* **195**, 755–761 (2015).
4. Haydon, G. H. & Neuberger, J. Liver transplantation of patients in end-stage cirrhosis. *Best Pract. Res. Clin. Gastroenterol.* **14**, 1049–1073 (2000).
5. Schuppan, D. & Afdhal, N. H. Liver cirrhosis. *Lancet* **371**, 838–851 (2008).
6. D’Amore, A. *et al.* Bi-layered polyurethane – Extracellular matrix cardiac patch improves ischemic ventricular wall remodeling in a rat model. *Biomaterials* **107**, 1–14 (2016).
7. Pardridge, W. M. Blood–brain barrier delivery. *Drug Discov. Today* **12**, 54–61 (2007).
8. Luissint, A.-C., Artus, C., Glacial, F., Ganeshamoorthy, K. & Couraud, P.-O. Tight junctions at the blood brain barrier: physiological architecture and disease-associated dysregulation. *Fluids Barriers CNS* **9**, 23 (2012).

Appendix

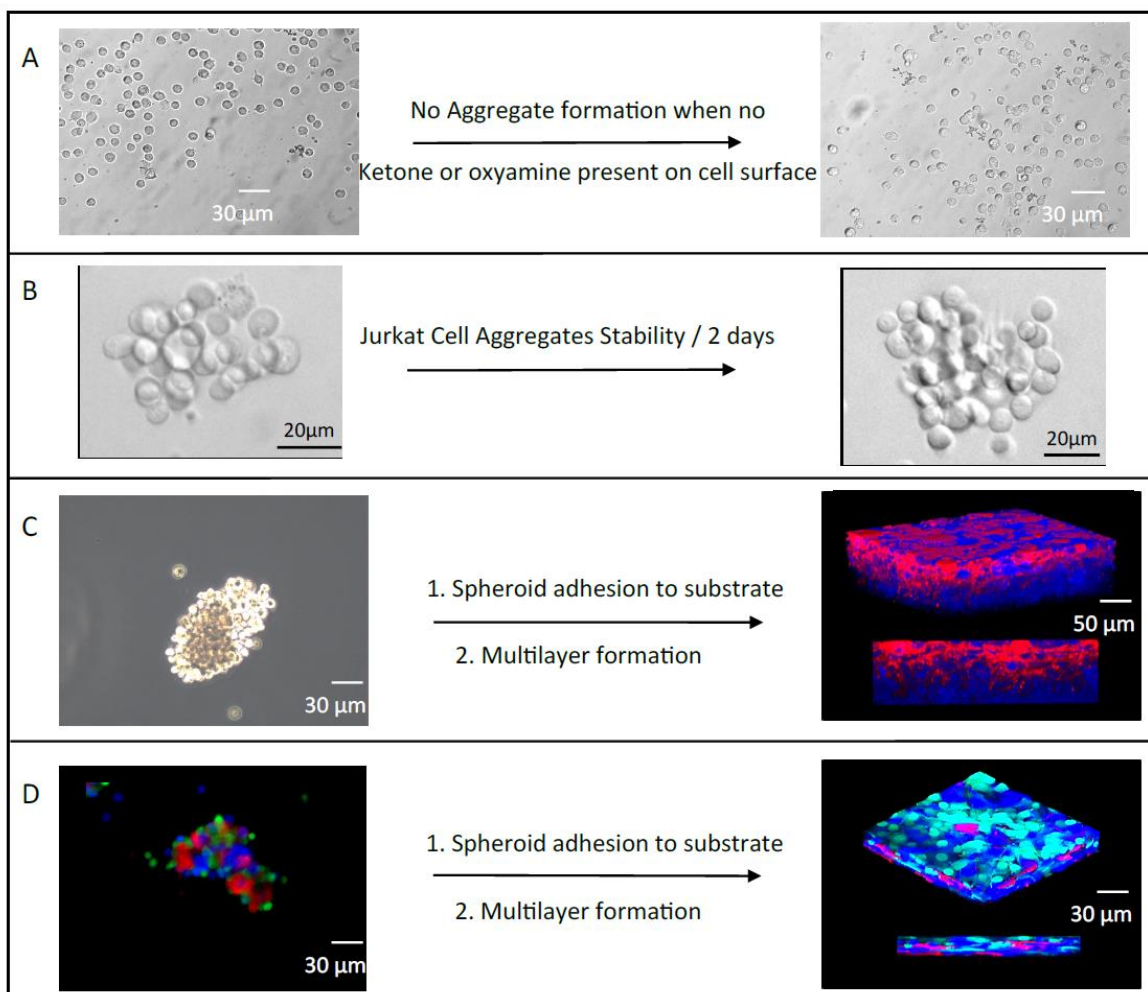


Figure A1. Control and stability studies for the formation of cell aggregates and multilayers. **(A)** Representative control images of fibroblast cells that do not form aggregates/spheroids when no bio-orthogonal lipids are delivered to the cell surface. **(B)** Suspension cells (Jurkat Cells) that form spheroids through the interfacial oxime click reaction are stable for several days without the use of polymer scaffolds or encapsulating materials. **(C)** Adhesive cells that form aggregates in solution and then deposit and adhere to cell culture substrate surfaces to generate multilayers. Without the interfacial oxime click reaction the cells would not form 3D multilayers but would only form standard monolayers in culture. **(D)** 3 colored cell lines form spheroids via the interfacial oxime click reaction and then form multilayers upon deposition to a cell culture substrate